Department of Civil, Environmental and Geomatic Engineering

University College London



Influence of coincident cracks in concrete on reinforcement corrosion

Takhmina Myrzakulova

A thesis submitted for the degree of

Doctor of Philosophy in Civil Engineering

September 2022

Statement of Originality

I, Takhmina Myrzakulova, confirm that the work presented in this thesis is my own. Where information has been derived from other sources, I confirm that this has been indicated in the thesis.

Signed: Takhmina Myrzakulova

Date: 1th September 2022

Abstract

Cracks can accelerate the penetration of aggressive substances such as chloride and carbon dioxide into concrete leading to premature corrosion of embedded reinforcing bars. Cracks may be coincident i.e. lie above and follow the line of the reinforcing bars, or intersecting i.e. cross reinforcing bars. The former type is widely acknowledged to present a more serious threat to reinforcement corrosion and would appear to be unavoidable in concrete construction. Yet, the research on coincident cracks is almost non-existent. The aim of this project is to investigate the influence of coincident crack width, depth and cement composition on chloride-induced corrosion. Three designs of specimens were employed. Type A consists of concrete slabs with a maximum surface crack width of 0.4mm. Type B contains parallel-sided cracks which were achieved by inserting steel shims into green concrete of equal depth, 0.1mm, 0.2mm, 0.3mm or 0.4mm wide which terminate approximately 9mm above reinforcing bars. Type C contains artificial cracks with identical widths to those of type B specimens but unlike these, the cracks extend to the surface of reinforcing bars. The binder types investigated were 100% Portland cement, 35%Portland cement /65% Ground granulated blast-furnace slag and 70%Portland cement /30% Fly ash. There were 6 type A, 30 of type B and 15 of type C specimens made of all three binder compositions tested. Corrosion was monitored using half-cell potentials, linear polarisation resistance, and zero resistance ammeter. The data was analysed by ANOVA and post-hoc tests. Also, the chloride content of the specimens as well as gravimetric mass losses of the reinforcement were evaluated. The results show that there is no threshold crack width below which there is a low risk of corrosion. The results also show that concrete made of blended cement may offer better protection to embedded reinforcing bars than pure PC mixes.

Impact Statement

Codes and standards on design in reinforced concrete such as Eurocode 2 often contain limits on surface crack widths aimed at reducing the risk of reinforcement corrosion. These limits have been derived by testing concrete specimens containing cracks which lie perpendicular to reinforcing bars. Yet, it is widely accepted that cracks which lie over and are aligned with reinforcing bars, termed coincident cracks, present a greater risk of corrosion. This omission may account for the enormous annual expenditure on the repair and maintenance of structures suffering from reinforcement corrosion. The aim of this project is to examine the impact of coincident cracks on reinforcement corrosion in order to evaluate the efficacy of present recommendation on crack control and to propose improvements where deficiencies are found.

Acknowledgements

First of all, I would like to express my sincere gratitude to my supervisors Dr Chanakya Arya for his support, guidance, advice, and teaching throughout the course of my Ph.D. study and to Prof Julia Stegemann for her support at different stages of this journey. I have gained immense experience and knowledge during my Ph.D. years and would like to thank my supervisors for their contribution to that.

I would like to thank all the technical staff at the workshop in UCL Chadwick Building including Leslie Ansdell, Warren Gaynor, Leslie Irwin, Dr Shi Shi, Dr Judith Zhou, and Dr. Eral Bele. Special appreciation goes to Leslie Ansdell and Warren Gaynor for preparing and sending all my specimens to Kazakhstan so that I could complete my experimental work. I also want to thank Leslie Ansdell for providing a space in the Fluids lab and Prof Richard Simon for providing a tank for storing the second set of my specimens.

I am thankful for the financial support provided by the Center for International Programs Bolashaq.

I am grateful to have shared this journey with all my friends and colleagues at UCL. I met truly incredible people and thank them for their support and all the great memories.

I would also like to acknowledge the immeasurable support from my parents Roza and Momyn during my Ph.D. albeit from a distance. Thank you to all my siblings and sisters-in-law. A special appreciation goes to my brother Mukhan, for being always by my side and for endless encouragement.

Table of contents

Statement of Originality	ii
Abstract	
Impact Statement	iv
Acknowledgements	V
Table of contents	vii
List of Figures	х
List of Tables	xv
List of Abbreviationsx	
Chapter 1 Introduction	2
1.1 Background	2
1.2 Research aim and objectives	3
1.3 Testing paradigm	3
1.4 Thesis outline	
Chapter 2 Review of cracks and corrosion mechanisms	6
2.1 Introduction	
2.2 Cracks and corrosion	7
2.2.1 Causes of cracking	7
2.2.2 Mechanism of corrosion process in reinforced concrete	8
2.2.3 Carbonation	
2.2.4 Chlorides	10
2.2.5 Mechanism of crack-induced corrosion in chloride rich environment	12
2.3 Factors influencing crack-induced corrosion	14
2.3.1 Relationship between crack width and corrosion	14
2.3.2 Crack frequency and corrosion	19
2.3.3 Concrete cover	22
2.3.4 Concrete and steel properties	23
2.3.5 Binder type	
2.3.6 Water-binder ratio and cement content	27
2.3.7 Type of rebar	28
2.3.8 Crack orientation	30
2.3.8.1 Intersecting cracks	
2.3.8.2 Coincident cracks	
Chapter 3 Causes, consequences and existing research on coincid	
cracks	33
3.1 Causes of coincident cracking	33
3.1.1 Plastic settlement	33
3.1.2 Plastic shrinkage	34
3.1.3 Early thermal shrinkage	35
3.1.4 Long-term drying shrinkage	36
3.1.5 Direct loading	37
3.1.6 Flexural cracks	37
3.1.7 Bond cracks	39
3.2 Consequences	40
3.3 Existing research	
3.3.1 Dakhil & Cady, 1975	
3.3.2 Stillwell, 1988	43
3.3.3 Poursaee & Hansson, 2008	47
3.3.4 François & Arliquie, 1998	

3.4 Current practices with regard to coincident cracking and needed re	
3.5 Conclusion	
3.6 Overall comment	
Chapter 4 Review of crack control and corrosion recommendations	
4.1 American Standard: Building Code Requirements for Structural C	
(ACI 318, 2019)	
4.2 Eurocode 2 and BS 8500-1:2015+A2:2019 (BS EN 206, 2019)	
4.3 (IS 456, 2000) Indian Code of Practice	
4.4 (JSCE, 2007) Japanese Code	
4.5 Russian Code (CΠ 28.13330, 2017)	
4.6 Chinese Code GB50010-2010 (modified in 2015) (Guo et al., 2018).	66
4.7 Conclusion	
Chapter 5 Methodology	
5.1 Specimen design	
5.1.1 Type A specimens	
5.1.2 Type B specimens	
5.1.3 Type C	80
5.1.4 The second set of specimens	83
5.1.5 Mix proportions and test details	
5.1.6 Casting and curing	
5.1.7 Sealing	87
5.1.8 Corrosion initiation	87
5.2 Measurement techniques	87
5.2.1 Corrosion monitoring	
5.2.2 Open circuit potential (OCP) or Half-cell potential	
5.2.2.1 How it works	
5.2.2.2 Interpretation of results	89
5.2.2.3 Limitations	
5.2.3 Linear Polarization Resistance	
5.2.3.1 How it works	
5.2.3.2 Interpretation of results	
5.2.3.3 Limitations	93
5.2.4 Zero resistance ammeter (ZRA)	
5.2.4.1 How it works	
5.2.4.2 Interpretations of results	
5.3 Chloride profile	
5.4 Gravimetric mass loss	
5.5 Statistical analysis	99
Chapter 6 Results and Discussion	
6.1 Effect of coincident crack widths on corrosion of reinforcement	
6.1.1 Specimens made of 100% PC	
6.1.1.1 Half-cell potentials	
6.1.1.2 Corrosion rates	
6.1.1.3 Gravimetric mass loss	
6.1.1.4 Photos showing condition of reinforcing bars	
6.1.2 Specimens made of 35% PC /65% GGBS denoted as GGBS	
6.1.2.1 Half-cell potentials	
6.1.2.2 Corrosion rates	
	, , ,

6.1.2.4 Photos showing condition of reinforcing bars	120
6.1.3 Specimens made of 30% FA/70% PC (denoted as FA)	121
6.1.3.1 Half-cell potentials	121
6.1.3.2 Corrosion rates	
6.1.3.3 Gravimetric mass loss	
6.1.3.4 Photos showing condition of reinforcing bars	
6.1.4 Discussion on the effect of crack width in reinforcement corrosion	
6.2 Effect of depth of cracking on corrosion rates.	
6.2.1 Specimen designs A1 & B	
6.2.1.1 Half-cell potentials	
6.2.1.2 Corrosion rates	
6.2.1.3 Gravimetric mass loss	
6.2.1.4 Photographic evidence of reinforcement condition	
6.2.2 Specimen designs A2 & C	
6.2.2.1 Half-cell potentials	
6.2.2.2 Corrosion rates	
6.2.2.3 Gravimetric mass loss	
6.2.2.4 Photographic evidence of reinforcement condition	
6.2.3 Discussion on the effect of crack depth in reinforcement corrosion	
6.3 Effect of cement type on corrosion of the reinforcement	
6.3.1 Specimen type A	
6.3.1.1 Corrosion rates	
6.3.1.2 Chloride concentration in concrete made of different cement type.	
6.3.2 Specimen type B	
6.3.2.1 Corrosion rates	
6.3.2.2 Chloride concentration in concrete made of different cement type.	
6.3.3 Specimen type C	
6.3.3.1 Corrosion rates	
6.3.3.2 Chloride concentration in concrete made of different cement type .	
6.3.4 Discussion on the effect of cement type on corrosion rate	
Chapter 7 Conclusion	
7.1 Summary of findings	
7.2 Recommendations on crack control in codes of practice based on obtain	
results	
7.3 Recommendations for future work	
References	
Appendix A Monthly corrosion assessment	
Appendix B Raw data in a long format	195
Appendix C Codes used in R studio	230
Appendix D Analysis of the last 3, 6, and 9 months	
Appendix E Effect of crack depth	
	243 247

List of Figures

Fig. 1.1 Intersecting and coincident cracks (Concrete Society, 2015)	2
Fig. 2.1 Types of cracks (Concrete Society, 2010)	8
Fig. 2.2 An overview of the electrochemical and physical processes taking place during corrosion of steel reinforcement proposed by (Küter, 2009)	_
Fig. 2.3. (a) Process of pitting corrosion of steel in concrete (Bertolini et al., 2004), (corrosion pit located adjacent to a defect in the steel-concrete interface (Mohammed al., 2002).	et
Fig. 2.4. Location of anodic and cathodic areas due to localised loss of passivity (CE	
Fig. 2.5. Cracks and corrosion at multiple intersecting cracks BRE (1993)	14
Fig. 2.6. Mass loss due to macrocell corrosion after test period of a) 24 weeks and by years (Schießl & Raupach, 1997)	•
Fig. 2.7. Effect of crack frequency on cumulative weight loss due to corrosion – By line colarization resistance (LPR) measurements (Arya & Ofori-Darko, 1995)	
Fig. 2.8. Cracks patterns in beams reinforced with plain and deformed bars (Mohammet al., 2001)	
Fig. 2.9. Comparison of diffusion coefficients according to concrete strength (S15, S2 and S30), addition of fly ash (S30F20) and maximum aggregate size (S30G13) (Jang al., 2011).	et
Fig. 2.10. Impact of binder type on corrosion rate depending on concrete cover and crawidth (Scott & Alexander, 2007).	
Fig. 2.11. Average resistivity values for 40mm cover specimens from weeks 32 to (weeks 32 to 46 for SL and SH), (Scott & Alexander, 2007)	
Fig. 2.12. Steel-concrete interface after formation of the internal cracks (Käthler et a 2017).	
Fig. 2.13. Transverse cracks and corrosion (Concrete Society, 2015)	31
Fig. 2.14. Corrosion process in coincident crack (BRE, 1993)	32
Fig. 3.1 Plastic settlement cracks (Concrete Society, 2010)	34
Fig. 3.2 Plastic shrinkage cracks follow the pattern of the reinforcement (Concre	
Fig. 3.3 Example of flexural cracks coincident with stirrups (CEB, 1985)	38
Fig. 3.4 Excessive bond stress (CER. 1082)	40

Fig. 3.5 Formation of longitudinal cracks
Fig. 4.1 Adequate combination of design concrete cover c_d and design diffusion coefficient for chloride ion D_d (Smith, 2016)
Fig. 5.1 Plan view of reinforcement arrangement for Type A specimens74
Fig. 5.2 The schematic view of the specimen type A
Fig. 5.3 Coated mild steel rod to prevent corrosion
Fig. 5.4 Type A specimen subject to three-point loading
Fig. 5.5 Frame used to hold the crack open in Type A specimens
Fig. 5.6 Step-by-step progression of Specimen type A
Fig. 5.7 Plan view of reinforcement arrangement in Type B specimens
Fig. 5.8 Elevation view of reinforcement arrangement of the B test sample 78
Fig. 5.9 Schematic view of the Specimen type B79
Fig. 5.10 Step-by-step progression of Specimen type B
Fig. 5.11 The distance between the bottom of the shim and the top of the mild steel bar.
Fig. 5.12 Schematic of Specimen design C
Fig. 5.13 Elevation view of reinforcement arrangement of the C test sample 81
Fig. 5.14 Step-by-step progression of Specimen type C
Fig. 5.15 Crack-steel interface in the artificially created crack that reaches the rebar level, specimen type C
Fig. 5.16 Testing positions in slab specimens
Fig. 5.17 Crack formation in type B specimens and measurement points
Fig. 5.18 Linear polarisation curve (Poursaee, 2010)
Fig. 5.19 Schematic of ZRA performance for the beam specimens
Fig. 5.20 Schematic of chloride profile depth on the right side shown as a red broken line
Fig. 5.21 Schematics of chloride determination levels in cracked specimens 98
Fig. 5.22 Analytical grade scales used to determine the weight of rebars after the pickling with Clarck's solution
Fig. 6.1 Half-Cell potential readings for specimen types B and C made of PC with different crack widths

Fig. 6.2 Monthly Corrosion rate readings for specimen types B and C with various crack widths measured via LPR
Fig. 6.3 Monthly Corrosion rate readings for specimen types B and C with various crack widths measured via ZRA
Fig. 6.4 Corrosion rates ($\mu A/cm^2$) experienced by specimen types B and C made of PC with different crack widths
Fig. 6.5 The amount of rust formed on the surface of the rebar in specimen type B made of PC: (a) the visual appearance of the specimens after the splitting into halves; (b) the surface of the rebar facing the crack, (c) the reverse side of the rebar (d) the surface of the reinforcement facing the crack after the picking
Fig. 6.6 The amount of rust formed on the surface of the rebar in specimen type C made of PC: (a) the visual appearance of the specimens after the splitting into halves along the crack; (b) the surface of the rebar facing the crack, (c) the reverse side of the rebar (d) the surface of the reinforcement facing the crack after the picking
Fig. 6.7 Half-Cell potential readings for specimen types B and C made of GGBS with different crack widths
Fig. 6.8 Monthly Corrosion rate readings for specimen types B and C with various crack widths measured via LPR
Fig. 6.9 Monthly Corrosion rate readings for specimen types B and C with various crack widths measured via ZRA
Fig. 6.10 Corrosion rates ($\mu A/cm^2$) experienced by specimen types B and C made of GGBS with different crack widths
Fig. 6.11 The amount of rust formed on the surface of the rebar in specimen type B made of GGBS: (a) the visual appearance of the specimens after the splitting into halves; (b) the surface of the rebar facing the crack, (c) the side away from the crack (d) the surface of the bar facing the crack after the picking.
Fig. 6.12 The amount of rust formed on the surface of the rebar in specimen type C made of GGBS: (a) the visual appearance of the specimens after the splitting into halves along the crack; (b) the surface of the rebar facing the crack, (c) the side away from the crack (d) the surface of the reinforcement facing the crack after the picking
Fig. 6.13 Half-Cell potential readings for specimen types B and C made of FA with different crack widths
Fig. 6.14 Monthly Corrosion rate readings for specimen types B and C with various crack widths measured via LPR
Fig. 6.15 Monthly Corrosion rate readings for specimen types B and C with various crack widths measured via ZRA
Fig. 6.16 Corrosion rates (μA/cm²) experienced by specimen types B and C made of FA with different crack widths

Fig. 6.17 The amount of rust formed on the surface of the rebar in specimen type B made of FA: (a) the visual appearance of the specimens after the splitting into halves; (b) the surface of the rebar facing the crack, (c) the side away from the crack (d) the surface of the reinforcement facing the crack after the picking
Fig. 6.18 The amount of rust formed on the surface of the rebar in specimen type C made of FA: (a) the visual appearance of the specimens after the splitting into halves along the crack; (b) the surface of the rebar facing the crack, (c) the side away from the crack (d) the surface of the bar facing the crack after the picking.
Fig. 6.19 The corrosion mechanism in Specimen type B, adopted from (E. Chen et al. 2020)
Fig. 6.20 Chloride concentration by weight of concrete in Specimen design B made of al cement mixes and various crack widths
Fig. 6.21 Chloride concentration by weight of concrete in Specimen design C made of all cement mixes and various crack widths
Fig. 6.22. The appearance of V-shaped pitting corrosion formed along the crack in Specimen design C
Fig. 6.23 The variation in depth and width of pits formed in type C specimens with different crack widths
Fig. 6.24 Crack depths and concrete-steel interface disruption levels for all three specimen designs A, B and C
Fig. 6.25 Half-Cell potential readings for specimen types A1 and B made of all cementypes
Fig. 6.26 Corrosion rates ($\mu A/cm^2$) experienced by specimen designs A1 and B 138
Fig. 6.27 Gravimetric mass loss (in grams) in type A1 & B specimen designs made with PC, GGBS and FA
Fig. 6.28 The rust development on the surface of the reinforcement with various crack depths for the set of specimens A1 & B
Fig. 6.29 Half-Cell potential readings for specimen types A2 and C made of all cement types
Fig. 6.30. Corrosion rates (μA/cm²) experienced by specimen designs A2 and C 145
Fig. 6.31. Gravimetric mass loss (in grams) in all specimen designs made with PC GGBS and FA
Fig. 6.32. The rust development on the surface of the reinforcement with various crack depths for the set of specimens A1 & B
Fig. 6.33. The corrosion type on the surface of specimens with different crack depths

Fig. 6.34 Formation of cathodic and anodic areas on the surface of the reinforcement where the crack follows the rebar longitudinally, adopted from (Schiessl, 1986) 150
Fig. 6.35. The corrosion mechanism in Specimen type C, adopted from (E. Chen et al., 2020)
Fig. 6.36. The corrosion mechanism in Specimen type B, adopted from (E. Chen et al., 2020)
Fig. 6.37. Corrosion rates (μA/cm²) in Specimen type A1 obtained via LPR and ZRA
Fig. 6.38. The chloride content of control specimens made of all three cement types.
Fig. 6.39. A schematic of the levels where chloride profiles have been determined in Specimen design A
Fig. 6.40. The chloride content by weight of concrete in cracked A1 (exposed to an aggressive environment for 36 months) / A2 (exposed to an aggressive environment for 14 months) specimens made of all cement types
Fig. 6.41. Corrosion rates ($\mu A/cm^2$) in type B specimens obtained via LPR and ZRA 158
Fig. 6.42. A schematic of the levels where chloride profiles have been determined in Specimen design B
Fig. 6.43. The chloride content by weight of concrete in type B specimens with 0.4mm crack width only made of all cement types
Fig. 6.44. Corrosion rates ($\mu A/cm^2$) in type C specimen obtained via LPR and ZRA. 161
Fig. 6.45. A schematic of the levels where chloride profiles have been determined in Specimen design C
Fig. 6.46. The chloride content by weight of concrete in type C specimens with 0.4mm crack width only made of all cement types

List of Tables

Table 1.1 Overview of specimen specifications
Table 2.1. Weight loss due to corrosion in grams (Mohammed et al., 2001) 18
Table 2.2. Influence of cover, water/cement ratio and cement content on corrosion (Beeby, 1983)
Table 2.3. Average concrete resistivities as a function of binder composition, Ω m (Claus et al., 2007)
Table 2.4. Effect of bar type and crack width on corrosion length (Beeby, 1978) 28
Table 3.1 Potential readings (Dakhil & Cady, 1975)
Table 3.2 Mix proportions
Table 3.3 Effect of concrete grade and cement type on reinforcement corrosion 46
Table 3.4 Effect of crack width and cover on reinforcement corrosion 47
Table 4.1 Basic requirements of concrete mix design for corrosion protection together with allowable water-soluble chloride ion content in ACI 318
Table 4.2. Durability recommendations for reinforced elements with an intended working life of at least 100 years (BS EN 206, 2019)
Table 4.3. Minimum Cement Content, Maximum Water-Cement Ratio and Minimum Grade of Concrete for Different Exposures with Normal Weight Aggregates of 20 mm and Nominal concrete cover in IS 456, 2000.
Table 4.4. Maximum design diffusion coefficient, D _d (cm²/year), for a range of concrete convers, c _d , with different service lives for elements exposed to splash zone in JSCE 200759
Table 4.5 Requirements for concrete mix design in aggressive environment in JSCE 2007
Table 4.6. Durability requirements for reinforcement corrosion for deformed and plain bars (JSCE, 2007)
Table 4.7. Concrete cover prescribed for corrosive environment (CΠ 28.13330, 2017) 63
Table 4.8. Concrete mix design requirements (CΠ 28.13330, 2017)64
Table 4.9 Crack width limitation for aggressive environment (CΠ 28.13330, 2017) 65
Table 4.10 Minimum concrete cover specifications (Guo et al., 2018) 66
Table 4.11. Requirement for concrete mix design (Guo et al., 2018)67
Table 4.12 Allowable maximum crack width for exposure conditions (Guo et al., 2018)
n

Table 4.13 Comparison of different Codes of Practice
Table 5.1. Summary of concrete mix proportions
Table 5.2 Chemical composition of the binders (%)
Table 5.3. Test details
Table 5.4. ASTM criteria for corrosion of steel in concrete for different standard reference electrodes (Broomfield, 2006)
Table 5.5. Interpretation of corrosion rate (Rodriguez et al., 1994)
Table 6.1 ANOVA results for different crack widths in specimens made of PC and measured by both measurement techniques
Table 6.2 Post Hoc Test of multiple comparisons on the effect of crack width on corrosion for specimens B and C made of PC measured via LPR and ZRA
Table 6.3 Gravimetric mass loss of B and C specimens made of PC 112
Table 6.4 ANOVA results for different crack widths in type B and C specimens made of GGBS and measured with both measurement techniques
Table 6.5 Post Hoc Test of multiple comparisons on the effect of crack width on corrosion for specimens B and C made of GGBS measured via LPR and ZRA 118
Table 6.6 Gravimetric mass loss of B and C specimens made of GGBS 119
Table 6.7 ANOVA results for different crack widths in specimens made of FA and measured with both measurement techniques
Table 6.8 Post Hoc Test of multiple comparisons on the effect of crack width on corrosion for specimens B and C made of FA measured via LPR and ZRA
Table 6.9 Gravimetric mass loss of B and C specimens made of FA 125
Table 6.10 ANOVA results for different crack depths (Specimen types A1 and B) in specimens made of all cement types and measured through both measurement techniques
Table 6.11. ANOVA results for different crack depths (Specimen types A2 and C) in specimens made of all cement types and measured through both measurement techniques
Table 6.12. ANOVA results for Specimen type A1 through both measurement techniques
Table 6.13. Post Hoc Test of multiple comparisons on the effect of cement type on corrosion among specimen type A1 measured via LPR and ZRA
Table 6.14. ANOVA results for Specimen type B through both measurement techniques

Table 6.15 Post Hoc Test of multiple comparisons on the effect of cement type on corro	osion
among specimen type B measured via LPR and ZRA	. 158
Table 6.16. ANOVA results for Specimen type C through both measurement technic	•
Table 6.17. Post Hoc Test of multiple comparisons on the effect of cement type on corro	osion
3	

List of Abbreviations

PC Portland cement

GGBS Ground granulated blast furnace slag

FA Fly ash

daN. m Deca Newton Meter

OPCC Ordinary Portland cement concrete

SM Silica fume

HPC High performance concrete

OPC Open circuit potential

LPR Linear polarisation resistance

ZRA Zero resistance ammeter

WE Working electrode

RE Reference electrode

CE Counter electrode

EIS Electrochemical impedance spectroscopy

CVA Cyclic voltammetry

AC Alternating current

DC Direct current

XRF X-ray fluorescence

HSD Honestly significantly different

IQR Interquartile range

Q1 1 Quartile

Q3 3 Quartile

SCM Supplementary cementitious material

W/C Water cement ratio

Chapter 1 Introduction

1.1 Background

The tensile strength of concrete is only around 10% of its compressive strength. Therefore, when concrete is subjected to relatively low values of tensile stress, it will crack (Park, 2001). Although cracks are not necessarily the only entry point for aggressive substances such as chloride and carbon dioxide into concrete it is obvious that they provide a more rapid means of ingress to embedded reinforcing steel than penetration through sound concrete via mechanisms such as diffusion (Hong & Hooton, 1999), capillary absorption (Stanish et al., 1997), wick action and hydrostatic pressure (Aldred et al., 2004). For example, work by (Djerbi et al., 2008) has shown that a crack width of 0.2mm can increase the diffusion coefficient of high-performance concrete containing silica fume, high-performance concrete and ordinary concrete by approximately 3, 6 and 15 fold respectively. Thus, it is widely acknowledged that the presence of cracks in concrete will hasten the onset of reinforcement corrosion, though not necessarily the subsequent rate of corrosion propagation, and therefore it is necessary to control their occurrence.

Much of the literature on the effect of cracks in concrete on reinforcement corrosion refers to longitudinal and transverse cracks, respectively, cracks which occur parallel to the main reinforcement and cracks which occur at right-angles. However, according to (Arya et al., 1994) this terminology is ambiguous since reinforcement is usually present in two directions at right-angles in virtually all reinforced concrete elements/structures and in two-way spanning slabs, for instance, both sets of bars are main steel. To evaluate the risk of reinforcement corrosion it would be better to categorise cracks under the headings:

- Coincident cracks following the line of the reinforcement
- Intersecting cracks crossing the reinforcement (Figure 1.1)

Intersecting cracks include diagonal cracks. The term reinforcement in these definitions includes the main bars, secondary bars and stirrups/links.

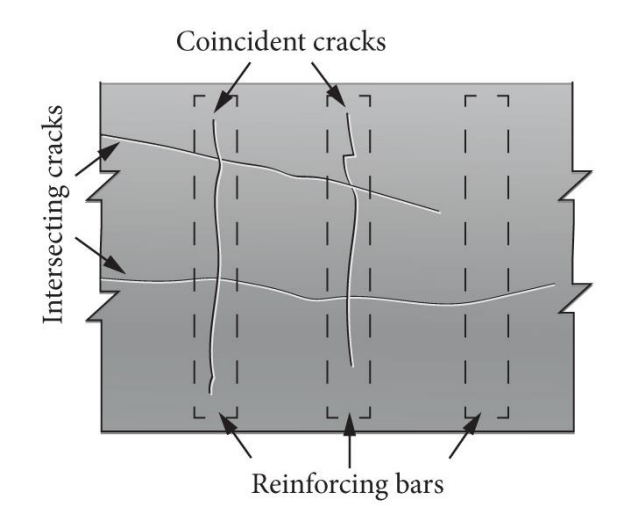


Fig. 1.1 Intersecting and coincident cracks (Concrete Society, 2015)

Although it is widely accepted that coincident cracks present a greater risk of corrosion than intersecting cracks, most of the work to-date on cracks and corrosion has focused on intersecting cracks. Apparently, the reasons for this are that it has generally been assumed that coincident cracks are:

- (a) relatively rare in practice,
- (b) can be eliminated by following good design, detailing and workmanship rules(The Concrete Society, 1992; Frosch, 2003),
- (c) will only give rise to corrosion of transverse or secondary bars which are largely unstressed and thus any corrosion will not significantly decrease the overall safety of concrete structures (CEB 1976, cited by (Beeby ,1978).

A useful starting point in this study would be to examine the accuracy of these statements via a desk study. This work would also help inform the laboratory studies to elucidate the influence of coincident cracks on corrosion. Width is a defining feature of cracks and would therefore seem to be an obvious parameter to consider. Moreover, many codes of practice recommend permissible crack widths in concrete structures for reasons of durability and thus work on this aspect would seem wholly justified. Plastic shrinkage and plastic settlement of concrete can give rise to coincident cracks. Plastic shrinkage cracks are typically 2-3mm wide, but their width rapidly decreases with depth (Concrete Society, 2010).

However, plastic settlement cracks normally extend to the surface of the top layer of reinforcing bars. Thus the effect of crack depth should also be examined.

Cement extenders play an important role in the transport mechanisms involved in reinforcement corrosion (Angst et al., 2019). Again most of the work on this aspect is based on specimens with intersecting cracks. The single piece of work which has compared the behaviour of concrete specimens with coincident cracks made of Portland and blended cement mixes by Poursaee and Hansson (2008) has suggested there are no advantages to be gained by using these materials. This is worrying given the latest advice in (BS EN 206, 2019) which warns against the use of pure PC concrete in structures exposed to chloride environments.

1.2 Research aim and objectives

The aim of the work were to

- (a) Produce a state of the art report on coincident cracks in concrete covering causes, consequences and existing research on the influence of reinforcement corrosion.
- (b) Elucidate the effect of coincident cracks with various widths both natural (achieved by 3 point bending) and parallel sided artificial (achieved by inserting steel shims into fresh concrete) on reinforcement corrosion.
- (c) Investigate the effect of coincident crack depths (both natural and artificial) on the reinforcement corrosion.
- (d) Explore the effect of Supplementary cementitious materials (SCM) on corrosion of reinforcement in concrete with coincident cracks.
- (e) Review and comment on the crack control recommendations in codes and standards on structural concrete design such as the (BS EN 1992, 2014), (ACI 318, 2019) and (GB50010-2010).

1.3 Testing paradigm

Two crack types (natural and artificial), three different crack depths (A, B and C) and four different crack widths (0.1; 0.2; 0.3; 0.4mm), three different cement types (100% Portland cement, 35%Portland cement /65% Ground granulated blast-furnace slag and 70% Portland cement /30% Fly ash) were studied in this work.

Table 1.1 shows all the variables used in this experimental work. There were two replicates for type A specimens where crack goes beyond the reinforcement made of all three cement types. Two replicates for each crack width in type B specimens made of all three cement types. Single sample for each crack width in type C specimens made of each cement type.

Table 1.1 Overview of specimen specifications.

Crack depths and types	Crack widths (mm)	Cement type	Number of specimens
A (Natural crack that exceeds the rebar)	≤ 0.4	PC, GGBS, FA	6
B (Artificial crack that stops short to the rebar)	0; 0.1; 0.2; 0.3; 0.4	PC, GGBS, FA	30
C (Artificial crack that stops at the top of the rebar)	0.1; 0.2; 0.3; 0.4	PC, GGBS, FA	12

Additional details, as well as descriptions of each specimen design and cement replacement ratio, are provided in the following chapters.

Estimates of corrosion probability and corrosion rates were obtained using three non-destructive test methods namely: half-cell potential, linear polarisation resistance (LPR) zero resistance ammeter (ZRA). Statistical analysis of results has been performed where appropriate.

Gravimetric mass losses of the rebars due to corrosion and chloride concentration in the concrete were also determined at the end of the experimental work.

1.4 Thesis outline

This thesis consists of 7 chapters.

Chapter 1 provides some background information on the areas of needed research as well as the research aims and objectives. A brief description of the

Chapter 1 Introduction

specimen types developed to achieve the various aims and objectives for this research is also provided.

Chapter 2 contains a broad literature review on general factors affecting corrosion of steel in cracked concrete.

Chapter 3 presents a state-of-the-art on causes, incidences, and consequences of coincident cracks.

Chapter 4 presents a critical review of crack control and corrosion recommendations in various codes of practice.

Chapter 5 discussed the development of the specimen design and test procedures used to answer the research questions.

Chapter 6 reveals the outcomes of the experimental work and their implications for rationalising the current code recommendations.

Chapter 7 summarises the main findings of the work as well as the limitations of this research. Also, recommendations for future research are outlined

Chapter 2 Review of cracks and corrosion mechanisms

2.1 Introduction

The life of reinforced concrete structures exposed to marine conditions or de-icing salts can be considerably shortened by the occurrence of reinforcement corrosion. Vast sums of money are required to repair these structures. It is important therefore that the advice in structural codes of practice governing durability design is sound.

Most reinforced concrete structures inevitably contain cracks which are formed as a result of various physical and chemical processes. The cracks can develop at different stages of the life of the structure. Cracks are believed to provide the preferential path for the ingress of aggressive substances such as chlorides into concrete cover and are assumed therefore that they will have a significant effect on reinforcement corrosion. To understand their role in this process it is convenient to divide cracks into two types: coincident cracks i.e. cracks which lie above and follow the line of steel reinforcing bars and intersecting cracks i.e. cracks which cross reinforcing bars. Coincident cracks are considered to be more dangerous of the two because they provide ready access to large areas of steel reinforcing bars to the substances needed for corrosion. Yet the advice on crack control in structural design codes appears to be based on the behaviour of intersecting cracks.

In general, the durability provisions in structural codes comprise a minimum thickness of concrete cover to steel reinforcing bars and corresponding concrete composition (BS 8500-1, 2019). They also specify permissible crack widths. However, there are significant differences in values of permissible crack widths specified in design codes around the world and it is also true that not all codes accept that the presence of cracks influences concrete durability (BS EN 1992, 2014) and (ACI 224, 2001) (see Chapter 4 for further details). It would seem that despite the fact that the relationship between cracks and corrosion has been investigated from all possible prospective, there is still no consensus. This chapter reviews the work to date on the influence of cracks on

reinforcement corrosion in order to discover why these differences in opinion exist and which if any of the advice is correct.

It is note worthy that the latest revision of (BS 8500-1, 2019) has recommended significant increases to minimum thicknesses of concrete cover for structures exposed to chloride environments. Although this move will be welcomed by many, this measure will increase surface crack widths which may in fact increase the risk of corrosion (Arya, 2016).

2.2 Cracks and corrosion

2.2.1 Causes of cracking

The tensile strength of concrete is around 10% of its compressive strength and when concrete experiences tensile stresses, the formation of cracks is unavoidable. The origin of these tensile stresses in reinforced concrete structures is shown in Figure 2.1. Here it can be seen that cracks can occur before hardening or after hardening. They may also be caused by loading, termed structural cracks, or as a result of various physical, chemical, thermal, handling processes, etc and give rise to non-structural or intrinsic cracks. Being aware of the causes of cracking can be helpful in determining whether a particular crack poses a potential risk to reinforcement corrosion (Concrete Society, 2015).

Irrespective of the cause, cracks will invariably facilitate the ingress of aggressive substances such as carbon dioxide and chlorides to embedded reinforcing bars, thereby accelerating the onset of reinforcement corrosion.

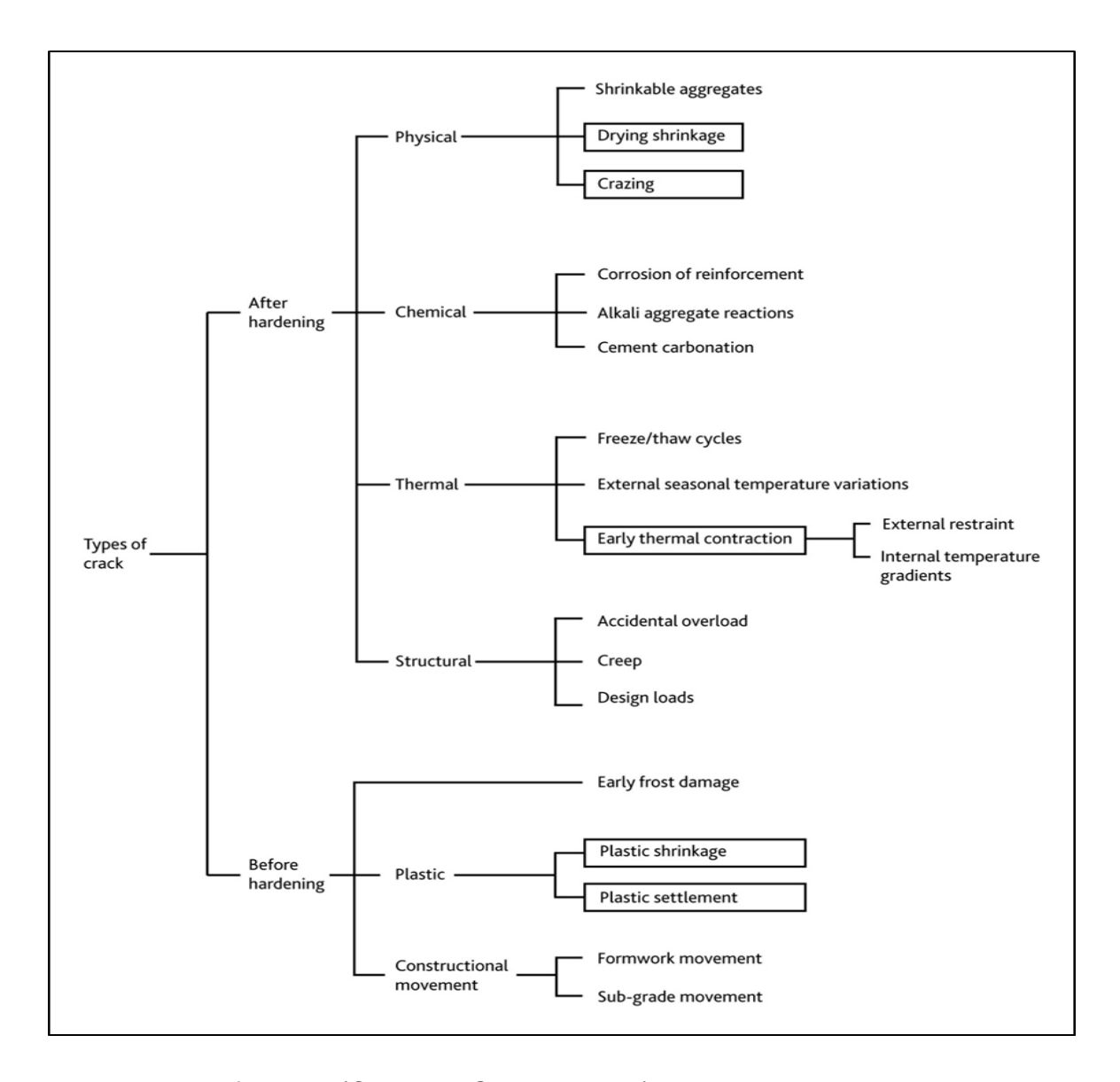


Fig. 2.1 Types of cracks (Concrete Society, 2010)

2.2.2 Mechanism of corrosion process in reinforced concrete

Generally, concrete provides an alkaline environment with a pH of around 13, thereby facilitating the formation of a thin protective layer of ferric oxide on the surface of embedded steel reinforcing bars. This ferric oxide film passivates the steel and prevents corrosion. However, it can be disrupted if the alkalinity of concrete reduces due to carbonation or the presence of chloride ions (Figure 2.2).

2.2.3 Carbonation

Carbonation occurs as a result of atmospheric carbon dioxide (CO₂) reacting with moisture in concrete to form carbonic acid (H₂CO₃) as shown in equation 2.1. In turn, the carbonic acid reacts with alkali hydroxides in the pore solution to form calcium carbonate (CaCO₃) as shown in equation 2.2. This lowers the pH of the concrete below 9, thereby causing the passivating oxide film to be destroyed and for corrosion to begin.

$$CO_2 + H_2O \rightarrow H_2CO_3$$
 Eq. 2.1

$$H_2CO_3 + Ca(OH)_2 \rightarrow CaCO_3 + 2H_2O$$
 Eq. 2.2

Rapid carbonation can occur in elements with low concrete cover to reinforcement. However, the most threatening causes are low cement content, high water/cement ratios leading to the formation of a well-connected open pore structure which allows rapid CO₂ ingress, and poor curing of concrete. Carbonation is possible even in elements with a deep concrete cover if the concrete quality is poor.

Bridges, indoor car parks and buildings are more vulnerable to carbonation induced corrosion as they experience high levels of carbon dioxide from vehicle exhaust gasses (Ofori-Darko, 1998). Another cause of fast rates of carbonation is the presence of cracks on concrete surfaces which accelerate penetration of CO₂ into the concrete interior (Beeby, 1978). However, there is a contradictory opinion about the influence of cracks on carbonation rate, which is that cracked areas may become polluted and covered, resulting in repassivation of steel surfaces. Thus, absorption of CO₂ may decrease or even stop (Schiessl, 1975).

Depths of carbonation can be assessed by spraying a freshly broken piece of concrete with phenolphthalein solution. If the sprayed surface doesn't change colour, it means that the pH is below 8 which indicates the concrete has carbonated. On the other hand, if the sprayed area changes to a pink or purple colour, this shows that the pH of the concrete is still above 8 or 9 (Blagovic', 2016).

A simplified carbonation model is presented in equation 2.3 (Bertolini et al., 2004):

$$x = K_{CO2} * t^{1/n}$$
 Eq. 2.3

where:

x - carbonation depth at time t;

K_{CO2} - carbonation factor which depends on concrete and environmental conditions;

n - exponent which is around 2;

a more sophisticated model has been proposed by (Papadakis, 2000) that gives a mathematical and physical meaning to the constant, K. However, carbonation-induced corrosion is outside the scope of this work and will not be discussed further. The following discusses chloride-induced corrosion which is considered to present a far greater threat to concrete durability (Bertolini et al., 2016).

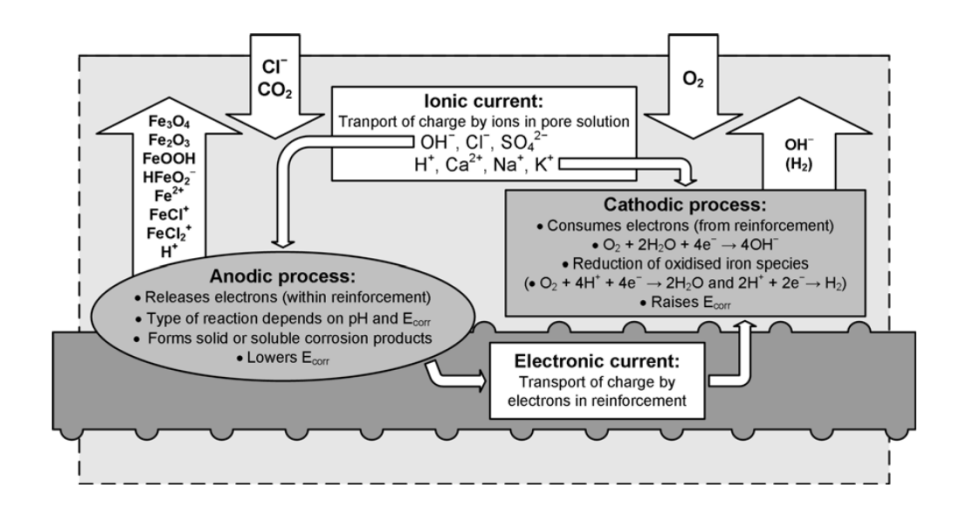


Fig. 2.2 An overview of the electrochemical and physical processes taking place during corrosion of steel reinforcement proposed by (Küter, 2009).

2.2.4 Chlorides

The mechanism of steel depassivation due to chloride ions is rather different to carbonation as uniform depassivation does not take place. Unlike carbonation, during chloride attack, the surface of the steel depassivates locally. A small amount of chloride is not able to break down the passive film; the concentration of chloride ions has to reach a threshold level. The threshold chloride level needed for depassivation depends of many factors including pH of the concrete mixture (the pH of different cement types can vary), level of chloride binding (whether it is chemically or physically bonded), and exposure conditions (% humidity and oxygen availability). 0.2% and 1%

chloride by weight of cement are considered to be the threshold levels for environments with and without moisture and oxygen availability respectively (Broomfield, 1997). Chlorides are not consumed during the process, rather they act as a catalyst that help to locally destroy the passive oxide film and allow pitting corrosion to occur (Equations 2.4 and 2.5).

$$Fe^{+2}+2Cl \rightarrow FeCl_2$$
 Eq. 2.4

$$Fe^{+2}+2Cl^{-}+2H_{2}O \rightarrow Fe (OH)_{2}+2HCl$$
 Eq. 2.5

Once chloride ions have sufficiently accumulated on the surface of steel, pitting corrosion takes place as shown in Fig. 2.3(a). Pitting corrosion normally initiates at places where the passive film is more vulnerable (Zhao & Jin, 2016). These places are usually thought to be where defects are present at the concrete-steel interface such as sulfide inclusion in the steel (Broomfield, 1997), cold joints (Yano et al., 2002), air voids as shown in Figure 2.3 (b) (Mohammed et al., 2002), bleed channels (Castel et al., 2003; Vidal et al., 2007) and cracks (Schiessl, 1986).

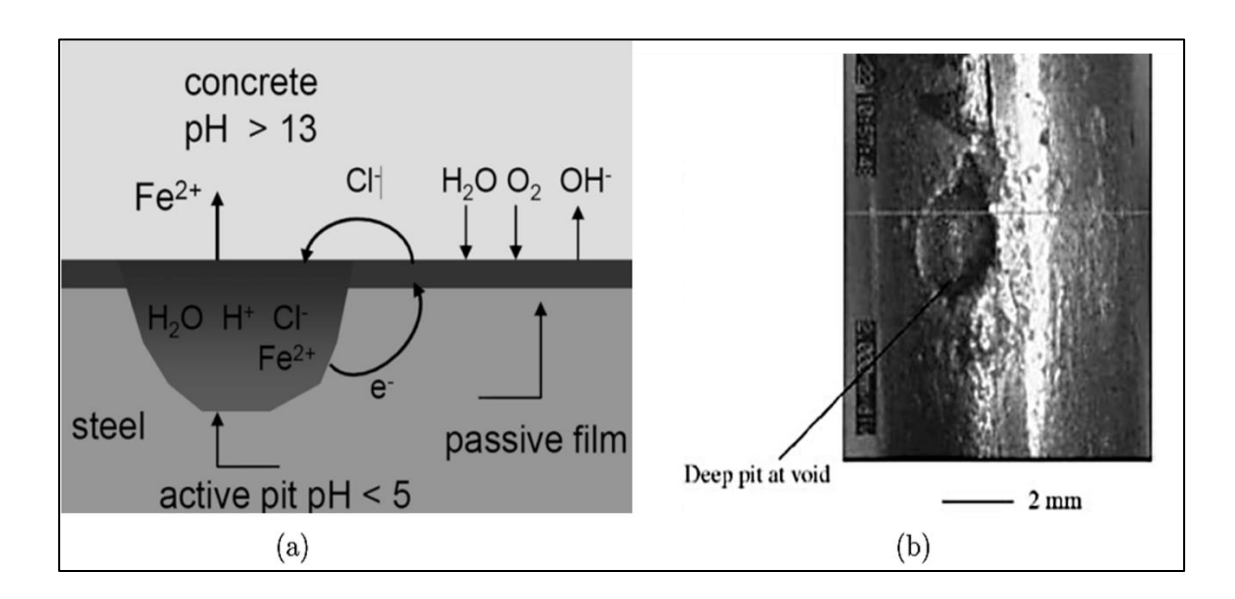


Fig. 2.3. (a) Process of pitting corrosion of steel in concrete (Bertolini et al., 2004), (b) corrosion pit located adjacent to a defect in the steel-concrete interface (Mohammed et al., 2002).

During the reaction between iron and chloride ions with water, the formation of hydrochloric acid takes place. This produces a very aggressive environment inside pits which leads to the formation of rust. Once hydrochloric acid separates back into

hydrogen and chloride ions, the whole process repeats becoming auto-catalytic and self-propagating (Pacheco, 2015). The surface of reinforcement is divided into large cathodes and small anodes, together known as a macro cell. Pitting corrosion due to chloride attack leads to the reduction of steel cross-sectional area, which in turn leads to a decrease in the load-bearing capacity of reinforced concrete members (Zhao & Jin, 2016).

2.2.5 Mechanism of crack-induced corrosion in chloride rich environment

The presence of cracks on the surface of concrete structures may well expose bars to substances such as chlorides, which make the reinforcing bars extremely susceptible to corrosion. Thus, when a cracked concrete member is exposed to a chloride-rich environment, any steel reinforcement at the crack will be rapidly depassivated. As a result of this, corrosion cells will form on the steel surface. Corrosion cells consist of anodic and cathodic areas and a conductor which is normally the concrete pore solution and facilitates ionic movement. The potential or voltage difference between the anode and cathode is the driving force for the electrochemical reactions taking place.

Four mechanisms of crack-induced corrosion in reinforcement subject to aggressive environments have been proposed. These suggest that both processes: cathodic-oxygen reduction and anodic-iron dissolution take place within the cracked area. They are illustrated in Figure 2.4, Models 2 and 3. In this case, the oxygen necessary for reaction development is also supplied through the crack. However, this requires that the crack is not constantly saturated with solution.

Model 1 in figure 2.4 suggests, however, that the anodic process occurs at the cracked area whereas the cathodic process mainly occur in the crack free areas. This model assumes oxygen is provided through the concrete cover. According to research by (Schiessl, 1986) the second mechanism is more representative of the corrosion process in cracked concrete. This mechanism assumes that concrete quality has a governing influence on corrosion propagation. Specifically, it suggests that the permeability and electrical resistivity of the concrete significantly influence the risk of corrosion in cracked concrete.

A further arrangement for anodic and cathodic areas is presented in Figure 2. 5, which is applicable to concrete members containing multiple cracks and shows the importance of crack spacing on rates of corrosion propagation in cracked concrete (see section 2.3.2 for further details).

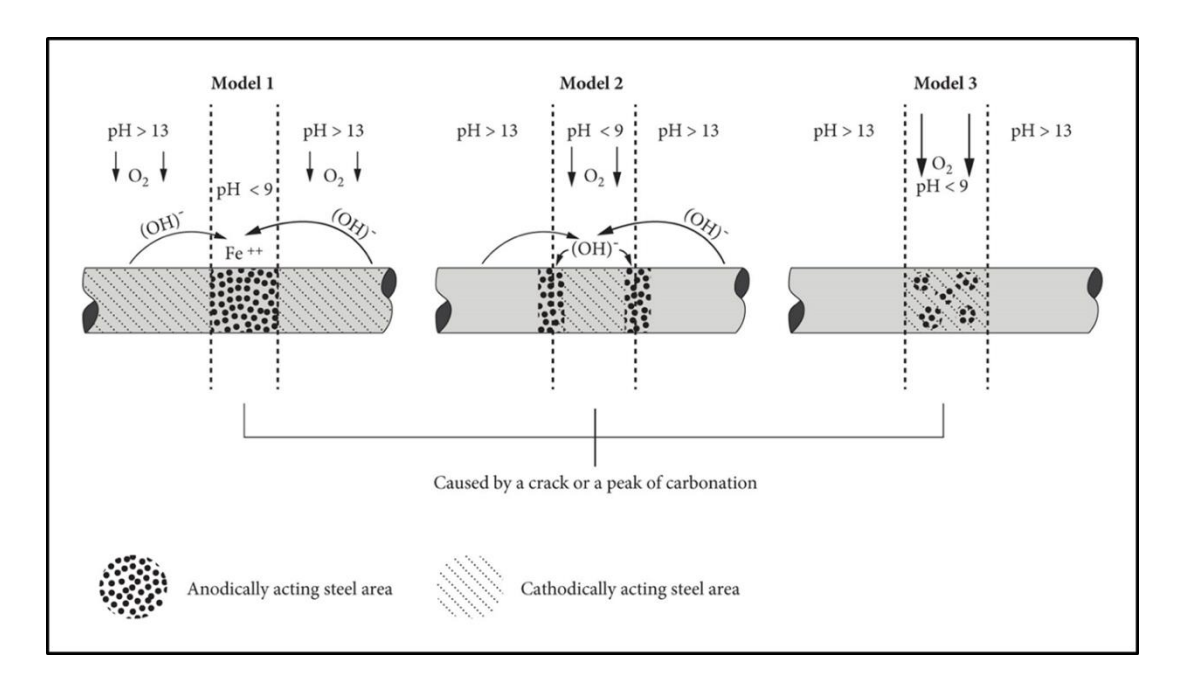


Fig. 2.4. Location of anodic and cathodic areas due to localised loss of passivity (CEB, 1982).

It is worth noting that the arrangement of anodic and cathodic areas shown in model 1 (Figure 2.4), where the anodic area is small and there is a large cathode, is likely to give rise to pitting corrosion. This mechanism of corrosion poses a higher safety risk as it can produce a rapid reduction in bar cross-section while showing minimal external signs of corrosion on the concrete surface.

In the case of reinforced concrete members with multiple cracks, the location of anodic and cathodic areas may be different. Corrosion starts at the widest cracks. (Suzuki et al., 1990) have termed this the "major cracks" and the steel at this location is predominantly anodic whereas the steel which intersects the narrower cracks is predominantly cathodic (Figure 2.5). Rehm and Moll (1964) found that in specimens with multiple cracks, narrower cracks did not show any corrosion. This suggests that these sites aided oxygen supply and primarily act as cathodes.

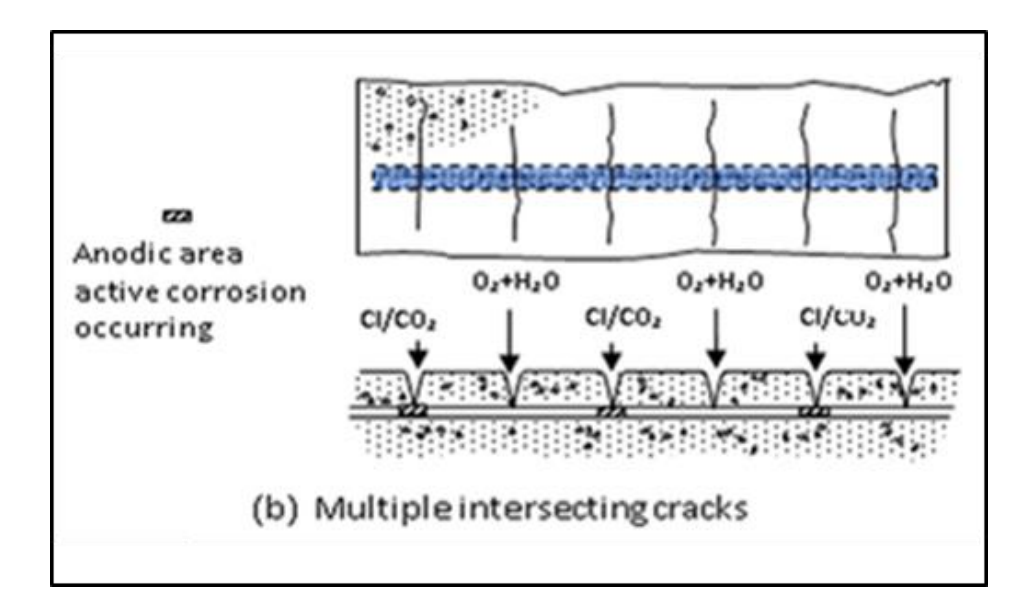


Fig. 2.5. Cracks and corrosion at multiple intersecting cracks BRE (1993).

2.3 Factors influencing crack-induced corrosion

Crack properties that influence chloride induced corrosion of reinforcement include the following:

- crack width,
- crack frequency,
- crack orientation with respect to embedded reinforcing steel,
- crack geometry and crack depth.

They are discussed next.

2.3.1 Relationship between crack width and corrosion

Corrosion of reinforcement in concrete is a complex process and needs to be examined from different perspectives. (Schiessl, 1975) showed that carbon dioxide penetration through cracks depends on crack width and the same was believed to be true of chloride ingress (Concrete Society, 2015). There have been numerous studies on the relationship between crack width and reinforcement corrosion with the aim of determining critical crack widths, under defined conditions, below which there is a low risk of corrosion. It is clear that cracks allow relatively rapid ingress of harmful substances to steel reinforcing bars and will eventually make the surface of the steel susceptible to corrosion. However, it is questionable whether crack widths influence the subsequent rate of corrosion.

Nevertheless, crack width was thought by many researchers to be the main parameter influencing chloride penetration, and there have been numerous attempts to determine critical crack widths for given exposure conditions below which cracks can be ignored. However, either the critical values determined have been found to be so small that they would be difficult to achieve in practice, or the results were so variable because of differences in experimental setup, exposure time, concrete mix and quality, thus affecting transport properties of concrete, that it has been difficult to reach a satisfactory answer.

(Reis et al., 1965) carried out a review of 18 sources of recommendations on permissible crack widths and proposed that crack width should not exceed 0.15mm for exterior members under aggressive environments, and 0.25mm and 0.35mm for exterior and interior exposure conditions respectively under natural environments. These crack widths are very similar to the allowable values mentioned in (ACI 224, 2001) and (BS 5400-4, 1990). However, the results of some more recent experiments on the relationship between crack width and transport properties of concrete have suggested that these values may not in fact be reasonable as discussed below. Moreover, these experiments have yielded values of crack widths below which concrete transport properties are so close to sound concrete that the presence of cracks can be ignored.

A study by (Rodriguez, 2003), investigated the influence of cracks on chloride ingress. By using artificially cracked concrete specimens with crack sizes ranging from 0.08 to 0.68 mm, it has been concluded that there was no relationship between crack width or crack wall roughness and chloride penetration.

(Yoon & Schlangen, 2010) found the following critical values: 0.012mm for short and 0.05mm for long term exposures. The authors attributed the difference in values to autogenous healing of concrete.

(Djerbi et al., 2008) found that in the case of crack widths between 0.03 and 0.08mm there was a moderate increase in chloride diffusion coefficient which became almost constant when crack widths exceeded 0.08 mm. Thus, it was concluded that the allowable crack width in concrete structures should not exceed 0.08mm.

(Marsavina et al., 2009) tested specimens with artificial cracks 0.2 and 0.3mm wide and depths of between 5mm and 20mm. They found that chloride ion penetration increased with increasing crack depth. They concluded that crack depth had more pronounced influence than crack width on chloride ingress. Their results also showed that crack widths less than 0.1mm have no influence on chloride penetration.

A study by (Jang et al., 2011) indicated that diffusion coefficients do not increase with increasing crack widths up to the so-called "threshold crack width." The threshold crack width for diffusion was found to be around 55–80µm. Above this threshold value, diffusion coefficients increased with crack width.

In a review paper on chloride transport properties of cracked concrete by (C. Gu et al., 2015) it was found that this phenomena is influenced by several factors including concrete composition and loading condition. It was further concluded that crack geometry is the vital factor that influences the chloride transport process in the crack and cracked concrete. This should include information on the width, depth, tortuosity, connectivity and surface roughness of the crack.

Regarding the effect of crack width on the chloride transport process, a consensus has not been reached and the need for further research is indicated. According to (C. Gu et al., 2015), focus should be placed on the influences of tortuosity, connectivity and surface roughness of the crack on the chloride transport process in the crack and cracked concrete.

Regarding the relationship between crack width and corrosion rate, there has been progressive research over a long period of time and two schools of thought have emerged, namely:

- 1) Although cracks will shorten the time to corrosion, there is no significant influence of crack width on corrosion propagation (Francois & Maso, 1988; Mohammed et al., 2001; Otsuki et al., 2000; Schießl & Raupach, 1997)
- 2) Cracks influence both the initiation and propagation phases (Otieno, 2010; Pettersson et al., 1996; Suzuki et al., 1990).

In 1964 work done by Rehm and Moll on cracked concrete specimens suggested there was a linear relationship between crack width and corrosion degree. This was based

on the results obtained after the first and second years of testing. However, the results of long-term tests (4-10 years) showed there was no significant influence of crack width on the amount of corrosion (Schiessl, 1975). Furthermore, it has been claimed that there was no link between crack width and corrosion rate, as for corrosion reaction to proceed, oxygen should be accessible in cathodic area and that electrical resistance between cathode and anode are of a higher significance in controlling corrosion rate (Beeby 1978) and (Tuutti, 1982).

(Schießl & Raupach, 1997) found that there was an increase in mass loss after 24 weeks period when the width of crack was increased, however, this relationship was negligible when they repeated the test procedure after 2 years as can be seen from Figures 2.6a and b. These authors also commented that the thickness of concrete cover and concrete composition have a more significant impact on the corrosion process and that this issue cannot be solved simply by limiting crack width between 0.3 and 0.5mm.

Another long term observation of this problem made by (François et al., 2006) was that there is no correlation between crack width and corrosion rate for cracks less than 0.5mm wide. According to these authors the type of applied loading may be more important in terms of corrosion behaviour of reinforcement.

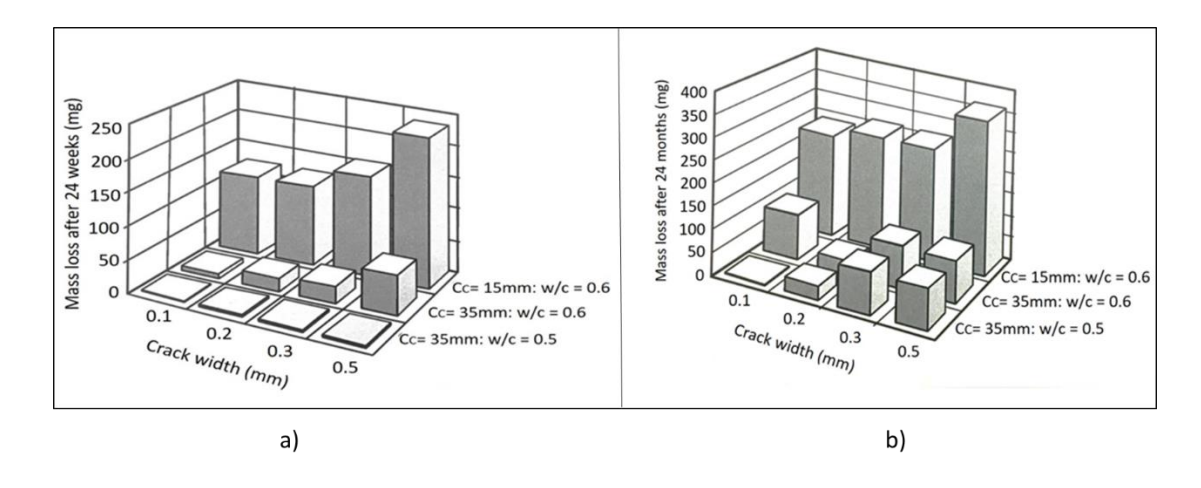


Fig. 2.6. Mass loss due to macrocell corrosion after test period of a) 24 weeks and b) 2 years (Schießl & Raupach, 1997).

In the work by (Otsuki et al., 2000) it was reported that the rate of corrosion is higher in cracked concrete due to increased availability of oxygen and water.

(Mohammed et al., 2001) tested single crack specimens with the following widths: 0.1; 0.3; and 0.7mm and the following w/c ratios: 0.3; 0.5; and 0.7. They concluded that at the beginning of testing (weeks 1-2), specimens with wider cracks experienced higher current densities, however after some time this changed and became less obvious. The researchers observed a stronger link between increased w/c ratio and corrosion rate rather than crack width and corrosion rate. Calculated mass loss values with respect to w/c ratio and crack width are shown in Table 2.1.

(Scott & Alexander, 2007) tested specimens made of various binder types with two different crack width (0.2 and 0.7mm) and two different concrete covers (20 and 40mm). They found that increased crack width cause increased corrosion rate. However, they also found that the corrosion rate decreased when a higher concrete cover was used.

(Otieno, 2010)using a similar test setup but different crack widths (0.4 and 0.7mm) observed that wider cracks lead to higher corrosion rates. They also noticed that deeper concrete covers resulted in reduced corrosion rates. Thus, both groups of researchers admitted a higher corrosion rate with wider cracks and a decrease in the amount of corrosion when deeper covers were provided. They proposed that the risk of corrosion should be defined in terms of concrete cover depth to surface crack width ratio. This approach seemed to be reasonable parameter to determine the risk of crack induced corrosion, however, ratio of crack width to cover depth is thought to be better (Concrete Society, 2015).

Table 2.1. Weight loss due to corrosion in grams (Mohammed et al., 2001)

W/C	Crack width (mm)		
	0.1	0.3	0.7
0.3	-	0.1775	-
0.5	0.265	0.373	0.3895
0.7	-	0.9765	-

To summarise, the impact of crack width on corrosion rate has still not been clarified, and further research work is needed.

2.3.2 Crack frequency and corrosion

A number of workers have shown that crack spacing (i.e. number of cracks per metre length or crack frequency) is another important parameter influencing crack-induced corrosion. (Schiessl, 1975) performed experimental work on cracked specimens and reported corrosion was independent of crack width as the distribution of corrosion depths was the same irrespective of crack width. Additionally, (Schießl & Raupach, 1997) aiming to clarify the corrosion mechanism and dominant influencing variables, tested cracked reinforced concrete beams. Using results and a simplified mathematical model, they calculated the effect of crack distance on corrosion rate. They found that by increasing the distance between cracks from 100mm to 200mm it is possible to reduce corrosion rate.

(Suzuki et al., 1990) looked at the corrosion process in specimens with a single crack and specimens with multiple cracks. In the latter, the cracks were induced by four-point loading which resembles natural cracking in concrete members such as beams and slabs. They found that specimens with single crack all showed corrosion, however in specimens with multiple cracks, corrosion occurred at the widest crack first. Half-cell potential readings at major cracks were more negative compared to narrower cracks adjacent. They assumed that major cracks delayed or suppressed the corrosion rate at smaller cracks as they experienced less corrosion.

In a study completed by (Arya & Ofori-Darko, 1995) the effect of crack frequency on corrosion rate was investigated. Specimens 1.36m long containing 0, 1, 4, 8, 12, 16 and 20 parallel sided cracks with constant concrete cover (42mm), crack depth (40mm) and w/c ratio of 0.65 were sprayed with a chloride solution and cumulative weight losses due to corrosion of embedded reinforcing bars were measured. It was reported that increasing the number of cracks lead to a higher corrosion rate, except for a specimen containing 20 cracks where self-healing of some cracks took place. Their results are shown in Figure 2.7. Similar to Schiessl's findings, these authors observed that the rate of corrosion at cracks was not uniform, although all the crack widths were identical. This is another proof of absence of a strong relationship between crack width and corrosion.

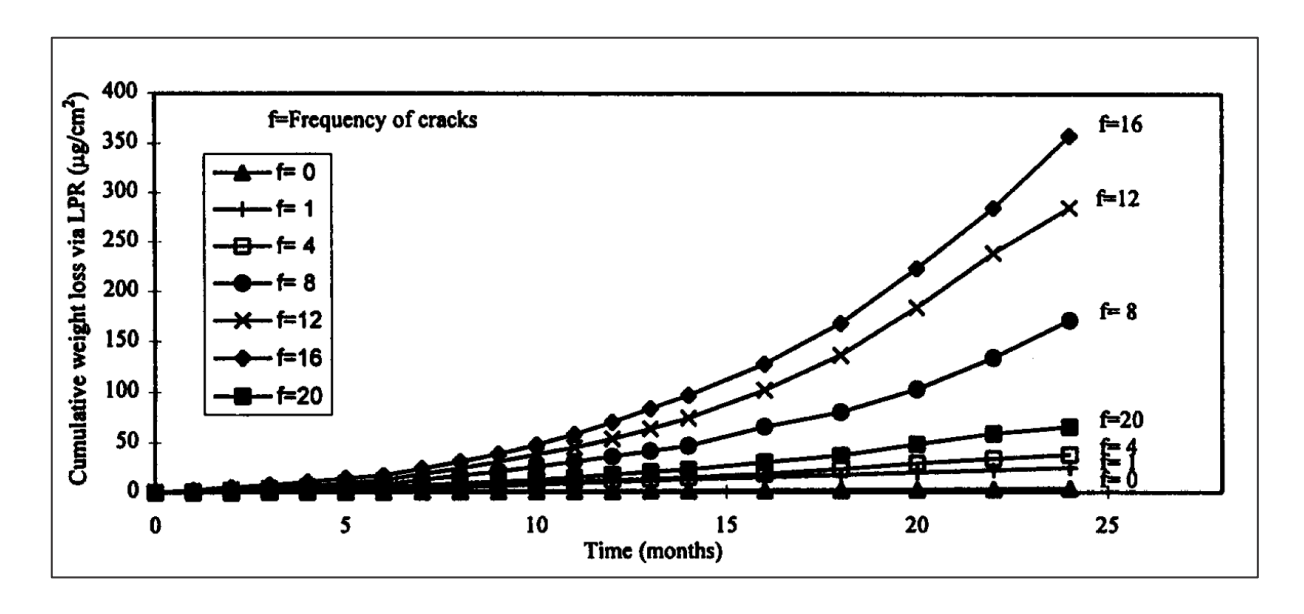


Fig. 2.7. Effect of crack frequency on cumulative weight loss due to corrosion – By linear polarization resistance (LPR) measurements (Arya & Ofori-Darko, 1995).

A relatively recent study by (Mohammed et al., 2001), looked at the effect of crack width and bar type on corrosion rate of reinforcement. These authors tested specimens with both single and multiple cracks. Three different crack widths were created in specimens with single crack: 0.1; 0.3; and 0.5mm and three w/c ratios: 0.3; 0.5; and 0.7. The specimens with multiple cracks were made of concrete of 0.5 and 0.7 water cement ratio and were cracked by applying loading of 5500 and 4500kg respectively. As a result of using deformed and plain reinforcing bars, they achieved a greater number of cracks in specimens with deformed bars and a lower number in specimens reinforced with plain bars. The crack patterns achieved can be seen in Figure 2.8. The cracks in specimens with deformed bar were narrower than the ones achieved in specimens reinforced with plain bars.

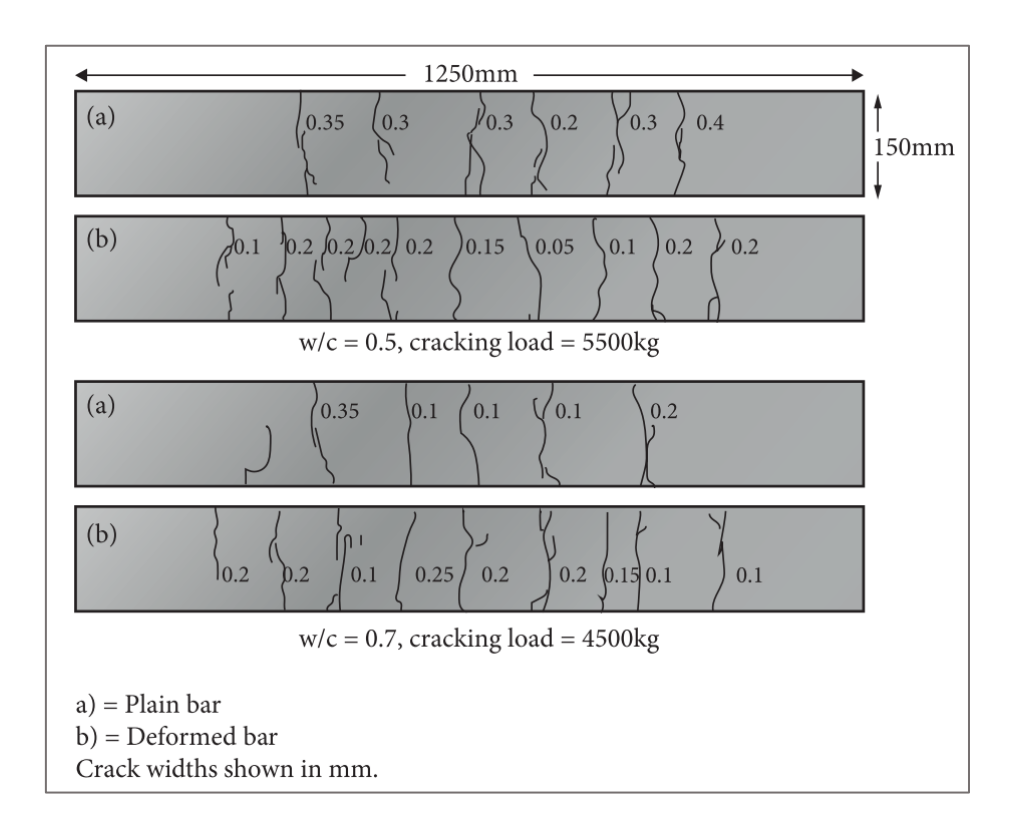


Fig. 2.8. Cracks patterns in beams reinforced with plain and deformed bars (Mohammed et al., 2001).

However, specimens with deformed bar had greater oxygen permeability and higher corrosion rates compared to specimens with plain bars. They concluded that the impact of crack width was noticeable only at the very beginning of the experiment. Water cement ratio was more significant than crack width and specimens with a greater number of cracks corroded at higher rates. This was thought to be due to the cathodic regions which occur mainly in the crack-free regions of concrete and extend over relatively large distances. The oxygen supply to these regions may be limited due to the concrete cover, and hence the subsequent rate of corrosion will be small. If, on the other hand, the same member contains a larger number of cracks, albeit of narrower widths, the cracks will not only increase the oxygen supply to the steel surface but also reduce the distance between anodes and cathodes, thereby resulting in a higher combined amount of corrosion.

Although this work provides good insight to the influence of crack frequency to reinforcement corrosion, it would be interesting to compare the behaviour of two specimens with the same reinforcement type and different number of cracks being as steel-concrete interface will be different when deformed rebars are used.

2.3.3 Concrete cover

Several workers including (Lea & Watkins, 1960) and (Houston et al., 1972) noted a reduction in the amount of corrosion damage to specimens when the thickness of concrete cover to embedded bars was increased (Table 2.2).

Interestingly, this finding is consistent with the results of the experiments on crack frequency described above. Here it was found that increasing the frequency (number) of cracks increased the total amount of corrosion damage. Increasing the frequency is the same as decreasing crack spacing. Studies on reinforced concrete beams show that crack spacing is a function of both the cover to the reinforcement and the bar diameter to steel percentage ratio (ϕ/ρ). However, the cover is the most important variable controlling crack spacing and the influence of ϕ/ρ in flexural situations is usually secondary. Increasing the cover therefore increases crack spacing which results in fewer (albeit wider) cracks. Based on the finding of the crack frequency experiments this should reduce the amount of corrosion damage as indeed was found to be the case by the authors cited in Table 2.2.

It is worth noting that restricting crack widths to permissible values effectively prevents engineers specifying deeper covers to steel bars despite the fact that the benefits of deeper covers are not disputed whereas the merits of controlling crack widths is still controversial.

Table 2.2. Influence of cover, water/cement ratio and cement content on corrosion (Beeby, 1983)

Investigators	Cement content (kg/m³)	Water/cement ratio	Cover (mm)	Measure of corrosion
(Dalamatal 4077)		0.66	12 37	25 5
(Baker et al., 1977)	296	0.71	12 37	64 12
	593	0.37	50 25	0 25
(Lea & Watkins, 1960)	356	0.55	50 25	10 82
,	214	0.96	50 25	75 100
	558	0.49	50 38 25 20	0 22 44 49
(Houston et al., 1972)	446	0.55	25 20	60 88
	335	0.62	50 38 25 20	75 98 100 100

2.3.4 Concrete and steel properties

Corrosion of reinforcing steel occurs by an electrochemical process and the quality of concrete plays an important role in the manner in which corrosion progresses. Although cracks accelerate the penetration of aggressive agents into concrete cover, thereby rapidly initiating corrosion, corrosion propagation is a function of the cathodic reaction. The cathodic areas are normally situated between cracks and oxygen availability is influenced by concrete permeability, and in turn by the type of binder used. It has been generally accepted that using supplementary cementitious materials such as blends of Portland cement with ground granulated blast furnace slag, fly ash and silica fume lead to production of concretes with higher resistance to movement of chloride ions. The pore structure of blended cement concretes is also preferable for slowing down the rate of corrosion propagation.

2.3.5 Binder type

Study by (Konin et al., 1998) looked at the effect of cement blends with addition of silica fume in cracked concrete specimens. They found a decrease in chloride ingress with specimens containing silica fume. According to these authors concrete composition is of major importance to chloride penetration.

According to (Otieno et al., 2012) there is a strong link between the concrete's transport properties and corrosion propagation in cracked concrete.

Assuming that diffusion is one of the main mechanisms responsible for chloride ingress into concrete, (Jang et al., 2011) investigated the chloride diffusion coefficient of cracked concrete of varying strengths and addition of fly ash. It can be seen from Fig. 2.9 that the chloride diffusion coefficient decreases with increasing concrete strength. The figure also shows that 20% replacement with FA reduced the chloride diffusion coefficient still further. This author also reported the chloride diffusion trends for specimens with crack width ranging between 110-130µm were similar to that of uncracked concrete. This led the author to conclude that the presence of cracks within specified limits does not alter the beneficial effect of fly ash on transport properties of concrete.

(Scott & Alexander, 2007) investigated the influence of binder type on corrosion rate. They used seven different binder types comprised of pure Portland cement and its blends with silica fume, fly ash and ground granulated blast furnace slags at various replacement levels.

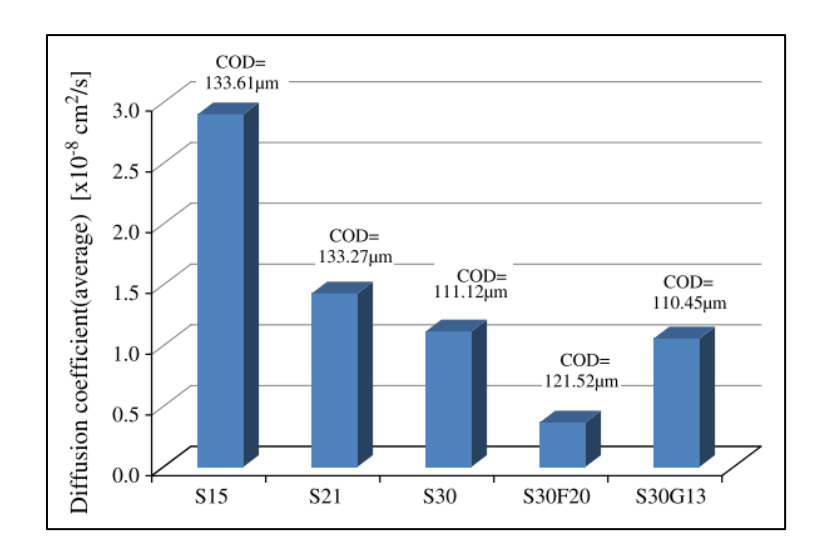


Fig. 2.9. Comparison of diffusion coefficients according to concrete strength (S15, S21, and S30), addition of fly ash (S30F20) and maximum aggregate size (S30G13) (Jang et al., 2011).

All mixes had a water/cement ratio of 0.58. All specimens contained a single crack either 0.2mm or 0.7mm wide and the thickness of the concrete cover was either 20mm or 40mm. The specimens were exposed to wetting (3 days) with 5% sodium chloride solution and drying (4 days) cycles under 30° C. From their results, it can be seen that specimens with blended cements experienced considerably smaller rates of corrosion compared to similar specimens made of 100% Portland cement (Figure 2.10).

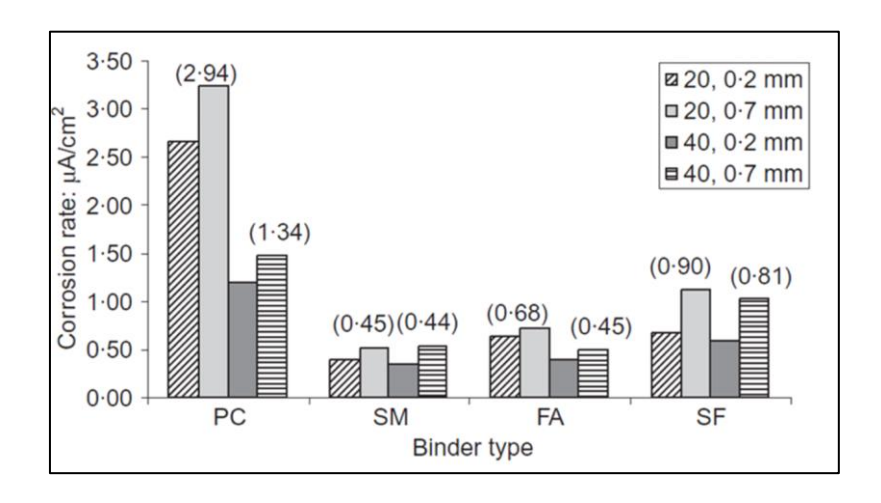


Fig. 2.10. Impact of binder type on corrosion rate depending on concrete cover and crack width (Scott & Alexander, 2007).

(Polder, 1996) and (Whiting et al.,2003) reported that the use of supplementary cementitious materials results in concrete mixes with high resistivity and lower

permeability which explains their regular use in the aggressive environment for preventing concrete deterioration. A significant increase in resistivity of FA blended concretes (Table 2.3.) has been shown to occur in the long-term according to research conducted by (Claus et al., 2007). The resistivities of the mixes tested by (Scott & Alexander, 2007) are shown in Figure 2.11.

Table 2.3. Average concrete resistivities as a function of binder composition, Ω m (Claus et al., 2007).

Binder comp.	All beams initially			All beams after 8 years		
Billaci comp.	Pos. a)	Pos. b)	Pos. c)	Pos. a)	Pos. b)	Pos. c)
FA blended	216	201	173	2447	1955	1193
CSF blended	323	288	295	729	630	483

Note, Pos a),b) and c) corresponds to exposure conditions such as: air, tidal and submerged respectively.

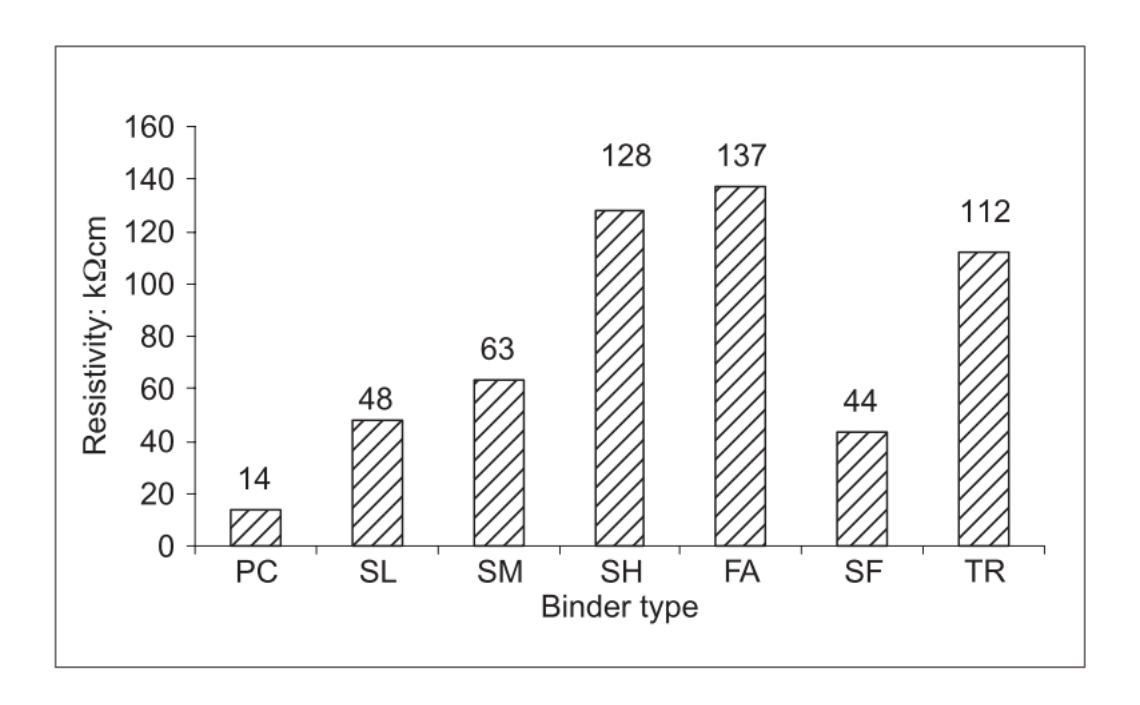


Fig. 2.11. Average resistivity values for 40mm cover specimens from weeks 32 to 56 (weeks 32 to 46 for SL and SH), (Scott & Alexander, 2007)

The authors conclude that the use of supplementary cementitious materials increase the resistivity of concrete and their results show at least a tripling of the resistivity can occur in specimen made of blended cements rather than pure Portland cement. However, these authors warn that the use of high resistivity concrete mixes alone may not be sufficient in decreasing corrosion rates. Other factors such as oxygen availability and cover depth should also be taken into account. This is attributable to the results obtained for specimens made of fly ash and silica fume. Despite the fact that fly ash specimens had twice the resistivity of the silica fume specimens, both mixes experienced similar corrosion rates (Figure 2.11).

Although the above-mentioned results indicate the benefits of using blended types of cement in corrosion protection it should be remembered that, the experimental results discussed are based on tests on specimens with transverse cracks. However, the results of tests on specimens with coincident cracks show that there may be no benefits of using blended cements (Poursaee & Hansson, 2008) and (Balakumaran et al., 2018) or their use might even lead to higher rates of corrosion compared to pure Portland cement mixes (Stillwell, 1988) as discussed in Chapter 3.

2.3.6 Water-binder ratio and cement content

Water-binder ratio is another factor influencing chloride penetration both in sound and cracked concrete. Higher water-binder ratios lead to permeable concrete thus, faster rates of corrosion of reinforcement. The impact of water-binder ratio on the corrosion process of cracked concrete has been investigated by many authors, usually in conjunction with cement content.

(Win et al., 2004) carried out a detailed study on the penetration profile of chloride ions through and around a crack in reinforced concrete structures. They also looked at the effect of a number of factors influencing corrosion rate such as water to cement ratio (w/c= 0.25; 0.45; 0.65), exposed direction, single and multicracks, crack width, cover thickness and NaCl solution concentration. Higher water-cement ratio led to increased chloride penetration both in the exposure surface and around the cracks. They concluded that transportation of chloride ion was strongly influenced by the bulk movement of the solution inside the concrete and this they believed would have a greater impact than diffusion on chloride penetration. These authors used Portland cement in their work and more research is needed using different binder types.

(Schießl & Raupach, 1997) reported that water-binder ratio influences corrosion mass loss in the crack zone. These authors further found that this effect was more

pronounced at the beginning of the experiment (the first 24 weeks) but became less obvious after two years of exposure. Other studies by (Djerbi et al., 2008; Konin et al., 1998; Otieno et al., 2012; Otieno, 2010) have also shown corrosion rate is higher in specimens with increased water-binder ratio.

Work by (Marsavina et al., 2009) and (Audenaert, 2009) found that an increase in cement content from 300 to 400kg/m³ at constant water-cement ratio resulted in decreased chloride penetration depth in the vicinity of the crack. Surprisingly, (Wassermann et al., 2009) reported that total water absorption, capillary absorption and chloride ingress reduced with reducing cement content for a given water/cement ratio. In such case cement content might be the prevailing factor according to results by (Baker et al., 1977), where water-cement ratio was reduced from 0.66 to 0.71 keeping cement content constant, a significant difference was found in the percentage of rusted surface area. Their results are shown in Table 2.2 together with some other author's results for comparison.

2.3.7 Type of rebar

Properties of reinforcing bars such as composition and surface finish on corrosion have been studied by (Ofori-Darko, 1998). The influence of steel composition on corrosion process can be seen from the results obtained by (Tremper, 1947). He investigated the effect of three different bar types on corrosion length of cracked specimens, namely: 16 gauge annealed wire, 7 gauge cold-drawn wire, and 6.3 mm square deformed bars. His findings are shown in Table 4. Here it can be seen that steel type has a significant effect on corrosion length.

Table 2.4. Effect of bar type and crack width on corrosion length (Beeby, 1978).

Bar type			Crack width mm				
Bai type		0.13	0.25	0.51	1.27	Mean	
16 gauge annealed wire	Average	5.60	7.40	8.60	9.90	7.90	
7 gauge cold-drawn wire	corroded	10.40	13.50	9.40	16.50	12.50	
6.3mm square deformed bar	length mm	11.70	17.80	20.60	17.20	16.80	

The early studies on the impact of surface finish of rebar on corrosion rate found that plain rebars experience higher corrosion than deformed bars (Schießl & Martin, 1969). It was thought that this was attributable to the fact that deformed bars have a better bond at the concrete steel interface, thus minimising the length of the slip zone. However (Goto & Otsuka, 1971) shed light on the development of cracks in concrete around steel reinforcement. He reported on the formation of internal cracks along the rebar when deformed steel is used (Figure 2.12), and they enhance further corrosion process allowing oxygen access to the cathodic area. Additionally, more recent studies confirmed that deformed bars lead to higher corrosion rates. Such results can be observed from work done by (Mohammed et al., 2001) and (Beeby & Scott, 2005).

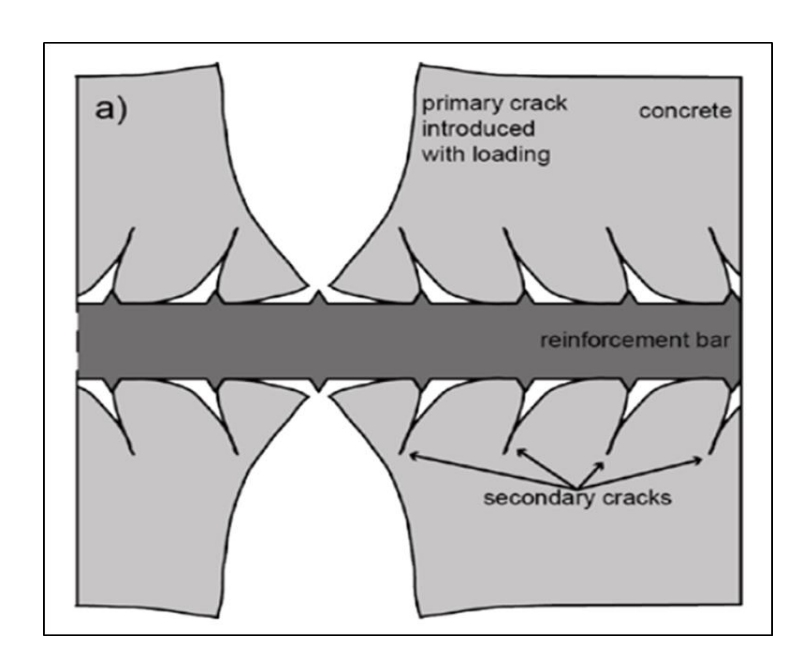


Fig. 2.12. Steel-concrete interface after formation of the internal cracks (Käthler et al., 2017).

On the other hand, more recent study by (Steen et al., 2019) on the effect of bond behavior of corroded and non-corroded rebars with ribbed and smooth finishes concluded that ribbed bars had a higher bond strength compared to smooth ones in both corroded and non-corroded samples. This is attributable to the formation of a mechanical interlock between rib pattern and concrete and this strong bond remained till the formation of rust-induced cracks in the rebar concrete interface. Whereas the bond between smooth rebar and concrete was formed due to chemical adhesion only between the bar and cement paste interface. The results of the authors are in a good agreement with other studies such as (Fang et al., 2004, 2006).

Based on the literature on the effect of reinforcement finish on corrosion of bar, no consensus has been reached and more research is needed to confirm above mentioned findings as research on smooth bars is scarce.

2.3.8 Crack orientation

This usually refers to the orientation of cracks with respect to reinforcing bars but this is not always the case. Two possibilities exist: (1) Longitudinal cracks i.e. cracks that occur parallel to the main reinforcement and (2) Transverse cracks i.e. cracks which occur at right angles to the main rebar. According to (Concrete Society, 2015) this classification is not very clear as reinforcement is usually present in two directions at right angles in practically all concrete members. In two way spanning slabs both sets of bars are considered to be main rebar. Therefore it would be better to use the terms: coincident cracks which refers to cracks which follow the line of reinforcement irrespective of function i.e. main steel, secondary steel or links and intersecting cracks i.e. crack that cross reinforcing bars.

2.3.8.1 Intersecting cracks

As discussed earlier, intersecting cracks normally form perpendicular to the reinforcement as shown in Figure 2.13. Thus, although they may shorten the time for corrosion onset by enabling aggressive substances to the depth of the concrete cover, they are relatively less dangerous as they may not significantly affect the corrosion propagation process. The propagation phase of corrosion is dependent on oxygen and moisture availability in cathodic areas which are located at crack free parts of concrete.

There are many factors influencing corrosion propagation such as crack properties, concrete and steel properties, exposure conditions and chloride concentration. Due to the complexity of this process and a number of influencing variables, effect of transverse cracks on corrosion rate is still an open question as previously discussed.

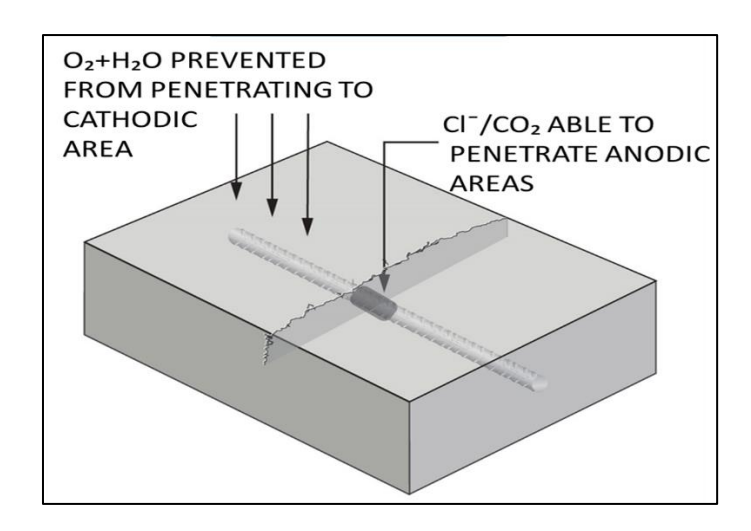


Fig. 2.13. Transverse cracks and corrosion (Concrete Society, 2015)

2.3.8.2 Coincident cracks

Coincident cracks are believed to present a greater risk of corrosion than intersecting cracks because they can accelerate both corrosion initiation as well as corrosion propagation. The passive film on the surface of reinforcing bars may be broken at several locations in the presence of coincident cracks. Oxygen and moisture are also readily transmitted to the cathodic sites through the same crack (Figure 2.14). Many authors have commented on the serious risk to corrosion due to the presence of coincident cracks and that all possible means should be used to prevent their occurrence (Alarab et al., 2020; Arya & Ofori-Darko, 1995; Beeby, 1978; Bentur, 1997; Blagovic', 2016; Wilkins & Stillwell, 1986). However, beyond this, there is very little known about coincident cracks. Codes and standards on structural concrete design mostly focus on flexural cracks and the risk of corrosion to longitudinal bars. Yet, given that reinforcement is usually present in two directions at right angles in virtually all reinforced concrete members, the chances of flexural cracks coinciding with transverse reinforcement must be quite high. The following chapter presents a state of the art on coincident cracks.

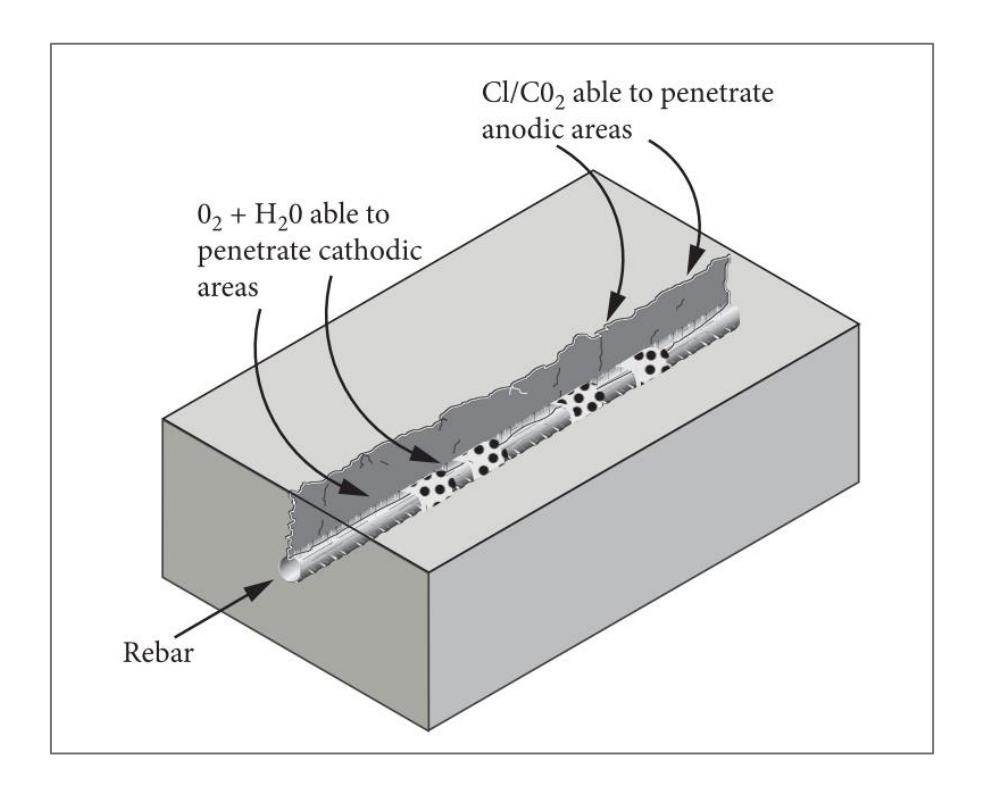


Fig. 2.14. Corrosion process in coincident crack (BRE, 1993)

Based on the information presented in this chapter, the following list of key points were considered to narrow down the research objectives and test campaign:

- Importance of chloride induced corrosion;
- Effect of crack orientation with respect to the reinforcement;
- Effect of crack depth on the development and rate of corrosion process;
- Effect of concrete cover to the reinforcement;
- Effect of binder type on the corrosion process of reinforcement;

Chapter 3 Causes, consequences and existing research on coincident cracks

The aim of this chapter to examine the principal causes and nature of coincident cracking in concrete structures. It also considers their significance as well as describes the existing research which has been carried out on coincident cracks.

3.1 Causes of coincident cracking

A literature review on types of cracks in concrete has revealed that coincident cracks can arise due to a number of causes including:

- Plastic settlement
- Plastic shrinkage
- Early thermal shrinkage
- Drying shrinkage
- · Direct loading.

Mechanisms such as frost attack and alkali-silica/aggregate reaction will give rise to crazing or map cracking. No doubt some of the resulting cracks will be coincident with embedded reinforcing bars but these mechanisms are excluded from the discussion. Rather, the work focuses on the causes bullet pointed above and in each case briefly describes the mechanisms involved and comments on the affected reinforcement.

3.1.1 Plastic settlement

Plastic settlement occurs when heavier solid particles in plastic concrete settle under gravity and drive clear "bleed" water to the concrete surface. Cracks form if settlement is relatively high and is restrained from occurring due to, for example, reinforcement which is near the top of the member. Coring can reveal the presence of crescent shaped voids under steel reinforcing bars as shown in Figure 4.1 or, in extreme cases, horizontal delamination. Cracking over the line of the reinforcement and the presence of voids under the reinforcement can act as channels for chloride and/or carbon

dioxide ingress, leading to depassivation and hence corrosion. Work by (Dakhil & Cady, 1975) shows that the tendency for plastic settlement cracking is related to concrete cover, bar diameter and the concrete slump. This tendency increases with decreasing cover. It also increases with increasing bar diameter and higher slump concrete but to a considerably lower degree than cover. Plastic settlement cracks often form in deep sections and will expose the top layer of reinforcement to corrosion (Concrete Society, 2010). In walls this will be the U-bars whereas in slabs this could include longitudinal bars and the tops of links. In thin slabs both the top and bottom layers of reinforcement may be affected (Ramey et al., 1997).

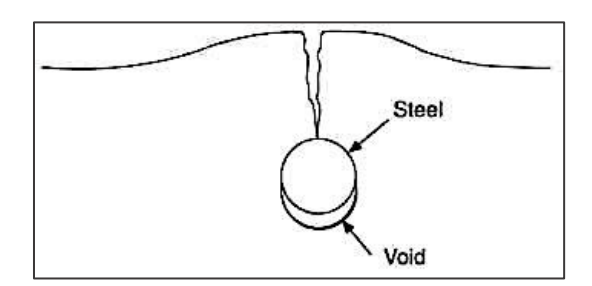


Fig. 3.1 Plastic settlement cracks (Concrete Society, 2010)

3.1.2 Plastic shrinkage

When evaporation exceeds the rate of bleeding, plastic concrete begins to dry out and capillary tensile forces result in shrinkage of the concrete. This occurs when the tensile strain capacity of plastic concrete is least and cracks can result. The cracks form within hours of placement but may not be noticeable until later. Plastic shrinkage cracks can typically be 2-3mm wide but their width rapidly decreases away from the surface. However, over time they can deepen and penetrate through the full depth of the slab due to restrained drying shrinkage.



Fig. 3.2 Plastic shrinkage cracks follow the pattern of the reinforcement (Concrete Society, 2010).

Plastic shrinkage cracks can follow the line of both the longitudinal and transverse reinforcing bars (CEB, 1985; Concrete Society, 2010; Richardson Mark, 2002). They most commonly occur in slabs exposed to wind and sun and can potentially expose top and bottom layers of reinforcing bars to corrosion illustrated in Figure 3.2.

3.1.3 Early thermal shrinkage

This type of cracking is relatively common and is associated with the heat released during cement hydration. During this phase the rate of heat development can exceed the rate of heat loss, resulting in an increase in the concrete temperature. When hydration slows the concrete cools and contracts. But if it is restrained from doing so, either internally or externally, cracks may develop.

Cracks caused by early thermal contraction will normally occur within the first two weeks of placement. Elements most likely to experience early thermal contraction cracking are cantilever walls used in, for example, retaining structures, bridge abutments and basements. A survey of 200 highway bridges in the UK, for instance, revealed that the commonest form of cracking was vertical cracks, which occurred on the face of abutments, wingwalls and wide piers (Wallbank, 1989). It was further noted that these cracks varied in width, length and spacing, but appeared on both full height elements and on exposed parts of buried abutments. The fact that the cracks were mostly vertical is probably attributable to the vertical reinforcement which is normally placed in front of transverse bars and act as a stress raiser. Thus, it will be appreciated

that early thermal cracking can also give rise to coincident cracks, thereby increasing the risk of corrosion of embedded reinforcing bars.

3.1.4 Long-term drying shrinkage

Drying shrinkage cracks occur when concrete contracts as it loses moisture during its early life. Drying shrinkage cracks are often confused with early thermal contraction cracks and are similar in that the cracking occurs due to restraint such as the friction between the concrete bridge deck and supporting girders (Krauss & Rogalla, 1996).

(Concrete Society, 2010) suggests that drying shrinkage occurs relatively infrequently in structures in the UK. But this is contradicted by studies on bridge deck cracking carried out in the US and by implication bridge structures in the UK which are reported to exhibit a similar pattern of cracking (Wallbank, 1989).

Based on a survey of all US department of transportation agencies it was found that more than 100,000 bridges in the US, some 50% of the total surveyed, suffered from cracks perpendicular to the direction of deck girders, referred to as "transverse cracks" (McDonald et al., 1995). There was a greater incidence of transverse cracking on bridge decks with steel girder superstructures rather than concrete superstructures (Krauss & Rogalla, 1996). Transverse cracking was also found to increase with span length and the use of continuous construction (NCHRP Synthesis 333., 2004). The cracks spaced 1m-3m apart typically occurred before the concrete was one month old and were full depth. By examining core samples (Purvis et al., 1995) further found that the crack position predominantly coincided with transverse reinforcement, which acts as a stress raiser.

In an effort to identify the possible cause of these cracks a team of researchers in Indiana, USA, monitored newly constructed bridges using strain gauges and thermocouples. They found that the predominant cause was restrained drying shrinkage, which was subsequently confirmed by laboratory tests (Frosch, 2003).

(Miller & Darwin, 2000) reported chloride levels in bridge decks at both cracked and uncracked locations. Their results showed significantly higher chloride contents at crack locations. At the level of the transverse reinforcement, the chloride content exceeded the threshold level for corrosion in as little as 1,000 days (NCHRP Synthesis 333., 2004). It was further noted that because the cracks are full depth, the bottom

layer of reinforcement as well as supporting beams and the substructure were also at risk of corrosion.

3.1.5 Direct loading

The above are all examples of non-structural cracks. Normal load effects such as bending, shear, torsion, etc, applied to sections can give rise to structural cracks. This category of crack, in particular cracks due to bending, has been the most extensively studied by researchers. The fundamental principle involved in governing such cracking is now well established and has been used to develop the crack width and spacing equations found in national Codes and Standards such as ACI 318 and Eurocode 2. The investigations on bending behaviour have further showed that direct loading can give rise to two types of cracks: flexural and bond, which present a significant risk of corrosion as discussed next.

3.1.6 Flexural cracks

Beams and slabs subject to bending due to transverse loading will experience a series of distributed flexural cracks as shown in Figure 3.3. These cracks will be perpendicular to the direction of longitudinal bars and being as the cracks extend beyond the cover no doubt will increase the risk of corrosion of these bars. If the flexural cracks coincide with any transverse reinforcement in the member i.e. distribution steel in the case of one-way spanning slabs, main steel in the case of two-way spanning slabs or stirrups in the case of beams, they will also expose transverse bars to corrosion. Indeed, test evidence suggests that transverse reinforcement frequently act as crack initiators. In some circumstances it has been found that this effect is so strong that the distribution of cracking is completely dominated by the arrangement of transverse bars (CEB, 1985).

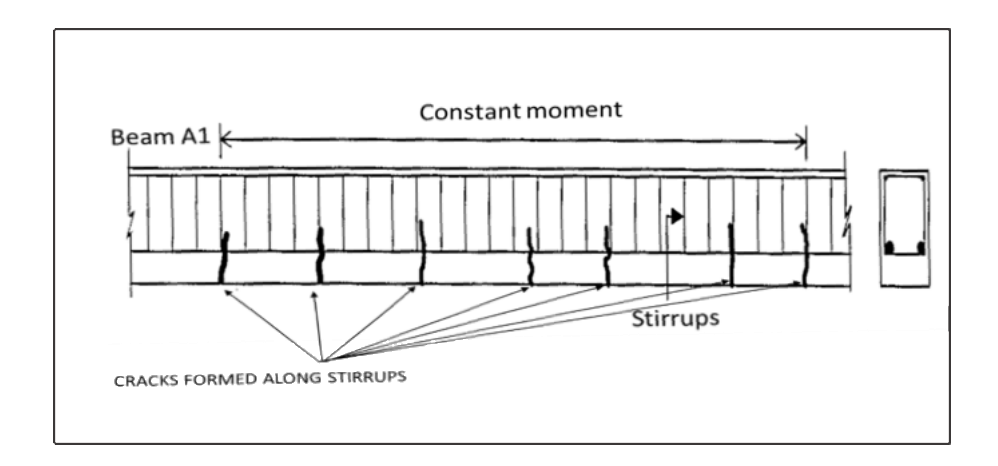


Fig. 3.3 Example of flexural cracks coincident with stirrups (CEB, 1985).

For example, (Caldentey et al., 2013) who investigated among other aspects the effect of cover and stirrup spacing on the position of flexural cracks found that stirrups tended to act as crack inducers. This effect was found to be strongest in beams with smaller covers of the order of 20mm. The beams with 70mm cover also showed in a general manner a tendency for cracks to coincide with the position of stirrups albeit in a less homogeneous way than in the case of beams with 20mm cover.

(François & Arliguie, 1998) tested beams 150mm wide × 280 mm deep × 3m long with two arrangements of reinforcing bars. Type A beams were reinforced with 2, 16mm diameter longitudinal bars and 8mm diameter stirrups at 220mm centres. The cover to the stirrups was 40mm. Type B beams were reinforced with 2, 12mm diameter longitudinal bars and 6mm diameter stirrups also at 220mm centres. The cover to stirrups in this case was 10mm. Half of both types of beams were loaded in three point bending to 1350 daN.m (Deca Newton Meter) and the remaining halves similarly loaded to 2120 daN.m. In the case of Type A beams it was found that in the central area of the beam each crack occurred in front of a stirrup. Moreover, it was found that increasing the load did not result in an increase in crack density since the cracks remained associated with a stirrup. Type B beams, however, experienced an increase in crack density, with a crack between stirrups in addition to the cracks located at each stirrup.

(Micallef & Vollum, 2017) who carried out four-point bending tests on concrete beams 450mm wide \times 250 mm deep \times 4250mm long reinforced with longitudinal bars in the top and bottom faces with a cover of 30mm and 10mm diameter stirrups at 200mm

centres in the constant moment zone reported that transverse cracking developed over and midway between stirrups.

Given that stirrups are placed on the outside face of the primary bars in beams and that they are, in general, manufactured using smaller diameter bars (Shehab et al., 2020), it would appear that stirrups are manifestly at higher risk of corrosion in chloriderich environments. This is probably more so in the case of structures designed to Eurocode 2 which permits a surface crack width of 0.3mm under quasi permanent loading.

3.1.7 Bond cracks

Bending due to direct loading also gives rise to shear/bond stresses acting parallel to longitudinal reinforcing bars at the interface between the bar and the concrete, which can produce cracking along the line of reinforcing bars (Kong & Evans, 1987). These cracks, referred to as bond cracks shown in Figure 3.4, frequently start from a flexural crack and are likely to be quite narrow, perhaps less than 0.1mm wide, under service loading (CEB, 1982). Nevertheless, bond cracks are capable of transmitting via the flexural cracks aggressive substances from the service environment to the surface of longitudinal bars, thereby promoting corrosion. Whereas the results of earlier studies suggested that corrosion of longitudinal bars was limited to around 3 bar diameters away from an intersecting crack (Beeby, 1978), presumably because of the existence of bond cracks, the more recent studies suggest corrosion can occur as far away as 13 bar diameters (Krauss & Rogalla, 1996).

Further evidence that bond cracks can damage the quality of the steel-concrete layer and promote corrosion of longitudinal reinforcing bars can be found in work presented by (François & Arliguie, 1998). Details of the beams used in their work was provided earlier. The beams were cracked by subjecting the specimens to two levels of three point loading and exposure to a chloride environment over a 12-year period. Whereas the results from type B beams are somewhat confusing the results from the type A beams show that they experienced longitudinal cracks which began at the intersection of the flexural crack and the tensile reinforcement. This was more pronounced in the case of beams subjected to the higher level of loading and was undoubtedly due to corrosion of the underlying reinforcing bars. These authors attributed the corrosion to three factors, namely (a) the presence of flexural cracks, (b) bond cracks and (c) poor

quality of the steel-concrete interface due to bleeding of concrete, given that these beams were cast upside down.

As noted above (BS EN 206, 2019) permits a crack width of 0.3mm under quasi permanent loading whereas its UK predecessor (BS8110, 1997) limited crack widths to 0.3mm under working load. This change in code provision is likely to increase the length of bond cracks and hence the length of bar which is susceptible to corrosion.

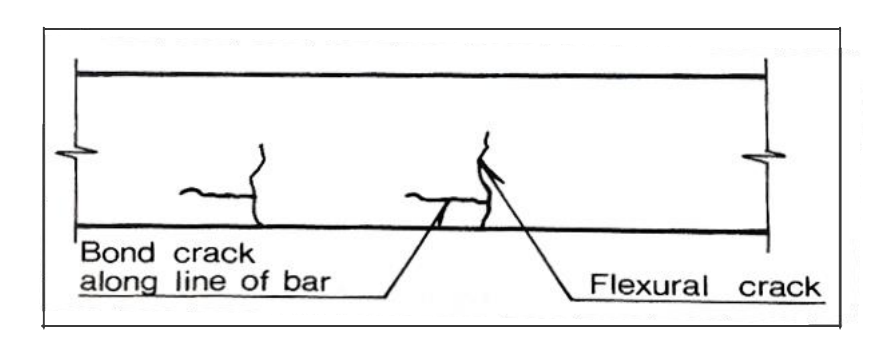


Fig. 3.4 Excessive bond stress (CEB, 1982).

3.2 Consequences

From the foregoing, it will be appreciated that coincident cracks can arise in a range of elements including beams, slabs, piers and walls. In beams and slabs both the top and bottom layers of reinforcing bars in both directions as well as any shear reinforcement that may be present can experience coincident cracking. Similarly, the reinforcement in the front face and tops of bridge abutment and wing walls can also suffer coincident cracking (Wallbank, 1989). It is not surprising therefore that in aggressive environments such as the coastal areas of the Arabian Gulf characterised by severe ground and ambient salinity and high temperatures/humidity or cold climates such as the USA, Canada and Europe where deicing salts are used on highways that corrosion of these elements has been found within a few years of construction.

Investigations on the effects of corrosion of concrete elements such as beams and slabs have been ongoing for some years. The results are being used to develop models for predicting both the present and future strength of deteriorated concrete structures (Hanjari et al., 2011). The availability of these models would enable bridge engineers, for example, to prioritize repair and maintenance work, which is imperative in many countries given the number of structures in need of treatment and the limited amount of annual funding available for this activity (Vassie & Arya, 2006). Most of the

information on this subject has been amassed by testing specimens subjected to accelerated corrosion using impressed currents. Unlike natural exposures, this method results in uniform corrosion of steel reinforcing bars and the accelerated rate of corrosion may alter the nature of the corrosion products formed (Williamson & Clark, 2006). Nevertheless, the trends reported appear to be reasonable. Thus, it has been found that corrosion of steel reinforcing bars results in cracks in the concrete above the bar. Corrosion of closely spaced stirrups can give rise to spalling of the concrete (Higgins & Farrow, 2006; Tuutti, 1982). Corrosion of longitudinal reinforcement can result in a reduction in the ultimate strength as well as the stiffness of flexural members (Almusallam et al., 1996). The resulting higher deflections may lead to serviceability problems (Azad et al., 2007). Localised corrosion can induce brittle fracture of flexural members (Almusallam, 2001). Corrosion of longitudinal bars has further been found to reduce shear strength (Rodriguez et al., 1997).

Cracking of the concrete arises due to the formation of corrosion products which have a lower density than the parent metal and result in the generation of tensile forces in the concrete which it is unable to sustain. As corrosion progresses spalling of concrete may occur. This represents a safety risk as the concrete could strike pedestrians, road users, vehicles, etc (Webster & Clark, 2016). The loss in flexural strength has been attributed to three primary causes, namely (i) cracking of concrete (ii) reduction in the area of steel reinforcement (Almusallam et al., 1996; Uomoto & Misra, 1988) and (iii) deterioration of the bond between the steel reinforcement and the concrete (Azad et al., 2007).

The loss in shear strength has been attributed to a reduction in both dowel action and aggregate interlock capacity (Xin Xue & Seki, 2010). However, if the longitudinal bars are adequately anchored these effects may be less significant (Azad et al., 2007).

Some authors have investigated the effect of corroded stirrups on the shear behaviour of flexural members and predictably it has been found that a loss in cross-sectional area will lead to a reduction in the shear capacity of members (Higgins & Farrow, 2006). Work by (Xue et al., 2014) shows that if the stirrups experience severe corrosion, in addition to the loss in shear resistance, the stiffness and ductility of members can also be reduced, thereby increasing the risk of brittle failure.

These results show that reinforcement corrosion can have serious structural consequences if left untreated. Elements such as beams and slabs would appear to be particularly vulnerable to this problem given their susceptibility to coincident cracking. The presence of coincident cracks no doubt hastens the onset of corrosion and may well increase the rate of corrosion propagation.

The following review the existing studies on the effect of coincident cracks on reinforcement corrosion in order to understand the current state of knowledge on this subject and, perhaps, to identify suitable strategies for reducing their impact.

3.3 Existing research

To date, it appears that only three studies have been carried out to elucidate the effect of coincident cracks on corrosion: (Dakhil & Cady, 1975; Poursaee & Hansson, 2008; Stillwell, 1988). The study by Stillwell is arguably the most comprehensive but appears to have gone unnoticed and is therefore described in some detail. Also included in this review is the study by (François & Arliguie, 1998). Although not directly aimed at developing a deeper understanding of this phenomenon it nevertheless includes some comments which are relatable to the present discussion and has therefore been included here. The following provides details of each of these studies and highlights key findings.

3.3.1 Dakhil & Cady, 1975

These authors investigated the effect of "subsidence cracking" i.e. plastic settlement cracking on reinforcement corrosion using blocks made of concrete mixes with slumps of 2, 3 and 4 inches (51, 76 and 102 mm) containing 5/8 inch (17.1mm) diameter reinforcing bars and ¾ and 1½ inch (19mm and 25mm) covers. The specimens were periodically exposed to a 5% NaCl solution and corrosion was monitored by measuring half-cell potentials using a copper/copper sulphate electrode. It was found that all the blocks with cracks registered higher ultimate potentials than those which did not have cracks as shown in table 3.1. The potentials of specimens 1-3 were less than -0.5V which indicates a severe risk of corrosion. The potentials for specimens 4-6 were in the range -0.35 to -0.5V which indicates a high risk of corrosion. The uncracked specimens registered potentials in the range -0.2V to -0.35V which indicates an intermediate risk of corrosion. Interestingly, neither slump nor cover were found to be

significant, which perhaps implies that there is no correlation between surface crack width and corrosion.

Table 3.1 Potential readings (Dakhil & Cady, 1975)

mm)	
	- 0.59
	- 0.57
2	- 0.56
	- 0.52
	- 0.49
2	- 0.47
	- 0.33
2	- 0.32
	- 0.31
	- 0.30
6 0 1 1 0 1 0	6 02 61 61 02 61 02 6

3.3.2 Stillwell, 1988

This work formed part of the Concrete in the Oceans research programme, whose aim was to provide additional knowledge to improve the design, construction and long-term performance of concrete oil production platforms in the North Sea. It was carried out in two Phases. Phase I tests were of 5-year duration and Phase II tests of 2.5 years duration. Both phases involved tests on beams which were around 1.3m and 250 mm wide and either 200mm or 150mm deep. All the beams were reinforced with a single 25 mm diameter bar placed longitudinally to which short lengths of bar of the same bar diameter were welded at right angles in positions where (flexural) cracks were likely to form (Figure 3.5). The effective depth of the welded bars was about 112mm giving rise to a cover of 25mm in the case of the 150 mm deep beams and 75mm in the case of the 200mm deep beams.

The cracks were induced by stressing pairs of beams back to back. Three concrete mixes were tested namely, standard grade, FA and low grade. The mix proportions

are shown in Table 3.2. The characteristic strength of the standard grade concrete was 55 N/mm² whereas that of the low grade concrete was 30 N/mm².

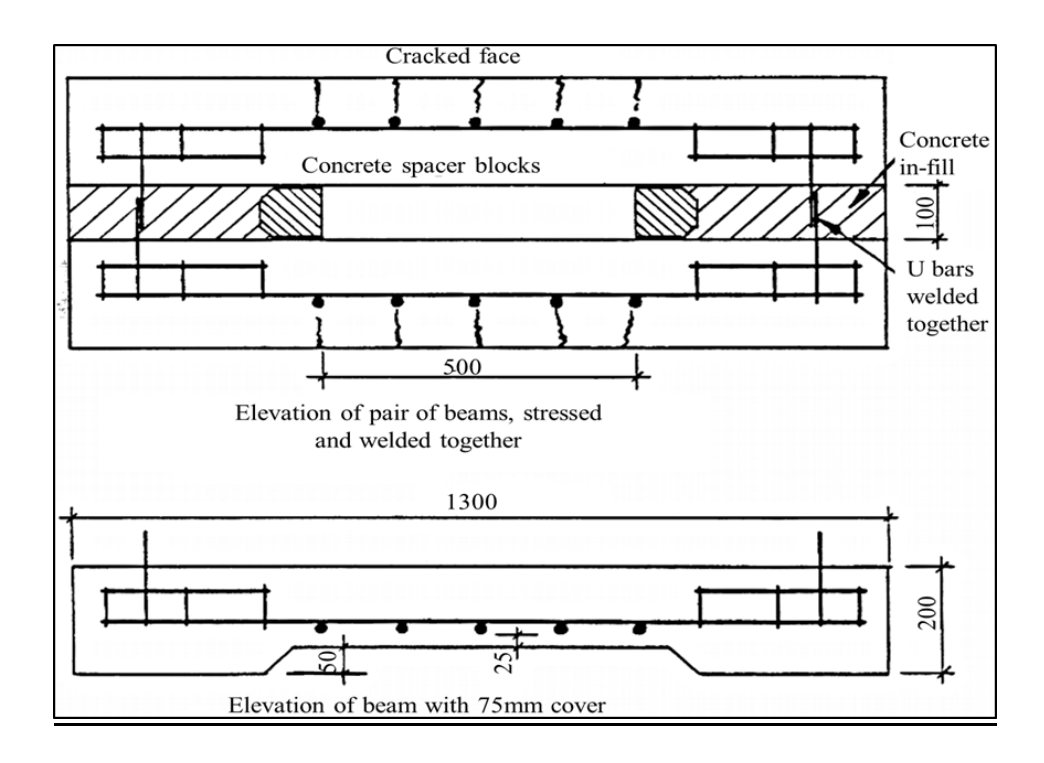


Fig. 3.5 Formation of longitudinal cracks.

Table 3.2 Mix proportions

Materials	Standard grade	FA	Low grade
PC	1.00	0.80	1.00
FA	-	0.20	-
20 mm aggregate	1.70	1.70	2.55
10 mm aggregate	0.80	0.80	1.20
Sand	1.50	1.50	2.25
w/c ratio	0.45	0.44	0.69

The specimens were subject to two main types of exposure:

- Deep immersion, in which the specimens were suspended continuously in sea water at a depth of 140mm.
- Splash zone, where the specimens were located on a jetty and subjected to periodic spraying with sea water.

The beams manufactured using standard and low grade concretes were tested for up to 5 years. The tests on beams manufactured with FA were started later and lasted for up to two and half years. After 1, 2.5 and 5 years, the beams were removed from the exposure sites and corrosion was assessed in terms of a grade from 1 to 5, defined as follows:

- 1 No corrosion
- 2 Traces of corrosion, negligible thickness of rust
- 3 Slight patches of corrosion, rust thickness ≤ 0.5 mm
- 4 Moderate corrosion, rust thickness ≤ 1.0 mm
- 5 Considerable corrosion, rust thickness ≤ 1.5 mm

The specimens exposed to the deep immersion zone did not experience any significant corrosion. However, when the specimens were removed after one year's exposure, despite preventing the specimens from drying out, significant corrosion developed at some of the large crack width positions along the beams. Chloride measurements taken of the concrete suggested that passivity of the reinforcement had been impaired under submerged condition but the fact that no corrosion had occurred was probably due to various factors such as the lack of oxygen availability at the reinforcement and the presence of marine growth which would have tended to block cracks while they were submerged. However, when the specimens were exposed to the atmosphere they dried out allowing access to oxygen and corrosion to develop.

A summary of the results obtained for specimens exposed to the splash zone are presented in Table 3.3. It was found that:

- All specimens were affected by corrosion of the reinforcement to varying degrees. Cores removed from beams exposed for five years showed significant corrosion of the reinforcement in all cases, irrespective of grade of concrete, cement type and thickness of concrete cover to reinforcement.
- Horizontal cracks developed just above the welded reinforcing bars in most of the samples manufactured using the low grade concrete due to the production

- of corrosion products. The authors further noted that it seemed likely that after a further period of time, spalling might have occurred.
- Cores removed from beams exposed for 2.5 years also showed significant corrosion at longitudinal crack positions, irrespective of grade of concrete, crack width or cover to reinforcement.
- The FA specimens sustained slightly higher levels of corrosion than the specimens manufactured using PC and which were in fact equivalent to the levels experienced by standard grade specimens after 5 years exposure.
- The level of corrosion damage sustained by specimens increased with exposure time but the rate of change reduced.

Table 3.3 Effect of concrete grade and cement type on reinforcement corrosion

Concrete grade and	Cover to reinforcement	Condition of reinforcement corrosion Age in years			
type	(mm)	1	2.5	5	
Standard	75	4½	3½	4½	
Standard	25	3½	4	4	
Low	75	3½	4	5	
Low	25	2½	4	4½	
FA	75	3½	5	-	
FA	25	4	4½		
Standard voided Standard voided Standard large cracks	75 25 75	- - 4	- - 4½	- - -	

Table 3.4 shows the effect of crack width and cover to reinforcement on the mean degree of corrosion for the three test mixes. It can be seen that

- (i) The worst corrosion was associated with the largest crack widths, although the difference is not very significant. The authors noted, however, that it was possible that even this difference could reduce after a longer period of exposure.
- (ii) The results of the tests on the standard grade specimens suggest that for a given crack width, beams with 75mm cover experienced less corrosion than

beams with 25mm cover. This implies that the crack width at the concrete/steel interface is more critical than the surface crack width.

Table 3.4 Effect of crack width and cover on reinforcement corrosion

Range of	Condition of reinforcement					
crack widths	Standard grade		Low grade		FA	
(mm)	75mm	25mm	75mm	25mm	75mm	25mm
0-0.3	2½	4	-	41/2	4	4
0.4-0.7	4	4	4	4	41/2	4½
0.8+	4½	-	5	5	5	-

3.3.3 Poursaee & Hansson, 2008

These authors examined the behaviour of longitudinally cracked concrete prisms made from three different concrete types: pure Portland cement concrete (OPCC) and two high performance concretes (HPC), which consisted of 75% silica fume cement and either 25% class C fly ash and or 25% blast furnace slag.

The prisms were 100 x 100 x 500 mm long and contained five embedded plain carbon steel probes (10mm diameter x 30mm long) attached to a polymethylmethacrylate (PPMA) rod. The prisms were stored outdoors. The temperature fluctuations and the difference between thermal expansion coefficients of the PPMA plastic rod and that of the cement paste caused the prisms to crack parallel to the PPMA rods. The resulting cracks were approximately 0.1mm wide at the surface. The prisms were covered with rock salt solution and kept wet and the corrosion activity of the carbon steel probes monitored using LPR over a 124 week period.

No significant difference was observed between the specimens made of OPCC and any of the HPC mixes regarding the resistance to corrosion when cracks (~0.1mm) are formed longitudinally to the reinforcement. This finding is consistent with the results of the Stillwell study discussed above.

3.3.4 François & Arliguie, 1998

These authors tested the behaviour of two types of concrete beams which were exposed to a chloride environments for up to a 12 year period (see 2.5.2 for details).

Although their investigation was aimed at developing a better general understanding of the relationship between cracking in concrete and the incidence of reinforcement corrosion, they have provided some comments on the behaviour of coincident cracks which are relevant to this discussion.

As previously noted, these authors found that the flexural cracks coincided with the position of stirrups. Surprisingly, however, there was no secondary cracking along the line of the stirrups which the authors suggested was due to the absence of corrosion of the underlying reinforcement. The authors attributed the lack of corrosion, despite the lower cover and the presence of coincident cracks, to the absence of bond stress and hence any deterioration/disruption at the steel-concrete interface.

Based on the literature, it is clear that a very limited work has been done on the effect of coincident cracks on corrosion of reinforcement. The results are somewhat contradicting as Dukhil and Candy found no correlation between crack widths and corrosion whereas Stillwell did note that samples with wider cracks underwent heavier corrosion. Regarding the effect of different binder types, now the current codes of practice recommend the replacement of PC with mineral admixtures, however, according to Stillwell and Poursaee results, blended mixes showed higher corrosion activity. Therefore, more research is needed to clarify this question.

3.4 Current practices with regard to coincident cracking and needed research

The literature review on types of cracks revealed that coincident cracks can result from a range of mechanisms including plastic settlement, plastic shrinkage, restrained thermal/long term drying shrinkage and direct loading. Although a great deal of research has been carried out on the first three of these causes/mechanisms of cracking, the measures proposed do not appear to have eradicated the problem (Concrete Society, 2010; Kochanski et al., 1990; NCHRP Synthesis 333., 2004). It is probably impossible to avoid coincident cracks from direct loading and it is highly likely, therefore, that coincident cracks are actually quite common in concrete structures. Affected reinforcement includes not just secondary reinforcement but also the main reinforcement and stirrups, where present.

There is both field and laboratory data which shows that cracks will facilitate the penetration of chlorides significantly faster than sound concrete, thereby shortening

the service life and increasing the maintenance cost of concrete structures (Dakhil & Cady, 1975; Djerbi et al., 2008; NCHRP Synthesis 333., 2004). Corrosion of embedded reinforcing bars increases the amount of coincident cracking, which in turn increases the risk of delamination and spalling of concrete. As discussed, corrosion of longitudinal bars and stirrups results in the loss of steel section and bond which reduces the strength, stiffness and ductility of concrete members.

Premature deterioration of concrete infrastructure such as bridges impedes economic growth, depletes natural and non-renewable resources and, more significantly, threatens human safety. Perhaps even more worrying is the fact that the advice on crack control in Codes and Standards does not draw attention to the existence of coincident cracks let alone include measures to reduce their impact. The recommendations on permissible crack widths are actually based on research on intersecting cracks i.e. cracking crossing reinforcement, the findings of which are contentious and do not appear to be applicable to coincident cracks. In the case of coincident cracks there appears to be no critical crack width below which there is a zero or low risk of corrosion. More generally, existing recommendations governing design for durability in Codes and Standards stress the importance of concrete quality, cement type and thickness of concrete cover. But the evidence from the tests conducted by (Stillwell, 1988) would appear to suggest that none of these measures will help reduce the risk of corrosion induced by coincident cracks. Researchers investigating the problem of "transverse cracking" in bridge decks have suggested a number of methods for reducing the associated risk of corrosion including the use of concrete mixes with a low tendency for cracking, sealing visible cracks using epoxy injection, waterproofing membranes/concrete overlays and epoxy-coated/FRP composite reinforcement. However, all these methods have drawbacks. The use of prestressing to reduce/eliminate cracking is another possibility that has been suggested but may be impracticable/uneconomic in the majority of cases (Krauss & Rogalla, 1996).

Stirrups would appear to be at particular risk of corrosion being as they act as crack initiators, have the least thickness of concrete cover and are usually made of smaller diameter reinforcement. Perhaps the only way of reducing the risk of corrosion of these bars is by encouraging the cracks to form away from the bars. A method of achieving this might be by introducing bars made of non-corrodible reinforcement in

the concrete cover. Preliminary tests on this method have shown that the cover reinforcement does indeed dominate crack formation but that further work is needed to establish if this approach will in fact reduce/eliminate the risk of corrosion as well as consider its practicability and the additional cost of construction.

Although the existing investigations on the effect of coincident cracks on reinforcement corrosion provide some useful insights, there is still a lack of understanding of the fundamental principles involved. For example, (François & Arliquie, 1998) found that coincident cracks did not invariably give rise to reinforcement corrosion. Perhaps this is related to the depth of cracking or possibly the stress state of the reinforcement which influences the degree of disruption at the steel concrete interface. As discussed in section 3.1, some mechanisms give rise to coincident cracks which predominantly extend to the surface of the steel reinforcement whereas other mechanisms give rise to coincident cracks which extend beyond the reinforcement. This will influence the area of bar at risk of corrosion as well as the distribution of anodic and cathodic regions, which together influence rates of corrosion. Very little information is currently available on these aspects or indeed how rates of corrosion associated with coincident and intersecting cracks compare. Information on how corrosion varies along the crack would also be of interest. Moreover, whilst it seems reasonable to assume that cement type has an effect on chloride penetration in cracked concrete and hence the time to corrosion initiation it would be surprising if cement type had no influence on the subsequent rate of corrosion propagation. The evidence from the tests carried out thus far suggest cement type has no influence on corrosion propagation but this seems unreasonable and more data on this aspect would be welcome. Similarly, the experiments to elucidate the effect of crack width on corrosion need to be more carefully conducted as this aspect seems critical to rationalising the recommendations on crack control in Codes and Standards, and given the scale of the problem of steel corrosion in concrete should be carried out as a matter of urgency.

3.5 Conclusion

 Coincident cracks in concrete structures can arise due to a number of mechanisms including plastic settlement, plastic shrinkage, early thermal shrinkage, long term drying shrinkage and direct loading.

- The chances of obtaining coincident cracking in concrete structures is high and there would appear to be no obvious way of avoiding these cracks in concrete construction.
- Coincident cracks can decrease the overall safety of concrete structures because they can promote corrosion of both longitudinal and transverse bars as well as stirrups in beams and slabs, which reduces their strength, stiffness and ductility.
- The recommendations on crack control in Codes and Standards are based on research on intersecting cracks and would appear to be unsuited to preventing corrosion due to coincident cracking.
- The research on coincident cracks is at present rather limited and more should be carried out to better understand the mechanisms involved and to propose cost-effective solutions to this problem.

3.6 Overall comment

Based on the literature above, the existence of cracks with different depths in practice was identified and lead to the development of specimen types with three different crack depths.

Chapter 4 Review of crack control and corrosion recommendations

Many codes and standards on structural concrete design specify values of maximum allowable crack widths primarily because of durability (specifically, to minimise the risk of reinforcement corrosion) but also because of aesthetics and/or water tightness. The cracks invariably referred to in these documents are those that occur transverse to longitudinal reinforcement. However, there are significant differences in the values of permissible crack widths specified as well as the method of specification. This section reviews the durability requirements in several building/design codes and standards in order to highlight some of the differences which exist, why this has occurred and to suggest how the advice might be rationalised. In general, there are five basic aspects governing the durability of reinforced concrete structures:

- 1. Minimum concrete cover to the reinforcement
- 2. Concrete mix design
- 3. Maximum chloride ion content
- 4. Maximum permissible crack width
- 5. Equation for crack width calculation

Equations for crack width control in codes of practice invariably aimed at estimating crack width induced by flexure due to imposed loading (Martin, 2006)

The following presents a comparison of code recommendations on each of the above assuming the exposure is either the splash zone or the most severe exposure listed in the code.

4.1 American Standard: Building Code Requirements for Structural Concrete (ACI 318, 2019)

1. Minimum concrete cover

According to this code the recommended minimum concrete cover for corrosion protection of the reinforcement should not be less than 51mm (2in) for walls and slabs, and not less than 64mm (2.5in) for other members.

2. Concrete mix design

(ACI 301, 2016) specifies limits on the maximum w/c ratio as well as the minimum compressive strength and maximum allowable water- soluble chloride content of concrete, as shown in Table 4.1. Section 4.2.3 of the code further recommends that the level of replacement of PC by SCM should not exceed 50 % by weight.

3. Maximum chloride ion content

Table 4.1 Basic requirements of concrete mix design for corrosion protection together with allowable water-soluble chloride ion content in ACI 318.

Exposure Class	Maximum w/c	Minimum f_c' , psi	Maximum water-soluble chloride ion (CI–) content in concrete, % by mass of cementitious materials
C0 ^[1]	N/A	2500	1
C1 ^[2]	N/A	2500	0.30
C2 ^[3]	0.40	5000	0.15

^[1] Dry or protected from moisture concrete

From Table 4.1 it can be seen that in chloride environments the maximum permissible water-soluble chloride content is 0.15% per mass of cementitious material which is equivalent to 0.45kg Cl⁻/m³ of concrete

4. Permissible crack width

Because of the lack of agreement between researchers on the effect of crack width on corrosion, ACI 318 does not include advice on permissible crack widths in reinforced concrete structures. However, this is achieved by setting limits on the reinforcement spacing. The reason cited by the code for the lack of advice on crack widths is because research by (Darwin et al., 1985; Oesterle, 1997) has shown that there is no correlation between surface crack widths under service load levels and corrosion. Thus, there is also no differentiation in allowable crack width between exterior and interior exposures. The Code recommendations suggest there will be more visible cracks where service loads give rise to high stresses in the reinforcement, however, formation

^[2] Concrete subjected to moisture without external chloride

^[3] Concrete exposed to moisture and an external source of chlorides from deicing chemicals, salt, brackish water, seawater, or spray from these sources.

of many narrow cracks is more desirable than a few wide cracks. This can be achieved by proper distribution of reinforcement over the zone of maximum concrete tension. The research by (Schießl & Raupach, 1997) has been referred to which indicate the greater importance of concrete quality, proper consolidation and sufficient concrete cover for corrosion protection rather than surface crack width.

5. Crack width equation

As mentioned above, there are no specific crack width limits prescribed in this or indeed the latest edition of (ACI 318, 2014), as the code's approach to crack control remains unchanged since 1999 and is through the requirements of minimum area of reinforcement and maximum reinforcement spacing.

4.2 Eurocode 2 and BS 8500-1:2015+A2:2019 (BS EN 206, 2019)

1. Minimum concrete cover to the reinforcement.

The recommended minimum concrete covers are shown in a Table 4.2 together with the associated mix design.

- 2. Specifications for concrete mix design.
- 3. Maximum chloride ion concentration

The allowable total chloride content for reinforced concrete subjected to environmental classes XD (corrosion induced by chlorides) and XS (corrosion induced by chlorides from seawater) is recommended to be 0.30 % by mass of cement, i.e chloride class 0.3, which corresponds to less than 0.60 kg Cl/m³ of concrete.

4. Permissible crack width

Eurocode 2 recommends a maximum permissible crack width of 0.3mm under quasipermanent load irrespective of service environment.

5. Crack width equation

The crack width, w_k , may be calculated from equation 4.1.

$$W_k = S_{r,max} (\varepsilon_{sm} - \varepsilon_{cm})$$
 Eq. 4.1

where:

S_{r,max} is the maximum crack spacing

 $\varepsilon_{\rm sm}$ is the mean strain in the reinforcement under the relevant combination of loads, including the effect of imposed deformations and taking into account the effect of tension stiffening. Only the additional tensile strain beyond the state of zero strain of the concrete at the same level is considered

 $\varepsilon_{\rm sm}$ is the mean strain in the concrete between cracks

 ε_{sm} - ε_{cm} can be calculated using equation 4.2:

$$\varepsilon_{\rm sm} - \varepsilon_{\rm cm} = \frac{\sigma_{\rm s} - k_t \frac{f_{\rm ct,eff}}{\rho_{\rm p,eff}} (1 + \alpha_e \, \rho_{\rm p,eff})}{E_{\rm s}} \ge 0.6 \frac{\sigma_{\rm s}}{E_{\rm s}}$$
 Eq. 4.2

where:

 σ_s is the stress in the tension reinforcement assuming a cracked section.

 α_e is the ratio E_s/E_{cm} Eq.4.3

Es design value of modulus of elasticity of reinforcing steel

Ecm secant modulus of elasticity of concrete

$$\rho_{\text{n,eff}} = (A_{\text{s}} + \xi_{1} A_{\text{p}}) / A_{\text{c,eff}}$$
 Eq. 4.4

 A_p is the area of pre or post-tensioned tendons within $A_{c,eff}$

 $A_{c,eff}$ is the effective area of concrete in tension surrounding the reinforcement prestressing tendons of depth, $h_{c,ef}$, where $h_{c,ef}$, is lesser 2.5 (h-d), (h-x)/3 or h/2

 ξ_1 is the adjusted ratio of bond strength taking into account the different diameters of prestressing and reinforcing steel:

$$= \sqrt{\xi * \frac{\phi_s}{\phi_s}}$$
 Eq. 4.5

- ξ is the ratio of bond strength of prestressing and reinforcing steel, can be found in section 6.8.2. and Table 6.2 of the actual Eurocode 2.
- φ_s is the largest bar diameter of reinforcing steel
- φ_p equivalent diameter of tendon according to section 6.8.2. of the actual Eurocode 2
- k_t is a factor dependent on the duration of the load: k_t = 0.6 for short term loading and k_t = 0.4 for long term loading.

4.3 (IS 456, 2000) Indian Code of Practice

1. Minimum concrete cover to the reinforcement

The Indian code identifies three exposure classes which can lead to reinforcement corrosion. They are shown in Table 4.3 together with the associated recommended nominal concrete covers.

2. Concrete mix design

The code specifies limits on the minimum cement content, maximum water cement ratio and the minimum concrete strength of members as shown in Table 4.3

3. Maximum chloride ion concentration

The maximum acid soluble chloride content in reinforced concrete should not exceed 0.6 kg Cl/m³ of concrete.

4. Permissible crack width

For aggressive environment, such as the 'severe' category noted in Table 4.3, surface crack widths should not exceed 0.1 mm under working load.

Table 4.2. Durability recommendations for reinforced elements with an intended working life of at least 100 years (BS EN 206, 2019).

Nominal		npressive stren ation content fo	Cement/combination type				
cover, mm	45+∆c	50+∆c	55+∆c	60+∆c	70+∆c	80+∆c	
		S					
			C45/55 0.35 ^{G)} ;380	C40/50 0.40;380	C35/45 0.45;360	C35/45 0.45;360	CEM I, IIA, A ₂ IIB- A ₂ M, IIB-S, CEM I-SRO, CEM I-SR3
XD3	C40/50 0.40; 360	C35/45 0.40;380	C32/40 0.45;360	C28/35 0.50;340	A ₁ C25/30 0.55;320	A ₁ C25/30 A ₁ 0.55;320	A ₂ IIB-P, A ₂ IIB-Q IIB-V, IIIA
AD3	C32/40 0.40;380	C28/35 0.45;360	C25/30 0.50;340	A ₁ C25/30 0.55;320 A ₁	C25/30 0.55;320	C25/30 0.55;320	IIIB, A ₂ IVB-P, IVB A ₂ Q, IVB-V
		C40/50 0.35; 380	C40/50 0.35 ^{G)} ; 380	C35/45 0.40;380	C32/40 0.45;360	C28/35 0.50;340	IIB-P, (A ₂) IVB-Q IIB-V, IIIA
		C40/50 0.35 ^{G)} ; 380	C35/45 0.40;380	C32/40 0.45;360	C25/30 0.55;320	C25/30 0.55;320	A₂ IIB-P or Q ≥ 25% pozzalana, IIB V ≥ 25% fly ash, IIIA ≥ 46% ggbs
XS3		C35/45 0.35 ^{G)} ; 380	C32/40 0.40;380	C28/35 0.45;360	A ₁ C25/30 0.55;320	A ₁ C25/30 0.55;320	IVB-P, (A ₂ IVB-Q, IVB-V, IIIB

G) In some parts of the UK it is not possible to produce a practical concrete with a maximum w/c ratio of 0.35

Text introduced or altered by Amendments No. 1 and No. 2, respectively is indicated in the text by tags (A) and (A) (A) and (A)

5. Crack width equation

The Indian code recommends use of the following equation for calculating crack width, $w_{\rm Cr}$

$$w_{cr} = \frac{3_a * \varepsilon_m}{1 + \frac{2(a_{cr} - c_{min})}{h - x}}$$
 Eq. 4.6

where

a_{cr} is distance from the point considered to the surface of the nearest

longitudinal bar,

C_{min} minimum cover to the longitudinal bar,

 ε_m average steel strain at the level considered,

h overall depth of member,

x depth of the neutral axis.

Table 4.3. Minimum Cement Content, Maximum Water-Cement Ratio and Minimum Grade of Concrete for Different Exposures with Normal Weight Aggregates of 20 mm and Nominal concrete cover in IS 456, 2000.

Exposure conditions	Nominal	Minimum Maximu		Minimum
	Concrete	cement		grade of
	cover, mm	content kg/m ³	w/c	concrete
Severe	45	320	0.45	M 30
Very Severe	50	340	0.45	M 35
Extreme	75	360	0.40	M 40

4.4 (JSCE, 2007) Japanese Code

1. Minimum concrete cover to the reinforcement.

The Japanese code uses a performance based approach to durability design. Thus, there is no fixed value of minimum concrete cover prescribed for a particular exposure class. Rather the Code presents a design curve which can be used for this purpose (see Figure 4.1). The procedure involves calculating the ratio of surface chloride ion concentration C_0 , and threshold chloride concentration C_{lim} , which is used in turn to estimate the ratio of the concrete cover c_0 and the design diffusion coefficient D_0 as shown in Figure 4.1 (Smith, 2016). Table 4.4 shows examples of the concrete covers necessary to achieve given service lives for elements exposed to the splash zone. Further details are provided in Part 3 of the code under "Durability Design".

Table 4.4. Maximum design diffusion coefficient, D_d (cm²/year), for a range of concrete convers, c_d, with different service lives for elements exposed to splash zone in JSCE, 2007.

Service		Design concrete cover, c _d (mm)								
life(years)	25	30	35	40	50	60	70	100	150	200
20	-	-	-	0.123	0.192	0.276	0.376	0.767	1.72	3.07
30	-	ı	ı	-	0.128	0.184	0.250	0.511	1.15	2.04
50	-	1	1	1	1	0.110	0.150	0.307	0.690	1.23
100	-	1	-	-	-	-	-	0.153	0.345	0.613

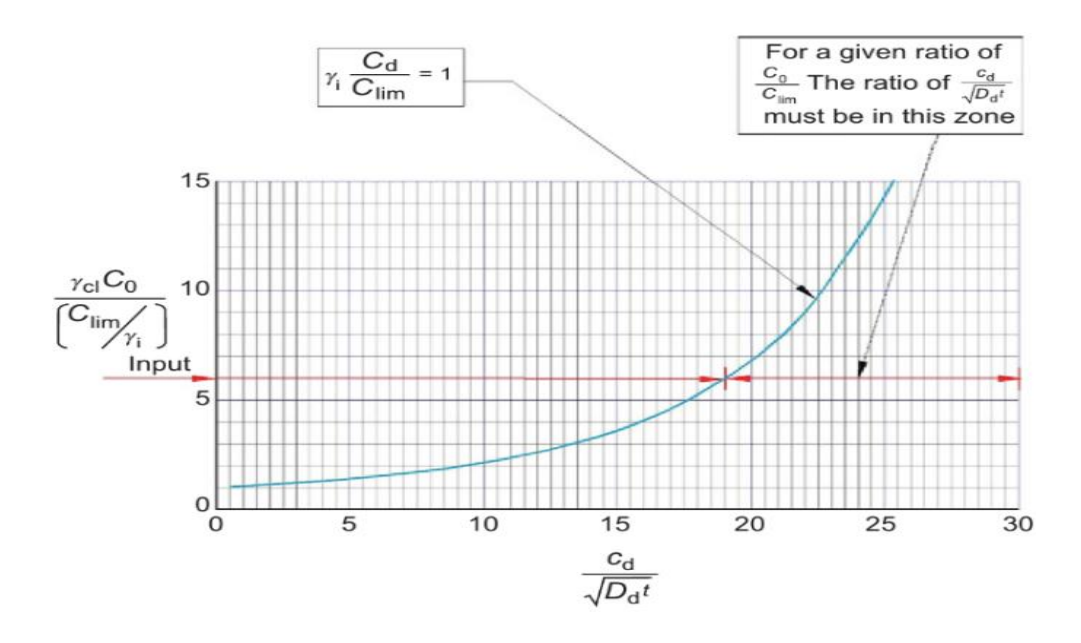


Fig. 4.1 Adequate combination of design concrete cover c_d and design diffusion coefficient for chloride ion D_d (Smith, 2016).

2. Concrete mix design.

Although as noted the Japanese code is performance-based, it nevertheless includes some mandatory requirements regarding maximum w/c ratio and minimum cement content for concrete in aggressive environments as shown in Table 4.5.

Table 4.5 Requirements for concrete mix design in aggressive environment in JSCE, 2007.

Requirements	Exposure conditions			
Requirements	Offshore, air	Splash zone	Undersea	
Maximum water-cement ratios for	45	45	50	
ordinary construction %	45	40	50	
Maximum water-cement ratios for				
construction with concrete products or	50	45	50	
products with equal or higher quality %				
Minimum cement content (kg/m³), with	330	330	300	
coarse aggregate size of 20 or 25 mm.	000	000	300	
Minimum cement content (kg/m³), with	300	300	280	
coarse aggregate size of 40mm.	500	550	200	

3. Maximum chloride ion content

The code specifies that the maximum chloride ion content should not exceed 0.3kg Cl/ m³ in corrosive environments and 0.60 kg Cl/m³ in the normal environment depending on the type of structure and with the permission of the owner.

4. Permissible crack width

The code distinguishes between three exposure environments for concrete structures as follows:

- Severely corrosive environment (tidal zones and structures exposed to frequent use of de-icing salts);
- Corrosive environment (permanently submerged in seawater or structures located near shoreline where air contains salt);
- Normal environment (Ordinary outdoor environment without any airborne salt)

The permissible crack width can be determined in accordance with guidance shown in Table 4.6.

Table 4.6. Durability requirements for reinforcement corrosion for deformed and plain bars (JSCE, 2007)

Environment	Maximum w/cm	Minimum concrete cover (mm)	Crack width
Normal	0.50 ^b / P ^c	40 ^b / P	0.005c
Corrosive	0.50 ^b / P ^c	40 ^b / P	0.004c
Severely corrosive	Р	Р	0.0035c

^a c is the thickness of concrete cover and should not exceed 100mm.

From Table 4.6 it can be seen that the values of permissible crack width are not fixed but a function of the service environment and thickness of concrete cover. Because of the latter, the permissible crack widths in the Japanese standard may

^b Values for carbonation processes, beam elements and intended working life of 100 years.

^c P designates the values determined by performance-based approach.

appear to be more onerous than those in other codes and standards. For example, in normal environments, assuming the cover is 40mm the permissible crack width is 0.2mm. In corrosive and severely corrosive environments and again assuming the cover is 40mm the permissible crack widths are 0.16mm and 0.14mm respectively. However, assuming a concrete cover of 65mm which is more reasonable for concrete in marine environment, the permissible crack width is ~ 0.23mm which is similar to values in other codes.

5. Crack width equation

The Japanese code recommends the following equation (4.7) for calculating crack width, w:

$$w = 1.1k_1 k_2 k_3 \{4_c + 0.7 (c_s - \phi)\} \left[\frac{\sigma_{se}}{E_s} \left(or \frac{\sigma_{pe}}{E_p} \right) + \varepsilon'_{csd} \right]$$
 Eq. 4.7

where

n

 k_1 a constant to take into account the effect of surface geometry of reinforcement on crack width. It may be taken to be 1.0 for deformed bars, 1.3 for plain bars and prestressing steel.

k₂ constant to take into account the effect of concrete quality oncrack width. It can be calculated through equation 4.8.

$$k_2 = \frac{15}{f'_c + 20} + 0.7$$
 Eq. 4.8

 f'_c compressive strength of concrete (N/mm²). In general, it may be taken to be equal to the design compressive strength, f'_{cd} .

 k_3 a constant to take into account the effect of multiple layers of tensile reinforcement on crack width. It may be calculated using equation 4.9.

$$k_3 = \frac{5(n+2)}{7_n+8}$$
 Eq. 4.9

number of the layers of tensile reinforcement.

- c concrete cover (mm).
- center-to-center distance of tensile reinforcements (mm).
- ϕ diameter of tensile reinforcement (mm).
- σ_{se} increment of stress of reinforcement from the state in which concrete stress at the portion of reinforcement is zero (N/mm²).
- σ_{pe} increment of stress of prestressing steel from the state in which concrete stress at the portion of reinforcement is zero (N/mm2).

4.5 Russian Code (CΠ 28.13330, 2017)

1. Concrete cover to the reinforcement.

In corrosive environments the code recommends values of concrete cover depending upon the chloride concentration of the exposure liquid and the permeability of concrete as shown in Table 4.7.

2. Concrete mix design.

The recommendations governing maximum w/c ratio, minimum concrete strength, minimum cement concrete and cement type for concrete in aggressive service environments are shown in Table 4.8.

Table 4.7. Concrete cover prescribed for corrosive environment (CΠ 28.13330, 2017)

Level of aggressiveness (corrosiveness)	Concrete cover,	liquid environm	ble chloride concer nent, ml/dm³, for co nt, cm²/c (water tigl	ncrete with
of the environment	mm	< 5 ·10 ⁻⁸ till 1 ·10 ⁻⁸ (W6 –W8)	< 1 ·10 ⁻⁸ till 5 ·10 ⁻⁹ (W10 – W14)	< 5 ·10 ⁻⁹ (W16 –W20)
Slightly	20	500	1300	4100
Moderately	30	700	1850	8300
Highly	50	1000	2700	18000

Table 4.8. Concrete mix design requirements (CΠ 28.13330, 2017)

Requirements for	Relevant exposure classes			
concrete	XS3	XD3		
W/c ratio	0.45	0.45		
Minimum compressive				
strength class, B	45	45		
Minimum cement content, kg/m³	340	320		
	CEM I(++)*, CEM II/A-S	CEM I(++), CEM II/A-S (+),		
	(++), CEM II/A-D (++), CEM	CEM II/A-D (++), CEM II/A-L		
Cement/ combination	II/A-L or LL (i), CEM II/A-M	or LL (+), CEM II/A-M (i),		
	(i), CEM III/A (++), CEM V/A	CEM III/A (++), CEM V/A (i),		
type	(i), CEM I-SR (++), CEM	CEM I-SR (+), CEM III/A-SR		
	III/A-SR (++)	(+)		

^{*}Designations such as "(++), (+)" and "(i)" in recommended cement types correspond to "recommended, allowed" and "testing is needed".

3. Maximum chloride content

The maximum allowable chloride content in concrete is 0.4% by mass of cement or combination type i.e chloride class of Cl 0.4

4. Permissible crack width

The code identifies four service environments for concrete structures: not aggressive, slightly aggressive, moderately aggressive and highly aggressive. Permissible crack widths are provided for the last three environments under dead and imposed loads separately as shown in Table 4.9.

Table 4.9 Crack width limitation for aggressive environment (C∏ 28.13330, 2017)

Paguiramento	Slightly	Moderately	Highly
Requirements	aggressive	aggressive	aggressive
Crack width under dead load, mm	0.2	0.15	0.1
Crack width under imposed load, mm	0.15	0.1	0.05
Concrete cover ¹ and Water tightness	20	20*	25
class	$\overline{W6}$	$\overline{W4}$	$\overline{W8}$

¹ Concrete cover and water tightness are shown as a nominator and a denominator respectively. *Concrete cover and water tightness indicated in moderately and highly aggressive environments are shown in case where additional protection such as isolation cover is used. These values should be increased if necessary depending on the type of the structure or harshness of the environment.

5. Crack width equation

In cases where cracks may affect the durability of reinforced concrete elements, the opening of different crack widths should be calculated. Calculation of crack opening is completed through such conditions where the width of crack opening from the external loads a_{crc} should not exceed maximum permissible values of crack width opening $a_{crc,ult}$ in accordance with equation 4.10.

$$a_{crc} \le a_{crc,ult}$$
 Eq. 4.10

Calculation of reinforced concrete elements should be done by considering the opening of cracks due to increased bending and shear stresses under dead and imposed loadings.

Crack width under imposed load is calculated through equation 4.11.

$$a_{crc} = a_{crc1}$$
 Eq. 4.11

Crack width under dead load is calculated through equation 4.12.

$$a_{crc} = a_{crc1} + a_{crc2} - a_{crc3}$$
 Eq. 4.12

where:

a_{crc1} crack width formed under permanent and temporary long-term imposed loads;

Chapter 4 A review of crack control and corrosion recommendations

a_{crc2} crack width formed under permanent and temporary (short and long-term) dead loads;

acrc3 crack width formed under permanent and temporary long-term dead loads;

4.6 Chinese Code GB50010-2010 (modified in 2015) (Guo et al., 2018)

1. Minimum concrete cover to the reinforcement.

The code identifies three main exposure categories for concrete: I, II and III. Categories II and III are divided into two subcategories: IIa and IIb, and IIIa and IIIb. Categories IIIa and IIIb are relevant to the design of structures exposed to corrosive environments. Recommended values of concrete cover for various elements of structure with design lives of 50 or 100 years are shown in Table 4.10.

Table 4.10 Minimum concrete cover specifications (Guo et al., 2018).

Environment	Concrete cove intended work	•	Concrete cover for 100 years intended working life (mm)	
Categories	Slab, Wall, Shell	Beam, Column	Slab, Wall, Shell	Beam, Column
I	15	20	21	28
IIa	20	25	28	35
II _b	25	35	35	49
IIIa	30	40	42	56
III _b	40	50	56	70

^{*} In case where not more than C25 concrete strength grade is used, the cover should be increased up to 5 mm.

2. Concrete mix design

Table 4.11 shows recommended values of the maximum w/c ratio and minimum concrete strength for each exposure environment

Table 4.11. Requirement for concrete mix design (Guo et al., 2018).

		Minimum concrete	Maximum Chloride
Environment	W/C Ratio	strength	content % by cement
		grade	mass
I	0.60	C 20	0.30
IIa	0.55	C 25	0.20
II _b	0.50 (0.55)	C 30 (C 25)	0.15
IIIa	0.45 (0.50)	C 35 (C 30)	0.15
III _b	0.40	C 40	0.1

^{*} Values under () should be used in case where air-entraining agents are used.

3. Maximum chloride content

Table 4.11 also shows values of the recommended maximum water-soluble chloride ion content of concrete.

4. Permissible crack width

Table 4.12 shows the allowable crack widths for various exposure conditions

Table 4.12 Allowable maximum crack width for exposure conditions (Guo et al., 2018).

Environmental	Crack control levels	Reinforced concrete structures	
Categories	Crack control levels	w _{lim} (mm)	
I	III	0.3 (0.4)	
II	III	0.2	
III	III	0.2	

5. Crack width equation

The formula recommended in the code to calculate crack width is somewhat similar to the expression in Eurocode 2, as shown in equation 4.13.

$$w_{max} = \alpha_{cr} \psi \frac{\sigma_s}{E_s} \left(1.9 c_s + 0.08 \frac{d_{eq}}{\rho_{te}} \right)$$
 Eq. 4.13

$$\psi = 1.1 - 0.65 \frac{f_{tk}}{\rho_{te} \sigma_s}$$
 Eq. 4.14

$$d_{eq} = \frac{\sum n_i d_i^2}{\sum n_i v_i d_i}$$
 Eq. 4.15

$$\rho_{te} = \frac{A_s + A_p}{A_{te}}$$
 Eq. 4.16

where

 C_S

 α_{cr} coefficient regarding component bearing characteristics, use according to table 7.1.2-1of the original Code;

 ψ non-uniformity coefficient of tensile strain on the reinforcement between adjacent cracks;

σs representative tensile of prestress concrete component longitudinal reinforcements calculated through standard load combinations or tensile of normal reinforced concrete component longitudinal reinforcements through quasi-permanent load combinations:

Es elastic modulus of the reinforcement, use according to 4.2.5 of the original Code;

the distance from the bottom of the tension zone in the section to the outer edge of reinforcement of the outer layer (mm), when c_s <20, take c_s =20, when c_s >65, take c_s =65;

 ρ_{te} the reinforcement calculated from the effective area of the tension zone, with pte = 0.01 when pte < 0.01;

As area of cross section of normal longitudinal reinforcement tensile zone;

A_p area of cross section of prestress longitudinal reinforcement tensile zone;

the representative diameter of tensile reinforcements (mm), for non-bond post-tensioning components, only use the representative diameter of cross section of normal longitudinal reinforcement tensile zone;

 d_i nominal diameter of the type i longitudinal reinforcement, for bonding prestressing multi-strands tendon, take diameter as $\sqrt{n_1 \ d_{pl}}$, d_{pl} is the diameter of single strand, n_1 is the number of strands;

n_i the number of type i reinforcements in tensile zone, for bonding prestressing multi-strands tendon, take the number of strands;

vi relative bonding characteristic coefficient of type i longitudinal reinforcement in tensile zone, use according to table 7.1.2-2 from the original Code.

4.7 Conclusion

Based on the above review of code provisions on durability design of reinforced concrete structures, it appears the advice on crack control can be divided into four groups:

- Codes of Practice that accept cracks influence concrete durability but do not specify permissible crack widths (ACI 318, 2019).
- II. Codes of practice that state cracks influence reinforcement corrosion but only specify a single permissible crack width irrespective of service environment, thicknesses of concrete cover and concrete composition (BS EN 1992, 2014).
- III. Codes of practice that accept there is a relationship between crack width and corrosion such that the more aggressive the exposure conditions the narrower the permissible crack width (GB50010-2010; IS 456, 2000; CΠ 28.13330, 2017)
- IV. Performance/hybrid codes which base their recommendations on the service environment and thickness of concrete cover (JSCE, 2007).

For ease of comparison of code recommendations, the key factors influencing corrosion protection are summarised in Table 4.13. Here it can be seen that there are considerable differences in the recommended values of concrete cover and permissible chloride content for similar exposure conditions noted in the codes. The codes also vary in their advice on cement type and SCM replacement ratios in chloride environments. For example, (ACI 318, 2019) limits the use of SCM to 50 % whereas (BS EN 206, 2019) and (CП 28.13330, 2017) recommend considerably higher percentages and provide more detailed guidance on replacement levels.

Table 4.13 Comparison of different Codes of Practice.

Codes	Regulation	Concrete cover (mm)	crack width (mm)	Chloride content
American	Prescription Based	51 and 64	Silent	0.45 kg/m ³
Eurocode 2	Prescription Based	45, 50, 55, 60, 70, 80 +Δc	0.3	0.60 kg/m ³
Indian	Prescription Based	45, 50, 75	0.1	0.60 kg/m ³
Japanese	Hybrid	Performance based	Performance based	0.30 kg/m ³
Russian	Prescription Based	20, 30, 50	0.1	0.4%
Chinese	Prescription Based	42, 56, 70	0.2	0.15/0.1 %

There is no clear guidance on SCM replacement ratios provided in the Japanese code, however. Nevertheless, the code does encourage the use of SCMs and recommends prior to their use, their efficacy and replacement ratio should be verified by test results or based on successful past projects. The Indian code also recommends the use of SCMs but like the Japanese code contains no guidance on this subject. The equations for calculating crack widths (where present) are quite dissimilar. Although all codes appear to accept that the presence of cracks increases the risk of reinforcement corrosion, however the measures advocated for achieving durability differ. For example, allowable crack widths for structures exposed to chloride environments range between 0.1 and 0.3mm.

None of the above-mentioned codes discusses the orientation of cracks with respect to reinforcing bars. Most of the work to date on the relationship between cracks and corrosion has focused on intersecting cracks, because it has been assumed that coincident cracks are:

- (a) relatively rare in practice;
- (b) can be eliminated by following good design, detailing and workmanship rules (Concrete Society, 1992; Frosch, 2003);
- (c) will only give rise to corrosion of transverse or secondary bars which are largely unstressed and thus any corrosion will not significantly decrease the overall safety of concrete structures (CEB 1976, cited by (Beeby, 1978);

However, it can be seen from the discussion in chapter 3 that coincident cracks are far from rare in practice, and they can give rise to structurally significant corrosion of reinforcing bars. It is important therefore that more research on the effect of coincident cracking is conducted. Details of the work carried out to elucidate the effect of coincident cracks on reinforcement corrosion are presented in the following chapter.

Chapter 5 Methodology

This chapter describes the test specimens and procedures used to assess the effect of coincident cracks on reinforcement corrosion. It also outlines the way in which the results were analysed.

5.1 Specimen design

As discussed in chapter 3, coincident cracks can occur due to many causes including plastic shrinkage, plastic settlement and bending. Plastic shrinkage cracks are typically 2-3mm wide but their width rapidly decreases away from the surface. As such these cracks may not reach the level of the underlying reinforcing bars. On the other hand, plastic settlement cracks normally extend to the surface of the top layer of reinforcing bars. Beams and slabs subject to bending due to transverse loading will experience a series of distributed flexural cracks some of which will be aligned with the shear reinforcement in beams and the distribution steel in slabs. The depth of these cracks will invariably exceed the depth of reinforcing bars in the tension face. Moreover, the width of these cracks increases with increasing loading. Thus, it will be appreciated that coincident cracks with varying depths and widths can form in concrete members and therefore the test specimens should be capable of investigating these two aspects of coincident cracking on rates of corrosion.

The results presented by Stillwell (1988) show that the FA specimens sustained slightly higher levels of corrosion than similar specimens manufactured using PC and which were in fact equivalent to the levels experienced by standard grade specimens after 5 years exposure. Poursaee & Hansson (2008) found no significant differences in the amounts of corrosion between specimens made of ordinary Portland cement concrete (OPCC) and two high performance (HPC) mixes.

These results are worrying as they cast doubt on the wisdom of making the use of blended cements concretes mandatory in chloride rich environments and merit further consideration.

Chapter 5 Methodology

Thus, the following aspects of coincident cracks were identified as requiring investigation as to their influence on rates of reinforcement corrosion:

- 1. Surface crack width
- 2. Crack depth
- 3. Cement type

Generally, all specimen designs are related to each crack parameter mentioned above, therefore it is impossible to look at a single parameter in isolation. To investigate the effect of crack width on corrosion specimen designs B and C were cast with varying crack widths (0; 0.1; 0.2; 0.3; and 0.4mm). Since it is impossible to control the crack width along the concrete cover, the crack widths were achieved by inserting steel shims with varying widths into the slots made in timber moulds, and removing them at an appropriate time. However, although B and C specimens had the same crack widths, their depths were different. Type B specimens had a clearance of ~ 9mm to the reinforcement level, whereas cracks stopped just on top of the rebar in type C specimens. Therefore, both sets of specimens were applied to investigate the effect of crack width as well as depth. Moreover, type A specimens were also employed to study the crack depths as the cracks in those specimens go beyond the reinforcement level. This was achieved by subjecting the samples under three-point loading where the load applied was gradually increased to ensure the initiation of the crack, which was then controlled by placing the specimens under the loading frames made of rigid steel shown in Figure 5.5. To investigate the effect of binder type on corrosion process, all three specimen designs had replicates made of three different cement mixes.

The details of each specimen design are presented below.

5.1.1 Type A specimens

Type A specimens consist of concrete slabs 500mm long \times 300mm wide \times 100mm deep. The slabs are reinforced with three longitudinal 10mm mild steel bars, arranged as shown in Figure 5.1. The depth of concrete cover to the longitudinal bars is 57mm as shown in Figure 5.2.

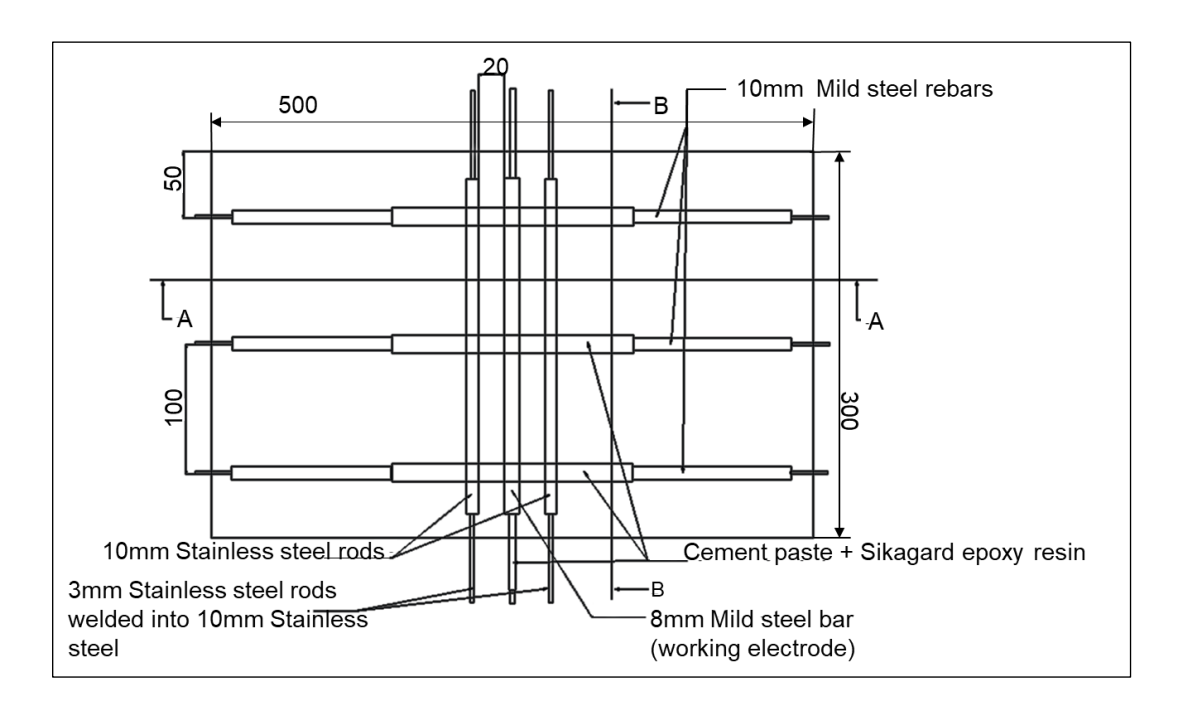


Fig. 5.1 Plan view of reinforcement arrangement for Type A specimens

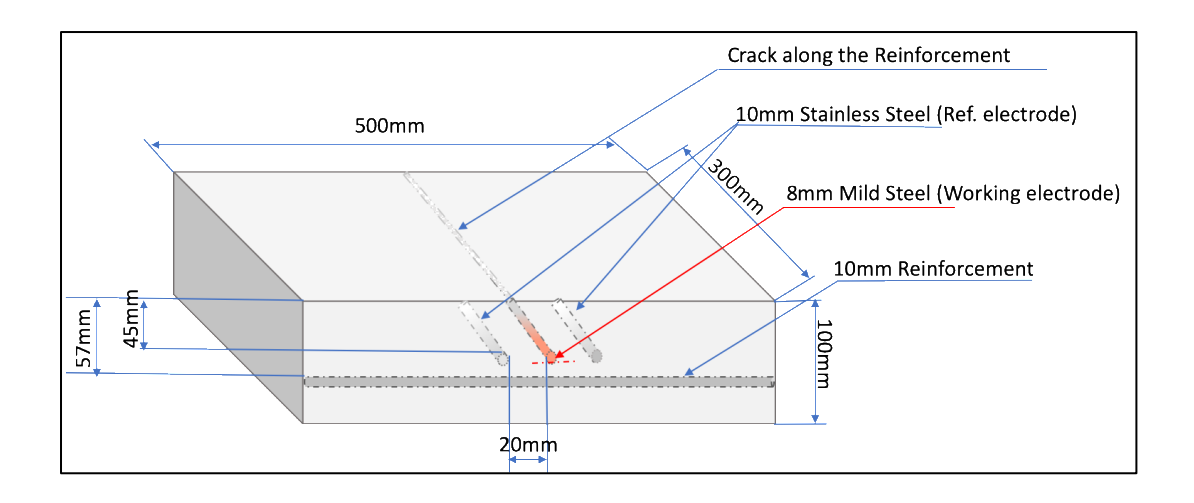


Fig. 5.2 The schematic view of the specimen type A.

The working electrode, which is positioned in the centre of the specimen in the transverse (y-y) direction, consists of an 8mm diameter × 260mm long mild steel bar. The cover to the working electrode is 45mm. The cover to the reinforcement was decided based on the minimal cover recommended in BS EN 206, 2019 which is shewn in table 4.2 of the 4th Section of this work. The ends of the working electrode were drilled with 4mm diameter holes and fitted with mild steel wires using push connections and welding. The wires enabled the electrode to be held in position during concreting and also electrically connect the bars to the corrosion monitoring equipment. Prior to concreting the exposed end of the wires

Chapter 5 Methodology

were coated with a polymer modified cementitious grout and covered in heat shrink sleeving in order to minimise the risk of crevice corrosion (Figure 5.3).

The working electrodes were cleaned by wire brushing, degreased with acetone and weighed prior to placing in the moulds.

The specimen also includes two 10mm stainless steel rods positioned either side of the working electrode which act as a counter electrode and enable the corrosion rate on the working electrode to be estimated using linear polarisation resistance and zero resistance ammeter. Half-cell potentials of the working electrode are also monitored. The ends of these two stainless steel rods were also drilled with 3mm diameter holes and fitted with 3mm stainless steel wires using push connections and welding.

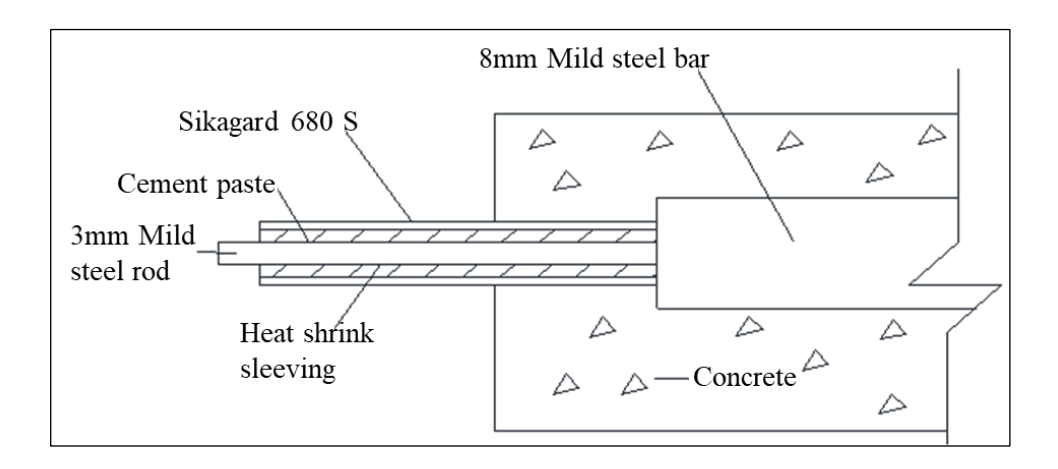


Fig. 5.3 Coated mild steel rod to prevent corrosion.

In order to induce a crack along the line of the working electrode, a 0.1mm thick × 5mm deep steel shim was inserted into the green concrete and removed after 6 hours. The specimens were actually cracked when they were between 28-31 days old. This was achieved by turning the slabs upside down and subjecting them to three-point bending as shown in Figure 5.4.

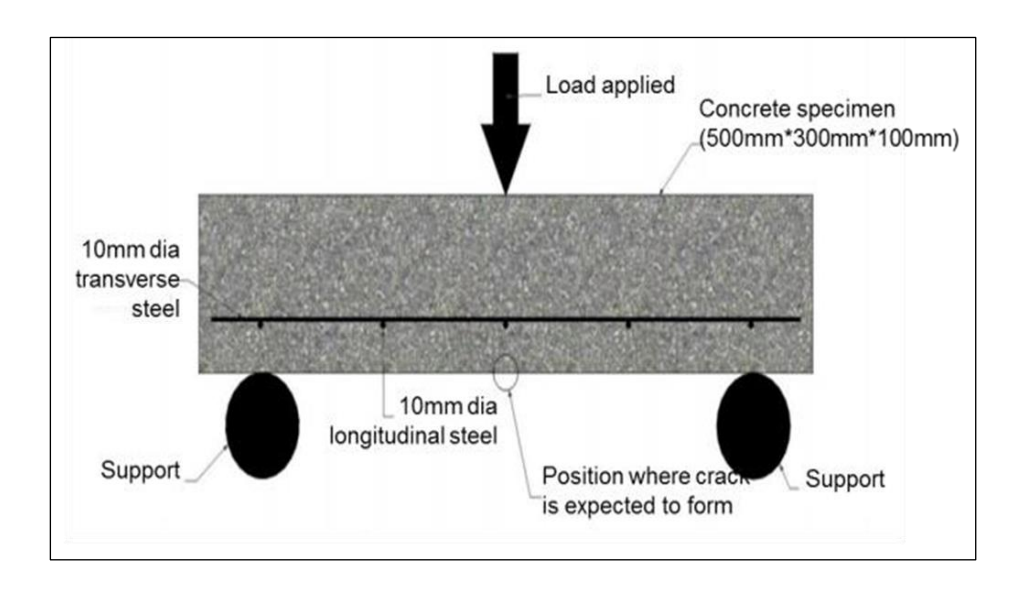


Fig. 5.4 Type A specimen subject to three-point loading.

The slabs were then removed and positioned the right way up in a rigid loading frame (Figure 5.5). By adjusting the screws, a crack with a maximum surface width of 0.4mm above the working electrode was obtained. The obtained crack width was measured with crack width microscope UTC 31 with 40x magnification and 4 mm measuring range with 0.02 mm subdivisions as well as crack width ruler. The slabs were left in the loading frames to ensure that the cracks remained open during the life of the experiment.

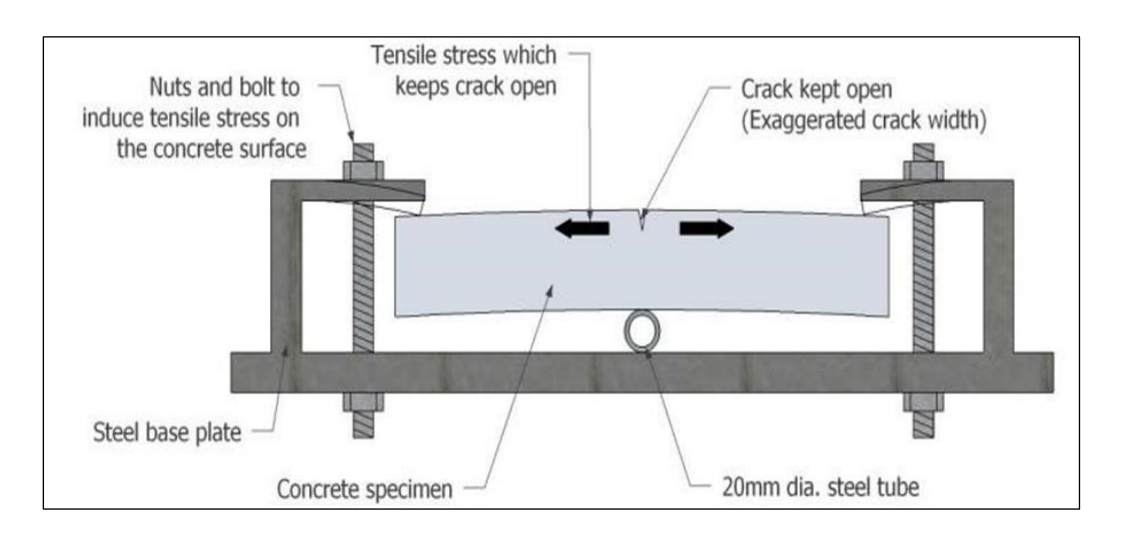


Fig. 5.5 Frame used to hold the crack open in Type A specimens.

Photos of the mould used (I), the means of crack induction (II, III), and the specimen in the loading frame (IV) which show the longitudinal crack typically

formed on the surface of type A specimens are presented in Figure 5.6 as recommended by (Burkan Isgor et al., 2019).

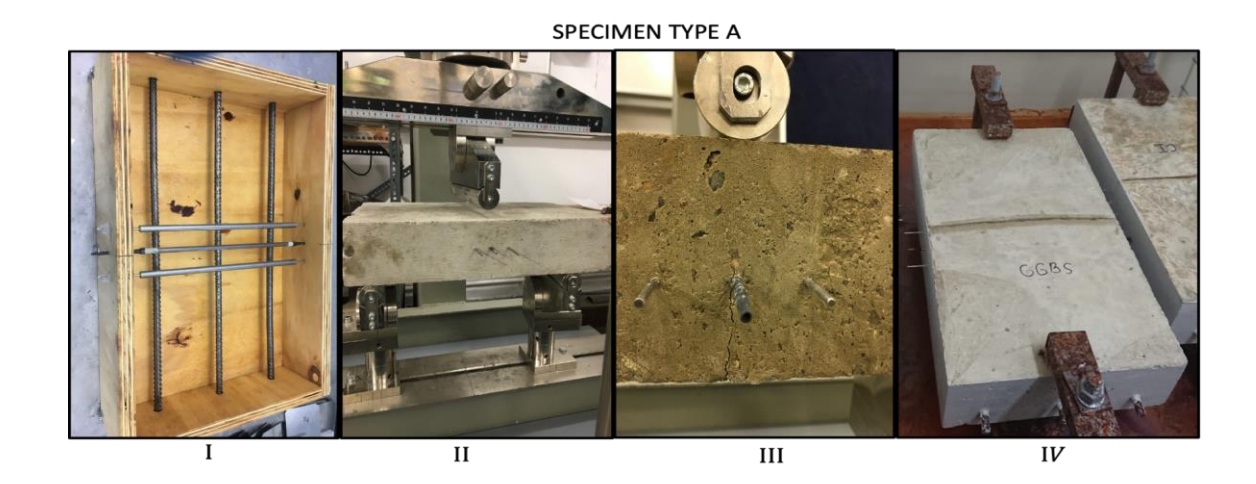


Fig. 5.6 Step-by-step progression of Specimen type A.

5.1.2 Type B specimens

Type B specimens are 500mm long × 135mm wide × 100mm deep beams. They contain two 8mm diameter × 460mm long mild steel and one 10mm diameter × 460 mm long stainless-steel bars, arranged as shown in Figure 5.7. The cover to all bars is 45mm.

As in the case of Type A specimens, both the mild steel and stainless steel bars were drilled at their ends to make smaller wholes on their circumference and fitted with 3mm diameter wires. The working electrodes were cleaned by wire brushing, degreased with acetone and weighed prior to placing in the moulds.

In Type B specimens the cracks above the mild steel bars were formed artificially. This was achieved by casting oiled steel shims of 0.1mm, 0.2mm, 0.3mm or 0.4mm thicknesses in the beams above the bars. The shims were held in position by inserting them in slots cut into the timber moulds. To prevent the shims from moving during casting, they were held in place using bridges and the concrete carefully placed around them and compacted by vibration.

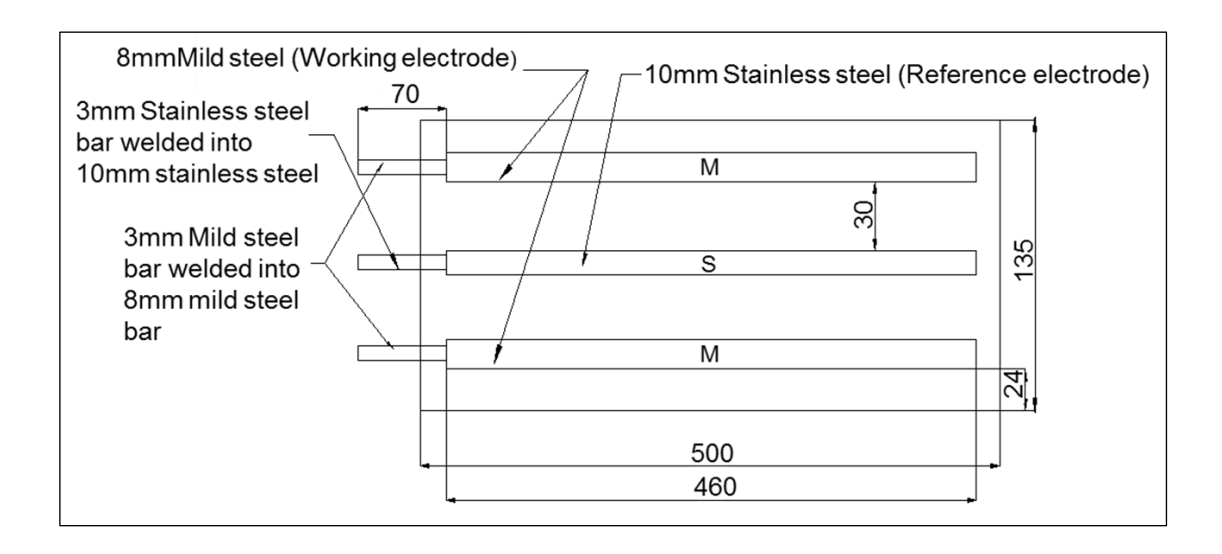


Fig. 5.7 Plan view of reinforcement arrangement in Type B specimens

The clearance between the bottom of the shims and the top of the mild steel bars was 5mm as shown in Figure 5.8. The shims were removed 6 hours after casting. The time for removing the steel shim was determined by trial and error this suggested removal of the shims 6 hours after casting was ideal as the concrete was strong enough to maintain the shape of the crack but allow the shims to be removed without disturbing the concrete.

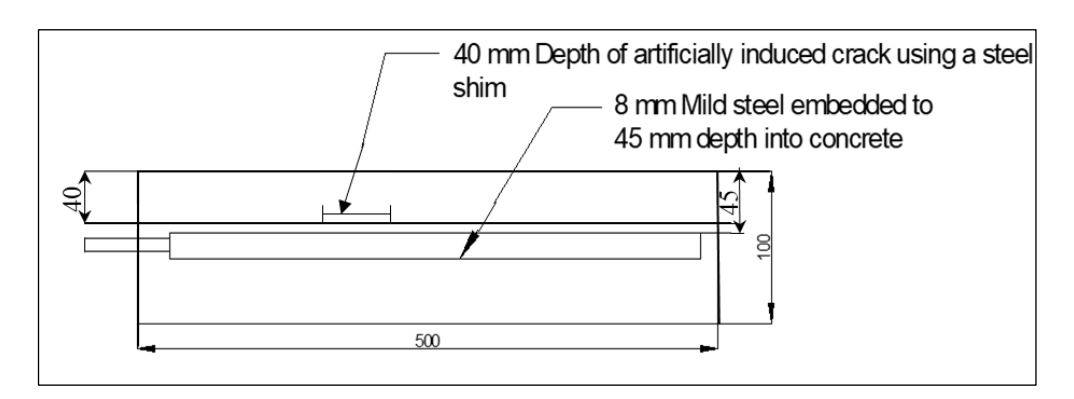


Fig. 5.8 Elevation view of reinforcement arrangement of the B test sample.

Figure 5.9 shows an isometric view of type B specimens.

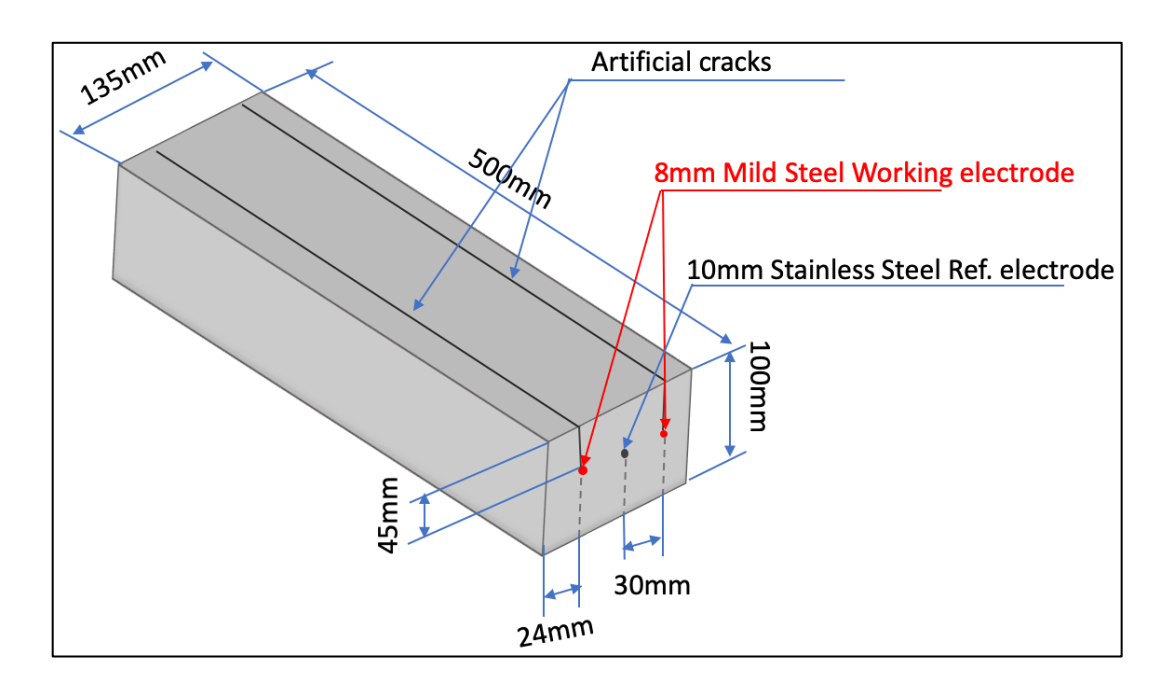


Fig. 5.9 Schematic view of the Specimen type B

Photos of the moulds used (I), the method of crack induction (II, III), and specimens after demoulding of type B specimens (IV) are shown in Figure 5.10.



Fig. 5.10 Step-by-step progression of Specimen type B.

During the specimen design stage of this work, it has been planned that the space between crack end and rebar be 5mm, however, due to possible shifts during vibration, the still shims used to induce cracks moved upwards resulting in a clearance of ~10mm. When the specimens were demoulded, it was noted that

Chapter 5 Methodology

some movement of the shims may have taken place. This was actually confirmed to be the case at the end of the experimental work as shown in Figure 5.11. This movement resulted in clearance of ~10mm rather than 5 mm originally envisaged. C clamps were found to be useful in avoiding this problem as the steel shims inserted to the slots should be positioned and kept stable during vibration.

Ideally, it would be useful to test specimens with intersecting crack parallel in this work, however, due to limited space availability in the laboratory this wasn't possible. Besides, there is a lot of data on the effect of intersecting cracks on corrosion, therefore it was impractical to carry out this test.

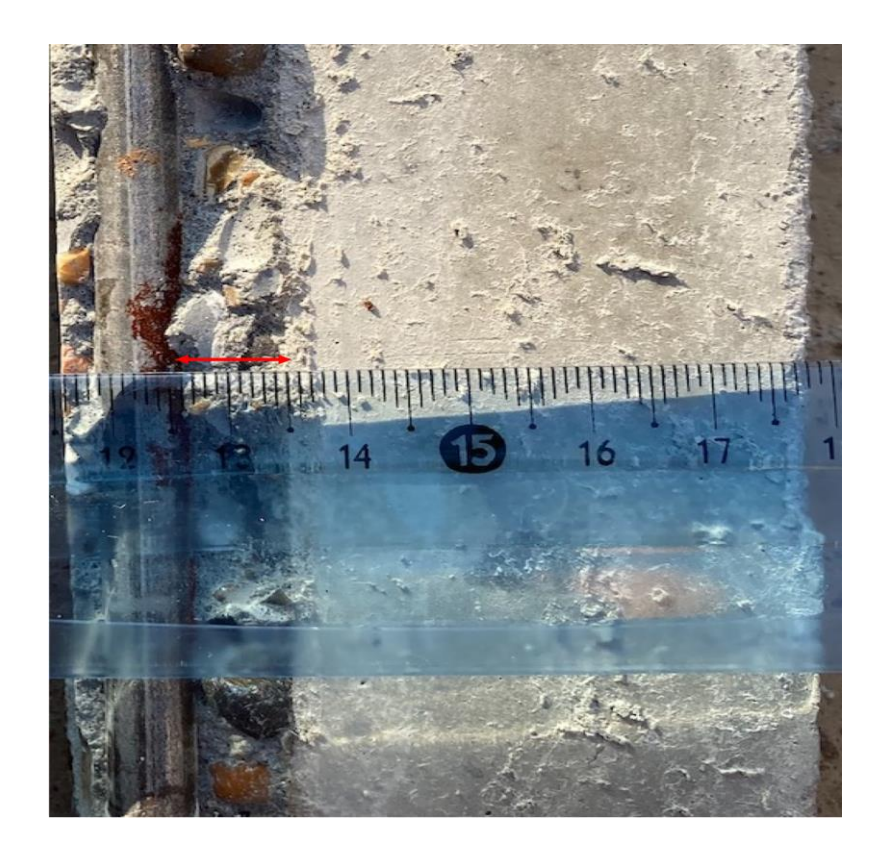


Fig. 5.11 The distance between the bottom of the shim and the top of the mild steel bar.

5.1.3 Type C

Type C specimens also consist of concrete slabs with the following dimensions: 350mm long × 300mm wide × 100mm deep. The slabs are reinforced with seven

longitudinal bars placed at two different levels arranged as shown in figures 5.12 and 5.13. The first level has 32mm deep concrete cover and consist of four 8mm diameter × 260mm long mild (Working Electrode) steel bars. The second level of reinforcement has 60mm deep concrete cover and contain three 10mm diameter × 260mm long stainless (Reference Electrode) steel bars. This two level reinforcement has been used in order to minimise the width and general size of the specimen. Similar to Type A and B specimens, both the mild steel and stainless steel bars were drilled at their ends and fitted with 3mm diameter wires.

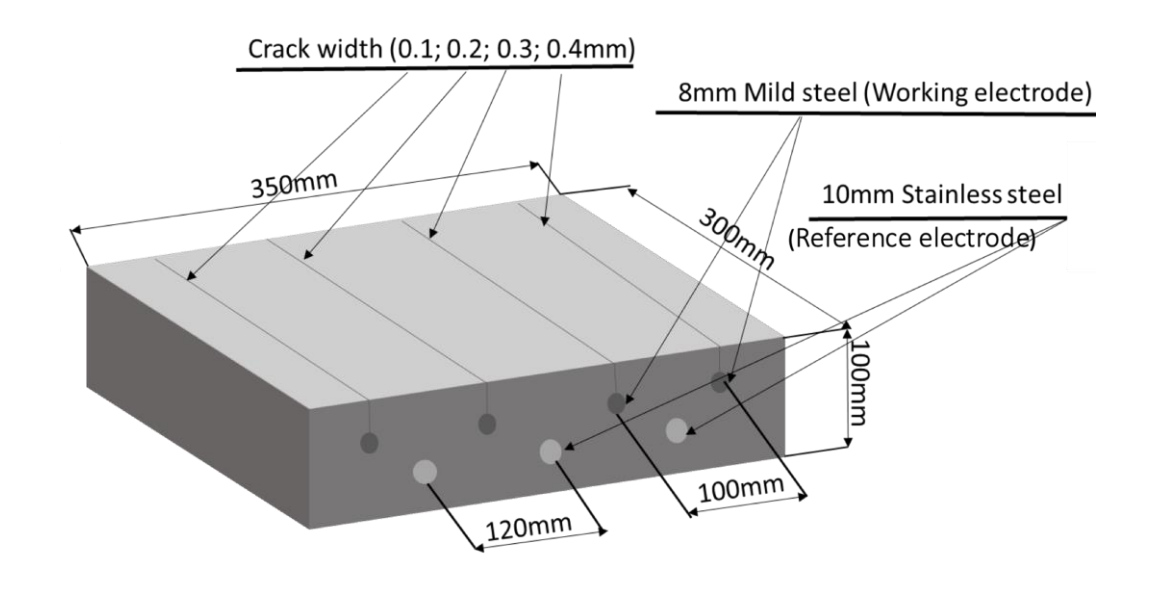


Fig. 5.12 Schematic of Specimen design C

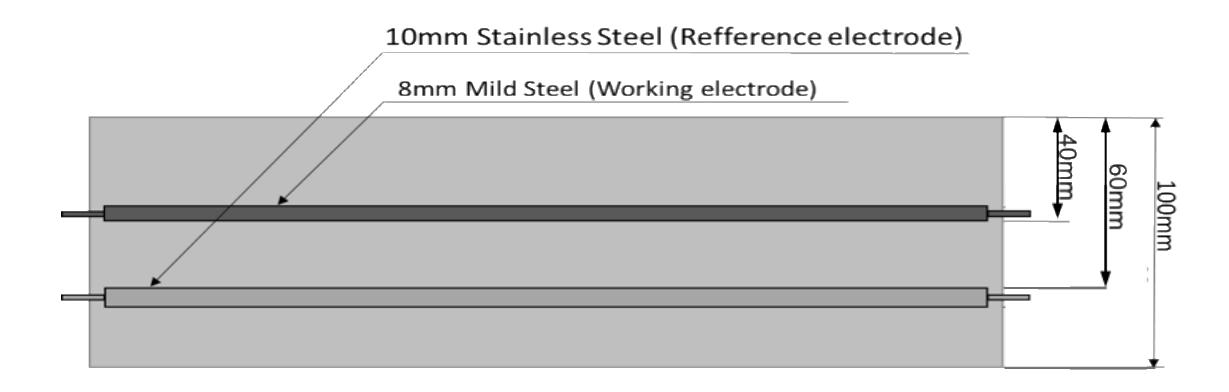


Fig. 5.13 Elevation view of reinforcement arrangement of the C test sample.

The working electrodes were cleaned by wire brushing, degreased with acetone and weighed prior to placing in the moulds. Indent letters were formed on one

end of the rods used as a working electrode, and their exact weight was taken in order to distinguish them at the end of the experimental work for obtaining final gravimetric weight loss. As in the type B specimens, the cracks were also formed above the mild steel bars artificially, however, this time there was no distance between the bottom of the shims and the top of the mild steel bars and the shims were touching the top surface of mild steel rods. Each mould had four slots for placing in the steel shims that would act as crack inducers and specimen with four different crack widths were produced. Thus, the cracks were formed by slotting in four oiled steel shims with 0.1mm, 0.2mm, 0.3mm and 0.4mm thicknesses into the mould and carefully placing the concrete around them. Type C specimens were produced using the same concrete mixture as previously cast specimens.

Photos of the moulds used (I), the method of crack induction (II, III and specimens after demoulding of type C specimens (IV) are shown in Figure 5.14.

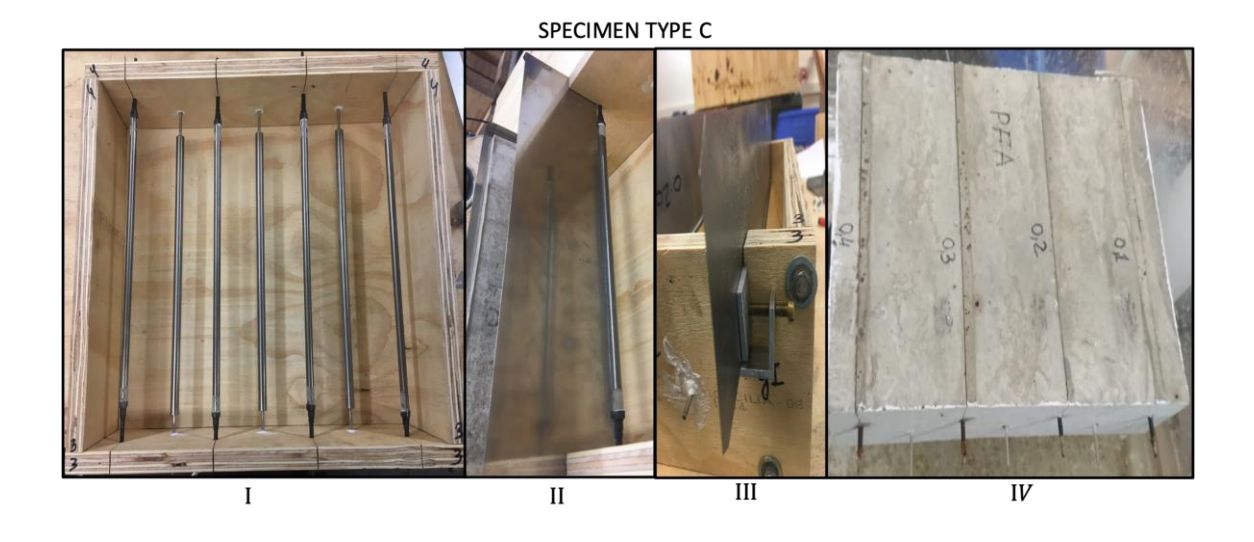


Fig. 5.14 Step-by-step progression of Specimen type C.

A better fixation arrangement for steel shims has been employed this time to prevent the movement of shims during casting (Figure 5.14, *III*). This arrangement was more successful in achieving the desired outcome as illustrated in Figure 5.15, where specimens have been opened along the crack and it was observed that the level of crack reached the reinforcement. C clamp has been used to secure the position of the steel shim in place during concrete casting).



Fig. 5.15 Crack-steel interface in the artificially created crack that reaches the rebar level, specimen type C.

5.1.4 The second set of specimens

About one and a half years later, another set of A2 and C specimens were cast at a later stage of the experimental period, thereby the first set of A specimens was denoted as A1. In total there are two type A specimens with different experimental exposure times such as A1 (older) and A2 (newer), type B specimens that were cast at the same time as A1 specimens and type C specimens which have been cast together with A2 specimens.

The primary reason was the thought of examining the effect of crack depth that stop on top of the reinforcement (type C specimens). Initially, two crack depths were considered to be studied A1 and B where cracks extend the rebar level and stop short before the reinforcement respectively. Upon careful literature review, it has been decided to study the effect of all possible coincident cracks present in practice. Thus, Specimen design A was treated as a representative of Flexural cracks, specimen type B formed due to Plastic shrinkage and type C specimens as Plastic settlement cracks.

Another reason was the storage space in Fluid's lab became available where type C and A2 specimens could be stored under the right conditions. The reason for casting the second set of A specimens was to have sample replicates to ensure the confidence of results.

Chapter 5 Methodology

Thereby A1 and B specimens were exposed to an aggressive environment longer (36 months), while the set of A2 and C specimens were exposed for 14 months.

5.1.5 Mix proportions and test details

The mix proportions of the concretes used in Type A and Type B specimens are shown in Table 5.1. The specimens were manufactured using three cement types: 100% PC (Mix 1), 65% GGBS /35% PC (Mix 2) and 30% FA /70% PC (Mix 3). The replacement ratio was decided not based on the constant compressive strength, but by keeping the percentage of replacement constant. This approach has been employed by other researchers such as (Poursaee & Hansson, 2008; Stillwell, 1988).

Table 5.1. Summary of concrete mix proportions

Test Reference	100% PC	65% GGBS /35% PC	30% FA /70% PC
rest Reference	Mix 1	Mix 2	Mix 3
PC	1.00	0.35	0.70
GGBS	-	0.65	-
FA	-	-	0.30
Sand	2.15	2.15	2.15
Aggregate (10mm)	1.64	1.64	1.64
Aggregate (20mm)	2.34	2.34	2.34
w/b	0.55	0.55	0.55
7-day compressive strength (N/mm²)	29.4	16.3	16.5
14-day compressive strength (N/mm²)	33.0	22.2	22.7
28-day compressive strength (N/mm²)	39.5	26.9	28.0

The chemical and mineralogical composition (in percentage) of the binders employed in the current investigation are provided in Table 5.2

Table 5.2 Chemical composition of the binders (%)

Binder type	MgO	Al2O3	SiO2	SO3	K2O	CaO	TiO2	V2O5	MnO	Fe2O3
PC	1.14	3.96	17.2	4.27	0.86	70.1	0.39		0.04	2.95
GGBS	8.12	12.3	34.1	2.59	0.56	44.2	0.96	0.02	0.25	0.41
FA	2	22.9	50.3	0.58	3.55	3.38	1.15	0.06	0.08	8.17

In total, there were six Type A specimens cast, fifteen Type B and 12 Type C specimens as summarised in Table 5.3. In Type B specimens cracks of the same widths were formed on both sides of the specimens, this was done to reduce the size of the specimens as there was extreme storage space shortage in the `laboratory. The same applies to specimen type C, where one specimen made of PC for example contains 4 different crack widths (0.1, 0.2, 0.3, and 0.4mm).

Here it can be seen that there two Type A specimens (A1 and A2) were made of the same concrete mixture design with a maximum surface crack width of 0.4mm, however they were cast at different times. The results of these tests will be used to assess the effect of natural coincident cracks that exceed the reinforcement level on corrosion behaviour (Flexural cracks).

Table 5.3. Test details

Test Ref	Mix	Crack width (mm) Number of specime	
A1	PC	≤ 0.4	1
A1	GGBS	≤ 0.4	1
A1	FA	≤ 0.4	1
A2	PC	≤ 0.4	1
A2	GGBS	≤ 0.4	1
A2	FA	≤ 0.4	1
В	PC	0	2
В	PC	0.1	2
В	PC	0.2	2
В	PC	0.3	2
В	PC	0.4	2
В	GGBS	0	2
В	GGBS	0.1	2

В	GGBS	0.2	2
В	GGBS	0.3	2
В	GGBS	0.4	2
В	FA	0	2
В	FA	0.1	2
В	FA	0.2	2
В	FA	0.3	2
В	FA	0.4	2
С	PC	0.1	1
С	PC	0.2	1
С	PC	0.3	1
С	PC	0.4	1
С	GGBS	0.1	1
С	GGBS	0.2	1
С	GGBS	0.3	1
С	GGBS	0.4	1
С	FA	0.1	1
С	FA	0.2	1
С	FA	0.3	1
С	FA	0.4	1
Total			51

Type B specimens were all made using three different cement types and had crack widths of 0mm, 0.1mm, 0.2mm, 0.3mm and 0.4mm. The results from Type B specimens will be used to investigate the effect of artificial cracks that don't reach the reinforcement but the crack width at the end of the crack was different. This crack type can be representative of Plastic shrinkage cracks.

Type C specimens were also made of all three cement types and had crack widths of 0.1mm, 0.2mm, 0.3mm and 0.4mm. The result from type C samples will be used to evaluate the effect of artificial cracks that reach the rebar and stops on top of it. This type of crack can represent Plastic settlement cracks.

5.1.6 Casting and curing

All specimens were cast in timber moulds and compacted by vibration. The specimens were initially cured in their moulds under polythene sheeting for 24 hours. The next day specimens were demoulded and allowed to continue curing by covering with damp hessian for further 6 days. At the end of these curing

periods the specimens were conditioned by storing in covered steel tanks (RH = 95%, temperature = 20°C) until they reach an age of 28 days.

Type A specimens were cracked between 28-31 days.

The oiled steel shims were removed from Type B and C specimens 6 hour after casting.

Four 100x100mm cube specimens were cast from each concrete mix. They were cured and conditioned in the same way as Type A, B and C specimens and tested after 28 days in order to establish the compressive strength of each mix.

5.1.7 Sealing

The surface sealing treatment is used to prevent moisture evaporation, to avoid concrete drying out under dry environment. The surfaces of samples were kept clean and dry before the start of application of sealant. All sample sides, except the top surface, were sealed by several layers of Sikagard resin. It is a one component solvent containing coating, used for moisture control and protection against ingress of substances on the concrete surface.

5.1.8 Corrosion initiation

Base half-cell potential, LPR and ZRA readings were taken before application of NaCl solution. Thereafter, the surface of the specimen along the cracks were sprayed with 3.5% NaCl solution once a week in order to initiate corrosion of the underlying steel bars.

5.2 Measurement techniques

For deriving the corrosion state of reinforcing steel, the most preferential methods are found to be non-destructive electrochemical techniques. They allow monitoring the reinforcement corrosion condition of the structure during their service life. The most popular electrochemical techniques in use today are open circuit potential (OCP), linear polarization resistance (LPR) and zero resistance ammeter (ZRA) methods, or more sophisticated ones such as electrochemical impedance spectroscopy (EIS), cyclic voltammetry (CVA), and etc. However, the

accuracy of these techniques in laboratory environments is not always equivalent for large concrete members in field conditions. Additionally, obtained values through monitoring can be difficult to interpret to quantitative corrosion rates, due to various influencing factors such as concrete cover, crack frequency, crack width, loads and general environmental conditions such as temperature and humidity. For determining the corrosion state of reinforcement in this work, three techniques have been used: Half-cell potential (OCP), Linear Polarisation Resistance (LPR), and Zero Resistance Ammeter (ZRA).

All of these techniques have benefits and drawbacks that are discussed further.

5.2.1 Corrosion monitoring

The instrument used for assessing corrosion degree of reinforcement, is GILL AC 2, provided by the company ACM Instruments. The equipment offers a Potentiostat, Galvanostat and Zero Resistance Ammeter with integrated Frequency Response Analyser and Sweep Generator in one. Electrochemical tests such as OCP, AC Impedance (EIS) and standard DC tests including LPR and current and voltage noise can be performed. The corrosion measurements were taken on a monthly basis since there were two sets of specimens cast at different times, Specimen types A1 and B had 36 measurements while types A2 and C specimens were tested 14 times.

5.2.2 Open circuit potential (OCP) or Half-cell potential

Open circuit potential has been a widely used standard and very straightforward technique in determining the corrosion state of rebar in concrete whether it is passive or active. This technique cannot be used to determine the amount of corrosion however can be used as an indicator of corrosion probability. Simply put, it allows the measurement of the voltage difference between embedded steel reinforcement and a reference electrode.

5.2.2.1 How it works

The reference electrode which can be external or internal (embedded into concrete) forms one half of the cell and the reinforcing steel (working electrode)

forms the other half, thus potential readings in millivolts can be obtained between the two half cells giving an indication of possible corrosion.

5.2.2.2 Interpretation of results

Obtained potential values can be interpreted by using (ASTM C 876, 2015) standard. The standard provides general guidelines for evaluating corrosion probability for different reference electrodes. They can be seen in Table 5.4, which gives estimated threshold values of potential indicating various degrees of corrosion.

The values on the standard were developed empirically in the USA and are widely used, however, they are based on test results of a regular concrete with cover thickness between 40 and 60mm. The guidelines may vary according to the environmental conditions and interpretation of results may need to be modified as well (Qian & Cusson, 2004). The readings of OCP may also be affected by electrical discontinuity of rebar, the presence of stray currents, chloride concentration, degree of saturation of concrete, electrical resistance and cover depth of concrete, ect. (Assouli et al., 2013). Thus, values of severe corrosion will vary in each case, however, more negative values correspond to higher corrosion risks (Qian et al., 2003). Therefore, it is necessary to conduct other non-destructive techniques simultaneously that can show corrosion rates, as OCP results can be misinterpreted (Assouli et al., 2013).

Table 5.4. ASTM criteria for corrosion of steel in concrete for different standard reference electrodes (Broomfield, 2006).

Copper/copper sulphate	Silver/silver chloride 1.0M KCL	Standard hydrogen electrode	Calomel	Corrosion condition
> - 200 mV	> - 100mV	+120 mV	> - 80 mV	Low (10% risk of corrosion)
> 200 to	- 100 to	+120 to	- 80 mV to	Intermediate
-350 mV	– 250mV	- 30 mV	-230 mV	corrosion risk
< -350 mV	< - 250 mV	- 30 mV	< -230 mV	High (> 90% risk of corrosion)
< -500 mV	< - 400 mV	- 180 mV	< -380 mV	Sever corrosion

5.2.2.3 Limitations

As mentioned above the conditions and environment of the place where measurements are taken affect the readings to varying degrees. Below is the list of possible error sources (Broomfield, 2006):

- Contact surface the surface of the concrete needs to be clean of contaminants, but it also needs to be wet to allow the flow of ions;
- Degree of saturation of concrete the lack of oxygen leads to a very negative reading;
- Presence of other metals other metals in the concrete can distort potential measurements;
- Stray currents nearby sources of DC can lead to shifts in potential;
- Electrochemical protection— cathodic protection, electrochemical chloride extraction and electrochemical realkalization are designed to shift the potential of the steel;
- Chemical contaminants any contamination leading to anodic or cathodic reactions on the steel surface cause misleading interpretation of potential measurements;

In this work, OCP measurements are performed with a Silver/silver chloride reference electrode and are taken before application of any NaCl solution in order to see the shift of potential to more negative value, then the testing is performed once a month. For type A (slab) specimens, the measurements are taken at three points and the distance between each point is ~70mm as well as specimen type C as the length of the working electrode was identical in both specimens. Depending on the starting point, the locations of testing positions are denoted as "close, middle and far", as shown in Figure 5.16.

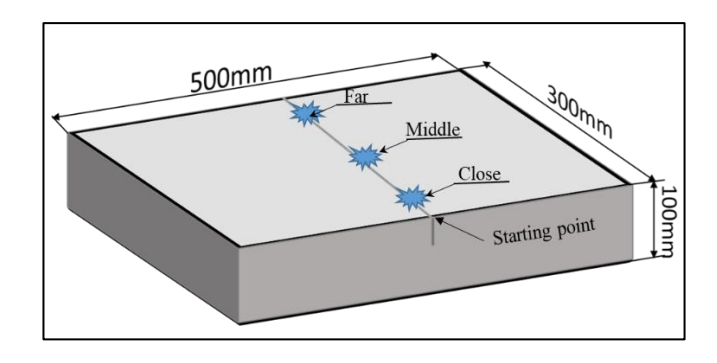


Fig. 5.16 Testing positions in slab specimens.

Type B beam specimens consists of two parallel sided cracks and the readings are taken from 5 points on each side as shown in Figure 5.17. The distance between each point is ~70mm. At the end of measurements the average result is taken.

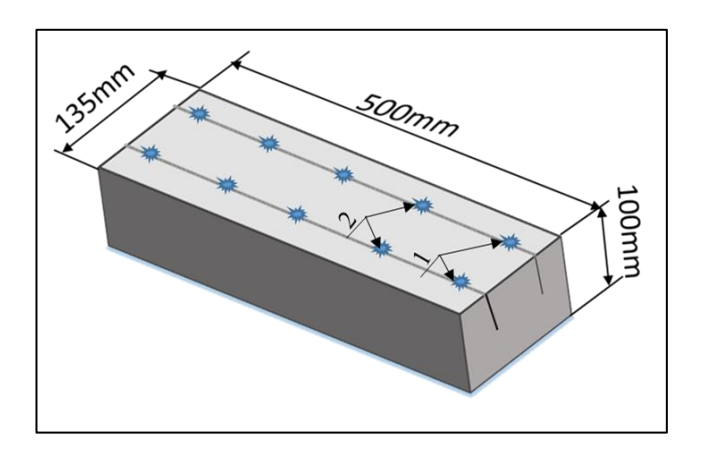


Fig. 5.17 Crack formation in type B specimens and measurement points.

Additionally, to OCP, in this work corrosion is monitored by Linear polarisation resistance and Zero resistance ammeter on a monthly basis.

5.2.3 Linear Polarization Resistance

5.2.3.1 How it works

LPR is another widely used and relatively straight forward technique that derives corrosion current of the reinforcement and corrosion rate can be calculated accordingly in real time. The working principle behind this technique is polarising the rebar where corrosion is expected to take place (working electrode) by applying an electric current in a range of at least ±10 mV and monitoring the response of reference electrode potential. Thus, ionic current has to pass

between the counter and the working electrodes through a low resistance connection and monitored by potentiostat. The chosen reference electrode should be kept stable during the test, in order to monitor and maintain potential at the working electrode (Broomfield, 2006). An example of schematic curve of linear polarisation resistance can be seen from Figure 5.18.

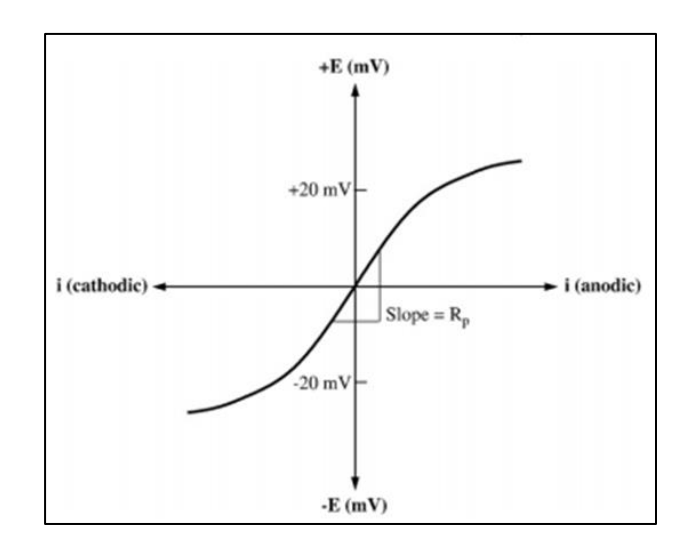


Fig. 5.18 Linear polarisation curve (Poursaee, 2010)

Polarisation resistance is the resistance of steel rebar during the application of external potential and can be calculated by the slope of the linear regression as shown in the graph (Eq. 3-1). Further, Stern-Geary equation (Eq. 3-2) can be employed for corrosion current calculation. The B value can be determined experimentally (Eq. 3-3) (through PDP tests and Tafel plot analysis) or a constant value of 26 mV for actively corroding state of rebar or 52mV for passive cases can be taken for calculation purposes. Thereafter for corrosion current density, i_{corr}, calculations (Eq. 3-4), the surface area of rebar that has been polarised should be known accurately.

$$Rp = \frac{\Delta E}{\Delta I}$$
 Eq. 5.1

$$Icorr = \frac{B}{R_p}$$
 Eq. 5.2

$$B = \frac{\beta a * \beta c}{2.3(\beta a + \beta c)}$$
 Eq. 5.3

$$icorr = \frac{Icorr}{A}$$
 Eq. 5.4

5.2.3.2 Interpretation of results

The equipment (ACM Instruments ,2000) used for corrosion monitoring in this work, allows the automatic conversion of the results to corrosion rate readings in µm/yr. Corrosion rates can be analysed using tables similar to the corrosion potential values which are provided by (ASTM C 876, 2015). While performing LPR tests, the corrosion potential and corrosion rate of the reinforcement can be obtained at once. For more accurate determination of corrosion rates, it is advised to use guard ring, device that can control the area of steel being polarised, hence more accurate value is derived. Criteria for corrosion rate values is shown in Table 5.5 as recommended by (Rodriguez et al., 1994).

Table 5.5. Interpretation of corrosion rate (Rodriguez et al., 1994)

Current density: μA/cm ²	Corrosion state
< 0.1	Passive condition
0.2-0.5	Low to moderate
0.5-1.0	Moderate to high
> 1.0	High

5.2.3.3 Limitations

Test conditions- During LPR measurements, the temperature and relative humidity of the surrounding environment affects the results (Broomfield, 2006).

Stern-Geary constant - The Stern-Geary constant B has a significant effect on the accuracy of calculated corrosion rate (Escudero et al., 1985). Constant values are suggested depending on the state of steel being actively corroding or passive which correspond to 26 and 52mV respectively (Poursaee, 2010). These values are a simplification, as they are derived from steel saturated in Ca(OH)₂ solution, which presumably represents concrete pore solution. Some other values of 125mV and 191mV are suggested, which depend on whether the concrete is moist or at ambient humidity respectively (Alonso et al., 1998). (Poursaee, 2010) states that the Stern-Geary constant is highly affected by anodic and cathodic

reactions, which are themselves affected by the conditions of the surroundings. However, in case when advanced testing equipment and software are available, the constant B can be derived from an equation based on βa , βc extrapolated from the Tafel Slope (Rodrigues et al., 2020).

Area of polarised steel - Numerous authors have shown a lot of evidence to suggest that the current flowing from the auxiliary electrode is unconfined and can spread over an unknown or larger area of steel than expected (Feliu et al., 1989). Thus, the accuracy of polarised surface area of steel is important as it will result in an error in the calculation of the corrosion current density. This in turn, will produce wrong assessment of the condition of the structure under investigation (Andrade et al., 2004). To overcome this problem, guard rings can be used to confine the polarisation area of steel, however in cases where deep concrete covers are used, it cannot be achieved (Flis & Pickering, 1998).

iR drop - iR compensation might be necessary when Linear Polarisation Resistance measurements are taken, for deriving numerical results such as corrosion rate (Rodrigues et al., 2020). To determine whether it is necessary or not, two data curves with and without iR compensation should be compared, and if the curve changes significantly between the two, compensation is required. An underestimation of iR drop can result in overestimation of polarisation resistance and incorrect corrosion currents (Dhir & Newlands, 1999).

5.2.4 Zero resistance ammeter (ZRA)

5.2.4.1 How it works

Galvanic current for corrosion assessment can be used when anodic and cathodic areas are located separately (macrocell) (Rodríguez, 1999). The working principle of this technique involves a connection of working and reference electrodes and measurement of macro-cell current through ordinary multimeter (Isgor et al., 2019). Simply put, it is a measurement of voltage drop taking place across a shunt resistor in the circuit. According to Ohm's law, voltage is proportional to current, thus, the current flowing in the circuit can be estimated (Oelßner et al., 2006). However, owing to a voltage drop (caused by resistance in ammeter), measured current by ammeter is lower than the true galvanic current (Nayak & Hostel, 2013). This can be solved by using a zero resistance ammeter.

Chapter 5 Methodology

The Zero Resistance Ammeter applies a voltage across the resistor within the instrument that is exactly equal to the voltage drop across the resistor to ensure that the current measured in the circuit is the correct one (Oelßner et al., 2006).

5.2.4.2 Interpretations of results

The current measured is simply the reverse current. From this, the corrosion current density can be derived if the area of steel being investigated is known. Calculated corrosion current can be converted to weight loss at the time of the measurement using Faraday's law (Eq. 3-5) of electrolysis.

$$m = \frac{I_{corr} \times t \times a}{n \times F}$$
 Eq. 5.5

where

Icorr is the corrosion current measured at time t

t is the time the voltage is applied for

a is the atomic weight of steel (56)

n is the number of equivalents exchanged (generally 2)

F is Faraday's constant (96 500 coulomb/equivalent) (Dean & Poursaee, 2011)

ZRA measurement are performed using GILL AC 2 as other measurement techniques mentioned above. The schematic of the test set up is shown in Figure 5.19.

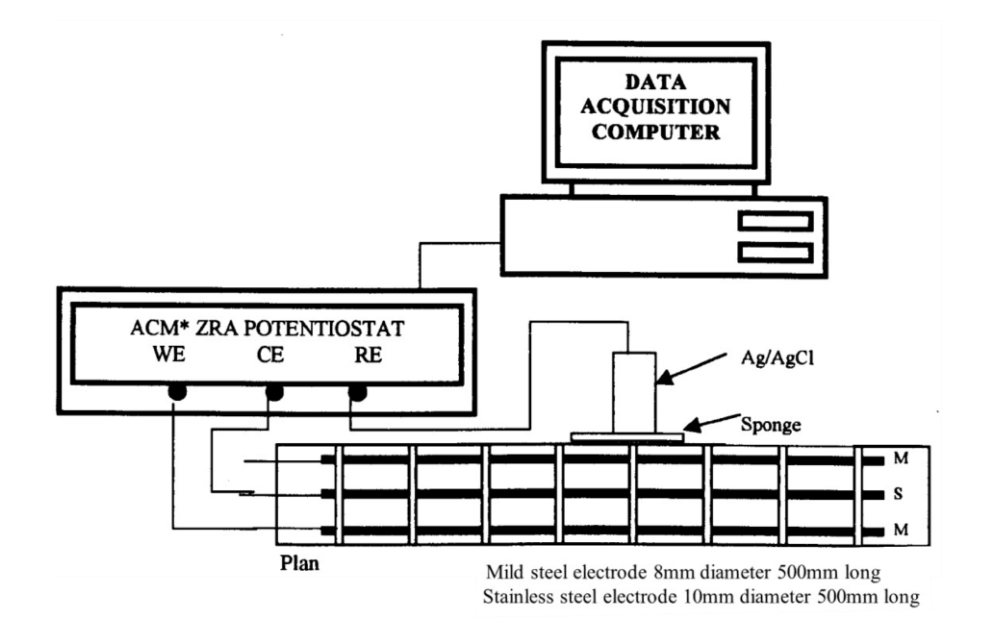


Fig. 5.19 Schematic of ZRA performance for the beam specimens.

5.3 Chloride profile

The chloride content in the concrete samples was determined using X-ray fluorescence (XRF) spectrum analysis by Bruker S8 Tiger. The manual of the equipment provides an extensive explanation of the procedure and can be found in two languages here (BRUKER, 2009; Spectrometer, 2008). This method identifies the total concentration of the chloride by measuring the solid state of the pressed powder. The precision of the results is found to be better than other available techniques (Bing Qi, Jianming Gao, 2017; Zhu et al., 2020).

Crushed concrete samples were oven-dried for 48 hours under 60°C, then after cooling down from crushed particles fine powder samples were obtained using a vertical spindle and pressed in a pressing machine into a tablet. The tablets then were subjected to XRF analysis. This technique has been used in a number of publications in determining the chloride content such as (Geiker et al., 2021). A detailed description and other advantages of the method can be found in the manual referred to above or through the company Bruker.

The specimens were transported to Kazakhstan (due to Covid 19) in order to complete the experimental work. Prior transportation, the specimens were wrapped with clean film and further wrapped with card board paper with several layers to ensure absence of contamination. Since the size and weight of the

specimens were large and heavy, their sides which were not of interest were trimmed at UCL prior to sending. The sizes of cut pieces are shown in Figure 5.21 Chloride profiles were determined in two different ways. From uncracked specimens, the dust samples were obtained out of four depth levels with 10mm intervals. This was achieved by drilling holes on top of the rebar and collecting the released powder from each 10mm increments. These powder samples were dried and milled further to increase the fineness level prior to testing. The schematic of the obtained samples from uncracked specimens is shown in Figure 5.20. However, from cracked specimens, chloride content was defined from two levels only: the top layer not reaching the rebar; and the lower level around the reinforcement. The chloride content in cracked specimens was identified from two levels only also due to Covid 19 when there was limited access to the laboratory and the equipment was heavily booked. The transferred specimens with reduced sizes were further cut into thinner blocks via an angle grinder (dry coring), after removing the reinforcement, the final size of the cut fractions are shown in Figure 5.21 with red dotted lines. Then those blocks were crushed further and milled into powder prior to testing using vibrating disc mill RS 200 for subsequent XRF analysis. The chloride content in uncracked samples was identified from two levels as well, in order to make a comparison with cracked ones, this is shown on the left side of the figure in a dotted red line as recommended in (Burkan Isgor et al., 2019).

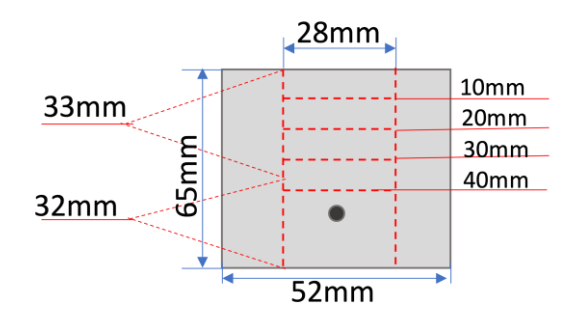


Fig. 5.20 Schematic of chloride profile depth on the right side shown as a red broken line.

Chapter 5 Methodology

The schematics of the samples made for chloride content determination in cracked concrete is shown in Figure 5.19. Since there were three different crack depths in specimen designs A, B and C, the top and bottom levels differed slightly.

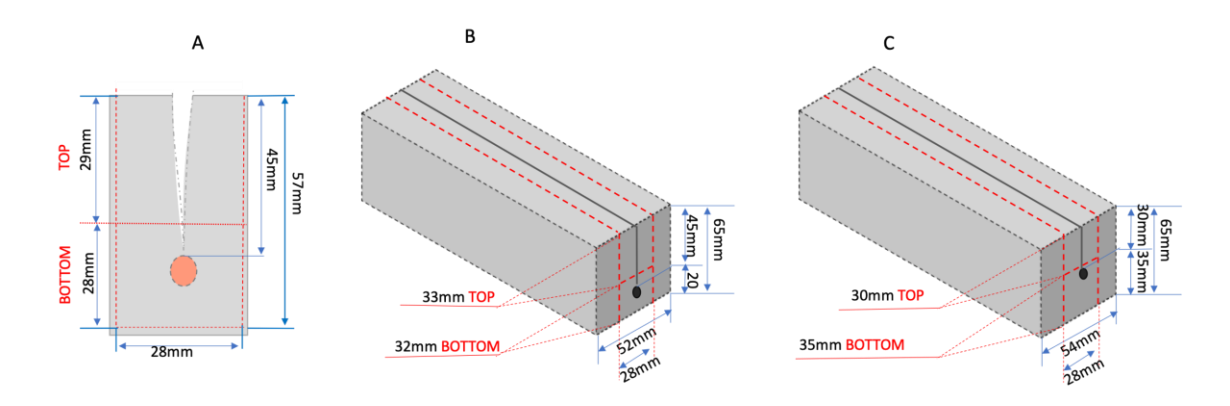


Fig. 5.21 Schematics of chloride determination levels in cracked specimens.

The chloride content was determined from three samples and the results were averaged.

5.4 Gravimetric mass loss

The Gravimetric mass loss of reinforcement due to corrosion was obtained following recommendations in (ASTM G 1 – 03, 2017). The Clark's solution was prepared by combining 1000 mL hydrochloric acid (HCl, sp gr 1.19), 20 g antimony trioxide (Sb2O3), and 50 g stannous chloride (SnCl2). This solution allows the removal of rust from the reinforcement surface at environmental temperature of 20- 25°C. Due to a high concentration of the hydrochloric acid, the whole procedure was completed strictly under a ventilation chamber. It took around 15 minutes to clear the surface of each rebar from rust by brushing it under the constantly stirred solution. The weight of the rebars were identified prior to casting of specimens, so that their gravimetric mass loss was determined accurately at the end of the experiment. Each reinforcement was labelled with letter on one end of the rebar, this was done to distinguish them at the end of the experimental work when specimens were broken open. The weight of rebars after the pickling has been determined by weighting them on scales with an appropriate precision as shown in Figure 5.20. The weight differences were

determined via equations provided in standard proceeding (ASTM G 1-03, 2017).



Fig. 5.22 Analytical grade scales used to determine the weight of rebars after the pickling with Clarck's solution.

5.5 Statistical analysis

For investigating the effects of crack width, crack depths and cement type on corrosion rates, statistical analysis is essential (ASTM International, 2014) as the results may show some differences however it is impossible to judge the extent of the variations with certainty. Thus, statistical tests such as ANOVA test of variance is useful in determining the influence of above-mentioned crack parameters on corrosion of reinforcement (Nieves-Mendoza et al., 2012).

ANOVA is an omnibus test and is used to test the null hypnotises that is "all group means are the same". In case the p-value obtained from ANOVA is significant the null hypothesis is rejected, meaning that at least one of the means in the group is significantly different from the rest. However, this test does not identify which ones out of all group means (e.g., which corrosion rates obtained from specimens with various crack widths are significantly different from each other) are different. Thus, there is a need for a follow-up test called a Post-Hoc Test (Hair et al., 2019).

The Post-Hoc test was used to compare pairs of all possible group combinations. There are several Post-Hoc tests, and Tukey's honestly significantly different (HSD) test is one of the most commonly used ones (Lee & Lee, 2018), also all group sizes analysed in this study was the same hence the selection of Tukey's HSD test (Chen et al., 2018). Thus Tukey's (HSD) test was followed up when ANOVA resulted in a significant p-value. Tukey's HSD test provides a deeper insight into the differences in significance level between all crack widths. This test uses pairwise post-hoc testing to define whether there is a difference between the means of all possible pairs using a studentized range distribution. Thus, it is useful in determining the significance level of every possible combination between all crack widths and other variables examined in this work.

To conduct ANOVA test, a data table was created where the results were arranged in a tabular format with the group variable and the outcome variable. Each row in the table represents an observation, and each column represents a variable. The first column contained the group labels, and the following columns contained the corresponding outcome values for each observation (Nieves-Mendoza et al., 2012). The software used for statistical analysis was R- Studio, it is a powerful and widely used tool for analysing the data statistically and visualising it in graph form. The tabulated data (of Half-cell potential reading as well as LPR and ZRA readings) used in this research is provided in Appendix A for all statistical analysis. Since R-Studio requires a specific arrangement of data to be analysed as an input to the software, all data is provided in a right format in Appendix B. Moreover, the software requires a certain code to execute the analysis, the codes used in this research are provided in Appendix C. The HSD test was performed after ANOVA simply by writing the necessary code and running the test.

Illustrating the estimated corrosion rate results obtained through two measurement techniques such as LPR and ZRA was found to be suitable in a form of a Boxplot. Boxplots are useful to show the spread of the data as well as mean and median values. The box ranges from the first quartile to the third quartile of the distribution and the range represents the IQR (interquartile range). The "whiskers" on box plots extend from Q1 and Q3 to the most extreme data points called outliers. The mean value is shown as a red dot in the middle of the

Chapter 5 Methodology

boxplot and the value is presented next to it, while the median value is shown as a black line crossing the boxplot.

The results obtained from non-destructive corrosion estimation techniques such as LPR and ZRA were statistically analysed using ANOVA and Post-Hoc tests. Generally, the results were divided into three parts where

- a) effect of crack widths,
- b) influence of crack depths,
- c) impact of various cement types

were presented and discussed separately.

a) Statistical analysis of the data on the effect of crack widths on corrosion.

In the investigation of the effect of crack widths, only Type B and C specimens were involved, type A specimens were omitted because the cracks were formed naturally, and their width was not controlled.

Since there were four different crack widths (0.1, 0.2, 0.3 and 0.4mm) as well as uncracked specimens, in both type B and C specimens, ANOVA test of variance has been performed for each specimen design separately. They were performed separately because the crack depth was different between B and C specimens. ANOVA test was utilised for LPR and ZRA readings separately as those corrosion rate estimation techniques measure different types of (microcell and macrocell) corrosion.

Another variable in this experimental programme is the cement types used, the results were presented for specimens made of PC followed by samples made of GGBS and FA respectively. Thus, the results are presented in a table form for specimens made of PC first, containing observations obtained from LPR (shown on the left side) and ZRA (shown on the right side) measurement techniques for type B and C specimens.

b) Statistical analysis of the data on the effect of crack depth on corrosion.

When the effect of crack depths has been investigated, the order of analysis was slightly different from the one used to study the effect of crack width. Since

specimens were cast at two different times, the results were presented by grouping the specimens by their exposure time to the experiment. Specimens A1 and B were tested for 36 months in total, whereas specimens A2 and C were tested for 14 months. Thereby the results on the effect of crack depth for A1 & B specimens are presented first and followed by specimens A2 and C as they were cast at the same time later.

Only One-way ANOVA test has been performed when analysing the effect of crack depth on corrosion rate as there were only two groups of specimens (either A1 & B or A2 & C) being analysed, thus there was no need for Post-Hoc test to be followed up.

The results for all cement types followed a similar trend when effect of crack depth investigated. Thereby ANOVA results were presented for (A1 & B samples first and then for A2 & C) specimens in one table containing observations for all cement types in the following order: PC, GGBS and FA.

For examining the effect of crack depth, specimens with 0.4mm crack widths only were selected (among B and C specimens with various cracks), this is because the cracks in A1/A2 specimens were formed naturally and their width was secured to be no more than 0.4mm.

c) Statistical analysis of the data on the effect of cement type on corrosion.

When examining the influence of cement type on corrosion rates, ANOVA and Post-Hoc tests were used to analyse the results. The specimen design was fixed this time and the results are presented first for A1/A2 specimens made with all three cement types as a table for ANOVA outcome. It was then followed by Post-Hoc test on occasions when ANOVA test resulted in significant p-value. Specimens with 0.4mm crack widths were selected this time as well due to the same reason mentioned above.

Chapter 6 Results and Discussion

This chapter is divided into three sections as three aspects of coincident cracks on corrosion of reinforcement in concrete have been investigated in the current work.

The first aspect is the effect of crack widths on corrosion of reinforcement as this is one of the main defining characteristics of cracks on the surface of the concrete.

The next aspect studied is the depth of cracks, this is reasonable to investigate as depending on the type and cause of the cracking, the depths vary, which can give rise to different types and amounts of corrosion.

The final aspect is the influence of cement type on corrosion rates. This is important as the propagation of the corrosion process is related to the quality of the concrete surrounding the reinforcement. Also, current recommendations in codes of practice prescribe the use of blended cement, in concrete exposed to an aggressive environment.

6.1 Effect of coincident crack widths on corrosion of reinforcement.

The effect of crack width was investigated using two designs of specimen: B & C, each manufactured using three cement types: 100% PC, 65% GGBS /35% PC and 30% FA /70% PC. Both designs consisted of uncracked and cracked specimens with 0.1, 0.2, 0.3 and 0.4mm wide parallel-sided cracks. In type B specimens the crack stopped approximately 9mm above the steel reinforcing bars whereas in type C specimens the cracks extended to the surface of the bars. Corrosion was monitored using half-cell potentials, linear polarisation resistance (LPR) and zero resistance ammeter (ZRA).

The results obtained from corrosion rate estimates via LPR and ZRA are displayed on a boxplot which indicates the mean, median, spread and skewness of the data.

At the conclusion of the experiments, the steel reinforcing bars were removed from the concrete beams and used to determine the mass losses resulting from

corrosion. Photos of the bars were also taken and used to evaluate the position, extent and type of corrosion damage sustained by the bars.

Subsections 6.1.1 - 6.1.3 show respectively the results obtained for type B and C specimens made of 100% PC, 35% PC /65% GGBS and 70% PC /30% FA. The results are presented/discussed in the following order:

- Half-cell potentials
- Corrosion rates
- Gravimetric mass loss
- Photos showing condition of reinforcing bars

6.1.1 Specimens made of 100% PC

6.1.1.1 Half-cell potentials

Figure 6.1 shows plots of the half-cell potential measurements for types B and C specimens obtained using a silver-silver chloride reference electrode. As previously discussed, the half-cell method is a non-destructive technique for assessing the risk of corrosion. It does not provide an indication of the rate of corrosion. According to (ASTM C 876, 2015) half-cell potentials greater than -100 mV suggest a low (10%) risk of corrosion, between -100mV and -250 mV an intermediate risk, between -250 mV and -400 mV a high risk and values less negative than -400 mV a severe risk. To ease discussion of the results, these ranges have been added to Figure 6.1.

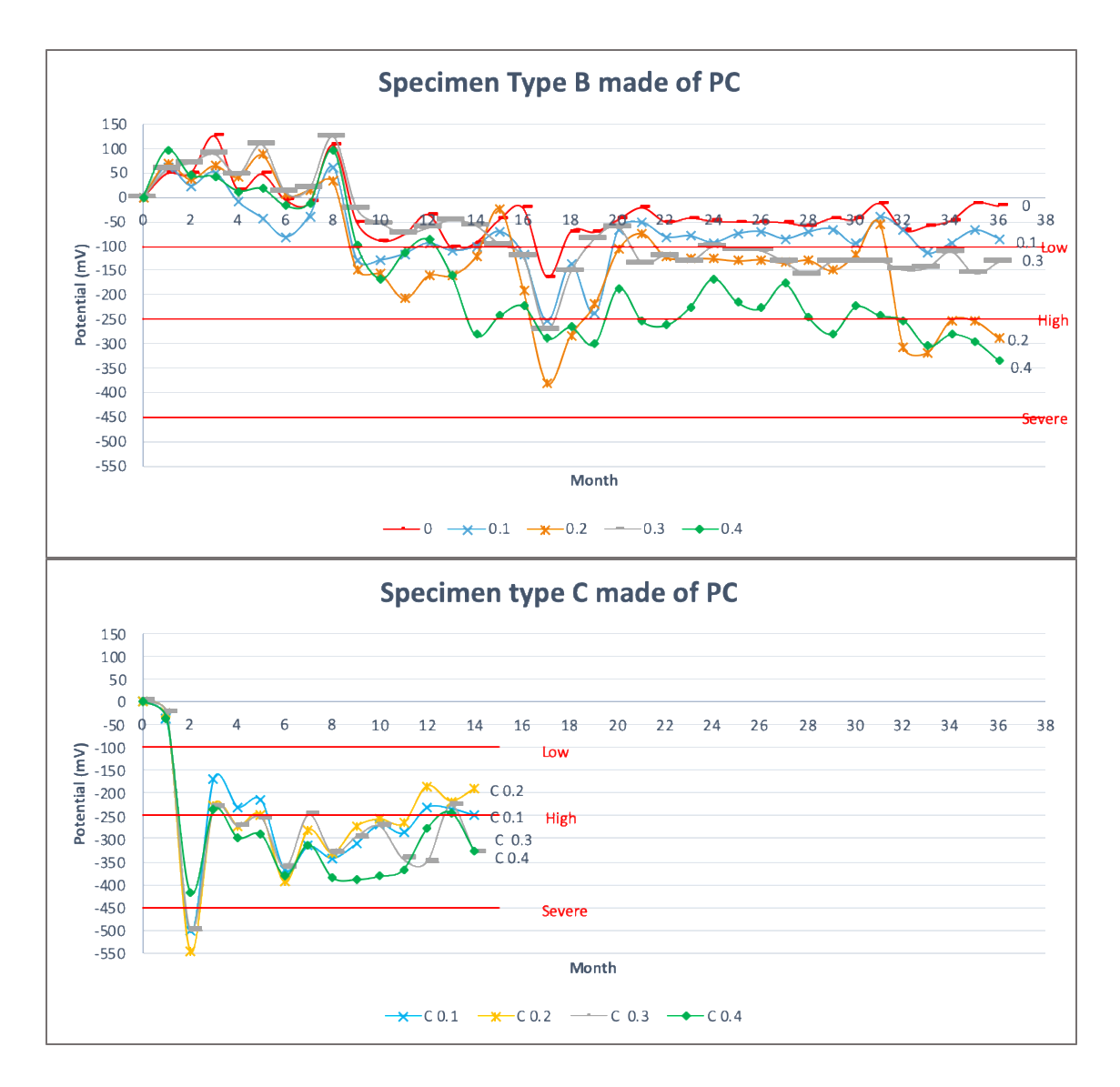


Fig. 6.1 Half-Cell potential readings for specimen types B and C made of PC with different crack widths.

The results for type B specimens suggest that corrosion initiation occurred at around 10 months from the start of the experiment. This is much longer than expected and was probably attributable to insufficient application of chloride solution to these samples. Concerns over ponding in cracks which could have affected the oxygen supply to reinforcing bars and hence corrosion rates led to this problem. Unfortunately, this cause was discounted when reviewing the experimental procedures and there was a delay in implementing corrective measures as mentioned on the methodology chapter.

Nevertheless, following corrosion initiation the half-cell potentials became more negative as expected. From Figure 6.1 it can be seen that the uncracked and

specimens with 0.1mm wide cracks remained at low risk of corrosion whereas specimens with crack widths in the range 0.2-0.4 experienced an intermediate risk of corrosion. In general, half-cell potentials were the least negative for specimens with crack widths of 0.1mm and most negative for specimens with crack widths of 0.4mm.

Corrosion was indicated in type C specimens from the second month onwards. This trend is reasonable given that the cracks extend to the surface of the reinforcing bars. Tests on these specimens began some 14 months after the tests on type B specimens. This meant that lessons learnt about the correct volume of chloride solution to apply to specimens were implemented right from the outset of this set of tests.

From Figure 6.1 it can be seen that these specimens experienced a very similar pattern of behaviour irrespective of crack widths and that in general all the specimens were at a high risk of corrosion throughout the test period.

6.1.1.2 Corrosion rates

Figures 6.2 and 6.3 show monthly readings of corrosion rate estimates for specimen types B and C made of PC measured via LPR and ZRA respectively. As it is evident from graph 6.2, the corrosion estimates show a good agreement with Half-cell potential readings shown above. Active corrosion seems to start from month 17 in specimen type B which can be confirmed by Half-cell potential results which indicate a high risk of corrosion for all cracked specimens except for control ones. Control samples revealed the least rate of corrosion risk which is also confirmed by Half-cell potential readings in Figure 6.1. Specimens with 0.4mm crack width ranged within high corrosion risk level according to Half-cell potential readings, however, corrosion rate estimates don't show a noticeable difference in trends compared with specimens with narrower crack widths, instead specimens with 0.2mm crack width showed the highest rates of corrosion towards the end of experimental work.

Corrosion rate estimates of Type C specimens also share generally good agreement with Half-cell potential readings. Since the crack reaches the reinforcement level, it seems like the passive film has broken down during the

first month of exposure to the aggressive environment, which is evident from Figure 6.1. where all specimens regardless of crack width exhibit high risk of corrosion.

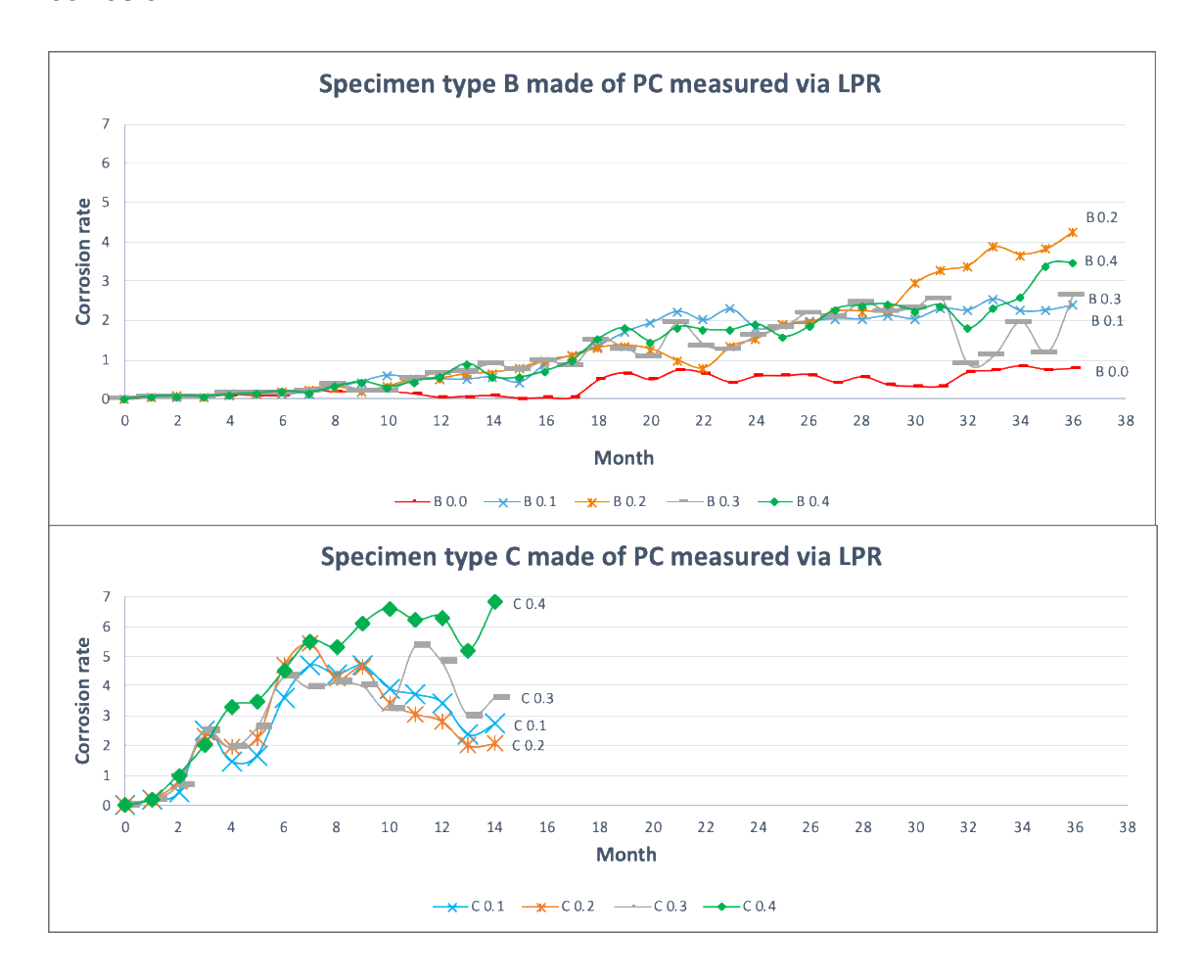


Fig. 6.2 Monthly Corrosion rate readings for specimen types B and C with various crack widths measured via LPR.

According to corrosion estimates obtained via ZRA, the results don't reveal a clear correlation with LPR results. This perhaps is attributable to the nature of macrocell corrosion being measured via this technique (Gu et al., 2018). Generally, based on type B specimen outcomes, some major fluctuations can be seen in the first 18 months of the experiment, mainly in specimens with 0.4 and 0.2mm crack widths, yet, the readings did stabilize during the next 16 months, then some minor fluctuations and increase in corrosion rate estimates took place. A high fluctuation after month 10 could be an indication of the decreased resistance between the rebar and reference electrode due to the formation of rust on the surface of the reinforcement. This decrease in resistance subsequently

could lead to those jumps in corrosion rates shown in the graph. This explanation is in a good agreement with Half-cell potential readings as they reached a low corrosion risk level starting from month 10. Further stabilization of corrosion rates could indicate the slowdown of corrosion process or stable rates, which is in a good agreement with half-cell potential readings except for specimens with 0.4mm crack width, which exhibited more negative readings.

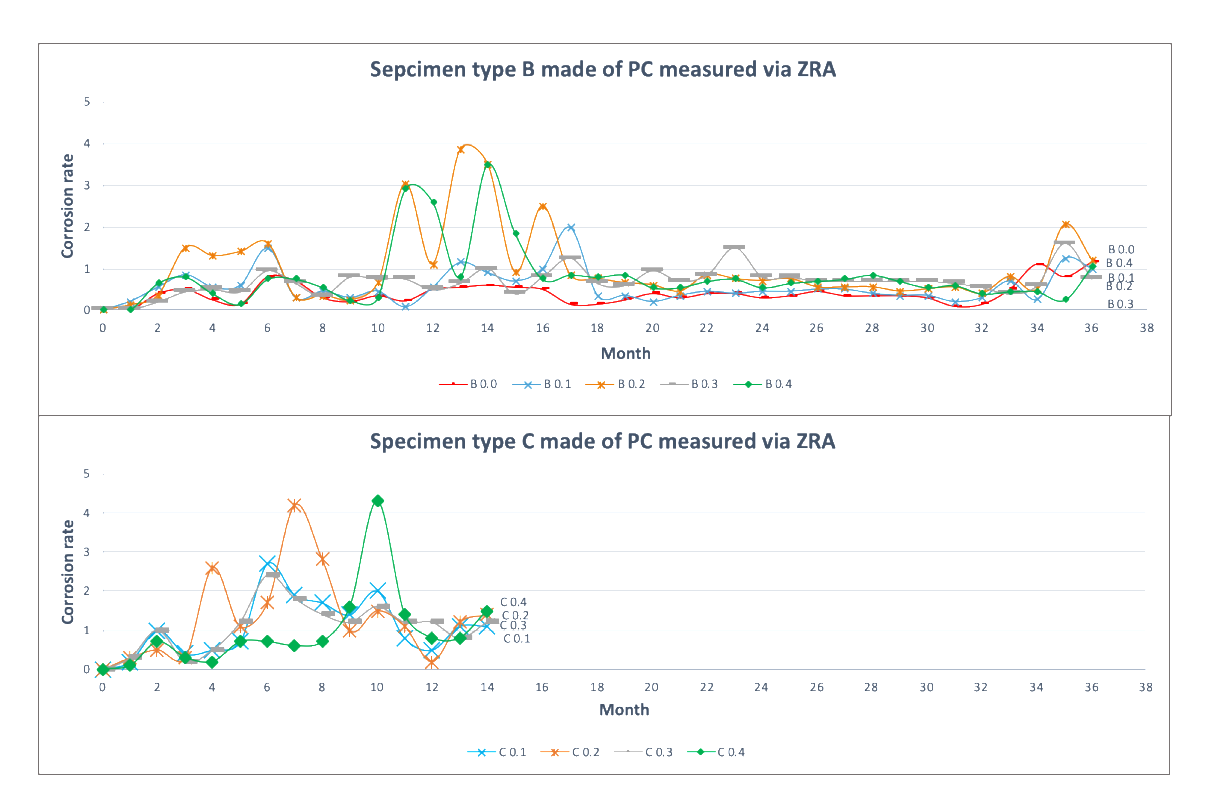


Fig. 6.3 Monthly Corrosion rate readings for specimen types B and C with various crack widths measured via ZRA.

Similar jumps can be seen in type C specimens, however, they are more pronounced starting from months 4-5, while in Half-cell potential readings to extremely negative from the first month onwards.

Although the LPR and ZRA measure different types of corrosion, the primary aim of this section is an investigation of the effect of crack width on corrosion of reinforcement. The question is, whether the corrosion rates increase as the crack widens, for this, an analysis of variance ANOVA test has been performed.

Table 6.1 shows the results of the ANOVA analysis on corrosion rates in type B and C specimens assessed using LPR and ZRA.

Table 6.1 ANOVA results for different crack widths in specimens made of PC and measured by both measurement techniques.

		Measurement	techniques	
Specimen	LPF	₹	ZI	RA
type	F Test statistic	Significance level	F Test statistic	Significance level
В	F(1)= 11.57	p < 0.05	F(1) =8.96	<i>p</i> < 0.05
С	<i>F(4)</i> = 11.15	p < 0.05	<i>F(4)</i> = 3.18	p < 0.05

Here it can be seen that both the LPR and ZRA results indicate that there is a significant effect of crack width on corrosion rate according to p-value. F-value is a statistic used to test the null hypothesis that the means of two or more groups are equal. It measures the ratio of the variance between groups to the variance within groups (Hair et al., 2019). In order to elucidate the precise nature of this relationship a Posthoc test - Tukey's HSD - was performed. This involves comparing the corrosion rates experienced by cracked and uncracked specimens as well as cracked specimens with each other. The results of this analysis are shown in Table 6.2. There are four different crack widths as well as uncracked specimens being examined, thus uncracked specimens have been denoted as 0.0 in the table.

The Posthoc test revealed that two measurement techniques (LPR and ZRA) show different outcomes. According to LPR results obtained from both type B and C specimens, there is a significant difference between uncracked and cracked specimens with every crack width, however, the difference in corrosion rates between specimens with 0.1, 0.2, 0.3 and 0.4 mm wide cracks are not significant.

Whereas ZRA results show slightly different outcomes, where significant differences are present between the following combinations: 0.2 vs 0; 0.4 vs 0; and 0.2 vs 0.1 in specimen design B and only a combination of 0.2 vs 0 in specimen type C. These differences in the results registered via two measurement techniques are likely to be due to the type of corrosion being examined such as microcell and macrocell (Ji et al., 2013).

Figure 6.4 shows boxplots produced from corrosion rates obtained non-destructively. The top two diagrams represent the corrosion rates of B specimen design, whereas the lower two diagrams illustrate the results for C specimen design. The graph on the left presents the spread of the data and the mean value (the figure in the middle of the boxplot) of the corrosion rates in each cracked specimen measured via LPR, while on the right side the same for ZRA measurements.

Table 6.2 Post Hoc Test of multiple comparisons on the effect of crack width on corrosion for specimens B and C made of PC measured via LPR and ZRA.

	Comparison	М	easurement	techniques	<u> </u>	
Specimen combinations between crack		Linear Polarisation Resistance			Zero Resistance Ammeter	
,,	widths 0; 0.1; 0.2; 0.3; 0.4	Mean Diff.	Sig.	Mean Diff.	Sig.	
	0.1 vs 0	0.91	<i>p</i> < 0.05	0.17	p = 0.60	
	0.2 vs 0	1.05	<i>p</i> < 0.05	0.60	<i>p</i> < 0.05	
	0.3 vs 0	0.74	<i>p</i> < 0.05	0.30	p = 0.75	
	0.4 vs 0	0.94	<i>p</i> < 0.05	0.34	<i>p</i> < 0.05	
В	0.2 vs 0.1	0.14	p = 0.96	0.43	<i>p</i> < 0.05	
Ь	0.3 vs 0.1	-0.16	p = 0.94	0.13	p = 0.78	
	0.4 vs 0.1	0.03	p = 0.99	0.17	p = 0.58	
	0.3 vs 0.2	-0.31	p = 0.61	-0.30	p = 0.08	
	0.4 vs 0.2	-0.11	p = 0.98	-0.26	p = 0.17	
	0.4 vs 0.3	0.19	p = 0.89	0.04	p = 0.99	
	0.1 vs 0	2.45	<i>p</i> < 0.05	7.52	p = 0.11	
	0.2 vs 0	2.45	<i>p</i> < 0.05	1.03	<i>p</i> < 0.05	
	0.3 vs 0	2.78	<i>p</i> < 0.05	7.52	p = 0.11	
	0.4 vs 0	2.30	<i>p</i> < 0.05	6.38	p = 0.23	
	0.2 vs 0.1	0.01	p = 1	2.78	p = 0.89	
	0.3 vs 0.1	0.33	p = 0.96	-4.44	<i>p</i> = 1	
С	0.4 vs 0.1	-0.15	p = 0.99	-1.14	p = 0.99	
	0.3 vs 0.2	0.32	p = 0.96	-2.78	p = 0.89	
	0.4 vs 0.2	-0.16	p = 0.99	-3.93	p = 0.70	
	0.4 vs 0.3	-0.48	p = 0.85	-1.14	p = 0.99	

Here it can be seen that the mean corrosion rates and the spread of results obtained via LPR are similar except for the uncracked specimens. However, the spread of results obtained via ZRA for type B specimens is rather erratic and has many outliers, especially in specimens with 0.2mm wide cracks. However, if we were to discount the outliers, the means are generally similar. The boxplots for type C specimens appear to exhibit similar trends.

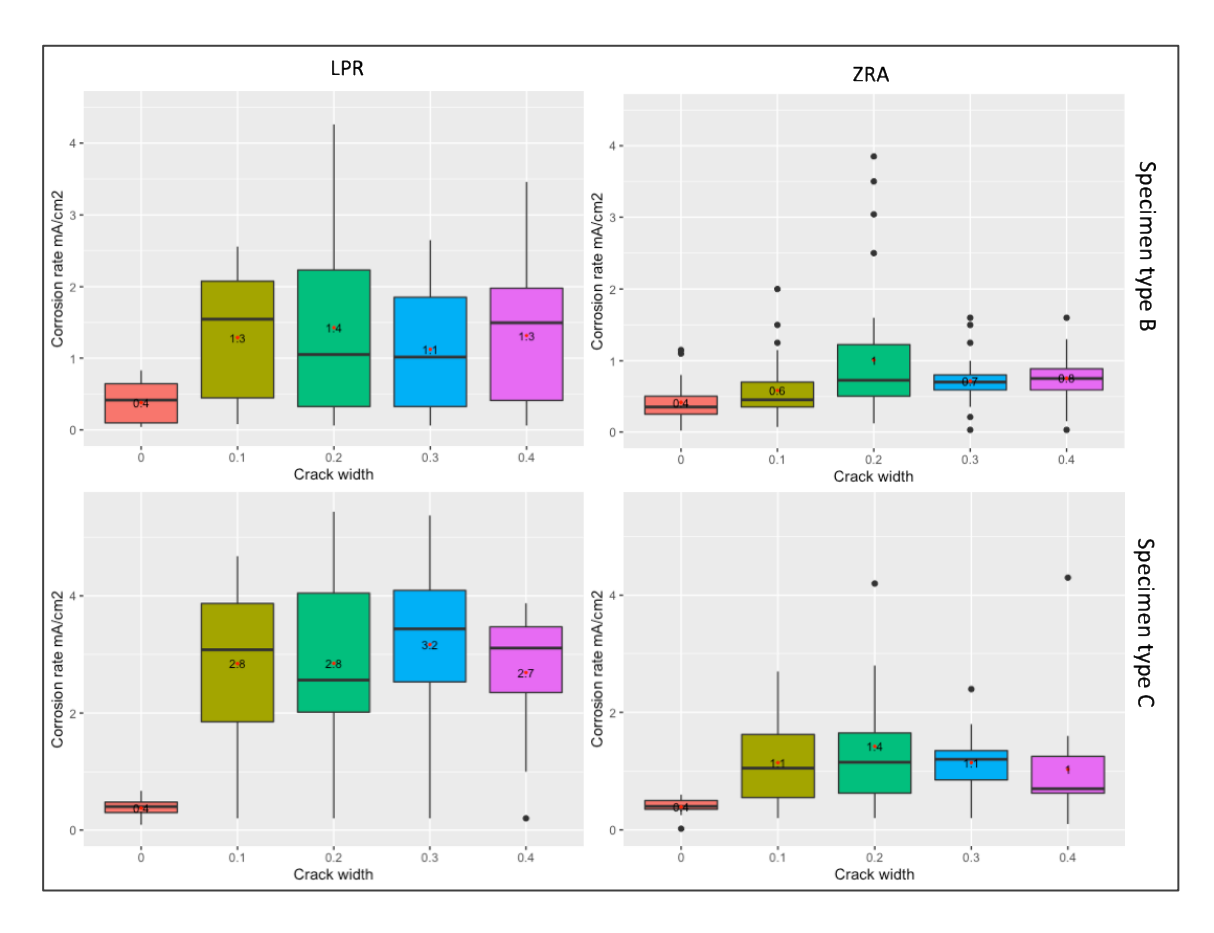


Fig. 6.4 Corrosion rates (μ A/cm²) experienced by specimen types B and C made of PC with different crack widths.

For the validity of the statistical analysis, the results were analysed for the last 3,6 and 9-month readings in isolation, graphs and ANOVA results are shown in Appendix D. The results for above mentioned months also confirmed the absence of a significant effect of the crack width range investigated in this work on the corrosion rate. This confirms the robustness of the statistical analysis employed above.

6.1.1.3 Gravimetric mass loss

At the end of the tests, the reinforcing bars were removed from the concrete beams and after pickling in Clark's solution the gravimetric mass losses were evaluated. Table 6.3 shows the results. It is worth noting that these measurements were made approximately 1.5 years after the termination of the experiments because of Covid 19. These results also appear to suggest there is no relationship between crack width and corrosion.

Table 6.3 Gravimetric mass loss of B and C specimens made of PC

Crack widths (mm)	Mass loss in (g) Specimen	Mass loss in (g) Specimens
Crack widths (min)	type B	type C
0.1	0.409	0.855
0.2	0.458	0.841
0.3	0.397	0.864
0.4	0.469	0.882

6.1.1.4 Photos showing condition of reinforcing bars

Figure 6.5 shows photos of a typical reinforcing bar from a type B specimen after splitting the concrete into halves (a), front and back of the rebar facing the crack (b and c), and after the cleaning of the rebar by pickling (d). Figure 6.6 shows the condition of a similar bar removed from specimen type C. From these figures, it can be seen that the bars in both types of specimens experienced rusting on both front and back faces. Moreover, it can be seen that the rust on the bar removed from the type C specimen is more extensive, which agrees with the gravimetric weight loss measurements presented in Table 6.3.

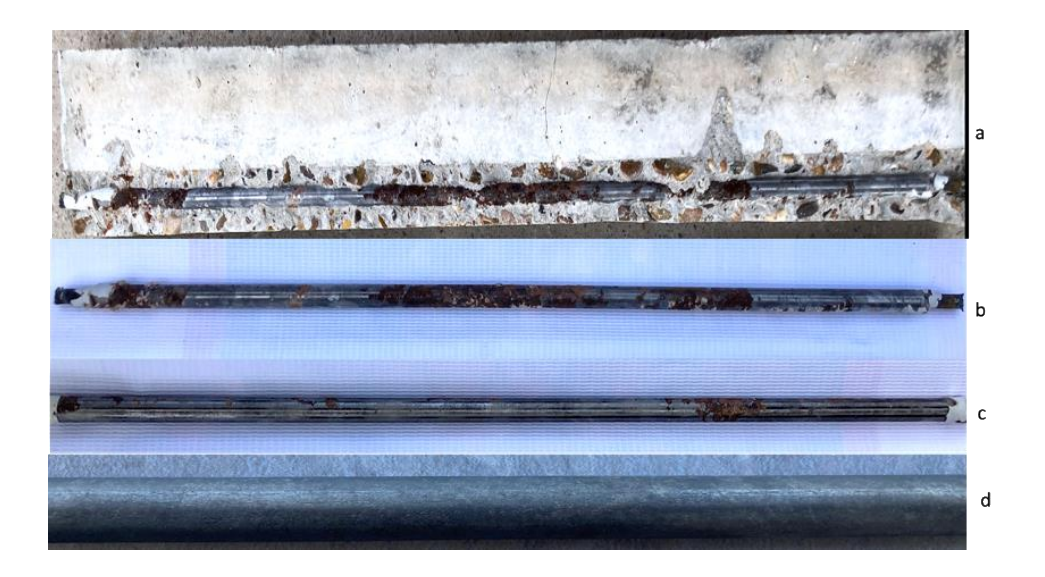


Fig. 6.5 The amount of rust formed on the surface of the rebar in specimen type B made of PC: (a) the visual appearance of the specimens after the splitting into halves; (b) the surface of the rebar facing the crack, (c) the reverse side of the rebar (d) the surface of the reinforcement facing the crack after the picking



Fig. 6.6 The amount of rust formed on the surface of the rebar in specimen type C made of PC: (a) the visual appearance of the specimens after the splitting into halves along the crack; (b) the surface of the rebar facing the crack, (c) the reverse side of the rebar (d) the surface of the reinforcement facing the crack after the picking

6.1.2 Specimens made of 35% PC /65% GGBS denoted as GGBS.

6.1.2.1 Half-cell potentials

Figure 6.7 shows plots of the half-cell potential measurements for types B and C specimens obtained using a silver-silver chloride reference electrode.

As can be seen from Fig. 6.5 the potential readings in B specimens, have dropped a lot earlier from the third month and fluctuated within the low and high corrosion possibility regions throughout the exposure time, except for specimens consisting of 0.1mm crack width. Overall, it can be assumed that the breakdown of the passive film took place between months 8 and 12 as the most negative readings started then. Surprisingly, specimens with 0.1mm crack widths remained at potential readings ranging between -270 and -300 mV, indicating a high risk of corrosion initiation, whereas specimens with wider cracks levelled off slightly.

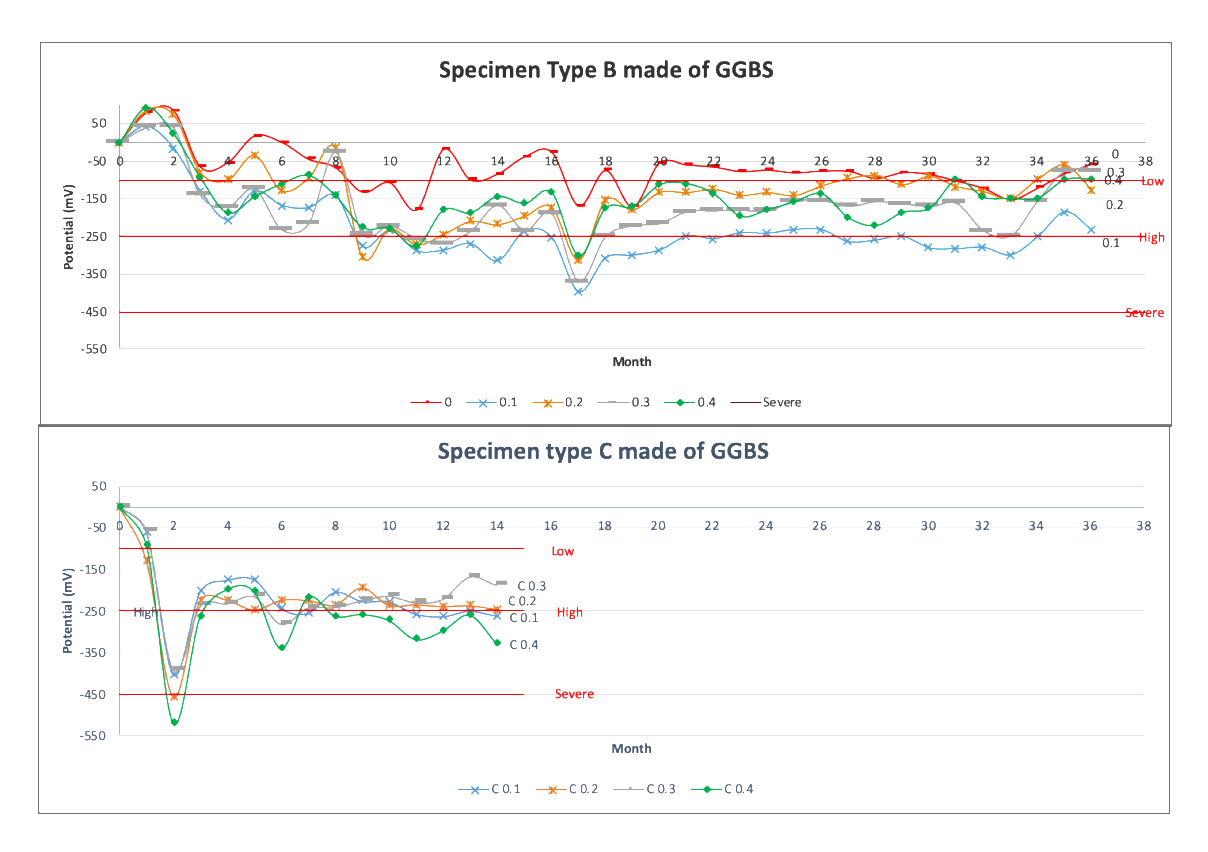


Fig. 6.7 Half-Cell potential readings for specimen types B and C made of GGBS with different crack widths.

In month 16, the potential readings exceeded the high corrosion risk level, this could be an indication of a passive film breakdown or starting point of active corrosion process which could be confirmed with LPR and ZRA readings.

Regarding the potentials in the C design, these specimens experienced remarkably similar potential readings regardless of crack widths which is more pronounced than in the B specimen design. The results fluctuated within the proximity of the high corrosion possibility region compared to that of specimen type B. The breakdown of passive films appears to happen during the second month of exposure to an aggressive environment. Overall, it is clear from the graphs above that there was no apparent difference in the transition state of the rebars from passive to active corrosion conditions with regard to different crack widths.

6.1.2.2 Corrosion rates

Monthly corrosion rate estimates are shown in Figures 6.8 and 6.9 for LPR and ZRA measurements.

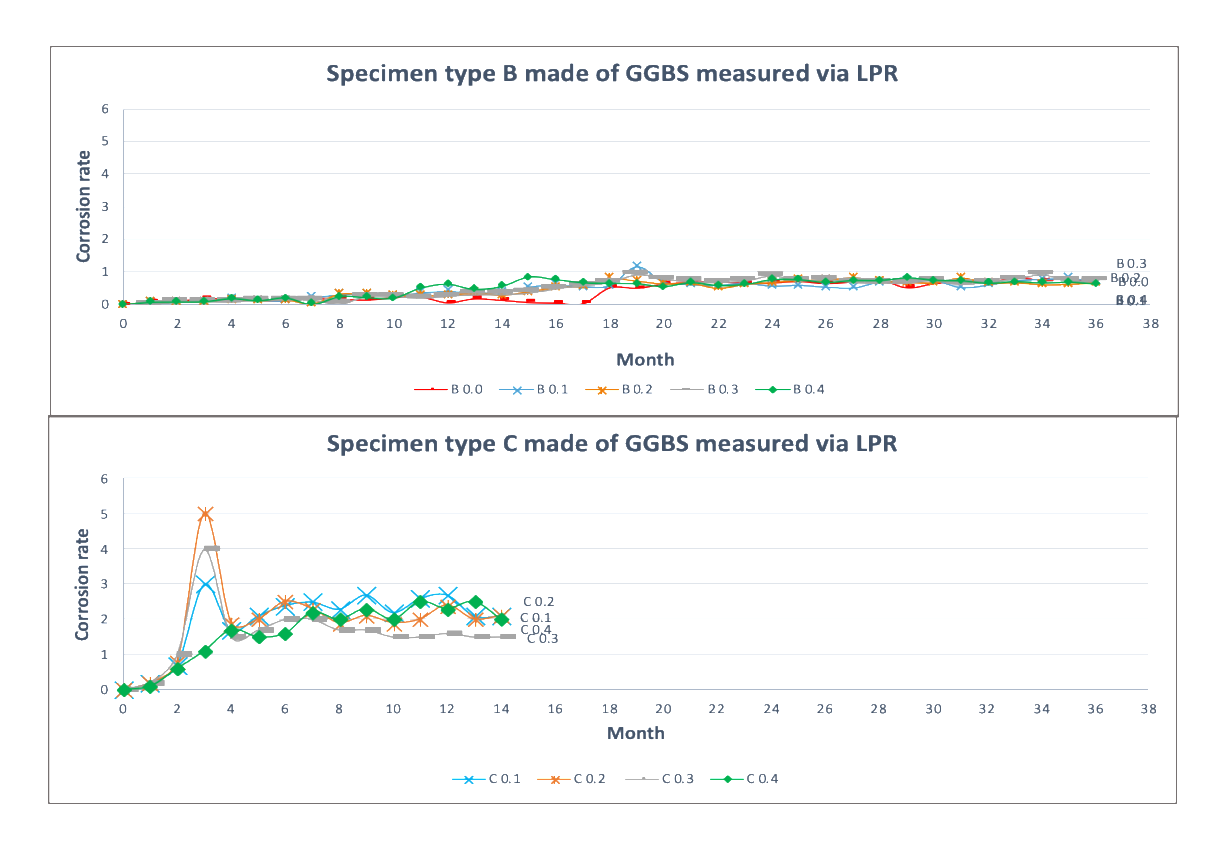


Fig. 6.8 Monthly Corrosion rate readings for specimen types B and C with various crack widths measured via LPR.

According to monthly LPR readings, type B specimens underwent a very mild corrosion rate. There was no indication of higher corrosion rates in month 16, which is evident from the half-cell potential readings. Another noticeable observation is the fact that all specimens with varying crack widths show similar corrosion rates including control specimens.

Regarding type C specimens, there was a sudden increase in month 3 for specimens with 0.1, 0.2 and 0.3mm crack widths, while Half-cell potential measurements experienced extreme drop in potential in the second month. Therefore, there was not a very accurate correlation between LPR and Half-cell potential readings. Although there are variations in corrosion rates among different crack widths, statistical analysis of variance is necessary to confirm whether it is significant or not.

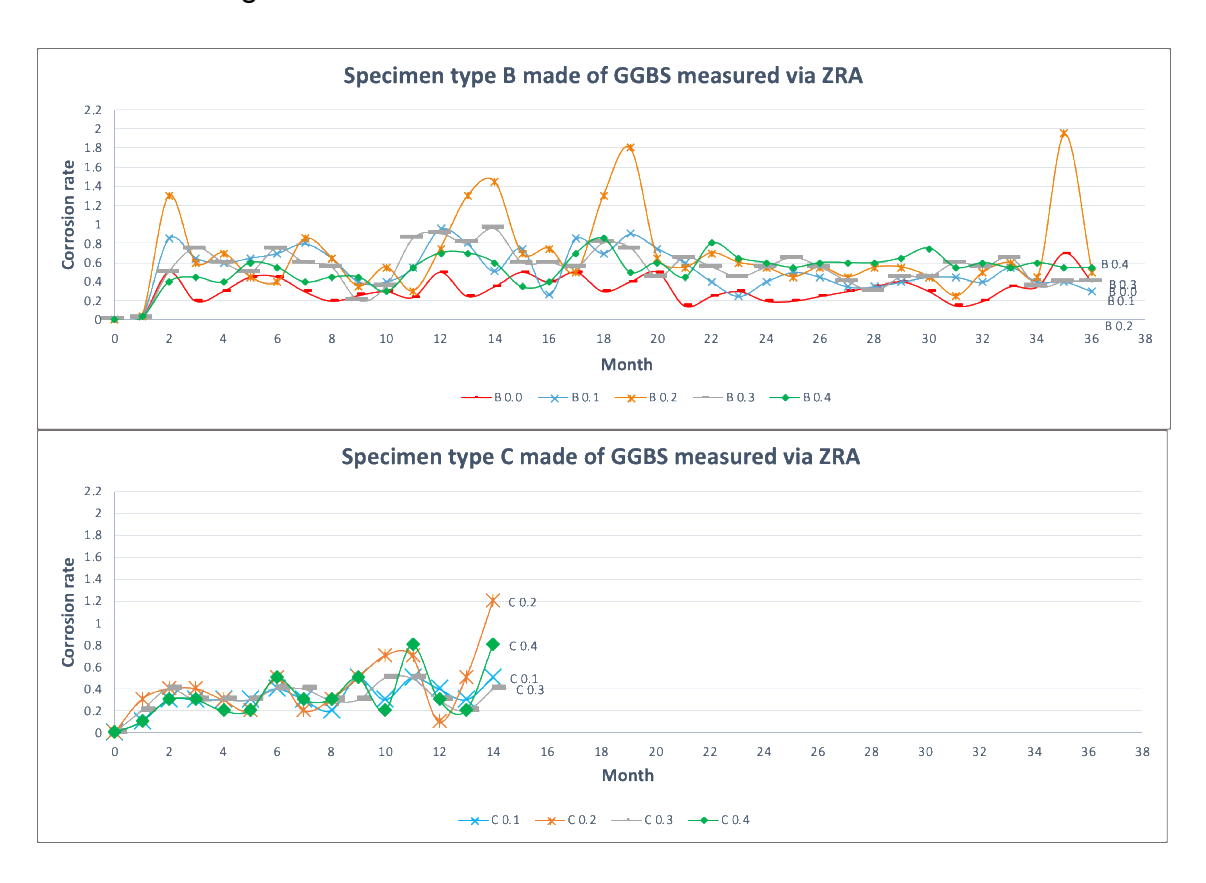


Fig. 6.9 Monthly Corrosion rate readings for specimen types B and C with various crack widths measured via ZRA.

According to ZRA readings for type B specimens, the results show relatively fluctuated rates especially for specimens with 0.2mm crack. There was a jump in rates in the second month which wasn't detected by Half-cell potential nor LPR

readings. Moreover, the dip in month 16 of Half-cell measurements cannot be spotted here either which could be the result of a change in ambient temperature or humidity levels as half-cell potential readings are sensitive to the testing environment (Yodsudjai & Pattarakittam, 2017).

ANOVA test results are presented in Table 6.4 and Post Hoc test results are shown in Table 6.5. According to ANOVA results, the effect of crack width appears to be controversial, where specimen type B results measured via LPR are not significant. In contrast, the ones measured via ZRA do suggest quite significant differences. A very opposite tendency is shown in specimen type C specimens, where LPR results revealed significant differences in crack widths and ZRA readings resulted in insignificant outcomes. Since the ANOVA results for Specimen type B measured by LPR and specimen type C results measured via ZRA revealed insignificant differences in corrosion rates with different crack widths, Post Hoc test was omitted. These controversial outcomes could be clarified by a graphical illustration of the corrosion rate results in a form of boxplots shown in Figure 6.10.

Table 6.4 ANOVA results for different crack widths in type B and C specimens made of GGBS and measured with both measurement techniques

	Measurement techniques			
Specimen	LPF	3	Z	RA
type	F Test statistic	Significance	F Test	Significance
	1 Test statistic	level	statistic	level
В	F(1)= 3.11	p = 0.08	F(1) =22.4	p < 0.05
С	<i>F(4)</i> = 11.7	p < 0.05	F(4)= 2.29	p =0.07

As can be seen from the table 6.5, in B specimen design, the Post Hoc test revealed a significant difference in corrosion rates (via ZRA) between uncracked samples and the ones with cracks except for the combination 0.1vs 0. There were significant differences among specimens with various crack widths as well, these appear to be due to specimens with 0.1mm crack width which experienced relatively low corrosion rates compared to other cracked specimens, which can

be seen in Figure 6.10. Whereas specimen design C (measured via LPR) revealed significant p-values between uncracked and cracked specimens only.

Table 6.5 Post Hoc Test of multiple comparisons on the effect of crack width on corrosion for specimens B and C made of GGBS measured via LPR and ZRA.

	Comparison		Measurement	techniques	
Specimen	combination	Linear	Linear Polarisation		esistance
type	between crack	Res	sistance	Amr	neter
турс	widths	Mean	Sig.	Mean	Sig.
	0; 0.1; 0.2; 0.3; 0.4	Diff.	olg.	Diff.	olg.
	0.1 vs 0	NA	NA	0.06	p = 0.83
	0.2 vs 0	NA	NA	0.37	<i>p</i> < 0.05
	0.3 vs 0	NA	NA	0.23	<i>p</i> < 0.05
	0.4 vs 0	NA	NA	0.23	<i>p</i> < 0.05
В	0.2 vs 0.1	NA	NA	0.31	<i>p</i> < 0.05
Ь	0.3 vs 0.1	NA	NA	0.17	<i>p</i> < 0.05
	0.4 vs 0.1	NA	NA	0.17	<i>p</i> < 0.05
	0.3 vs 0.2	NA	NA	-0.14	p = 0.09
	0.4 vs 0.2	NA	NA	-0.14	p = 0.08
	0.4 vs 0.3	NA	NA	0.01	p = 0.08
	0.1 vs 0	1.69	<i>p</i> < 0.05	NA	NA
	0.2 vs 0	1.67	<i>p</i> < 0.05	NA	NA
	0.3 vs 0	1.27	<i>p</i> < 0.05	NA	NA
	0.4 vs 0	1.34	<i>p</i> < 0.05	NA	NA
	0.2 vs 0.1	-0.01	p = 0.99	NA	NA
	0.3 vs 0.1	-0.42	p = 0.59	NA	NA
С	0.4 vs 0.1	-0.35	p = 0.74	NA	NA
	0.3 vs 0.2	-0.41	p = 0.62	NA	NA
	0.4 vs 0.2	-0.34	p = 0.77	NA	NA
	0.4 vs 0.3	0.07	p = 0.99	NA	NA

The insignificant outcome of the ANOVA test in B specimen design measured via LPR can be explained from Figure 6.10 where it is clear that all cracked specimens showed low corrosion rates and they were close in value to uncracked ones. A similar explanation in Specimen design C measured via ZRA where corrosion rates in cracked specimens show low rates that are close to uncracked ones. These results perhaps may indicate an underestimation of corrosion rates in cracked specimens as they were clearly corroding.

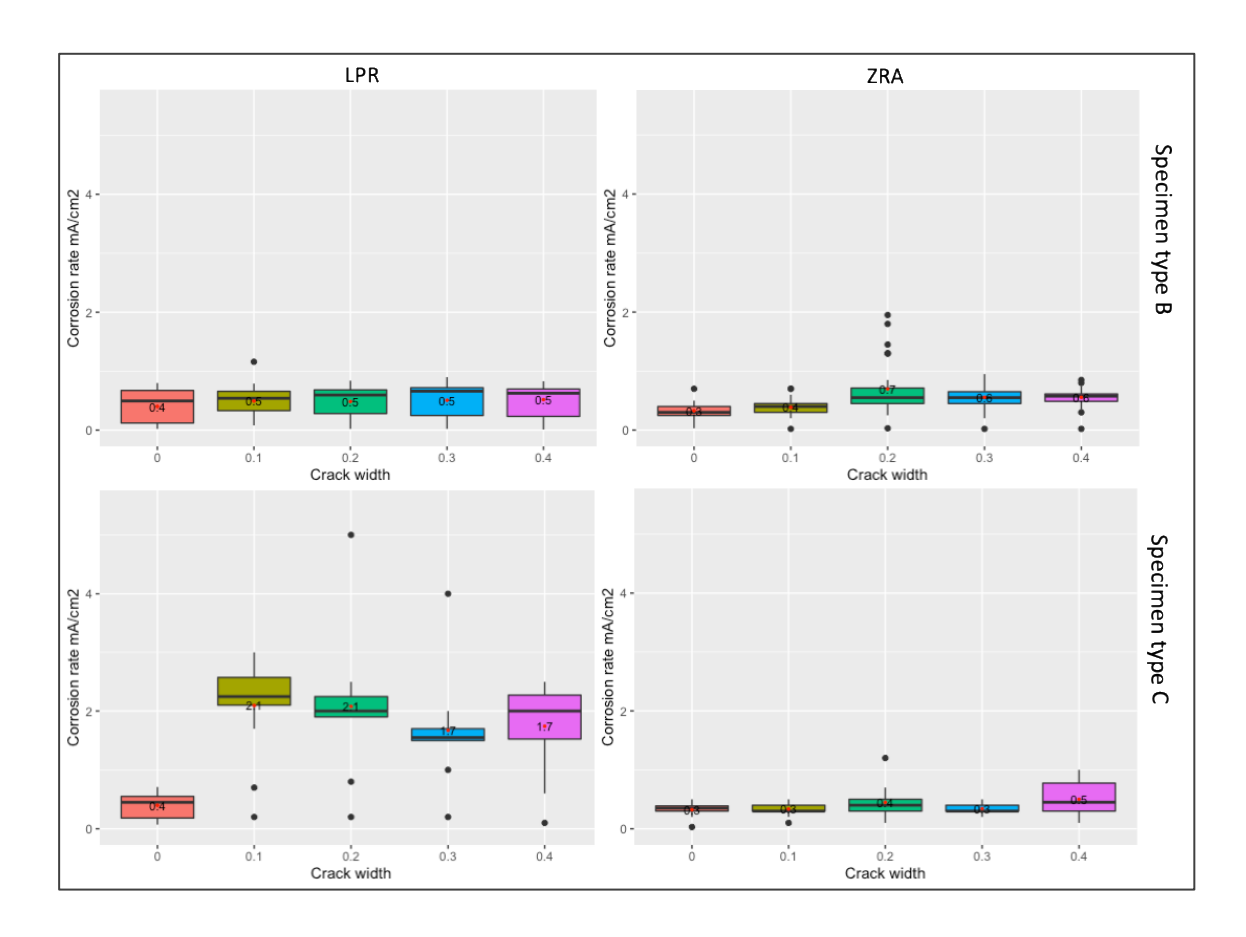


Fig. 6.10 Corrosion rates (μ A/cm²) experienced by specimen types B and C made of GGBS with different crack widths.

6.1.2.3 Gravimetric mass loss

Table 6.6 shows the gravimetric mass losses experienced by both specimen designs.

According to gravimetric mass loss results, there is no noticeable difference between various crack widths in both specimen designs B and C.

Table 6.6 Gravimetric mass loss of B and C specimens made of GGBS

Crack widths	Mass loss in (g) Specimen	Mass loss in (g)
(mm)	type B	Specimens type C
0.1	0.266	0.585
0.2	0.263	0.596
0.3	0.239	0.561
0.4	0.271	0.567

6.1.2.4 Photos showing condition of reinforcing bars

The Figures 6.11 and 6.12 represent the photographic evidence of the rust formed on the surface of specimen designs B and C respectively.

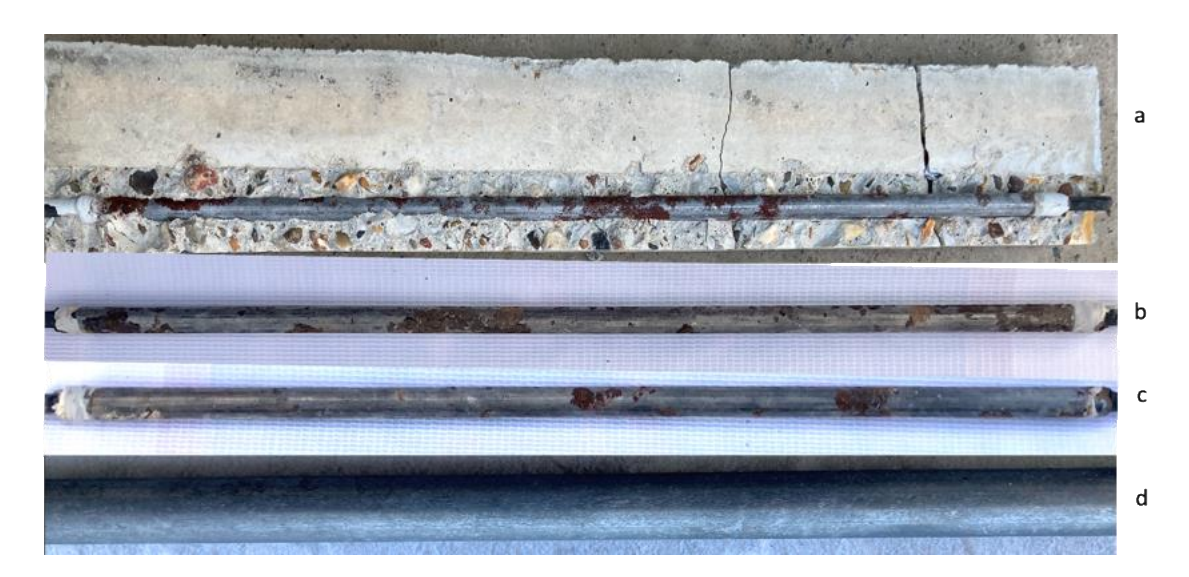


Fig. 6.11 The amount of rust formed on the surface of the rebar in specimen type B made of GGBS: (a) the visual appearance of the specimens after the splitting into halves; (b) the surface of the rebar facing the crack, (c) the side away from the crack (d) the surface of the bar facing the crack after the picking.



Fig. 6.12 The amount of rust formed on the surface of the rebar in specimen type C made of GGBS: (a) the visual appearance of the specimens after the splitting into halves along the crack; (b) the surface of the rebar facing the crack, (c) the side away from the crack (d) the surface of the reinforcement facing the crack after the picking.

6.1.3 Specimens made of 30% FA/70% PC (denoted as FA)

6.1.3.1 Half-cell potentials

Figure 6.13 depicts the average potential readings for type B and C specimens made with the addition of FA. The Half-cell potential readings follow similar trends obtained from specimens made of GGBS in both specimen designs. Where the breakdown of passive film and overall progression of readings are similar according to Figure 6.7. Again, the difference between cracked and uncracked specimens is clearly shown in the graph, whereas the cracked specimens exhibit similar potential readings on both designs.

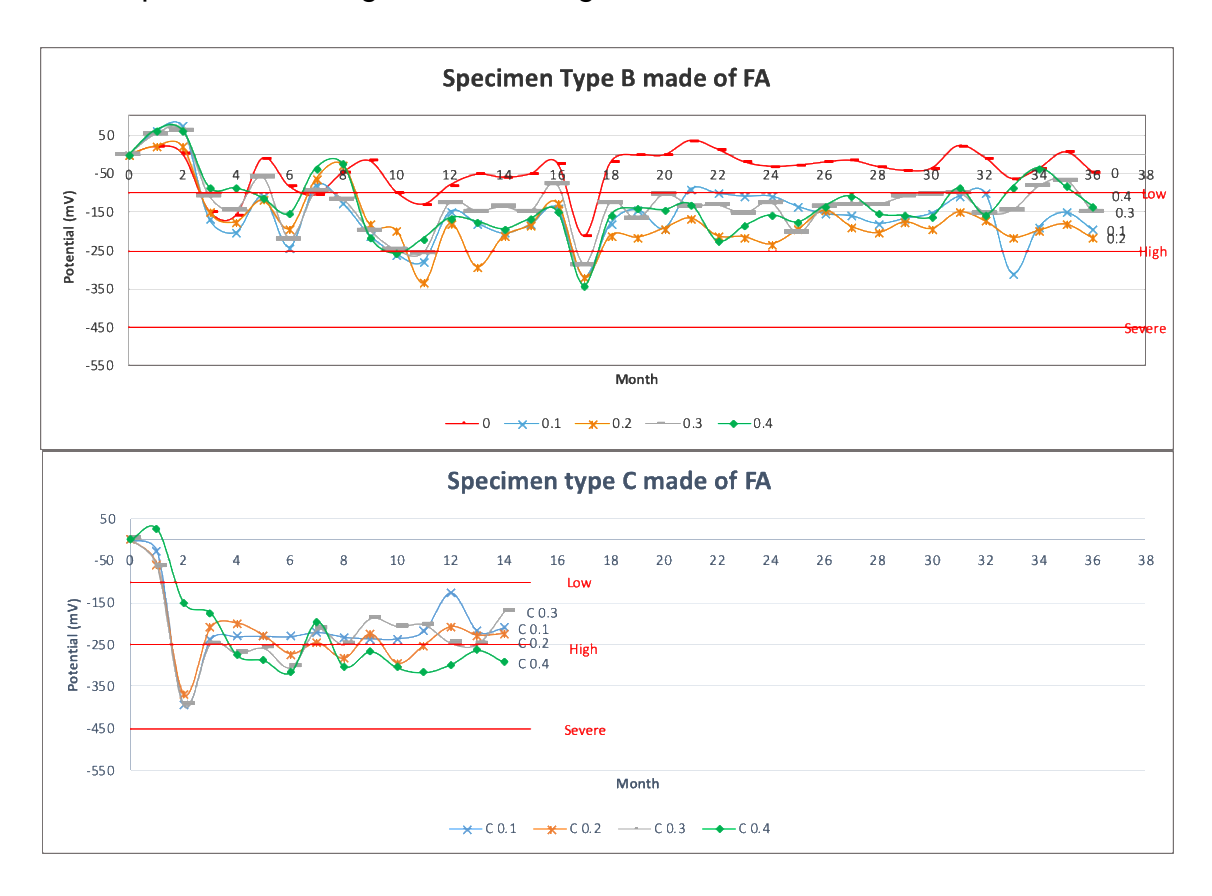


Fig. 6.13 Half-Cell potential readings for specimen types B and C made of FA with different crack widths.

6.1.3.2 Corrosion rates

Monthly corrosion rate readings are presented in Figures 6.14 and 6.15 for LPR and ZRA measurements respectively.

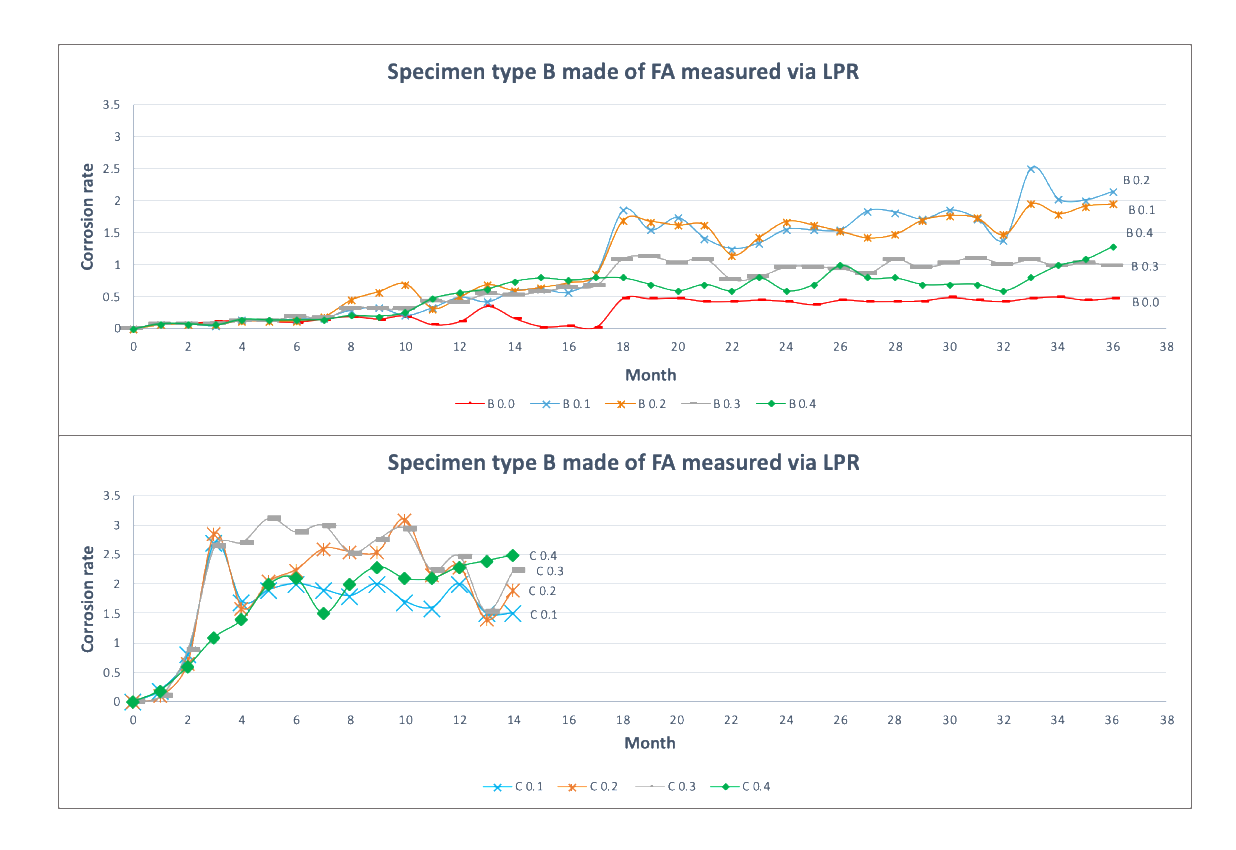


Fig. 6.14 Monthly Corrosion rate readings for specimen types B and C with various crack widths measured via LPR.

According to corrosion rate estimates measured via LPR, the values spread relatively more compared to specimens made of GGBS. In accordance with half-cell potential readings, which showed more negative potentials in month17, LPR results revealed a slight increase in corrosion activity around that same month.

Regarding type C specimens, LPR readings are in a good agreement with Half-cell potential outcomes, as both demonstrate active corrosion starting from month 2. Concerning the variation in corrosion rates depending on crack width, statistical analysis is needed to verify the significance levels.

Similar to ZRA measurements obtained for specimens made of PC and GGBS, there was no correlation between LPR readings measured in specimens made of FA. Generally, corrosion rates for specimens with different crack widths exhibit relatively scattered values throughout the experiment period.

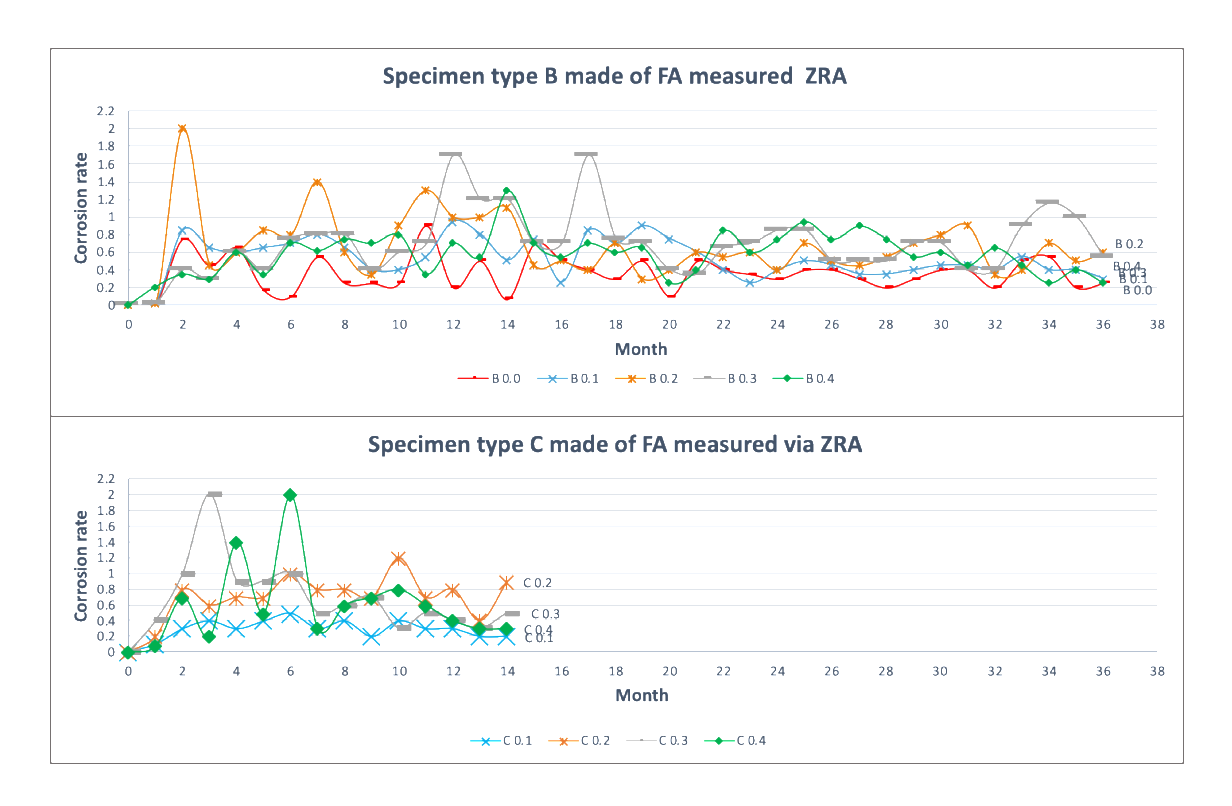


Fig. 6.15 Monthly Corrosion rate readings for specimen types B and C with various crack widths measured via ZRA.

Tables 6.7 and 6.8 show the results obtained from ANOVA and Posthoc tests respectively. According to ANOVA results, all specimen designs in both measurement techniques resulted in significant outcomes.

Regarding the Posthoc test results measured via LPR, both B and C specimen designs showed significant p values between combinations of uncracked and cracked specimens. This shows that corrosion rates between cracked specimens are not significant and they all proceed similar rates of corrosion irrespective of crack width. While corrosion rate estimates via ZRA in B specimens show significant results in all combinations of uncracked and cracked specimens except between 0.1 vs 0. While in C specimen designs significant p-value was between combinations of specimens with 0.2 and 0.1mm crack widths.

Table 6.7 ANOVA results for different crack widths in specimens made of FA and measured with both measurement techniques.

Specimen	Measurement techniques		
type	LPR	ZRA	

	F Test statistic	Significance	F Test	Significance
	i i est statistic	level	statistic	level
В	F(1)= 17.25	<i>p</i> < 0.05	F(1) =16.18	<i>p</i> < 0.05
С	F(4)= 18.63	<i>p</i> < 0.05	F(4)= 4.89	p < 0.05

Table 6.8 Post Hoc Test of multiple comparisons on the effect of crack width on corrosion for specimens B and C made of FA measured via LPR and ZRA.

	Comparison		Measurement	techniques	
Specimen	combination	Linear Polarisation		Zero Resistance	
type	between crack	Res	sistance	Amr	neter
турс	widths	Mean	Sig.	Mean	Sig.
	0; 0.1; 0.2; 0.3; 0.4	Diff.	Olg.	Diff.	Oig.
	0.1 vs 0	0.27	<i>p</i> < 0.05	0.17	p = 0.08
	0.2 vs 0	0.25	<i>p</i> < 0.05	0.31	<i>p</i> < 0.05
	0.3 vs 0	0.38	<i>p</i> < 0.05	0.34	<i>p</i> < 0.05
	0.4 vs 0	0.30	<i>p</i> < 0.05	0.22	<i>p</i> < 0.05
В	0.2 vs 0.1	-0.02	p = 0.99	0.14	p = 0.22
Ь	0.3 vs 0.1	0.12	p = 0.53	0.17	p = 0.07
	0.4 vs 0.1	0.03	p = 0.99	0.05	p = 0.93
	0.3 vs 0.2	0.13	p = 0.37	0.03	p = 0.99
	0.4 vs 0.2	0.05	p = 0.96	-0.09	p = 0.68
	0.4 vs 0.3	-0.09	p = 0.78	-0.11	p = 0.38
	0.1 vs 0	1.38	<i>p</i> < 0.05	-0.08	p = 0.96
	0.2 vs 0	1.72	<i>p</i> < 0.05	0.35	p = 0.06
	0.3 vs 0	2.00	<i>p</i> < 0.05	0.32	p = 0.08
	0.4 vs 0	1.41	<i>p</i> < 0.05	0.24	p = 0.30
	0.2 vs 0.1	0.34	p = 0.66	0.43	<i>p</i> < 0.05
С	0.3 vs 0.1	0.62	p = 0.11	0.41	p = 0.15
	0.4 vs 0.1	0.03	p = 0.99	0.33	p = 0.08
	0.3 vs 0.2	0.28	p = 0.79	-0.02	p = 0.99
	0.4 vs 0.2	-0.31	p = 0.73	-0.10	p = 0.93
	0.4 vs 0.3	-0.59	p = 0.14	-0.08	p = 0.97

Figure 6.16 shows the corrosion rates obtained via both measurement techniques.

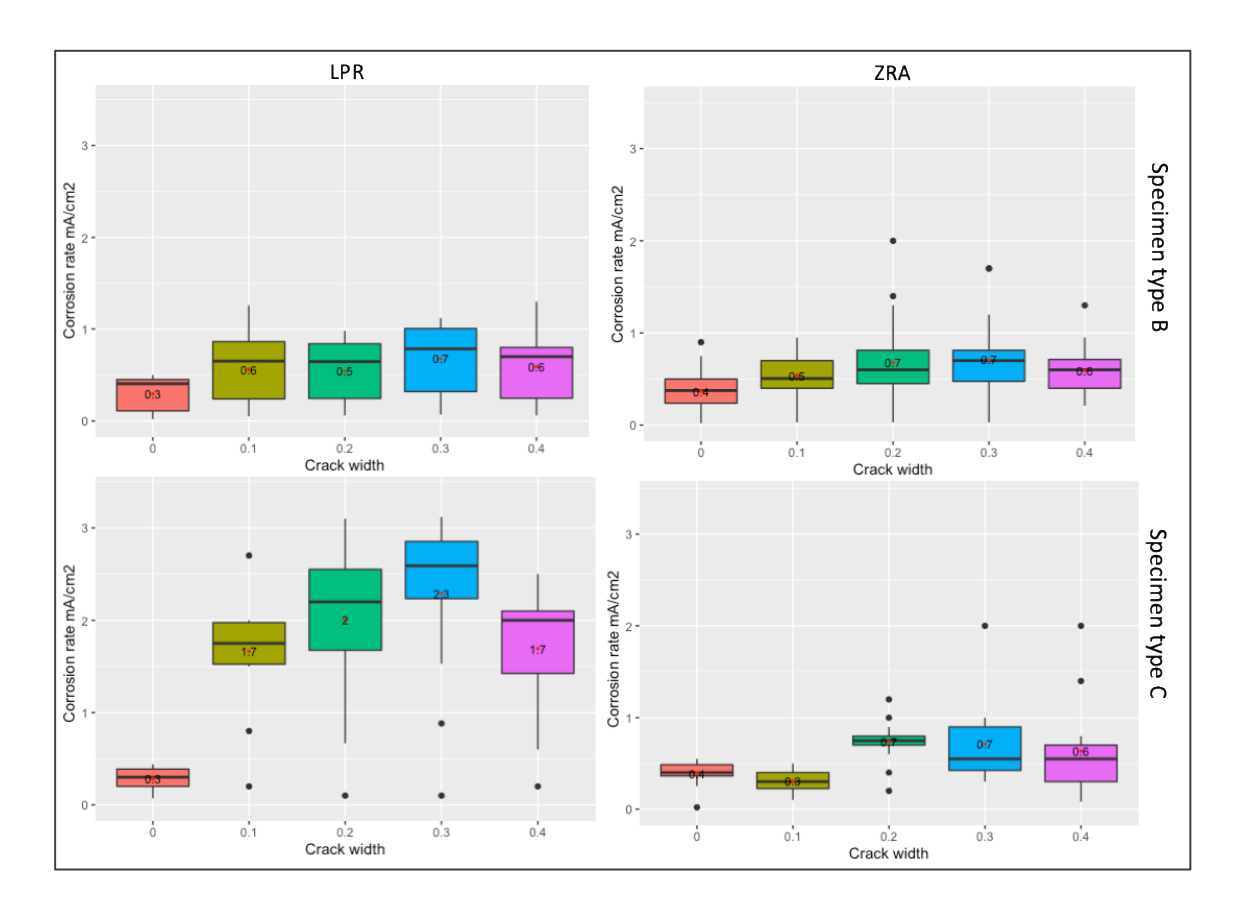


Fig. 6.16 Corrosion rates (μ A/cm²) experienced by specimen types B and C made of FA with different crack widths.

According to LPR results, the difference in corrosion rates between uncracked and cracked specimens is clearly shown in both type B and C specimens. Whereas ZRA readings show somewhat erratic results.

6.1.3.3 Gravimetric mass loss

Gravimetric mass losses experienced by specimens made with the addition of FA with varying cracks are shown in Table 6.9 for type B and C designs. The gravimetric mass losses experienced by these specimens are also extremely similar to the ones obtained from specimens made with the addition of GGBS.

Table 6.9 Gravimetric mass loss of B and C specimens made of FA

Crack widths	Mass loss in (g) Specimen	Mass loss in (g)
(mm)	type B	Specimens type C
0.1	0.281	0.569
0.2	0.270	0.555
0.3	0.271	0.536

0.4	0.280	0.575
• • •	0.200	0.0.0

6.1.3.4 Photos showing condition of reinforcing bars

The Figures 6.17 and 6.18 represent the photographic indication of rust formed on the surface of the rebar in both specimen designs B and C respectively.



Fig. 6.17 The amount of rust formed on the surface of the rebar in specimen type B made of FA: (a) the visual appearance of the specimens after the splitting into halves; (b) the surface of the rebar facing the crack, (c) the side away from the crack (d) the surface of the reinforcement facing the crack after the picking



Fig. 6.18 The amount of rust formed on the surface of the rebar in specimen type C made of FA: (a) the visual appearance of the specimens after the splitting into halves along the crack; (b) the surface of the rebar facing the crack, (c) the side away from the crack (d) the surface of the bar facing the crack after the picking.

Overall, the absence of the effect of crack width on corrosion of reinforcement can be seen from the various test results conducted above. Due to the differences in the design and crack extent between specimen types B and C, they experienced different types/amounts of corrosion. Thus, it is thought to discuss them separately, first specimen design B and followed by C.

Specimen type B

Regarding the corrosion mechanism in Specimen type B, where there is a clearance of around 10mm between crack end and reinforcement, a combination of both macrocell and microcell corrosions appears to take place.

During the specimen design stage of this work, it has been planned that the space between crack end and rebar be 5mm, however, due to possible shifts during vibration, the still shims used to induce cracks moved upwards resulting in a clearance of ~10mm. Thereby, in this case, a good quality oxidation film was formed on the rebar surface, and a time for a chloride build-up and penetration were necessary to break the passive film. Thus, in this specimen design, the exposure is similar to sound concrete with a thin concrete cover. The initiation of the corrosion process was slower than the other two specimen designs. Although the desired specimen configurations have not been achieved in this set of specimens, it can still be representative of a real structure condition in practice, where cracks with a certain width appear on the surface of the concrete, however, do not reach the reinforcement level fully. Overall, the corrosion process started in areas of the steel with relatively lower potential or in places with the highest chloride ion build-up. Due to uneven surface conditions and variations in chemical and physical properties, mild steel has a heterogeneous electrochemical state (Zou et al., 2012). Thereby the corrosion may start along the surface points with the presence of different site energies brought by various surface conditions (McCafferty, 2010). Steel properties such as metallurgy, and surface roughness as well as the content and spatial distribution of moisture in microscopic and macroscopic voids at the steel-concrete interface play a major role in the initiation of the corrosion process (Angst et al., 2019). As a result, corrosion patches started to appear in several areas, mainly on the top surface of the rebar facing the crack. The reinforcement areas with signs of corrosion acted as an anode

and the remaining parts acted as a cathode. This is demonstrated in figure 6.19. The corrosion formed on the surface of the reinforcement appears to be general as no sign of pitting was observed irrespective of crack width.

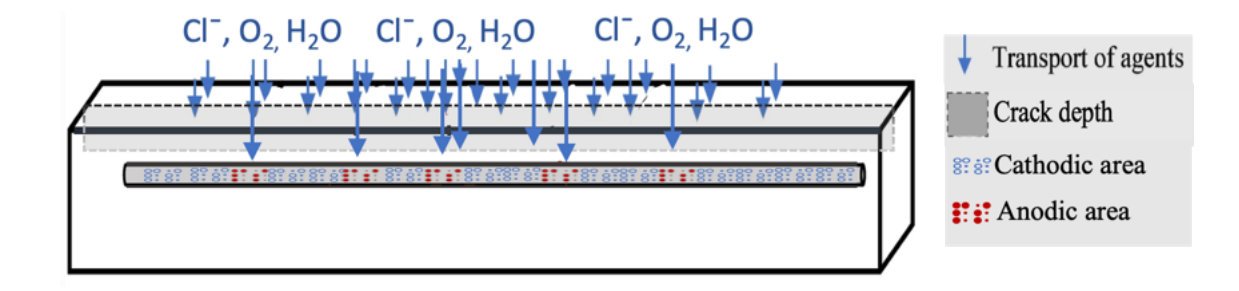


Fig. 6.19 The corrosion mechanism in Specimen type B, adopted from (E. Chen et al., 2020).

The corroded points were simply covered with a thin layer of rust and the cleaning process of the rebar with the Clarck's solution was relatively easy and fast as there was no pitting or any indentation as can be seen from figure 6.17 (d).

Overall, it could be said that the uncracked specimens in all cases did not show negative enough potentials, which was expected as the concrete cover was 45mm in them and they were highly unlikely to corrode. Regarding the results of cracked specimens, obtained from potential readings, it took some time before the rebars were depassivated from the chloride ingress, moreover, it appears that the oxide film did break at a roughly similar time in all cracked specimens regardless of crack widths. The potential readings simply appear to show that the steel was not initially corroding but the situation eventually changed.

According to chloride concentration in all specimens with varying cracks made of three cement mixes, shown in Figure 6.20, it appears that chloride content is higher in the top layer and lower in the crack vicinity (which was denoted as bottom). The position of the dust samples obtained for chloride content is shown in Section 5 Methodology and shown schematically in Figure 5.21. However, chloride content in concrete around the reinforcement shows similar concentration irrespective of crack width.

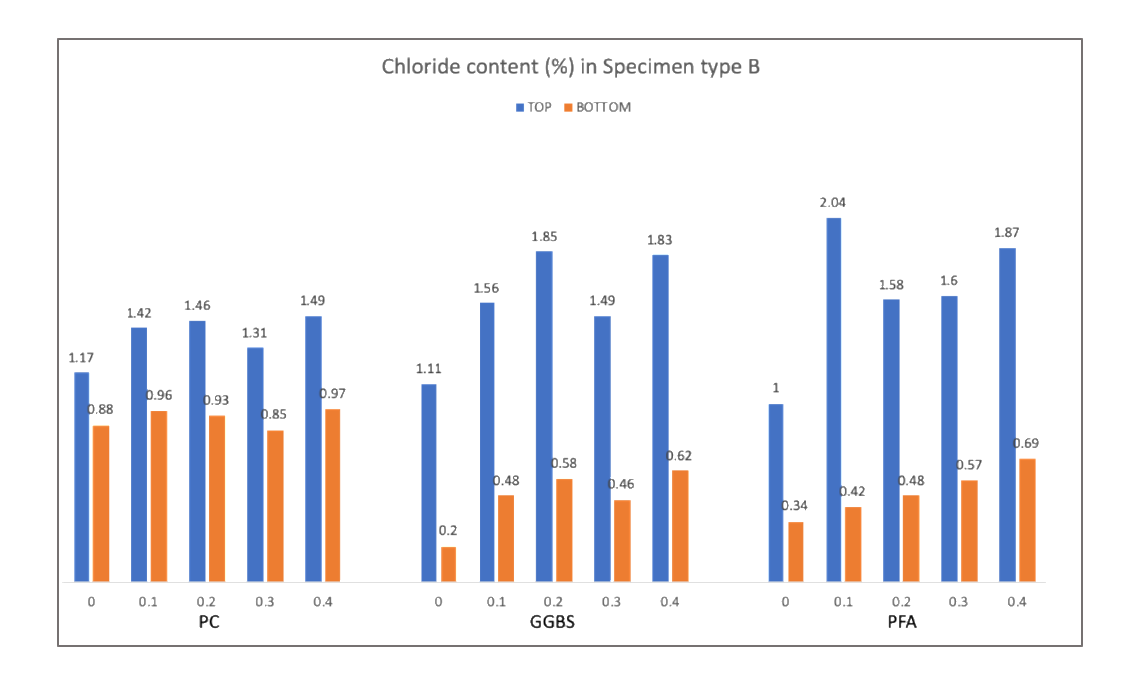


Fig. 6.20 Chloride concentration by weight of concrete in Specimen design B made of all cement mixes and various crack widths.

Whereas according to non-destructive corrosion rate measurements (figures 6.4, 6.10 and 6.16 Specimen type B), all specimens with varying crack widths experienced similar corrosion rates. Moreover, the final gravimetric mass loss outcomes were in good agreement with non-destructive corrosion measurements obtained via LPR and did not show much of a difference in mass losses due to corrosion with regard to crack widths.

Specimen type C

Specimen design C was cast later than Specimen design B samples and they were exposed to a chloride environment for a shorter period of time. However, it is evident from the figures above, pitting corrosion can be observed in all of these specimens that formed along the crack. As the crack in these specimens formed by inserting thin steel shims into the slots cut in the timber moulds and the concrete has been carefully placed on top of them, the formation of the oxide film in that particular area appears to be missing. Thus, the corrosion process appears to start very soon after the chloride solution application.

This can be observed from Half-cell potential readings (Figures 6.1, 6.7 and 6.13 Specimen design C), where the potential readings shifted towards extremely negative values and exceeded a line for severe corrosion possibility. Generally,

negative potential readings were ranging around the high corrosion probability zone. The plots do not vary between crack width i.e. both in terms of the time it took for corrosion initiation and the time taken for potentials to indicate, say, a high or severe risk of corrosion.

The chloride content of the cracked specimens made of all cement mixes is shown in figure 6.21. A similar trend to the type B specimens can be seen from the figure. The chloride concentration shows a similar values irrespective of crack width, specifically in the vicinity of the reinforcement.

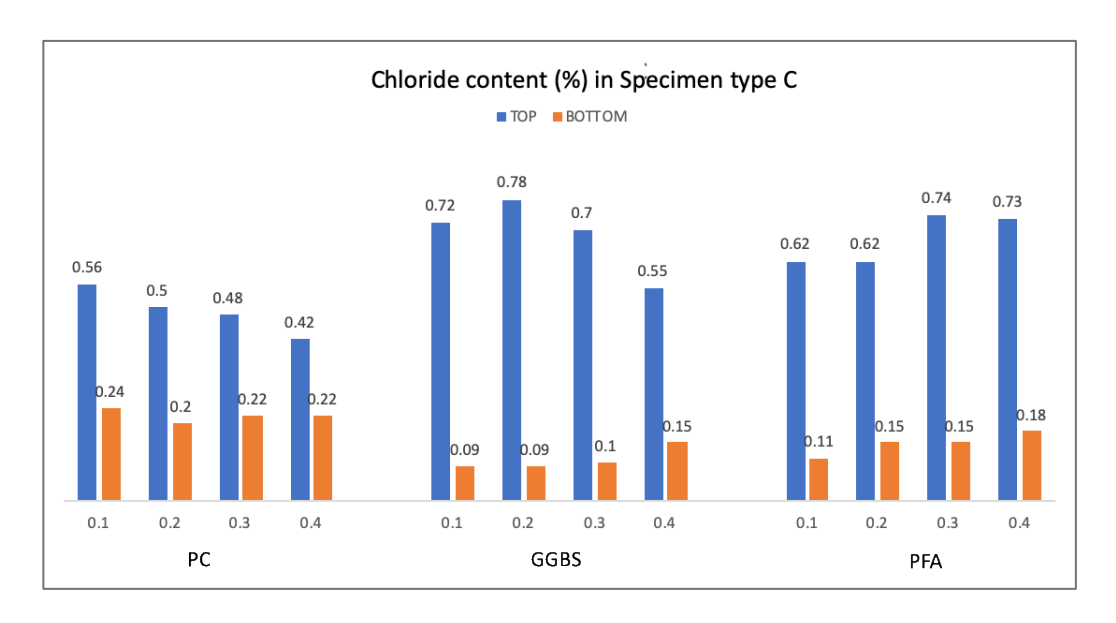


Fig. 6.21 Chloride concentration by weight of concrete in Specimen design C made of all cement mixes and various crack widths.

Along with pitting corrosion, general corrosion signs were observed upon breakage of the specimens as can be seen from photographs (figures 6.6, 6.12 and 6.18). The rust formed primarily on the top surface of the rebar facing the cracked side and it was relatively rust-free on the reverse side of the rebar. A thin v-shaped indentation was formed in the rebar along the crack due to pitting corrosion as shown in Figure 6.22. This was not the case in Specimen type B samples. After cleaning the bars from rust with Clarck's solution, it was possible to see the depth and width of pits formed on the surface of the bar shown in Figure 6.23. As can be seen from the photographs, the depths of the pits vary along the bar in some cases. However, when the long pits are shallow, the bars developed a couple of deeper and wider pits as can be seen from bars removed

from specimens with 0.2 and 0.3mm crack widths. Thus, according to the results obtained from various tests, and corrosion observations experienced by these specimens, there appears to be no relationship between the crack width and corrosion rates as well as mass losses caused by corrosion.



Fig. 6.22. The appearance of V-shaped pitting corrosion formed along the crack in Specimen design C.



Fig. 6.23 The variation in depth and width of pits formed in type C specimens with different crack widths.

6.1.4 Discussion on the effect of crack width in reinforcement corrosion

To-date, the work by (Stillwell, 1988) appear to be the only attempt to elucidate the effect of coincident crack width on reinforcement corrosion. As previously noted this author found that "the worst corrosion was associated with the largest crack widths, although the difference was not significant". Stillwell also noted that "it was possible that even this difference could reduce after a longer period of exposure".

Some information on this aspect can be gleaned from the study by (Balakumaran et al., 2018) although these authors examined a mixture of coincident and

intersecting cracks. These authors investigated the effect of cracks in bridge decks on corrosion and concluded that the effect of crack width on the amount of rust formed was not significant and no strong correlation was observed between surface crack width and chloride diffusion as well as rust appearance on the bar surface.

Broadly speaking, both conclusions agree with the findings of the present study and would suggest that there is no significant effect of crack width on corrosion. However, it is worth speculating why this should be case given that the opposite effect would intuitively seem more reasonable. We know that cracks aid chloride penetration into concrete. Where cracks extend to reinforcing bars they will also increase the degree of disruption at the concrete/steel interface. Both effects are likely to increase with increasing crack width and hence one might have expected to see an increase in corrosion with increasing crack width.

However, the fact that this was not found to be the case suggests there maybe some flaws in our understanding of the role of cracks in corrosion. In the case of type B specimens since the cracks were formed using shims and terminated approximately 9mm above the reinforcing bars, larger cracks would not be expected to increase the disruption at the concrete/steel interface. Under normal circumstance, narrow crack will increase the time taken for chloride to reach the surface of reinforcing bars thereby indicating a lower risk of corrosion at least in the short term. However, since the cracks used in this work extend to the same depth in the test specimens irrespective of width this aspect has largely been eliminated. In fact, analysis of the concrete around the bar shows that the chloride contents (shown in in figure 6.20) were similar irrespective of crack width which suggest that chloride contamination is more dependent on the properties of the uncracked concrete around the bar rather than the crack width. This is probably not too dissimilar to what occurs in the field in the long-term and would explain Balakumaran et al (2018) finding namely there was no strong correlation observed between surface crack width and chloride diffusion i.e. there were similar levels of chloride contamination of the concrete.

In the case of type C specimens, the cracks not only extend to the reinforcing bars but also the area of bar not in intimate contact with the concrete which

Chapter 6 Results and Discussion

increases with increasing crack width and probably explains why these specimens experienced higher rates of corrosion than type B specimens. But the fact that type C specimens with larger crack widths did not register higher rates again suggests that this is again related to the properties of the uncracked concrete around the bar which dominates behaviour and the size of the crack over the range investigated is unimportant. Moreover, the chloride content in the concrete around the rebar revealed similar values, which confirms the explanation above.

This behaviour would also appear to be applicable to concrete with natural cracks. If the test specimens used in this work had utilised natural cracks all that would have meant is that the tests would need to have been conducted over a much longer time period in order to minimise the effect of chloride initiation period on corrosion but that there would be no significant difference in the amount of rust that was formed as was found to be case by (Stillwell, 1988) and (Balakumaran et al., 2018).

6.2 Effect of depth of cracking on corrosion rates.

Different crack depths and concrete-steel interface disruption levels have been looked at in this work. Three different crack depths were investigated, one of which is a natural crack denoted as Specimen type A1/A2 and the other two are created artificially by inserting the steel shims into the fresh concrete denoted as B and C. The extent of contamination varied for each crack depth as illustrated in Figure 6.24. The contamination depth is shown as a white area following the crack, and the concrete-steel interface disruption level seems to affect the amount of corrosion obtained from each crack depth.

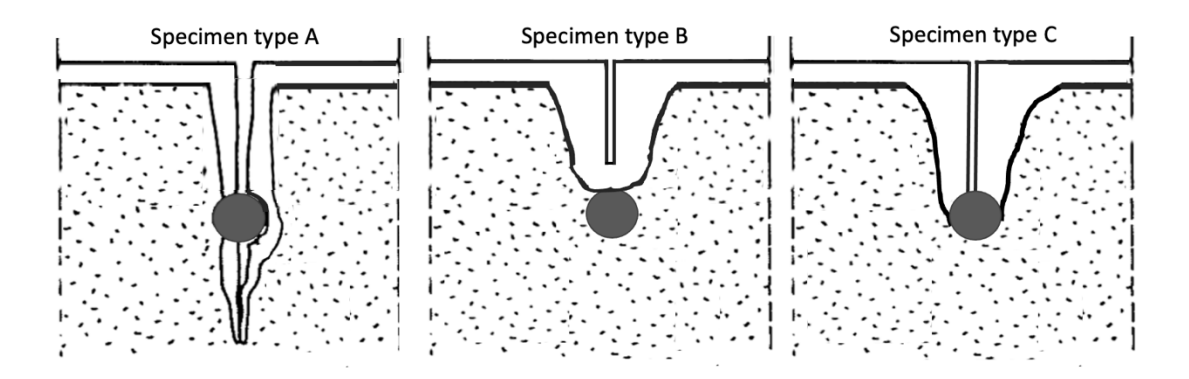


Fig. 6.24 Crack depths and concrete-steel interface disruption levels for all three specimen designs A, B and C.

As mentioned in the methodology part of this work, there are two sets of specimens cast at different times. The primary reason for casting the second set of specimens was the delayed corrosion initiation in specimen type A1 as well as the thought of examining the effect of crack depths that stop on top of the reinforcement (type C specimens). Initially, two crack depths were considered to be studied A1 and B where cracks extend the rebar level and stop short before the reinforcement respectively. After casting the second set of specimens, the initiation and progression of the corrosion process occurred at the expected pace as the chloride application technique and amount of chloride applied changed. Thereby A1 and B specimens were exposed to an aggressive environment longer (36 months), while the set of A2 and C specimens were exposed for 14 months. Thus, the first set of specimens A1 and B are presented first (subsection 6.2.1) and followed by the second set of specimens which consist of A2 and C

specimens (subsection 6.2.2). The order of results starts with the first set made of PC, GGBS and FA then follow by the second set made with the same cement types.

Although two specimen sets were cast at different times, some inferences can be made with regard to all three crack depths on the corrosion of reinforcement. Thus, the first question that arises from the results is which crack depth gives rise to more corrosion. To answer this question, the results are presented in the following order below:

- Half-cell potential readings to indicate the initiation time for corrosion
- Corrosion rates
- Gravimetric mass loss
- Photographic evidence of reinforcement condition

6.2.1 Specimen designs A1 & B

6.2.1.1 Half-cell potentials

Initial understanding of the effect of crack depth on corrosion can be obtained from Half-cell potential readings which are used to indicate a starting point of the corrosion process in these specimens with various crack depths and disruption levels in the steel-concrete interface.

Figure 6.25 present the Half-cell potential readings for A1 & B set made of all cement types. According to the potential readings shown in the figure, an obvious difference can be seen between the two specimen designs, as the steel-concrete interface disruption levels are significantly different. Generally, the trends are extremely similar in all cement types, where the breakdown of the passive film in Specimen type A1 took place a lot earlier than in B specimens. The depassivation in A1 specimens started after the 6, 4, and 2 months for specimens made of PC, GGBS and FA respectively, whereas, in type B specimens, it took around a year for the potential readings to get negative enough to indicate the breakdown of the oxide film. Overall, the corrosion possibility in B type specimens ranged between

low and high levels whereas in A1 specimens the trends fluctuated between high and severe corrosion probability zones.

6.2.1.2 Corrosion rates

Since there are only two groups being analysed in both sets, such as A1 and B in the first and A2 and C in the second set, a one-way ANOVA test has been performed. Unlike the effect of crack widths, where a number of width variations were considered (0: 0.1; 0.2; 0.3; 0.4mm), in this set, there are three crack depths and due to different cast times, the specimens were divided into two groups as mentioned above. The outcome of the test is shown in table 6.10 for all three cement types.

Table 6.10 ANOVA results for different crack depths (Specimen types A1 and B) in specimens made of all cement types and measured through both measurement techniques.

Specimen types A1 and B	Measurement techniques	F Test statistic	Significance level
PC	LPR	F (1)= 34.69	p < 0.05
	ZRA	F(1) =71.73	p < 0.05
GGBS	LPR	F (1)= 50.21	p < 0.05
	ZRA	F(1) = 23.66	p < 0.05
FA	LPR	F (1)= 51.21	p < 0.05
	ZRA	F(1) = 11.05	p < 0.05

According to One-way Anova results, the difference in corrosion rates between specimen designs A1 and B is significant in all cement types and via both measurement techniques. This highlights that corrosion propagation proceeds at different rates in these two crack depths.

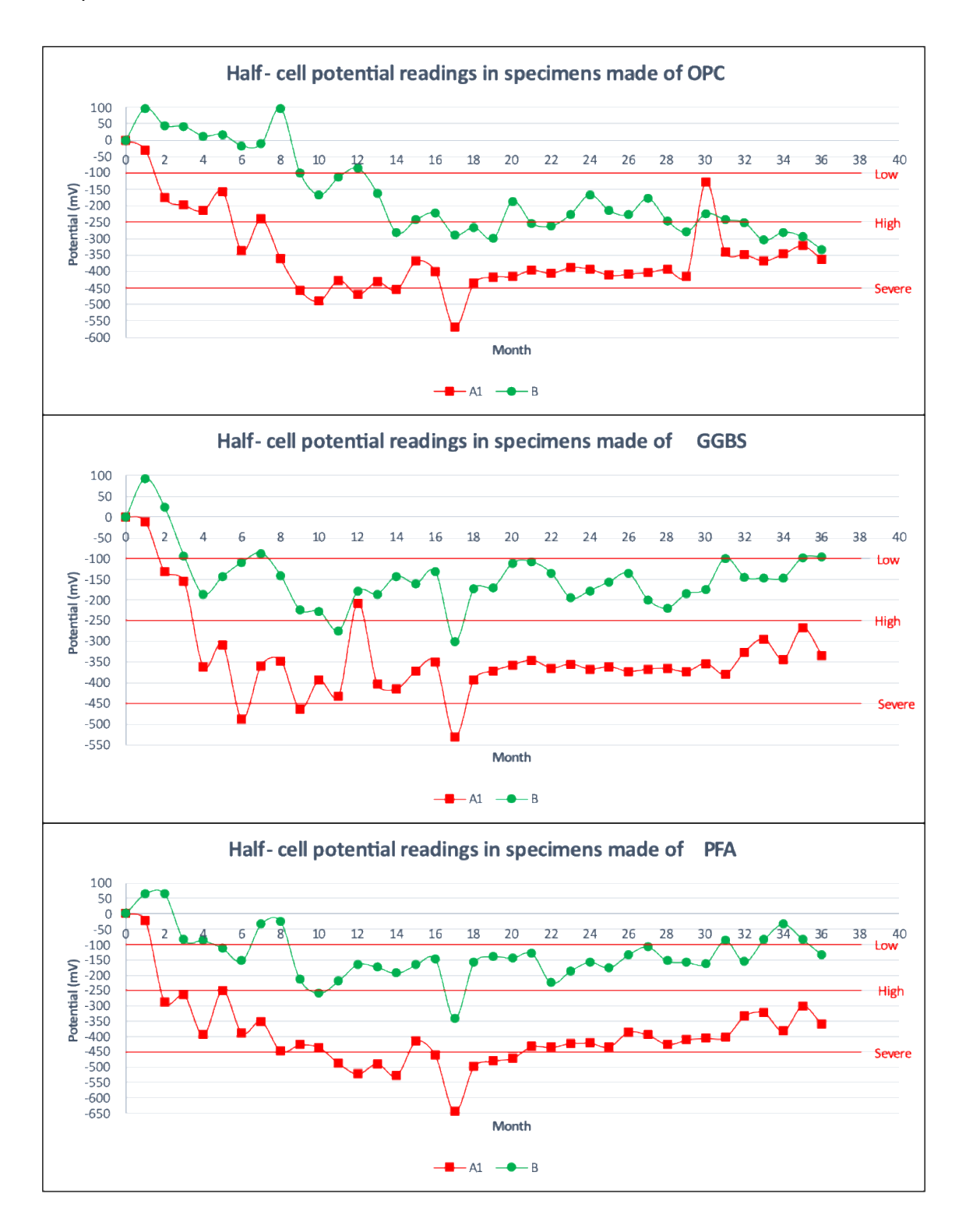


Fig. 6.25 Half-Cell potential readings for specimen types A1 and B made of all cement types.

Corrosion rates measured via both measurement techniques are shown as a boxplot in Figure 6.26. The boxplots represent the spread of the data, and the median (straight line on the body of the boxplot) as well as the mean values (the

red dot and a figure underneath it) of the readings. As can be seen from Fig. 6.26, there is a considerable difference in the spread of the data between specimen designs A1 and B measured via LPR, whereas ZRA readings show a number of outliers which might have affected the ANOVA results, but the spread of data is smaller compared to LPR readings. Furthermore, boxplots from the results including the last 26 months readings only are presented in Appendix E for specimens A1 and B.

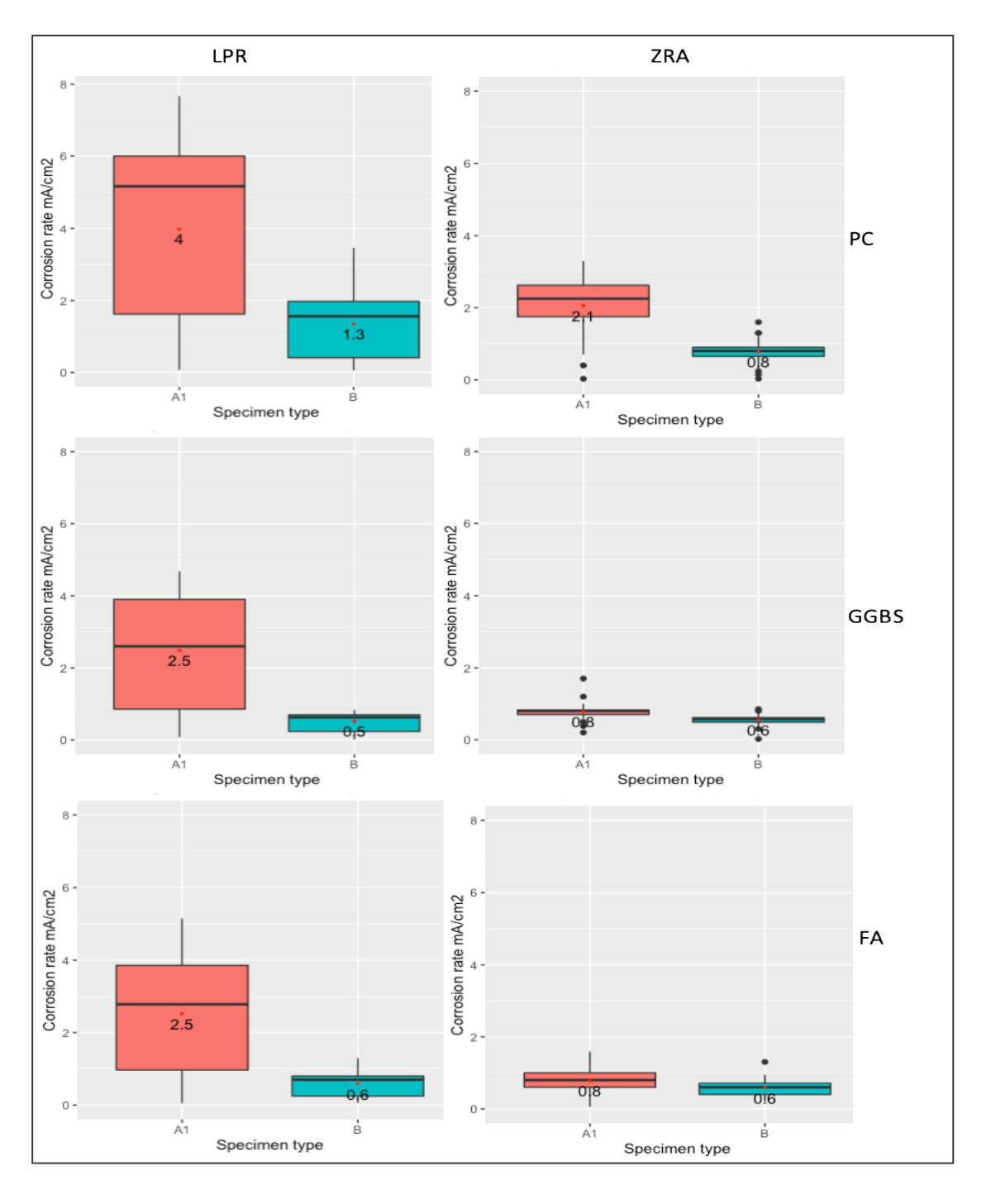


Fig. 6.26 Corrosion rates (μA/cm²) experienced by specimen designs A1 and B.

Generally, corrosion rates measured via ZRA appear to be substantially smaller than that of LPR, this is attributed to the fact that these measurement techniques measure two different types of corrosion that would coexist during the active corrosion process. Moreover, they can give an estimate of corrosion rates, however, there are many factors influencing the results, thus gravimetric mass loss is an essential measure in such experiments as a confirmation of the accuracy of non-destructive testing.

In the case of LPR readings, microcell current is measured through the slope of the Tafel plot, which is a graph of the anodic and cathodic polarization behaviour of the reinforcement. It is achieved by applying a small potential to the reinforcement and measuring the resulting current response.

In the case of ZRA technique, galvanic current between the two different kinds of metals is measured. Also, this technique asses the corrosion of the entire rebar under the study thus can be sensitive to the changes of the corrosion conditions, such as oxygen concentration, temperature, the passivation state of the metal (Yunze et. al. 2016).

Gravimetric mass loss on the other hand, is a common method to quantify the extent of corrosion in a laboratory setting. It involves weighing the steel reinforcement before and after exposure to a corrosive environment for a specific period. The difference in mass indicates the amount of material lost due to corrosion.

6.2.1.3 Gravimetric mass loss

Figure 6.27 represents a Gravimetric mass loss for all specimen designs combined together. The first line represents a mass loss in grams obtained from specimens made of PC whilst the second and the third lines stand for specimens made with the addition of GGBS and FA.

Chapter 6 Results and Discussion

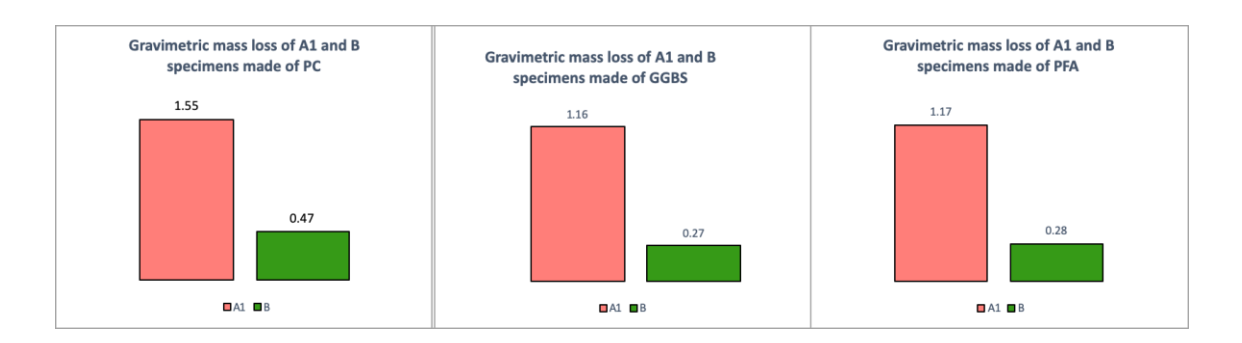


Fig. 6.27 Gravimetric mass loss (in grams) in type A1 & B specimen designs made with PC, GGBS and FA.

Gravimetric mass loss results can be considered as a confirmation of all the corrosion estimation tests performed above. As can be seen from the graph, all non-destructive test methods appear to be in good agreement with the Gravimetric mass losses. Gravimetric mass loss has been completed following (ASTM G 1-03, 2017) and described in detail at Subsection 5.4 of this work.

The difference in compressive strength of the concretes used in this work was not a primary focus of this work, however, it can be seen that specimens with the addition of mineral admixtures exhibited lower rates of corrosion, although they developed lower compressive strength.

6.2.1.4 Photographic evidence of reinforcement condition

A visual appearance of the rust formed on the rebar surface depending on each crack depth can be seen in Figure 6.28. The figure is divided into three parts according to the cement types used (shown on the left side), and according to specimen designs shown as A1 & B (on the right side). Since the rust formation differed on the sides facing the crack and the side away from the crack, the side of the rebar facing the crack is denoted as CS and the reverse side is denoted as RS in the graphs (shown on the right side of the graph). It appears from the photographs, that the surface facing the crack in type A1 specimens was fully covered in rust except for specimen made of GGBS which corroded from both ends and the central area kept a good contact with the surrounding concrete. This could be due to the nature of the crack formation. Although the crack was ensured to form above and along the reinforcement, the crack tortuosity as well as the alignment of coarse aggregates could have affected the degree of

disturbance between steel concrete interface. While the reverse side of the bar in type A1 specimens made of blended cements is relatively rust-free, whereas in specimen made of pure PC the reverse side is also covered in rust. Regarding the corrosion development in type B specimens, both sides have some patches of rust, but the corroded area is considerably smaller than in type A1 specimens. This is expected as the reinforcement was covered by concrete. The reverse side has substantially less rust patches compared to the side facing the crack.

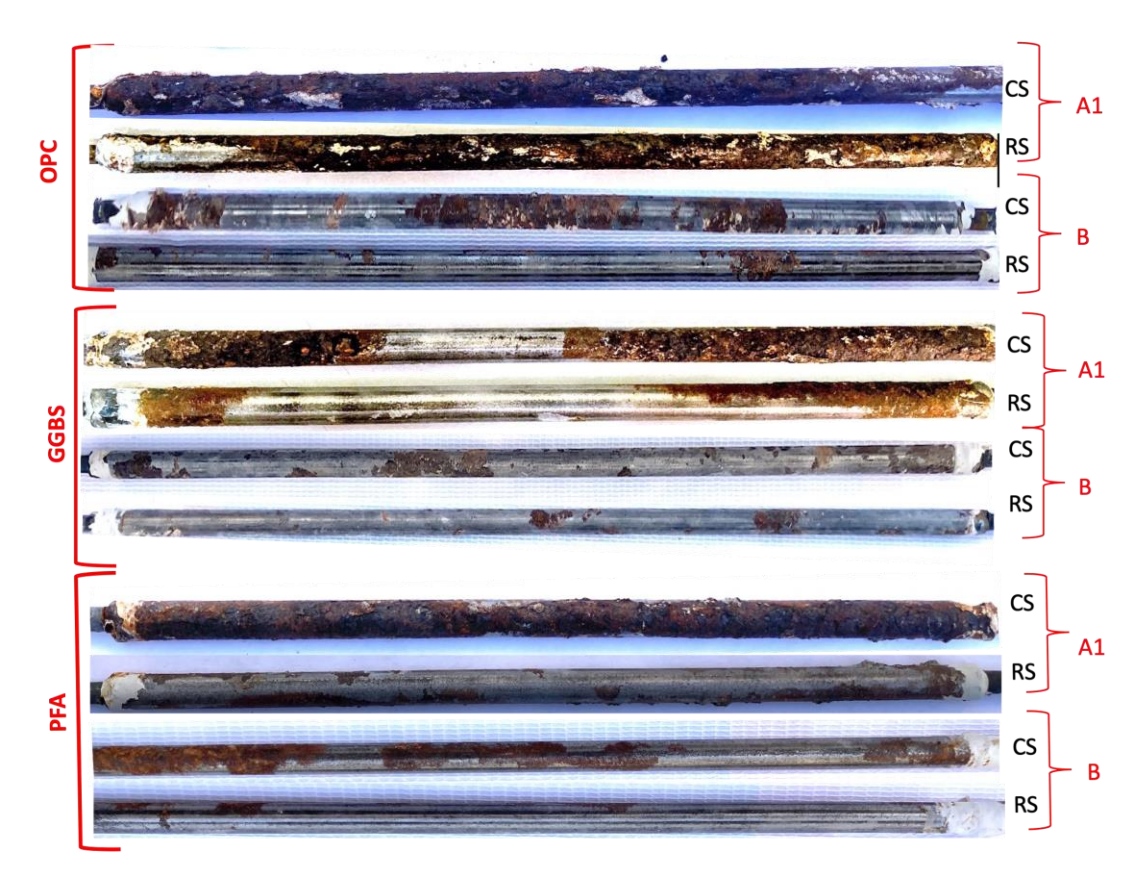


Fig. 6.28 The rust development on the surface of the reinforcement with various crack depths for the set of specimens A1 & B.

6.2.2 Specimen designs A2 & C

6.2.2.1 Half-cell potentials

According to Half-cell potential records shown in Figure 6.29 which represents the corrosion initiation time for specimen designs A2 and C, it appears that the breakdown of the passive film happened during the first couple of months in both specimen designs.

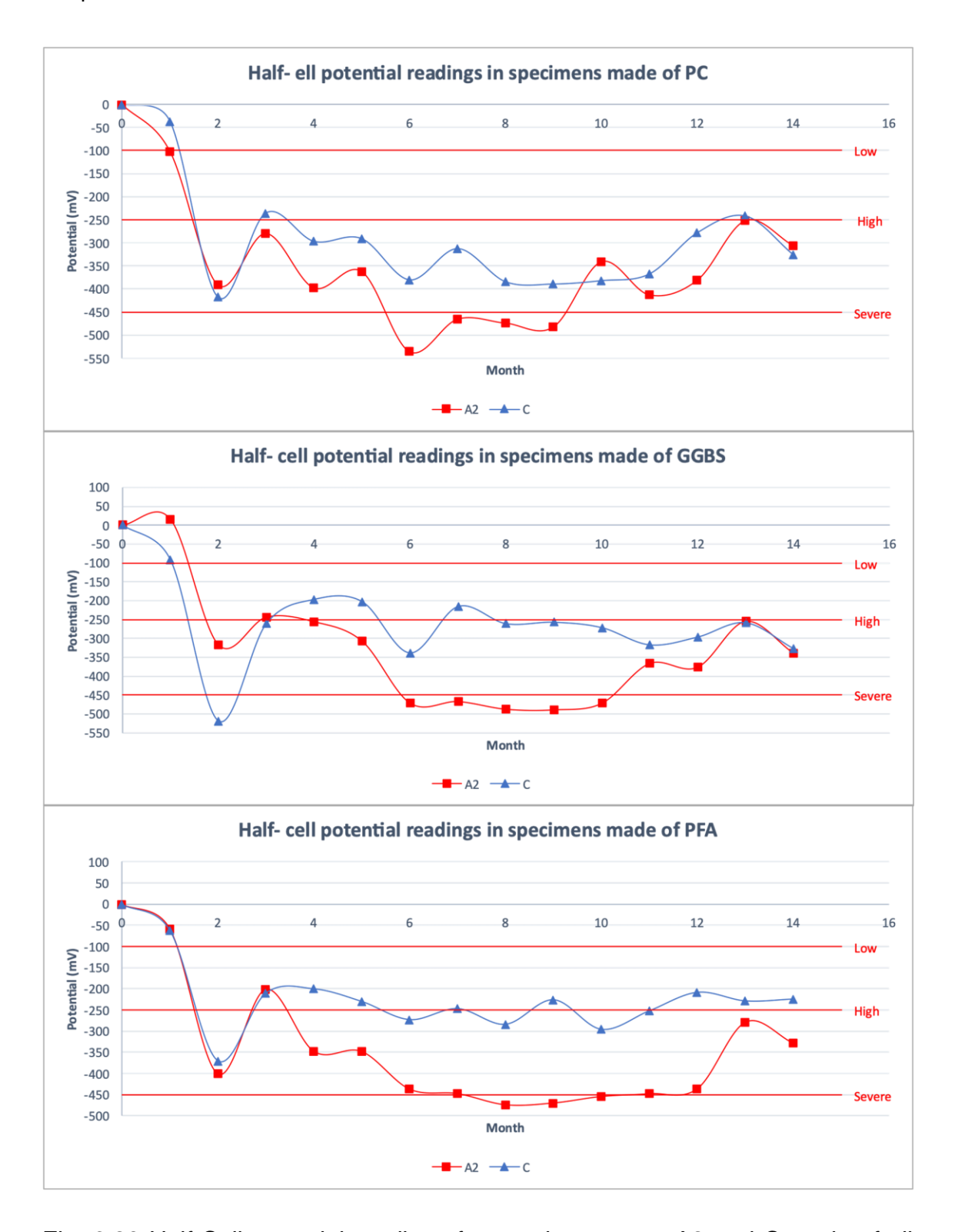


Fig. 6.29 Half-Cell potential readings for specimen types A2 and C made of all cement types.

Although the starting point of corrosion was identical in these specimens, the rates of corrosion seem to be different as the potential records for specimen type A2 indicated severe corrosion probability while that for type C specimens

fluctuated around the high corrosion possibility line, except for the second month where the potentials dropped significantly reaching the severe corrosion zone in almost all cement types. This is attributed to the disruption level in the steel-concrete interface. Overall, looking at various crack depths and disruption levels, examined so far, it appears that all three crack depths and disruption degrees give rise to different amounts of corrosion. The next test for clarifying this difference in corrosion progression is corrosion current measurements in these specimens.

6.2.2.2 Corrosion rates

ANOVA test results are shown in table 6.11. Regarding the second set of specimens where specimens A2 and C are analysed, it appears that the outcomes obtained via LPR technique revealed a significant result. Whereas in readings measured via ZRA, specimens made of PC only showed significant effect and the other cement types revealed insignificant outcomes. This is perhaps due to the differences in corrosion type being measured via ZRA and the rates of macrocell corrosion proceed at a similar rate in these cement types as well as crack depths.

Table 6.11. ANOVA results for different crack depths (Specimen types A2 and C) in specimens made of all cement types and measured through both measurement techniques.

Specimen types A2 and C	Measurement technique	F Test statistic	Significance level	
PC	LPR	F(1)= 10.79	p < 0.05	
FO	ZRA	F(1) =7.11	p < 0.05	
CCRS	GGBS LPR ZRA		p < 0.05	
GGBS			p = 0.113	
FA	LPR	F(1)= 16.57	<i>p</i> < 0.05	
1.4	ZRA		p = 0.339	

Boxplots produced from corrosion rates are shown in Figure 6.30. The spread of the data is considerably different between both specimens, although the crack reaches the reinforcement level in both specimen designs, it appears that specimens A2 underwent a higher corrosion magnitude compared to specimen

type C according to LPR readings which are in line with the half-cell potential records. However, the spread of the data measured via ZRA is quite similar in blended cements in both A2 and C specimens.

6.2.2.3 Gravimetric mass loss

Gravimetric mass losses experienced by these specimens are shown in Figure 6.31. According to the graph, the corrosion process was more intensive in A2 specimens compared to type C. This is also in agreement with all test results performed so far.

6.2.2.4 Photographic evidence of reinforcement condition

The spread and development of the rust on the bar surface can be seen from Figure 6.32. It can be seen that the surface facing the crack is almost fully covered in rust in both A2 and C specimens, while the surface away from the crack is partially clean and smooth. This indicates that there remained an intact contact of the reinforcement with the surrounding concrete. The surface facing the crack appears to suggest a similar corrosion magnitude irrespective of crack depth according to the figure.

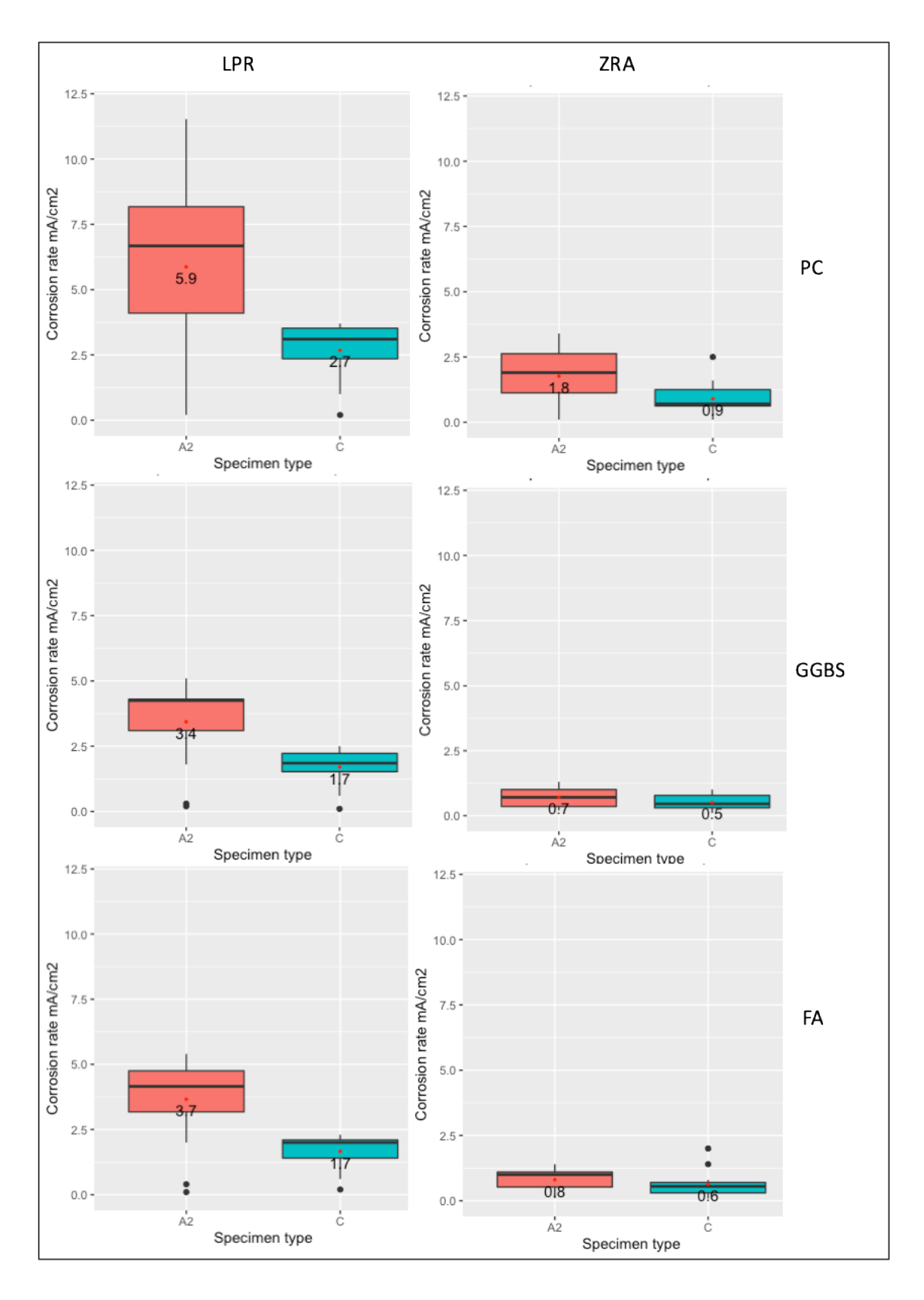


Fig. 6.30. Corrosion rates ($\mu A/cm^2$) experienced by specimen designs A2 and C.

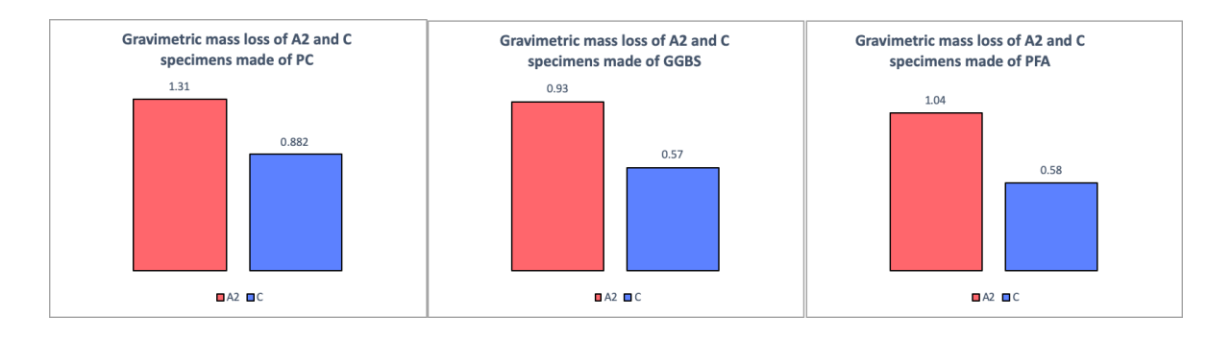


Fig. 6.31. Gravimetric mass loss (in grams) in all specimen designs made with PC, GGBS and FA

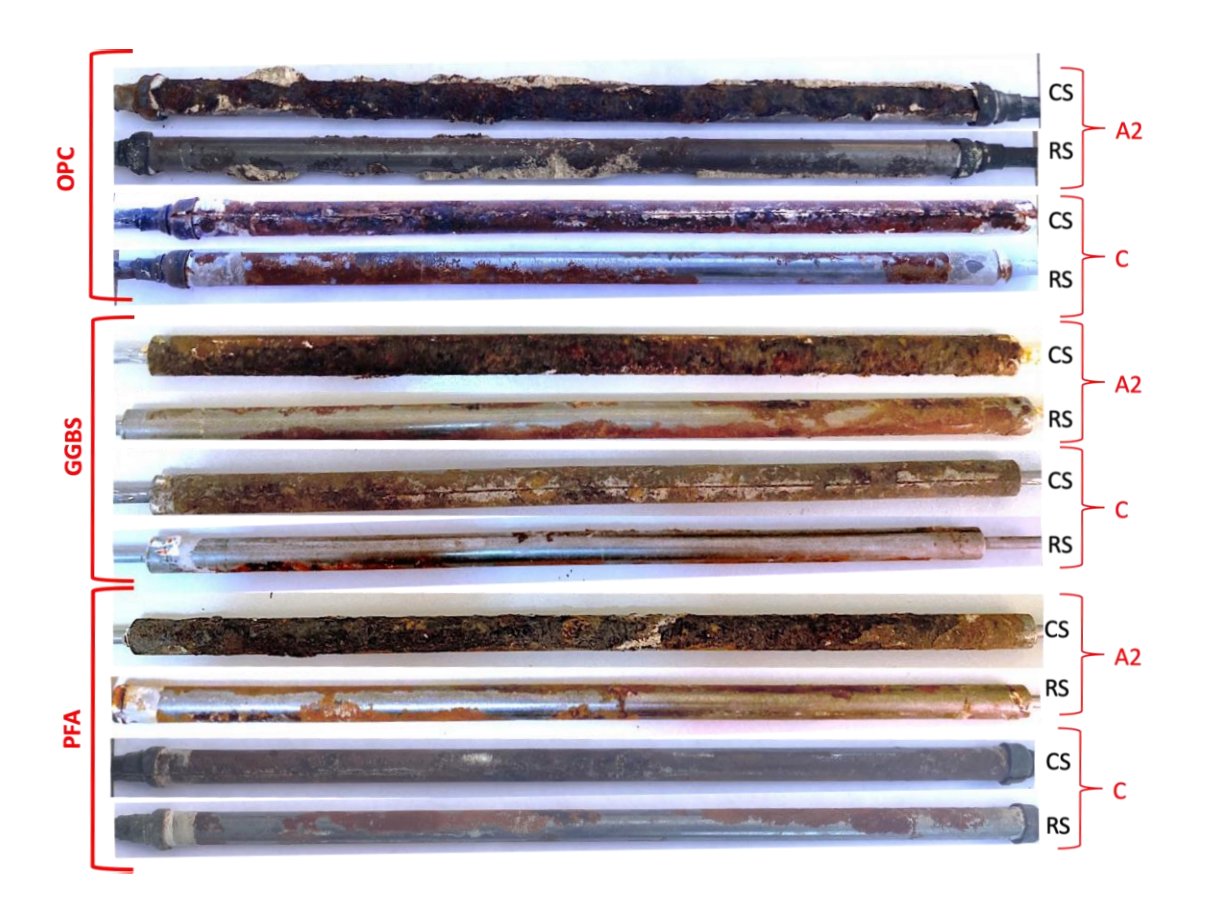


Fig. 6.32. The rust development on the surface of the reinforcement with various crack depths for the set of specimens A1 & B.

6.2.3 Discussion on the effect of crack depth in reinforcement corrosion

Overall, the effect of crack depth is evident from the results presented above, where a significant outcome was obtained in all cases according to LPR readings. This is due to the type of corrosion that occurred in these specimens which is explained below. Figure 6.33 presents photographic evidence of the difference between rust that developed on the rebar surface facing the crack before (denoted as A, B, and C) and after the pickling (denoted as A',B' and C') from closer proximity and bigger scale.

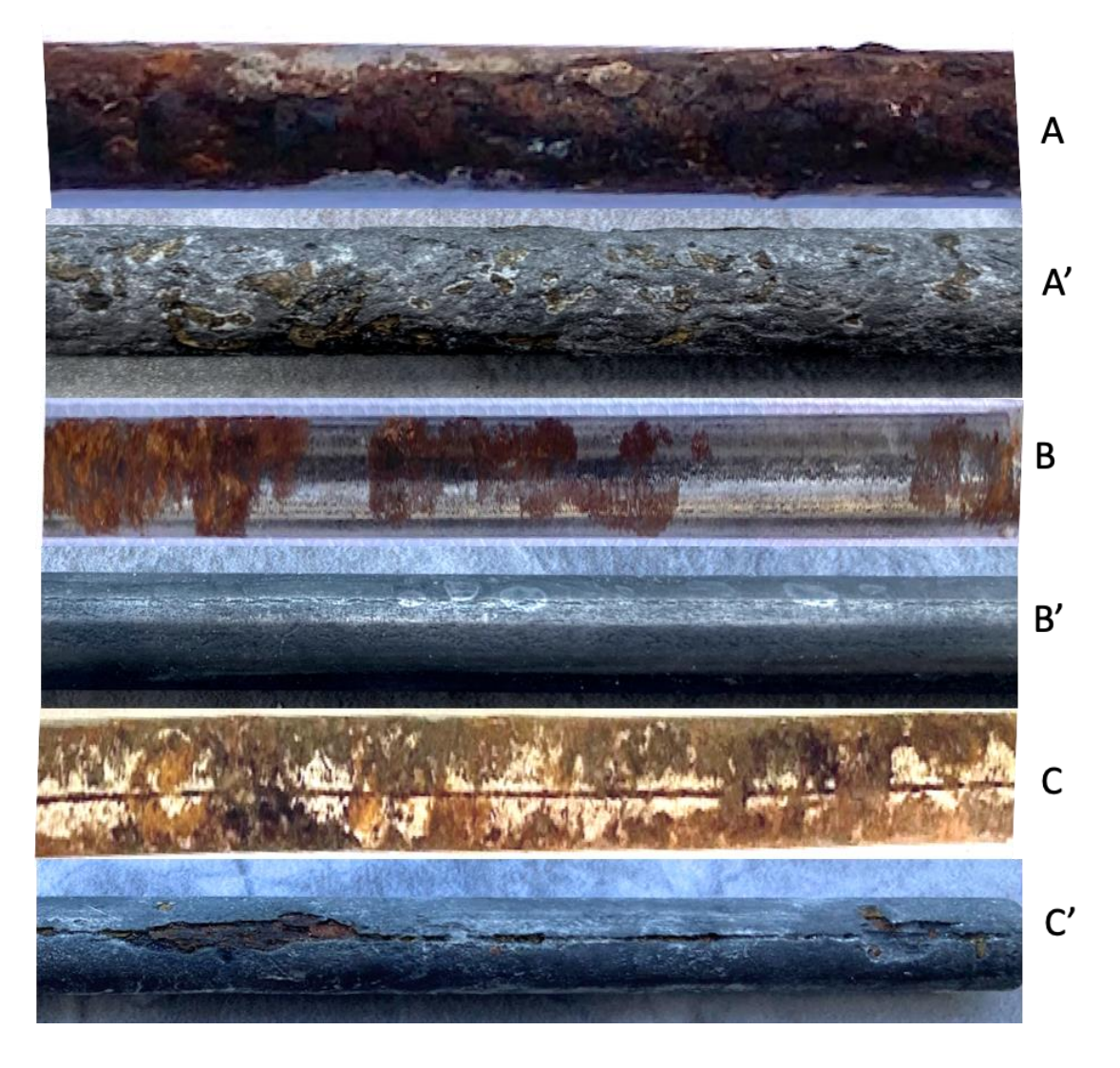


Fig. 6.33. The corrosion type on the surface of specimens with different crack depths.

Taken together, these results suggest that Specimen design A, where the longitudinal crack goes beyond the reinforcement level gives rise to the highest

amount of corrosion, followed by Specimen type C and ending with Specimen type B corresponding to the lowest corrosion rates. The crack depth in type A and C specimens gave rise to pitting corrosion, however, they were different in nature as can be seen from Figure 6.32. Although type A specimens exhibited higher corrosion magnitude and had more mass loss compared to type C, after the pickling it was noticed that the pits in type C specimens were deeper. In type A specimens extensive pitting can be noticed covering a wider area, but the pit depths were not more than 1mm, whereas in type C specimens the pits were more than 2mm in some places. This needs more research as the pits formed in type C specimens may impair the structural integrity of the reinforced concrete structures exposed to an aggressive environment faster leading to a reduction of load bearing capacity.

Another aspect in evaluating the corrosion extent is labelling/measuring the surface area rusted, this evaluation may lead to wrong interpretations. Looking at Figure 6.32, it can be seen that the rusted areas in type A2 and C are extremely similar, when attempting to measure the rust-covered area they revealed similar results as well. However, the nature of the pits and their depths are completely different, it was found that the area of the steel covered in rust is not an indication of the corrosion magnitude in these specimens. Thus, gravimetric mass loss and careful examination of the pits is necessary when categorising the corrosion extent.

These differences in the degree of corrosion rates in each specimen design could be due to the following causes:

- the disruption severity of the concrete-steel interface;
- the availability of oxygen to the cathodic regions;
- the corrosion type, whether it is microcell or macrocell corrosion;
- the ratio of cathodic to the anodic areas formed on the surface of the rebar;
- the quality of the oxide film on the surface of the rebar;

Regarding the amount of corrosion along the length of the reinforcement in specimen type A, it appears that although the crack exceeded the reinforcement

level, the top part and perhaps one side (right or left) of the rebar experienced severe disruption, whereas some parts on the other side maintained an intact contact with the surrounding concrete. When the specimens were opened along the length of the crack, the rebar inside the concrete looked like the whole circumference of the bar is covered in rust and uniform corrosion took place, however, when the bar was removed from the concrete completely, the other side was relatively rust-free as illustrated in figures 6.28 and 6.32. This is expected due to significant debonding of the steel-concrete interface throughout the length of the reinforcement. This has been confirmed when the rebars were cleaned from rust by pickling in order to obtain the gravimetric mass loss. The surfaces facing the crack were heavily pitted in most cases, whereas the surface that remained intact with concrete stayed smooth and rust-free similar to the B' in Figure 6.33. Thus, the rebar surface that kept an undamaged contact with the reinforcement is thought to act as a cathode, whereas the surface subjected to a severe debonding with the surrounding concrete acts as an anode.

Thus, it appears that in the case of specimen design A, where the crack exceeds the reinforcement level, microcell corrosion takes place. Higher rates of corrosion are caused by an extreme disruption along the length of the rebar which exposed a larger area of the rebar to the contaminated environment and allowed higher oxygen availability for the corrosion process to proceed. According to (Schiessl, 1986), the coincident cracks lead to the development of microcell corrosion which is illustrated in Figure 6.34. In this scenario, rebar with a coincident crack act as an anode and an intact part of the steel located underneath it acts as a cathode Coincident cracks do not confine the sites of possible corrosion initiation as in the case of transverse cracks, because the passive film on the surface of the steel might be lost in several positions and larger areas (Pease, 2010).

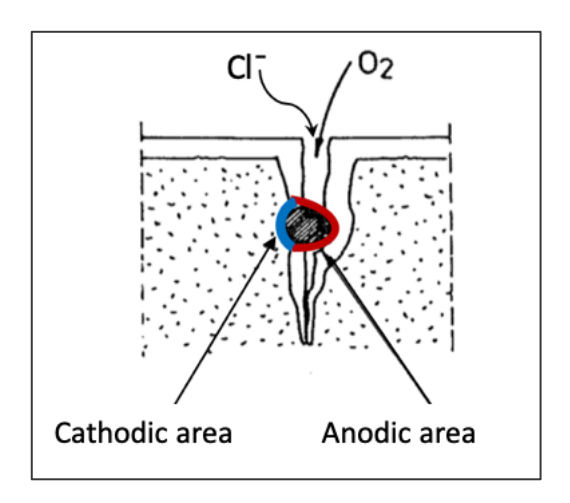


Fig. 6.34 Formation of cathodic and anodic areas on the surface of the reinforcement where the crack follows the rebar longitudinally, adopted from (Schiessl, 1986).

In the case of specimen type C where the crack stops on top of the reinforcement, microcell corrosion is also thought to occur. The severity of corrosion appears to be caused by the quality of the oxide film on the surface of the reinforcement. As in the case of Specimen type C, it is not clear whether the passive film has formed fully on the surface of the concrete as the steel shim was placed on top of the reinforcement during casting. The shims were removed before the end of the set time of the concrete. Thus, all the thermodynamic and kinetic conditions that were exemplified in the literature might not be applicable as the cracks formed during casting. According to research by (Hansson et al., 2006), it takes seven days for the formation of the passive film on the surface of the rebar in a mortar and three days in a synthetic pore solution. Whereas, in more recent research by (Hussain et al., 2015), it was found that it takes at least 20 days for the formation of passive film in Ordinary Portland cement concrete with a w/c ratio of 0.50. Thus, these specimens did not have neither 7 nor 20 days for the proper development of the passive film fully covering the bar. This explains the formation of V-shaped pitting along the crack, an instant corrosion process seems to be taking place, as no build-up of the chloride threshold was necessary to break the passive film. The area of bar where the steel shims were placed as crack inducers left bare. The suggested corrosion mechanism is illustrated in Figure 6.35, where the top surface of the rebar facing the crack end acts as an anode and the bottom side of the rebar acts as a cathodic area.

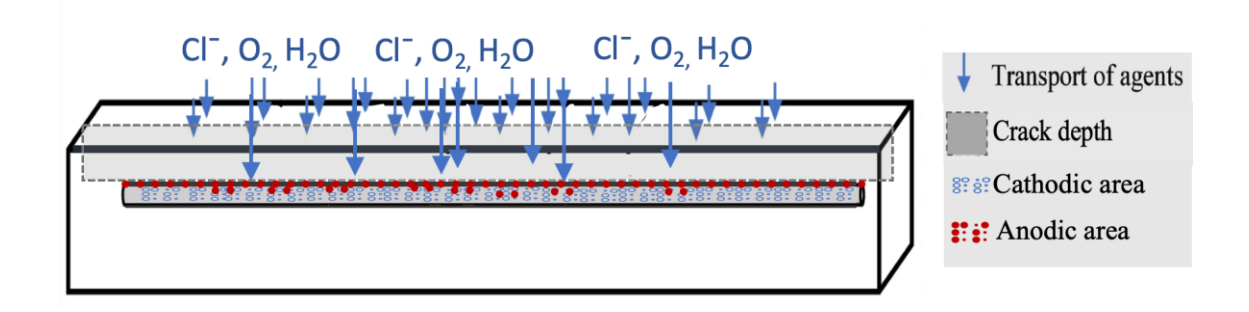


Fig. 6.35. The corrosion mechanism in Specimen type C, adopted from (E. Chen et al., 2020).

Regarding the corrosion mechanism in Specimen type B, where there is a clearance of around 10mm between crack end and reinforcement, a combination of both macrocell and microcell corrosions appears to take place. During the specimen design stage of this work, it has been planned that the space between crack end and rebar be 5mm, however, due to possible shifts during vibration, the still shims used to induce cracks moved upwards resulting in a clearance of 10mm. Thereby, in this case, a good quality oxidation film was formed on the rebar surface, and a time for a chloride build-up and penetration were necessary to break the passive film. Thus, in this specimen design, the exposure is similar to sound concrete with a thin concrete cover. The initiation of corrosion process was slower than the other two specimen designs. Although the desired specimen configurations have not been achieved in this set of specimens, it can still be representative of a real structure condition in practice, where cracks with a certain width appear on the surface of the concrete, however, do not reach the reinforcement level fully. Overall, the corrosion process started in areas of the steel with relatively lower potential or in places with the highest chloride ion buildup. As a result, corrosion patches started to appear in several areas, mainly on the top surface of the rebar facing the crack. The reinforcement areas with signs of corrosion acted as an anode and the remaining parts acted as a cathode. This is demonstrated in figure 6.36. Upon breakage of the specimen, it was observed that general corrosion took place in corroded areas, as no pitting signs have been noticed. The corroded points were simply covered with a thin layer of rust and were instantly removed with Clark's solution leaving a smooth surface which can be seen from Figure 6.33, B'.

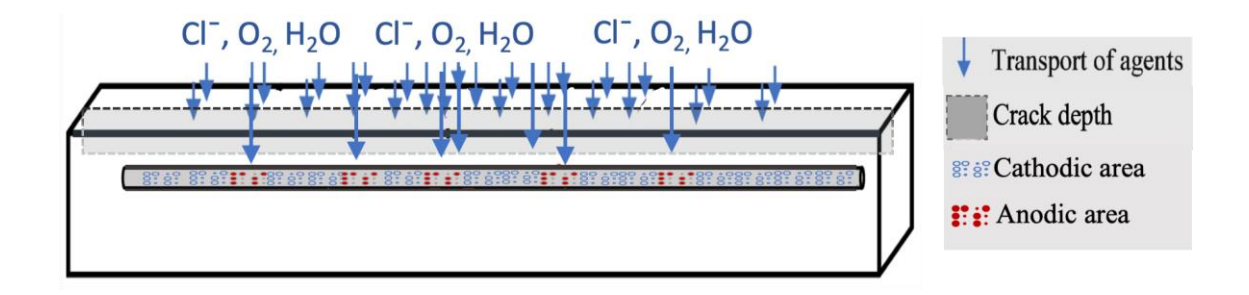


Fig. 6.36. The corrosion mechanism in Specimen type B, adopted from (E. Chen et al., 2020).

There is scarce research work that looked at the effect of a coincident crack depth on corrosion of reinforcement. Most of the research has focused on transverse cracks in terms of the effect of crack width (Mohammed et al., 2001; Montes et al., 2004; Otieno, 2010) and crack depth (Audenaert, 2009; Marsavina et al., 2009). The latter has been concentrated on the effect of crack depths on chloride penetration not the corrosion rate of the reinforcement.

According to the study by Brown, an inspection of 37 bridges in Virginia was analysed (Sansone & Brown, 2007). Overall, 30.5 % of the total 108 cracked cores, had crack depths extending or stopping at the level of the reinforcement. It was found that an increase in crack depths leads to a higher percentage of surface area corrosion. Another parameter that influences corrosion of reinforcement in bridges was found to be the orientation of the crack concerning the reinforcement. The highest amount of corrosion was observed in cores with cracks located directly above and parallel to the rebar regardless of reinforcement type.

6.3 Effect of cement type on corrosion of the reinforcement.

Three different cement mixes have been used in this research with the following combinations: 100% PC; 35% PC/65% GGBS and 70% PC/30% FA. According to the results, the binder type appears to significantly affect the corrosion rates of reinforcement in all specimen designs. Since there were three specimen designs as A1/A2, B and C, all of them had replicates made of three binder types.

Subsections from 6.3.1 to 6.3.3 will cover the results on the effect of cement type on corrosion rates for type A1, B and C specimens respectively. The results are presented in the following order:

- Corrosion rates
- Chloride profiles in each specimen design and cement type

6.3.1 Specimen type A

6.3.1.1 Corrosion rates

The results on corrosion rates obtained from A1 and A2 specimens follow the same trends, thus the outcome of the A2 specimens can be found in Appendix E.

Table 6.12 represents the ANOVA test results of specimen type A1 obtained from both measurement techniques. As can be seen from the table, the effect of cement type revealed significant values via both measurement techniques, thus it has been followed by Post-Hoc test which is shown in table 6.13.

Table 6.12. ANOVA results for Specimen type A1 through both measurement techniques

Measurement technique	F Test statistic	Significance level
LPR	F(2)=6.83	p < 0.05
ZRA	F (2) =70.82	<i>p</i> < 0.05

Table 6.13. Post Hoc Test of multiple comparisons on the effect of cement type on corrosion among specimen type A1 measured via LPR and ZRA.

Measurement techniques							
Linear Polarisation Resistance			Zero Resistance Ammeter				
Binder type	Compa rison	. SIQ. SIQ					Sig.
1. PC 100%	1-2	1.49	p < 0.05	1. PC 100%	1-2	1.28	<i>p</i> < 0.05
2. GGBS 65%	3-2	0.035	p = 0.99	2. GGBS 65%	3-2	0.002	p = 0.99
3 FA 30%	3-1	-1.46	p < 0.05	3. FA 30%	3-1	-1.27	p < 0.05

It is evident from table 6.13, that the corrosion rates experienced by specimens made with the addition of GGBS and FA are extremely similar, whereas the comparison combinations of PC vs GGBS and PC vs FA resulted in significant results. This is better illustrated in Figure 6.37, where corrosion rates are shown as a boxplot. As can be seen from corrosion rates, the specimens made of PC experienced higher rates of corrosion whereas the blended types of cement show extremely similar values. According to LPR readings, the spread of the data is similar specimens with SCM, whereas the spread of data in ZRA readings show slight differences although the mean values are $0.8~\mu\text{A/cm}^2$.

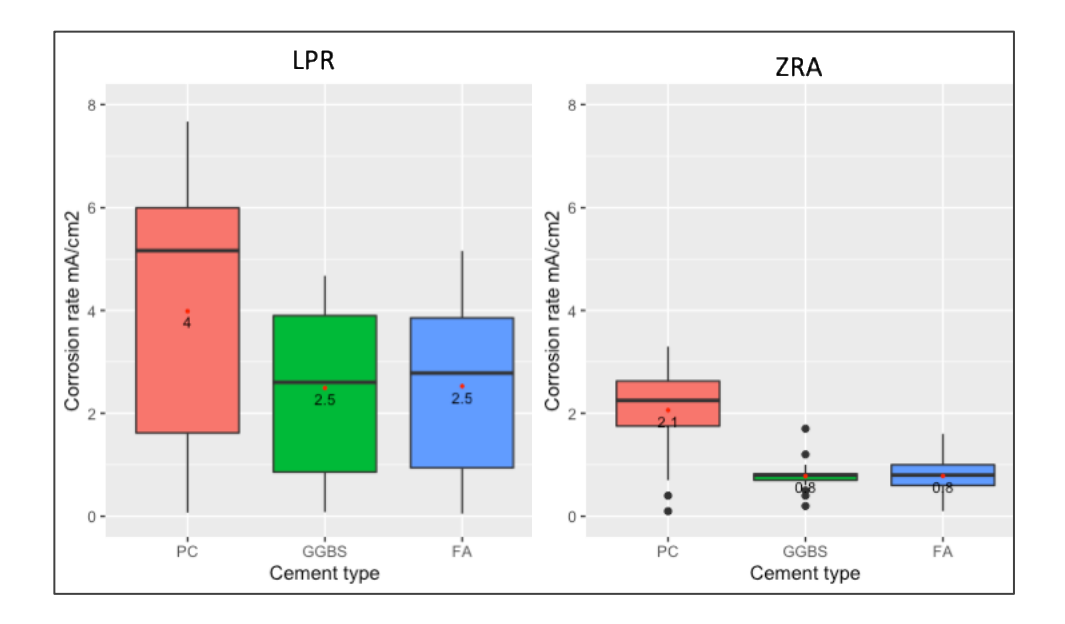


Fig. 6.37. Corrosion rates (μ A/cm²) in Specimen type A1 obtained via LPR and ZRA.

6.3.1.2 Chloride concentration in concrete made of different cement type

These differences in corrosion rates among various cement types might be due to differences in chloride concentration in the concretes. In control specimens the chloride profile has been identified by drilling a hole with intervals of 10mm and from the collected concrete powders, the chloride content has been acquired up until the depth of 40mm which is graphically shown in Figure 6.38. However, the chloride profiles in cracked specimens were not obtained following the same technique. Due to Covid 19, the specimens were transported to a different country in order to complete the experimental work and because of the busy schedule arranged for the equipment used in the laboratory of the university where the tests were carried out, the chloride content was determined only from two levels as shown in figure 6.39 and denoted as Top and Bottom levels. The specimens were cut into smaller blocks with the following dimensions: 28x57x300mm as shown as the red broken line representing the cut-out piece dimensions used to define the chloride content. The powder for determining the chloride content was collected from 3 points along the sample and the average chloride content was obtained. Since chloride profile was not a primary interest of this research and the test was not performed rigorously (the measurements were taken from two depth levels only in cracked specimens), it is thought to be useful in providing a better understanding and explanation of the corrosion mechanism in these cement types. As can be seen from figure 6.38, chloride content in each blended cement appears to be slightly higher than in specimens made of PC in the first 10mm layer of the concrete. However, compared to the first 10mm the chloride concentration dropped twice as much in the next 20mm depth in blended cement, whereas in samples made of PC the decrease was negligible. In the following 30mm depth, chloride content in the blended cement got reduced further and ended with 0.3 and 0.24 % in samples made of GGBS and FA respectively. However, chloride content in PC samples showed 0.94 and 0.86% in the 30 and 40mm depths respectively compared to the initial point of 1.54%. This difference in chloride penetration depth can be attributed to lower permeability as well as lower diffusion coefficient of blended cement compared to ordinary Portland cement. When the chloride comes into contact with blended cement, due to the low permeability of these types of cement, the chloride gets

highly concentrated on the top surface of the concrete and does not bind with the concrete as ordinary Portland cement does.

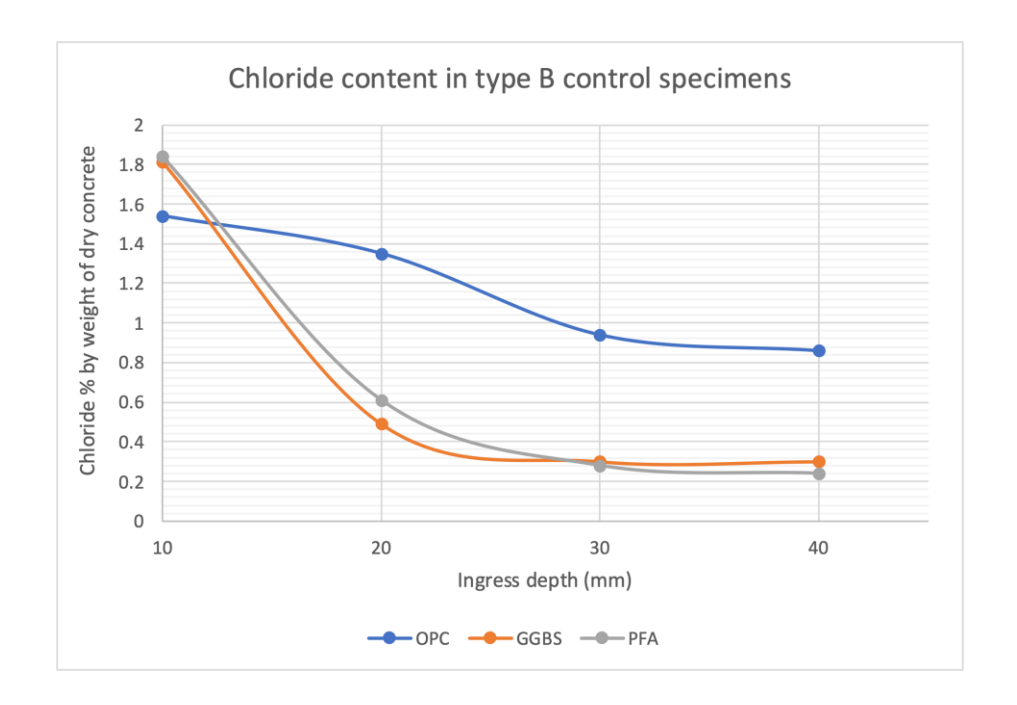


Fig. 6.38. The chloride content of control specimens made of all three cement types.

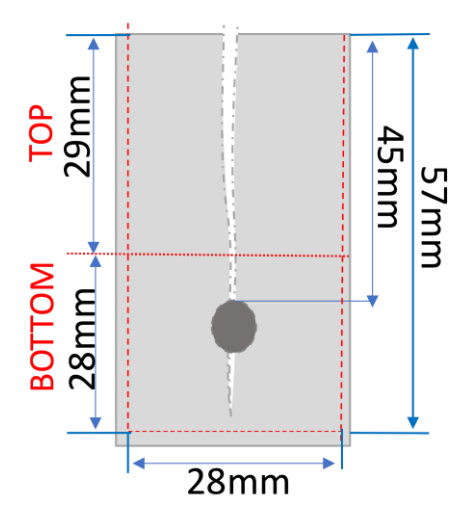


Fig. 6.39. A schematic of the levels where chloride profiles have been determined in Specimen design A.

The chloride content in cracked A1 and A2 specimens is shown in figure 6.40. These results appear to show that specimens made of blended types of cement had higher chloride levels in the top surface layers than corresponding specimens

made of pure PC but lower chloride levels at lower depth. Also, looking at both A1 and A2 samples (which have different exposure times) made of PC show a negligible difference between the two levels of chloride profiles. Whereas specimens with SCMs show considerable difference in chloride content found in the upper level and in the vicinity of the reinforcement. This is true for both A1 and A2 specimens which suggest the time dependence of chloride penetration in concrete with SCMs.

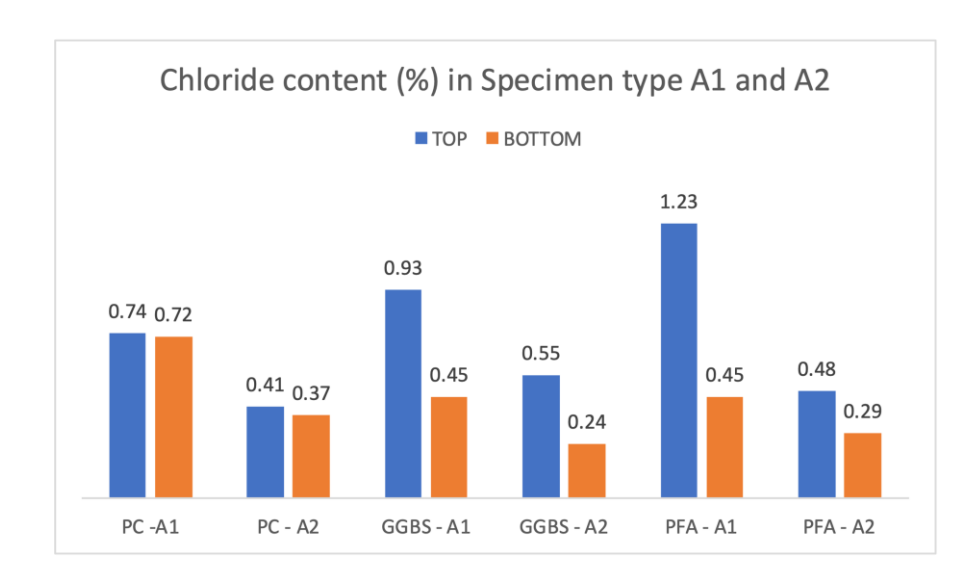


Fig. 6.40. The chloride content by weight of concrete in cracked A1 (exposed to an aggressive environment for 36 months) / A2 (exposed to an aggressive environment for 14 months) specimens made of all cement types.

6.3.2 Specimen type B

6.3.2.1 Corrosion rates

The next set of results represents Specimen type B with a crack width of 0.4mm, this crack width has been chosen because it is the widest crack, and specimen type A1/A2 had crack widths not exceeding 0.4mm. Tables 6.14 and 6.15 show the results of ANOVA and Post Hoc tests respectively, whereas Figure 6.41 displays the corrosion rate differences experienced by specimens made of different cement types.

Table 6.14. ANOVA results for Specimen type B through both measurement techniques

Measurement technique	F Test statistic	Significance level
LPR	F(2)=18.27	p=0.000
ZRA	F (2) =6.87	p = 0.000

Table 6.15 Post Hoc Test of multiple comparisons on the effect of cement type on corrosion among specimen type B measured via LPR and ZRA.

Measurement techniques								
Linear Polarisation Resistance			Zero Resistance Ammeter					
Dindor type	Compa	Mean	Sig	Binder	Compa	Mean	Cia	
bilider type	Binder type rison	Diff.	Sig.	type	rison	Diff.	Sig.	
1. PC	1-2	0.79	p < 0.00	1. PC	1-2	0.2	p < 0.00	
100%	1-2	0.79	$\rho < 0.00$	100%	1-2	0.2	ρ< 0.00	
2. GGBS	3-2	0.07	p < 0.87	2. GGBS	3-2	0.038	p < 0.78	
65%	5-2	0.07	p < 0.01	65%	5-2	0.030	ρ<0.70	
3. FA 30%	3-1	2.4 0.72	n -0.00	3. FA	3-1	-016	n = 0.00	
	3-1 $ -0.72 p = 0.00$		30%	J-1	-010	p = 0.00		

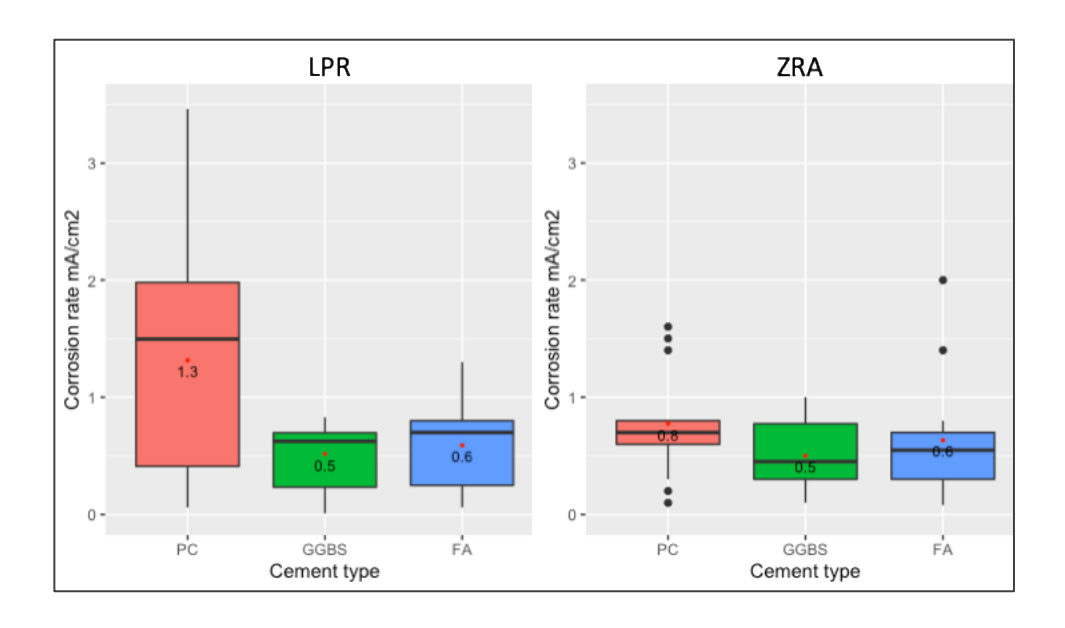


Fig. 6.41. Corrosion rates ($\mu A/cm^2$) in type B specimens obtained via LPR and ZRA

Generally, the corrosion trends in terms of cement type are extremely similar to the previous set of results. The specimens made of PC exhibit the highest amount of corrosion and blended cements show lower and similar trends.

6.3.2.2 Chloride concentration in concrete made of different cement type

Since the dimensions of these specimens were different from the previous model, Figure 6.42 shows the schematic of the cut-out piece of the sample for chloride content determination. The specimens were cut into smaller blocks with the following dimensions: 52x65x500mm as shown as the outer side of the specimen, whereas the thicker red broken line represents the cut-out piece dimensions used to define the chloride content. Figure 6.43 represents the chloride content of cracked B specimens where the same trends as in the case of specimen type A can be noticed.

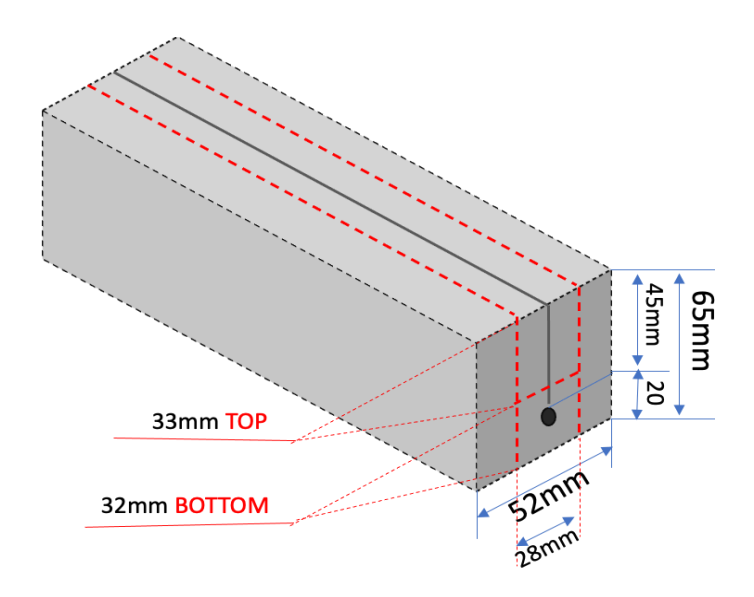


Fig. 6.42. A schematic of the levels where chloride profiles have been determined in Specimen design B.

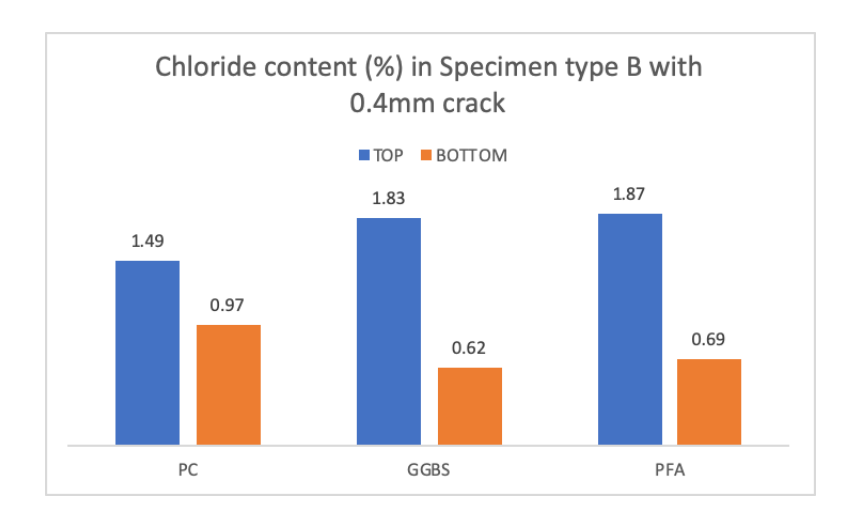


Fig. 6.43. The chloride content by weight of concrete in type B specimens with 0.4mm crack width only made of all cement types.

As can be seen from figure 6.35, the chloride concentration in the top layers is consistently higher in all samples which are expected from this set-up, however, in samples made of SCMs, the chloride content is higher than that of PC samples. The chloride content in the vicinity of the bar in specimens with SCMs however, show lower concentration percentages then samples with PC. Thus, it appears that even in specimens with coincident cracks the low permeability and diffusivity of blended cement take part in the corrosion mechanism.

6.3.3 Specimen type C

6.3.3.1 Corrosion rates

The following results show the effect of cement type on Specimen type C, where cracks stop directly over the reinforcement. Tables 6.16 and 6.17 show the outcomes of ANOVA and Post Hoc tests, while Figure 6.36 represents the corrosion rates experienced in specimens made with different cement types.

Table 6.16. ANOVA results for Specimen type C through both measurement techniques

Measurement technique	F Test statistic	Significance level
LPR	F(2)=6.84	p =0.002
ZRA	F(2) = 3.42	p = 0.123

ANOVA results revealed a significant p-value in the case of LPR measurements, however, ZRA measurements show an insignificant difference between cement types used, thus the Post Hoc test has not been continued for ZRA results. An insignificant difference in corrosion rates with regard to different cement types in ZRA reading can be seen in Figure 6.44, where the mean corrosion rates obtained from specimens made of PC is 1 μ A/cm² and 0.5 and 0.6 μ A/cm² from specimens with the addition of GGBS and FA respectively. This is likely due to

lower rates of macrocell corrosion in these specimen design and microcell corrosion is controlling the process.

Table 6.17. Post Hoc Test of multiple comparisons on the effect of cement type on corrosion among specimen type C measured via LPR and ZRA

Measurement				techniques			
Linear Polarisation Resistance			Zero Resistance Ammeter				
Binder	Compa	Mean	Sia	Binder	Compa	Mean	Cia
type	rison	Diff.	Sig.	type	rison	Diff.	Sig.
1. PC	1-2	4.70	p = 0.00	1. PC	1-2	NA	NA
100%	1-2	1.72		100%	1-2	INA	INA
2. GGBS	3-2	0.00	p = 0.87	2. GGBS	3-2	NA	NA
65%	3-2	0.39		65%	3-2	INA	INA
3. FA 30%	3-1	-1.33	p =0.02	3. FA30%	3-1	NA	NA

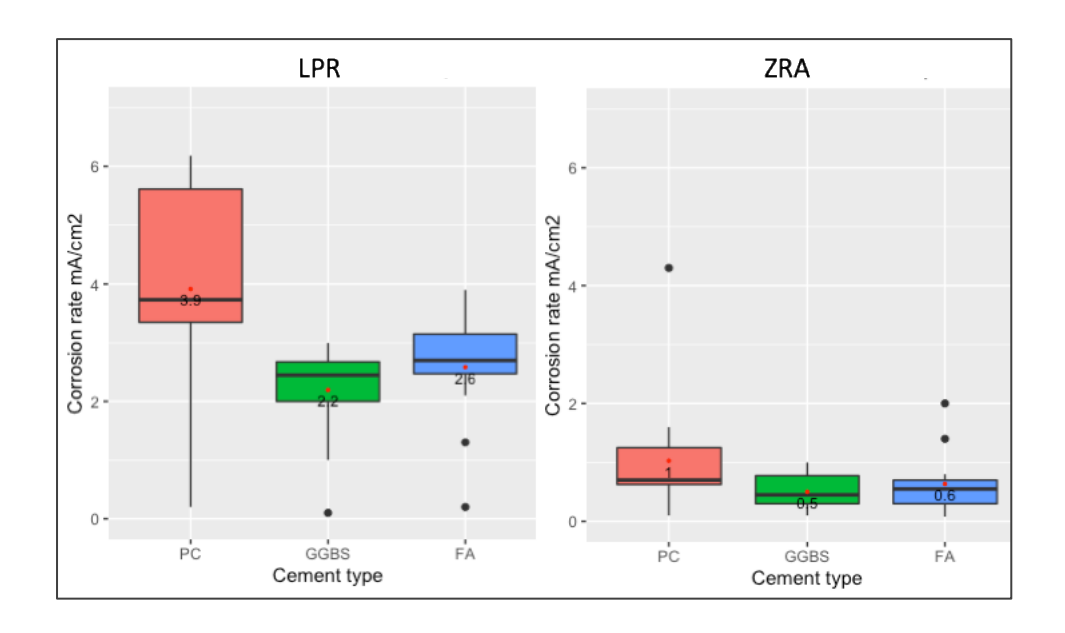


Fig. 6.44. Corrosion rates ($\mu A/cm^2$) in type C specimen obtained via LPR and ZRA.

6.3.3.2 Chloride concentration in concrete made of different cement type

The dimensions of the reduced sample for determining the chloride content are shown in the Figure 6.45.

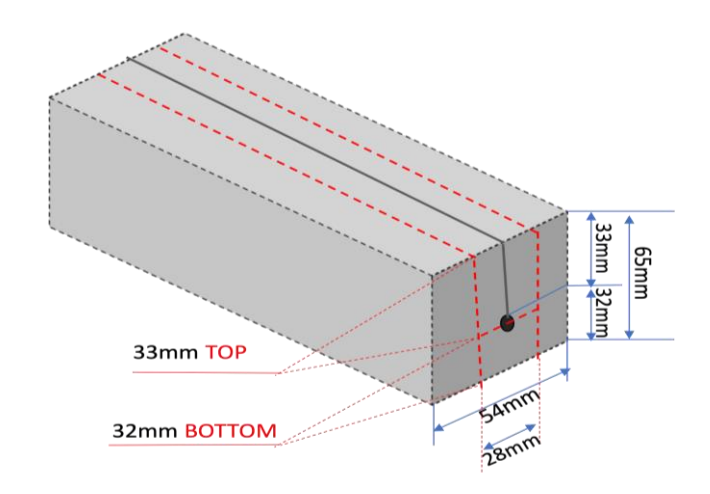


Fig. 6.45. A schematic of the levels where chloride profiles have been determined in Specimen design C.

Specimen design C was cast later than Specimen design B samples and they were exposed to a chloride environment for a shorter period of time. As can be seen from figure 6.46, the trends of chloride concentration follow the same order as previous sets of results. Although the cracks reach the reinforcement, the concentration of chloride is less pronounced in these specimen designs compared to B samples, this is due to the shorter exposure time to chloride solution.

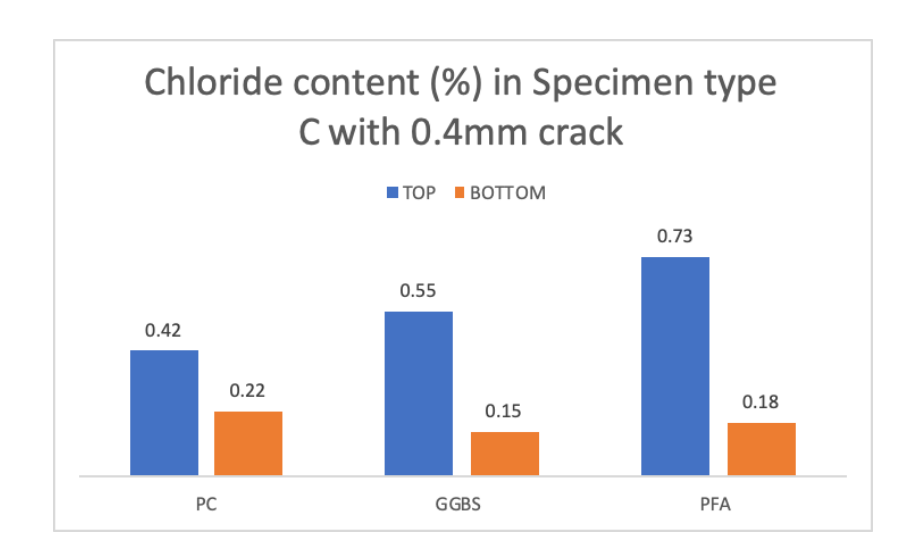


Fig. 6.46. The chloride content by weight of concrete in type C specimens with 0.4mm crack width only made of all cement types.

Generally, all cement types exhibit similar results regardless of specimen design.

6.3.4 Discussion on the effect of cement type on corrosion rate

There were only three pieces of research found in the literature concerning the effect of cement type on corrosion rate in specimens with coincident cracks which are (Stillwell, 1988), (Balakumaran et al., 2018; Poursaee & Hansson, 2008). The details of their experimental work can be found in the literature review chapter.

The outcome of the other researchers on the influence of cement type on corrosion rates is contradictory to the results obtained in this work. There was no effect of cement type in all three studies, in fact, Stillwell reported higher corrosion in cores made of FA, whereas Poursaee and Balakumaran reported no difference in corrosion rates on specimens with mineral admixtures. This could be due to different replacement ratios as in the study by Stillwell, the replacement rate of FA was 20% whereas, in Poursaee, it was 25% for either FA or GGBS. Whereas the replacement ratio of the SCM in the inspection of the bridges in Virginia has not been reported.

Generally, the influence of cracks on corrosion is governed by two aspects:

- a) they provide an easy ingress of chlorides;
- b) they provide various disruption levels between the steel-concrete interface; Generally according to all specimen designs, the chloride concentration in the vicinity of the reinforcement was lower in blended cement mixes which is attributed to lower permeability of these mixes.

Regarding the effect of cement type on corrosion in type A specimens, the chloride content in the vicinity of the reinforcement was higher in samples obtained from PC and lower in samples obtained from concretes with SCMs.

In terms of disruption level in these specimens, they had the most severe disruption level among all specimen designs, however, there was still part of the reinforcement intact with surrounding concrete, which has been noted in the discussion of the effect of crack depth earlier (shown in Figures 6.20 and 6.24). This suggests that higher resistivity of blended cement mixes is dominating the corrosion process.

Concerning the effect of blended cement mixes on corrosion in type B specimens, there is no bond loss between steel and concrete, thus the corrosion proceeds as in sound concrete, where the benefits of SMCs are in place. Surprisingly the half-cell potential reading did not demonstrate slower initiation time for corrosion in blended cements, however overall rates of corrosion were lower.

Whereas in type C specimens the corrosion initiation was similar in all mixes according to half-cell potential readings, whereas the propagation is slowed down due to a higher resistivity in these cement mixes as the disruption level in these specimens is milder than in type A specimens. As the nature of the corrosion process involves the flow of electrons and ions in order to complete the circuit, the concrete resistivity still affects the rate of corrosion propagation. Even after the corrosion initiation, the rate of corrosion seems to progress slower when there is a contact of concrete and steel remaining. Therefore, the electrical resistivity and hence resistance of the concrete to the flow of ions will affect the corrosion rate when coincident cracks are present.

This could be an explanation for contradicting results with Poursaee, as in their specimen design, the concrete steel interface was disrupted completely and if they would come to the same conclusion no matter what kind of cement is being used.

Chapter 7 Conclusion

This chapter presents a summary of the main findings of this research. It also sets out some proposals for revisions to the crack control recommendations in design codes on the structural use of concrete. Finally, it outlines some areas of needed research.

7.1 Summary of findings

The purpose of this research was to investigate the influence of coincident crack width, depth and various cement mixes on reinforcement corrosion in structures exposed to chloride bearing environments. An extensive literature review on the causes of coincident cracks shows that they are far from rare and can arise from a number of mechanisms. These cracks can promote corrosion of both longitudinal and transverse bars as well as stirrups, leading to reduced strength, stiffness and ductility of members and decreased overall safety of structures.

The current recommendations for crack control in design codes are based on the findings of research conducted on the effect of transverse cracks on corrosion which show the absence of a correlation between crack widths and corrosion, yet coincident cracks are more critical and very little work has been carried on their behaviour. These considerations led to the development of an experimental program to investigate the effect of the above mentioned parameters of coincident cracks on corrosion in reinforced concrete.

According to the findings of the experimental work, the following conclusions can be drawn:

- Coincident cracks are commonly present in structures according to an extensive literature review.
- Corrosion progression in reinforced concrete containing coincident cracks with the widths of 0.1, 0.2, 0.3 and 0.4mm was found to proceed at a similar

rate irrespective of the widths. This was concluded according to a statistical analysis of the obtained data which revealed insignificant differences in corrosion rates experienced by specimens with varying cracks. The chloride content in the vicinity of the reinforcement showed similar values irrespective of crack width. The absence of the correlation between coincident crack width and corrosion rates has been confirmed by gravimetric mass loss of the bars at the end of the experimental work.

- Investigated crack widths were collected from various code recommendations prescribed as permissible values. However, when cracks coincide with the reinforcement, no limit width was found below which there is a lower risk of corrosion. No threshold crack width value among studied ones (0.1, 0.2, 0.3 and 0.4mm) was found.
- Crack depth was found to have a significant influence on corrosion propagation. Three specimen designs with various crack depths were examined:
 - Specimen type A where cracks exceed the reinforcement level. These specimens experienced the most severe corrosion rates. Extensive pitting corrosion was observed on the areas of the rebar where the steel-concrete bond was lost;
 - Specimen type B where cracks terminate 9mm before the reinforcement. These specimens underwent the mildest corrosion rates among all. Mainly the surface of the rebars facing the cracks was covered with light rust patches. General corrosion was thought to take place in these specimens as the reinforcement maintained intact contact with the surrounding concrete which resulted in the lowest corrosion rates in these specimens.
 - Specimen type C where cracks stop at the top of the reinforcement. These specimens developed pitting corrosion along the crack. The depth of the pits was irregular along the length of the bar, while the deepest pit size was approximately 2mm. The rates of corrosion in

these specimens were significantly lower than the ones experienced by type A specimens.

- It was found that crack depth depends on the cause of cracking and various depth give rise to different corrosion types. Deeper cracks cause higher disruption to the concrete-steel interface which in turn results in more severe corrosion.
- The effect of blended cement mixes was found to be significant. Among studied mixes: 100% PC; 35% PC/65% GGBS and 70% PC/30% FA, the specimens made of blended cement showed extremely similar results and significantly lower rates of corrosion compared to pure PC. However, they still gave rise to extensive corrosion in the reinforcement. Thus, when cracks coincide with the reinforcement, SCMs can not provide adequate protection against corrosion perhaps as in the case of transverse cracks.
- It was found in this work that neither crack limits recommended in codes
 of practice nor advised cement mixes prevent or provide adequate
 protection from corrosion of reinforcement when cracks coincide with the
 underlying reinforcement.

7.2 Recommendations on crack control in codes of practice based on obtained results

The advice on crack control in design codes should draw attention to the existence of coincident cracks and the risk they present to the durability of structures exposed to chloride environments.

The code should highlight the common causes of coincident cracks. It should also include the latest advice on how their occurrence might be minimised.

To address the plastic settlement cracks, the measures recommended in codes of practice such as the use of blended cement mixes, and higher concrete covers for the reinforcement seem to be reasonable, however, those types of cracks still appear in structures. This implies poor workmanship in practice is one of the causes of the formation of those cracks. Thus, perhaps a better way would be to chase those cracks after the concrete hardening and sealing them.

Flexural cracks coinciding the reinforcement could be prevented by encouraging their formation away from the main reinforcement. This could be achieved by introducing a secondary layer of reinforcement made of noncorrosive material such as basalt fibre reinforced polymer bars.

7.3 Recommendations for future work

Considering the results and limitations of the current thesis, some recommendations for future investigations are suggested as follows:

- Since Plastic settlement cracks form during the initial hours of placing the concrete and they tend to follow the line of the reinforcement, it is not clear whether the passive oxide film develops fully in the area of the crack where reinforcement is exposed to the surrounding environment. Since a week time or 20 days is required for the development of passive film in the mortar and concrete respectively, a study on the behaviour and quality of the passive film in such an environment is needed.
- It was found in this work that deeper coincident cracks cause severe
 disruption to the steel concrete interface and result in higher amounts of
 corrosion, perhaps this is the function of distribution of anodic and cathodic
 regions, which together influence rates of corrosion. A more detailed study
 on this aspect is needed in improving the behaviour of corrosion in
 coincident cracks.
- Additionally, to the above, a comparison of rates of corrosion associated with coincident and intersecting cracks compare, and how blended cement mixes contribute to the corrosion propagation in both cases would be of interest.
- Information on how the service life models for structures would change if they considered including the data/threat of the existence of coincident cracks in structures.

References

- ACI 224. (2001). Control of Cracking in Concrete Structures. *ACI Committee* 224R-01, 1–46. https://doi.org/0097-8515
- ACI 318. (2014). Aci 318-14. 519. https://doi.org/10.2307/3466335
- ACI 318. (2019). Building Code Requirements Available for Public Review (ACI 318-19).
- ACM Instruments 2000. (2000). GILL AC 2 Operation Guide.
- Alarab, L. A., Ross, B. E., & Poursaee, A. (2020). Influence of Transverse Crack
 Opening Size on Chloride-Induced Corrosion of Steel Bars in Concrete. *Journal of Bridge Engineering*, 25(6), 04020027.

 https://doi.org/10.1061/(asce)be.1943-5592.0001555
- Aldred, J. M., Rangan, B. V, & Buenfeld, N. R. (2004). Effect of initial moisture content on wick action through concrete. 34, 907–912. https://doi.org/10.1016/S0008-8846(03)00202-3
- Almusallam, A. A. (2001). Effect of degree of corrosion on the properties of reinforcing steel bars. 361–368.
- Almusallam, A. A., Al.Gahtani, A., Aziz, A. R., & Dakhil, F. H. (1996). *EFFECT OF REINFORCEMENT CORROSION ON FLEXURAL BEHAVIOR OF A-A.* 8(August), 123–127.
- Alonso, C., Andrade, C., Izquerdo, M., Novoa, R., & Perez, C. (1998). Effect of protective oxide scales in the macrogalvanic behaviours of concrete reinforcement. *Corrosion Science*, Vol. 39(No 8), 268–278.
- Andrade, C., Alonso, C., Gulikers, J., Polder, R., Cigna, R., Vennesland, Salta, M., Raharinaivo, A., & Elsener, B. (2004). Test methods for on-site corrosion rate measurement of steel reinforcement in concrete by means of the polarization resistance method. *Materials and Structures/Materiaux et Constructions*, 37(273), 623–643. https://doi.org/10.1617/13952
- Angst, U. M., Geiker, M. R., Alonso, M. C., Polder, R., Isgor, O. B., Elsener, B.,
 Wong, H., Michel, A., Hornbostel, K., Gehlen, C., François, R., Sanchez, M.,
 Criado, M., Sørensen, H., Hansson, C., Pillai, R., Mundra, S., Gulikers, J.,
 Raupach, M., ... Sagüés, A. (2019). The effect of the steel–concrete

- interface on chloride-induced corrosion initiation in concrete: a critical review by RILEM TC 262-SCI. *Materials and Structures/Materiaux et Constructions*, 52(4). https://doi.org/10.1617/s11527-019-1387-0
- Arya, C. (2016). An examination of the crack control provision in BS EN 1992-2. *Proceedings of the Institution of Civil Engineers*, 169, 270–277.
- Arya, C., Newman, J. B., & Wood, L. A. (1994). Cracks and their implications for design. Synopsis in The Structural Engineer, Vol. 72, N.
- Arya, C., & Ofori-Darko, F. K. (1995). Influence of crack frequency on reinforcement corrosion in concrete. *Cement and Concrete Research*, *26*(3), 345–353. https://doi.org/10.1016/S0008-8846(96)85022-8
- Assouli, B., Ballivy, G., Rivard, P., Assouli, B., Ballivy, G., & Rivard, P. (2013). Influence of environmental parameters on application of standard ASTM C876-91: half cell potential measurements Influence of environmental parameters on application of standard ASTM C876-91: half cell potential measurements. 2782. https://doi.org/10.1179/174327807X214572
- ASTM C 876. (2015). Standard test method for corrosion potentials of uncoated reinforcing steel in concrete. ASTM C876 15. G01.14,. *ASTM International*, 1–8. https://doi.org/10.1520/C0876-15.2
- ASTM G 1 03. (2017). Standard Practice for Preparing, Cleaning, and Evaluating Corrosion Test Specimens. Designation: G1-03. *ASTM Special Technical Publication*, 505–510.
- ASTM International. (2014). Standard Guide for Applying Statistics to Analysis of Corrosion Data. *Astm*, *95*(Reapproved 2010), 1–14. https://doi.org/10.1520/G0016-13.2
- Audenaert, K. et. al. (2009). Influence of Cracks on the Service Life of Concrete Structures in a Marine Environment. *Key Engineering Materials*, 399(August), 153–160. https://doi.org/10.4028/www.scientific.net/KEM.399.153
- Azad, A. K., Ahmad, S., & Azher, S. A. (2007). Residual Strength of Corrosion-Damaged Reinforced Concrete Beams. 104.
- Baker, Money, & Sanborn. (1977). *Marine Corrosion Beiiavior of Bare and Metallic-Coated Steel Reinforcing Rods in Concrete*. 30–50.
- Balakumaran, S. S. G., Weyers, R. E., & Brown, M. C. (2018). *Linear Cracking in Bridge Decks*. 1–75.

- Beeby. (1983). Cracking, Cover, and Corrostion of Reinforcement. *Concrete International*, *5*(2).
- Beeby, A. (1978). Cracking and Corrosion. Concrete in the Oceans. Cement and Concerete Association, Slough, UK, Technical Report No. 1., 1.
- Beeby, & Scott. (2005). Cracking and deformation of axially reinforced members subjected to pure tension. *Magazine of Concrete Research*, *57*(10), 611–621.
- Bentur, A. (1997). Steel corrosion in concrete: fundamentals and civil engineering practice. CRC press.
- Bertolini, L., Carsana, M., Gastaldi, M., Lollini, F., & Redaelli, E. (2016). *Corrosion of Steel in Concrete and Its Prevention in Aggressive Chloride-Bearing Environments*.
- Bertolini, L., Pedeferri, P., Polder, R. B., & Elsener, B. (2004). *Corrosion of Steel in Concrete:Prevention Diagnosis, Repair*. Wiley-VCH.
- Bing Qi, Jianming Gao, F. C. and D. S. (2017). Evaluation of the damage process of recycled aggregate concrete under sulfate attack and wetting-drying cycles. *Construction and Building Materials*, *138*(May 1, 2017).
- Blagovic', A. (2016). The Influence of Cracks on the Durabiliitty and Service Life of Reinforced Concrete Structures in relation to Chloride-Induced Corrosion.

 Delft University of Technology.
- Broomfield, J. P. (1997). Corrosion of steel in concrete: understanding, investigation, and repair (1st ed.). London.
- Broomfield, J. P. (2006). Corrosion of Steel in Concrete: Understanding, Investigation and Repair, Second Edition. https://doi.org/10.4324/9780203414606
- BRUKER. (2009). S8 Tiger Operator's Manual. 203.
- BS 5400-4. (1990). Steel, concrete and composite bridges Part 4: Code of practice for design of concrete bridges (Issue December).
- BS 8500-1. (2019). BSI Standards Publication Concrete Complementary British Standard to BS EN 206 Part 1: Method of specifying and guidance for the specifier. *BSI Standards Publication*, 1.
- BS EN 1992. (2014). Eurocode 2 Design of concrete structures. *Part 2:* Concrete Bridges Design and Detailing Rules, 3(BS EN 1992-2:2005).
- BS EN 206. (2019). BS 8500-1; Concrete- Complementary British Standard to

- BS EN 206-1; Part 1:Method of specifying and guidance for the specifier. 1, 1–48.
- http://shop.bsigroup.com/en/ProductDetail/?pid=00000000030133675
- BS8110. (1997). "Structural use of concrete. part i: Code of practice for design and construction." *British Standards Institution*.
- Burkan Isgor, O., Angst, U., Geiker, M., Halmen, C., Hansson, C., Pacheco, J., Tepke, D., Trejo, D., & Vaddey, N. P. (2019). Recommended practice for reporting experimental data produced from studies on corrosion of steel in cementitious systems. *RILEM Technical Letters*, 4(July), 22–32. https://doi.org/10.21809/rilemtechlett.2019.90
- Caldentey, A. P., Corres Peiretti, H., Giraldo Soto, A., & Peset Iribarren, J. (2013). Cracking of RC members revisited: Influence of cover, φ/ρ s, ef and stirrup spacing An experimental and theoretical study. *Structural Concrete*, *14*(1), 69–78. https://doi.org/10.1002/suco.201200016
- Castel, A. Ã., Vidal, T. Ã., Franc, R., & Arliguie, G. Ã. (2003). *Influence of steel concrete interface quality on reinforcement corrosion induced by chlorides*. 2, 151–159.
- CEB. (1982). Durability of concrete structures: state-of-the-art report: (contribution à la 22e Session plénière du C.E.B., Munich, avril 1982). *N 148*.
- CEB. (1985). CEB design manual on cracking and deformations. *Euro-International Committee for Concrete*.
- Chen, E., Berrocal, C. G., Löfgren, I., & Lundgren, K. (2020). Correlation between concrete cracks and corrosion characteristics of steel reinforcement in precracked plain and fibre-reinforced concrete beams. *Materials and Structures/Materiaux* et Constructions, 53(2). https://doi.org/10.1617/s11527-020-01466-z
- Chen, T., Xu, M., Tu, J., Wang, H., & Niu, X. (2018). Relationship between Omnibus and Post-hoc Tests: An Investigation of performance of the F test in ANOVA. *Shanghai Archives of Psychiatry*, *30*(1), 60–64. https://doi.org/10.11919/j.issn.1002-0829.218014
- Claus, K. L., Østvik, J.-M., & Bjøntegaard, Ø. (2007). Compilation of 5 papers on (1) Electrical resistivity as a durability indicator and (2) Cracking tendency in hardening concrete. 2482, 1–67.
- Concrete Society. (1992). Non-Structural Cracks in Concrete. In Tecnical Report

- N° 22.
- Concrete Society. (2010). Non-Structural cracks in concrete. In *Concrete Society Technical Report TR* 22.
- Concrete Society. (2015). Relevance of cracking in concrete to reinforcement corrosion. *Concrete Society Report TR 44*.
- Dakhil, F. H., & Cady, P. D. (1975). Cracking of Fresh Concrete as Related to Reinforcement. American Concrete Institute, Journal Of, 72, 421–428. https://doi.org/10.14359/11145
- Darwin, D. ., Manning, D. G. ., & Hognestad, E. (1985). "Debate: Crack Width, Cover, and Corrosion,." *Concrete International, V. 7, No. 5, May*, 16.
- Dean, S., & Poursaee, A. (2011). Corrosion Measurement Techniques in Steel Reinforced Concrete. *Journal of ASTM International*, *8*, 103283. https://doi.org/10.1520/JAI103283
- Dhir, R. K., & Newlands, M. D. (1999). Controlling Concrete Degradation. *Creating with Concrete*, 260. https://doi.org/doi:10.1680/ccd.28197
- Djerbi, A., Bonnet, S., Khelidj, A., & Baroghel-bouny, V. (2008). Influence of traversing crack on chloride diffusion into concrete. *Cement and Concrete Research*, 38(6), 877–883. https://doi.org/10.1016/j.cemconres.2007.10.007
- Escudero, M. L., Gonzalez, A., Molina, A., & Andrade, C. (1985). *ERRORS IN THE ELECTROCHEMICAL E V A L U A T I O N OF V E R Y SMALL CORROSION R A T E S - I . P O L A R I Z A T I O N. 25*(10), 917–930.
- Fang, C., Lundgren, K., Chen, L., & Zhu, C. (2004). Corrosion influence on bond in reinforced concrete. 34, 2159–2167. https://doi.org/10.1016/j.cemconres.2004.04.006
- Fang, C., Lundgren, K., Plos, M., & Gylltoft, K. (2006). Bond behaviour of corroded reinforcing steel bars in concrete. 36, 1931–1938. https://doi.org/10.1016/j.cemconres.2006.05.008
- Feliu, S., Gonzalez, A., Andrade, M. C., & Feliu, V. (1989). Determining Polarization resistance in reinforced concrete slabs. *Corrosion Science*, 29(1), 105–113.
- Flis, J., & Pickering, H. W. (1998). *Interpretation of impedance data for reinforcing steel in alkaline solution containing chlorides and acetates. 43*(97), 1921–1929.

- François, Castel, A., Vidal, T., & Vu, N.-A. (2006). Long term corrosion behavior of reinforced concrete structures in chloride environnement. *JOURNAL DE PHYSIQUE IV*, *136*(NUCPERF 2006), 285–293.
- François, R., & Arliguie, G. (1998). Influence of Service Cracking on Reinforcement Steel Corrosion. *Journal of Materials in Civil Engineering*, 10(1), 14–20. https://doi.org/10.1061/(asce)0899-1561(1998)10:1(14)
- Francois, R., & Maso, J. C. (1988). Effect of damage in reinforced concrete on carbonation or chloride penetration. *Cement and Concrete Research*, *18*(6), 961–970. https://doi.org/10.1016/0008-8846(88)90033-6
- Frosch, R. J. (2003). Investigation of bridge deck cracking in various bridge superstructure systems. *Technology Transfer and Project Implementation Information*, February, 265.
- Geiker, M., Danner, T., Michel, A., Belda Revert, A., Linderoth, O., & Hornbostel, K. (2021). 25 Years of Field Exposure of Pre-Cracked Concrete Beams; Combined Impact of Spacers and Cracks on Reinforcement Corrosion. Construction and Building Materials, 286(March), 122801. https://doi.org/10.1016/j.conbuildmat.2021.122801
- Goto, Y., & Otsuka, K. (1971). Internal Cracks Formed in Concrete Around Deformed Tension Bars. 68, 160–162.
- Gu, C., Ye, G., & Sun, W. (2015). A review of the chloride transport properties of cracked concrete: experiments and simulations. *Journal of Zhejiang University-SCIENCE*A, 16(2), 81–92. https://doi.org/10.1631/jzus.A1400247
- Gu, X., Dong, Z., & Jin, Z. (2018). *Macrocell corrosion between crossed steel rebars embedded in concrete under chloride environments*. *04005*.
- Guo, Y., Gong, G., Chin, C., & Zhang, C. (2018). Structural design of concrete to EC2 and GB50010-2010: A comparison. *MATEC Web of Conferences*, *175*. https://doi.org/10.1051/matecconf/201817501039
- Hair, J. F., Babin, B. J., & Anderson, R. E. (2019). *Multivariate Data Analysis*. Cengage. https://books.google.kz/books?id=0R9ZswEACAAJ
- Hanjari, Z., Kettil, P., & Lundgren, K. (2011). Chalmers Publication Library Analysis of Mechanical Behavior of Corroded Reinforced Concrete Structures.
- Hansson, C. M., Poursaee, A., & Laurent, A. (2006). Macrocell and microcell

- corrosion of steel in ordinary Portland cement and high performance concretes. *Cement and Concrete Research*, *36*(11), 2098–2102. https://doi.org/10.1016/j.cemconres.2006.07.005
- Higgins, C., & Farrow, W. (2006). Tests of Reinforced Concrete Beams with Corrosion-Damaged Stirrups. ACI Structural Journal, 103(1). https://doi.org/10.14359/15094
- Hong, K., & Hooton, R. D. (1999). Effects of cyclic chloride exposure on penetration of concrete cover. 29(March 1998), 1379–1386.
- Houston, J., Atimtay, E., & Ferguson, P. . M. (1972). Corrosion of reinforcing steel embedded in structural concrete.
- Hussain, R. R., Alhozaimy, A., Al Negheimish, A., Al-Zaid, R., & Singh, D. D. N. (2015). Mechanism of nucleation and growth of passive film on steel reinforcing bar at different durations of its exposure in concrete pore solution at nanoscale. *ACI Materials Journal*, 112(4), 523–534. https://doi.org/10.14359/51687662
- IS 456. (2000). Concrete, Plain and Reinforced. *Bureau of Indian Standards,New Dehli*, 1–114.
- Isgor, B., Angst, U., Geiker, M., Halmen, C., Hansson, C., Pacheco, J., Tepke, D., Trejo, D., & Vaddey, P. (2019). Recommended practice for reporting experimental data produced from studies on corrosion of steel in cementitious systems. *RILEM Technical Letters*, 4, 22–32. https://doi.org/10.21809/rilemtechlett.2019.90
- Jang, S. Y., Kim, B. S., & Oh, B. H. (2011). Effect of crack width on chloride diffusion coefficients of concrete by steady-state migration tests. *Cement and Concrete Research*, 41(1), 9–19. https://doi.org/10.1016/j.cemconres.2010.08.018
- Ji, Y. S., Zhao, W., Zhou, M., Ma, H. R., & Zeng, P. (2013). Corrosion current distribution of macrocell and microcell of steel bar in concrete exposed to chloride environments. *Construction and Building Materials*, 47, 104–110. https://doi.org/10.1016/j.conbuildmat.2013.05.003
- JSCE. (2007). Standard specifications for concrete structures (Issue 15).
- Käthler, C. B., Angst, U. M., & Larsen, C. K. (2017). Effect of cracks on chloride-induced corrosion of reinforcing steel in concrete. September, 1–9.
- Kochanski, T., Parry, J., Pruess, D., Schuchardt, L., & Ziehr, J. (1990). Premature

- cracking of bridge decks study. Final Rep., Wisconsin Department of Transportation, October.
- Kong, F. K., & Evans, R. H. (1987). Reinforced and Prestressed Concrete. In Reinforced and Prestressed Concrete. https://doi.org/10.1007/978-1-4899-7134-0
- Konin, A., François, R., & Arliguie, G. (1998). Penetration of chlorides in relation to the microcracking state into reinforced ordinary and high strength concrete. *Materials and Structures*, 31(5), 310–316. https://doi.org/10.1007/BF02480672
- Krauss, P. D., & Rogalla, E. A. (1996). *Transverse cracking in newly constructed bridge decks*. Washington: National Academy Press, 1996.
- Küter, A. (2009). 'wwq Management of Reinforcement Corrosion a thermodynamic Approach. 228(April), 354.
- Lea, F. M., & Watkins, C. M. (1960). The durability of reinforced concrete in sea water. In *Twentieth Report of the Sea Action Committee of Institution of Civil Engineers. London: H.M.S.O.* wentieth Report of the Sea Action Committee of Institution of Civil Engineers. London: H.M.S.O.
- Lee, S., & Lee, D. K. (2018). What is the proper way to apply the multiple comparison test? *Korean Journal of Anesthesiology*, *71*(5), 353–360. https://doi.org/10.4097/kja.d.18.00242
- Marsavina, L., Audenaert, K., De Schutter, G., Faur, N., & Marsavina, D. (2009).
 Experimental and numerical determination of the chloride penetration in cracked concrete. *Construction and Building Materials*, 23(1), 264–274.
 https://doi.org/10.1016/j.conbuildmat.2007.12.015
- Martin, L. H. (Laurence H. (2006). Concrete design to EN 1992 / L.H. Martin, J.A. Purkiss. In *Concrete design to EN 1992* (2nd ed.). Butterworth-Heinemann.
- McCafferty, E. (2010). Introduction to corrosion science. In *Introduction to Corrosion Science*. https://doi.org/10.1007/978-1-4419-0455-3
- McDonald, D. B., Rogalla, E. A., & Krauss, P. D. (1995). Early-Age Transverse Deck Cracking. *Concrete International*, *17*(5).
- Micallef, M., & Vollum, R. (2017). The Effect of Shear and Lap Arrangement on Reinforcement Lap Strength. *Structures*, 12. https://doi.org/10.1016/j.istruc.2017.09.004
- Miller, G. G., & Darwin, D. (2000). Performance and constructability of silica fume

- bridge deck overlays. 57. https://rosap.ntl.bts.gov/view/dot/42134
- Mohammed, Otsuki, N., Makoto, H., & Tsunenori, S. (2001). Corrosion of Steel Reinforcement in Concrete. *Corrosion*, *13*(03), 1–4.
- Mohammed, U., Otsuki, N., Hamada, H., & Yamaji, T. (2002). Chloride-Induced Corrosion of Steel Bars in Concrete with the Presence of Gap at the Steel-concrete Interface Chloride-Induced Corrosion of Steel Bars in Concrete with Presence of Gap at Steel-Concrete Interface. August 2016.
- Montes, P., Bremner, T. W., & Lister, D. H. (2004). Influence of calcium nitrite inhibitor and crack width on corrosion of steel in high performance concrete subjected to a simulated marine environment. *Cement and Concrete Composites*, 26(3), 243–253. https://doi.org/10.1016/S0958-9465(03)00043-X
- Nayak, S., & Hostel, N. (2013). In this section of. April, 378–386.
- NCHRP Synthesis 333. (2004). Concrete Bridge Deck Performance. In *Concrete Bridge Deck Performance*. https://doi.org/10.17226/17608
- Nieves-Mendoza, D., Gaona-Tiburcio, C., Hervert-Zamora, H. L., Tobias, R. J., Castro-Borges, P., Colas, R. O., Zambrano Robledo, P., Martínez-Villafañe, A., & Almeraya-Calderón, F. (2012). Statistical analysis of factors influencing corrosion in concrete structures. *International Journal of Electrochemical Science*, 7(6), 5495–5509.
- Oelßner, W., Berthold, F., & Guth, U. (2006). The iR drop well-known but often underestimated in electrochemical polarization measurements and corrosion testing. 6, 455–466. https://doi.org/10.1002/maco.200603982
- Oesterle, R. G. (1997). The Role of Concrete Cover in Crack Control Criteria and Corrosion Protection. *PCA R&D Portland Cement Association, Skokie, IL, 87 Pp.*, 2054.
- Ofori-Darko, F. K. (1998). CRACK FREQUENCY AND THE MINIMISATION CORROSION IN CONCRETE REINFORCEMENT Francis Kwame OFORI-DARKO. South Bank University.
- Otieno, Beushausen, H., & Alexander, M. (2012). Towards incorporating the influence of cover cracking on steel corrosion in RC design codes: the concept of performance-based crack width limits. *Materials and Structures/Materiaux* et Constructions, 00, 1–12. https://doi.org/10.1617/s11527-012-9871-9

- Otieno, M. B. (2010). Corrosion in cracked and uncracked concrete influence of crack width, concrete quality and crack reopening. *Magazine of Concrete Research*, *9831*(6), 393–404. https://doi.org/10.1680/macr.2010.62.6.393
- Otsuki, N., Miyazato, S., Diola, N. B., & Suzuki, H. (2000). Influences of Bending Crack and Water-Cement Ratio on Chloride-Induced Corrosion of Main Reinforcing Bars and Stirrups. *Aci Materials Journal*, *97*, 454–464.
- Pacheco, J. F. (2015). Corrosion of reinforcing steel in cracked concrete. In *Journal* (Vol. 18).
- Papadakis, V. G. (2000). Effect of supplementary cementing materials on concrete resistance against carbonation and chloride ingress. 30, 291–299.
- Park, R. (2001). Concrete, Reinforced (R. A. Meyers (ed.); 3rd ed.).
- Pease, B. J. (2010). *Influence of concrete cracking on ingress and reinforcement corrosion and reinforcement corrosion* (Vol. 233, Issue December).
- Pettersson, Fidjestoll, P., & Jorgenson, O. (1996). The Effect of Cracks on Reinforcement Corrosion in High-Performance Concrete in a Marine Environment. *ACI Symposium Publication*, 163. https://doi.org/10.14359/1358
- Polder, R. B. (1996). The influence of blast furnace slag, fly ash and silica fume on corrosion of reinforced concrete in marine environment. *HERON, Vol. 41, No. 4*, 287–300.
- Poursaee. (2010). Cement and Concrete Research Potentiostatic transient technique, a simple approach to estimate the corrosion current density and Stern Geary constant of reinforcing steel in concrete. *Cement and Concrete Research*, 40(9), 1451–1458. https://doi.org/10.1016/j.cemconres.2010.04.006
- Poursaee, A., & Hansson, C. M. (2008). The influence of longitudinal cracks on the corrosion protection afforded reinforcing steel in high performance concrete. *Cement and Concrete Research*, 38(8–9), 1098–1105. https://doi.org/10.1016/j.cemconres.2008.03.018
- Purvis, R., Babaei, K., Associates, W. S., Williams, W., & Highway, F. (1995). Causes and Methods of Prevention.
- Qia, Cusson, D., & Chagnon, N. (2003). Evaluation of Reinforcement Corrosion in Repaired Concrete Bridge Slabs A Case Study. 59(5), 457–468.
- Qian, S., & Cusson, D. (2004). Electrochemical evaluation of the performance of

- corrosion-inhibiting systems in concrete bridges. 26, 217–233. https://doi.org/10.1016/S0958-9465(03)00041-6
- Ramey, G. E., Wolff, A., & Wright, R. (1997). STRUCTURAL DESIGN ACTIONS

 TO MITIGATE BRIDGE DECK CRACKING By George E. Ramey;

 Associate Member, ASCE, Angela R. WolfT / and. 2(3), 118–124.
- Reis, E. E., Mozer, J. D., Bianchini, A. C., & Kesler, C. E. (1965). Causes and control of cracking in concrete reinforced with high-strength steel bars: a review of research.
- Richardson Mark. (2002). Fundamentals of Durable Reinforced Concrete (1 Edition). Spon Press, London.
- Rodrigues, R., Gaboreau, S., Gance, J., Ignatiadis, I., Rodrigues, R., Gaboreau, S., Gance, J., Ignatiadis, I., & Re-, S. B. (2020). Reinforced concrete structures: A review of corrosion mechanisms and advances in electrical methods for corrosion monitoring To cite this version: HAL Id: hal-02979786.
- Rodriguez. (2003). Influence of cracks on chloride ingress into concrete. *ACI Materials Journal*, 100(2), 120–126. https://doi.org/10.14359/12551
- Rodriguez, L., Ortega, J., & Casal. (1997). LOAD CARRYING CAPACITY OF CONCRETE STRUCTURES WITH. II(4), 239–248.
- Rodríguez, P. (1999). Significance of coplanar macrocells to corrosion in concrete-embedded steel. *Corrosion*, *55*(3), 319–325. https://doi.org/10.5006/1.3283994
- Rodriguez, Ramirez, E., & González, J. A. (1994). Methods for studying corrosion in reinforced concrete. *Magazine of Concrete Research*, *46*(167), 81–90. https://doi.org/10.1680/macr.1994.46.167.81
- Sansone, J. M., & Brown, M. C. (2007). Paper No. 07282. 07282, 1-10.
- Schiessl, P. et al. (1986). EINFLUSS VON RISSEN AUF DIE DAUERHAFTIGKEIT VON STAHLBETON-UND SPANNBETONBAUTEILEN. Deutscher Ausschuss Fuer Stahlbeton, 370.
- Schießl, & Martin. (1969). The Influence of Time and Environmental Conditions on the Corrosion of Deformed Bars in Cracked Concrete. *RILEM-Symposium*.
- Schiessl, P. (1975). Admissible Crack Widths in Reinforced Concrete Structures. In *Behaviour in Service of Concrete Structures*. Liege.

- Schießl, P., & Raupach, M. (1997). Laboratory Studies and Calculations on the Influence of Crack Width on Chloride-Induced Corrosion of Steel in Concrete. *Materials*, *94*, 56–61.
- Scott, A., & Alexander, M. G. (2007). The influence of binder type, cracking and cover on corrosion rates of steel in chloride-contaminated concrete.

 Magazine of Concrete Research, 59(7), 495–505.

 https://doi.org/10.1680/macr.2007.59.7.495
- Shehab, R. H., Mahmoud, A. S., & Mansoor, Y. A. (2020). The effect of corroded stirrups on shear behavior of reinforced concrete beams. *IOP Conference Series: Materials Science and Engineering*, 745(1). https://doi.org/10.1088/1757-899X/745/1/012127
- Smith, P. E. (2016). Design and speci fi cation of marine concrete structures. https://doi.org/10.1016/B978-0-08-100081-6.00003-9
- Spectrometer, X. (2008). S8 Tiger ™. Power, November, 1–26.
- Stanish, K. D., Hooton, R. D., & Thomas, M. D. A. (1997). *Testing the Chloride Penetration Resistance of Concrete: A Literature Review* (U. of Toronto (ed.)). https://rosap.ntl.bts.gov/view/dot/35971
- Steen, C. Van, Verstrynge, E., Wevers, M., & Vandewalle, L. (2019). Cement and Concrete Research Assessing the bond behaviour of corroded smooth and ribbed rebars with acoustic emission monitoring. *Cement and Concrete Research*, 120(August 2018), 176–186. https://doi.org/10.1016/j.cemconres.2019.03.023
- Stillwell, J. A. (1988). Exposure tests on reinforced concrete in seawater.

 Concrete in the Oceans Technical Report No. 23.
- Suzuki, K., Ohno, Y., Praparntanatorn, S., & Tamura, H. (1990). *Mechanism of steel corrosion in cracked concrete. Corrosion of reinforcement in concrete.*Papers presented at the third international symposium on "corrosion of reinforcement in concrete construction", belfry hotel, wishaw, warwickshire, may 21-24, 1990.
- Tremper, B. (1947). The Corrosion of Reinforcing Steel in Cracked Concrete. *ACI Journal Proceedings*, *43*(6). https://doi.org/10.14359/8780
- Tuutti, K. (1982). Corrosion of steel in concrete. Swedish Cement and Concrete Research Institute.
- Uomoto, S., & Misra, T. (1988). Behavior of Concrete Beams and Columns in

- Marine Environment When Corrosion of Reinforcing Bars Takes Place. *ACI Symposium Publication*, *109*. https://doi.org/10.14359/2796
- Vassie, P. R., & Arya, C. (2006). Long-term maintenance strategies for highway bridges. 90(June), 83–90.
- Vidal, T., Castel, A., & François, R. (2007). Corrosion process and structural performance of a 17 year old reinforced concrete beam stored in chloride environment. *Cement and Concrete Research*, 37(11), 1551–1561. https://doi.org/10.1016/j.cemconres.2007.08.004
- Wallbank, E. J. (1989). The performance of concrete in bridges: a survey of 200 highway bridges. London: H.M.S.O.
- Wassermann, R., Katz, A., & Bentur, A. (2009). Minimum cement content requirements: A must or a myth? *Materials and Structures/Materiaux et Constructions*, *42*(7), 973–982. https://doi.org/10.1617/s11527-008-9436-0
- Webster, M., & Clark, L. (2016). The structural effects of corrosion an overview of the mechanisms. November.
- Wilkins, N. J. M., & Stillwell, J. A. (1986). The corrosion of steel reinforcement in cracked concrete immersed in seawater. *Proc. Marine Concrete*, *86*.
- Williamson, S., & Clark, L. (2006). Effect of Corrosion and Load on Reinforcement Bond Strength. *Structural Engineering International*, 12, 117–122. https://doi.org/10.2749/101686602777965559
- Win, P. P., Watanabe, M., & Machida, A. (2004). Penetration profile of chloride ion in cracked reinforced concrete. *Cement and Concrete Research*, 34(7), 1073–1079. https://doi.org/10.1016/j.cemconres.2003.11.020
- Xue, X, Seki, H., & Song, Y. (2014). Shear Behavior of RC Beams Containing Corroded Stirrups. 17(2), 165–177. https://doi.org/10.1260/1369-4332.17.2.165
- Xue, Xin, & Seki, H. (2010). *Influence of Longitudinal Bar Corrosion on Shear Behavior of RC Beams*. 8(2), 145–156.
- Yodsudjai, W., & Pattarakittam, T. (2017). Factors influencing half-cell potential measurement and its relationship with corrosion level. *Measurement*, *104*, 159–168. https://doi.org/10.1016/j.measurement.2017.03.027
- Yoon, I. S., & Schlangen, E. (2010). Long / Short Term Experimental Study on Chloride Penetration in Cracked Concrete. Key Engineering Materials, 417– 418, 765–768. https://doi.org/10.4028/www.scientific.net/KEM.417-418.765

References

- Zhao, Y., & Jin, W. (2016). 1.3.3 Concrete Cover Stressing and Cracking. In *Steel Corrosion-Induced Concrete Cracking*. Elsevier. https://app.knovel.com/hotlink/khtml/id:kt010W18L5/steel-corrosion-induced/concrete-cover-stressing
- Zhu, J., Gao, J., He, Z., & Chen, F. (2020). Degradation progress and protection of cement mortars partially immersed in sulfate-chloride solution. *Magazine of Concrete Research*, 72(22), 1135–1146. https://doi.org/10.1680/jmacr.19.00018
- Zou, Y., Wang, J., Bai, Q., Zhang, L. L., Peng, X., & Kong, X. F. (2012). Potential distribution characteristics of mild steel in seawater. *Corrosion Science*, *57*, 202–208. https://doi.org/10.1016/j.corsci.2011.12.017
- CΠ 28.13330. (2017). Concrete and reinforced concrete structures. General provisions.

Appendix A Monthly corrosion assessment

Table A- 1 Monthly average Half-cell potential readings for Specimens A 1 and B made of all binder types for the first year

Test reference	1 month	2 month	3 month	4 month	5 month	6 month	7 month	8 month	9 month	10 month	11 month	12 month
A1 PC	-30.0	-175.5	-198.2	-214.5	-156.4	-337.0	-240.3	-361.3	-457.3	-489.7	-426.7	-469.7
A1GGBS	-11.9	-132.1	-154.9	-361.4	-308.6	-487.3	-358.7	-346.7	-462.7	-393.7	-431.3	-207.7
A1 FA	-11.9	-132.1	-154.9	-361.4	-308.6	-487.3	-358.7	-346.7	-462.7	-393.7	-431.3	-207.7
B PC 0.0	48.9	50.1	126.3	16.3	47.9	-4.7	-10.0	107.6	-50.9	-88.6	-75.1	-34.9
B PC 0.1	61.5	23.2	50.6	-9.6	-42.7	-81.7	-37.9	60.4	-128.5	-128.7	-116.0	-94.0
B PC 0.2	70.6	37.7	66.0	42.9	88.3	8.1	15.6	32.1	-147.6	-157.1	-208.5	-160.9
B PC 0.3	55.9	69.3	87.1	46.7	107.1	9.5	18.0	123.1	-24.7	-54.1	-75.7	-63.9
B PC 0.4	95.7	44.2	41.1	12.1	16.7	-18.2	-12.1	95.2	-99.3	-167.2	-113.6	-86.7
B GGBS 0.0	77.2	83.6	-65.8	-54.2	16.2	23.4	-44.7	-67.0	-131.7	-106.5	-178.4	-18.8
B GGBS 0.1	41.3	-16.0	-130.2	-205.7	-129.6	-167.4	-174.0	-142.0	-276.8	-234.2	-287.5	-285.9
B GGBS 0.2	85.0	73.6	-79.3	-99.6	-33.6	-127.8	-95.0	-14.3	-304.9	-228.9	-271.3	-243.7
B GGBS 0.3	40.2	40.3	-141.3	-172.8	-123.5	-232.8	-217.5	-26.3	-244.7	-222.3	-256.3	-270.3
B GGBS 0.4	92.7	23.5	-93.7	-186.1	-143.7	-109.3	-87.2	-141.3	-224.5	-227.4	-274.4	-178.5
B FA 0.0	20.3	2.0	-147.1	-159.1	-9.4	-83.6	-105.0	-46.7	-16.8	-98.3	-129.7	-79.6
B FA 0.1	61.2	73.3	-167.9	-203.0	-109.4	-241.7	-80.1	-127.0	-210.3	-259.8	-279.2	-149.2
B FA 0.2	20.9	20.2	-149.9	-175.5	-119.2	-193.4	-63.2	-28.2	-182.1	-197.7	-334.0	-179.7
B FA 0.3	51.9	61.5	-108.4	-144.7	-59.4	-219.0	-96.5	-117.7	-197.7	-249.9	-256.8	-126.2
B FA 0.4	63.5	63.8	-85.3	-87.8	-113.3	-153.9	-34.8	-25.6	-214.4	-258.7	-219.1	-165.5

Table A- 2 Monthly average Half-cell potential readings for Specimens A 1 and B made of all binder types for the second year

Specimen design	13 month	14 month	15 month	16 month	17 month	18 month	19 month	20 month	21 month	22 month	23 month	24 month
A1 PC	-431.0	-456.0	-369.0	-399.3	-569.7	-435.7	-416.7	-415.0	-395.7	-405.0	-387.7	-392.3
A1GGBS	-403.3	-415.3	-371.7	-350.0	-531.3	-392.7	-371.7	-357.3	-345.7	-364.3	-355.0	-367.3
A1 FA	-403.3	-415.3	-371.7	-350.0	-531.3	-392.7	-371.7	-357.3	-345.7	-364.3	-355.0	-367.3
B PC 0.0	-103.2	-92.3	-45.2	-22.1	-162.9	-69.5	-70.4	-45.2	-20.7	-49.8	-41.9	-48.5
B PC 0.1	-109.7	-100.7	-70.7	-118.7	-254.1	-138.0	-239.4	-66.5	-52.4	-81.4	-79.6	-92.6
B PC 0.2	-160.0	-121.1	-22.7	-189.4	-381.8	-283.4	-220.1	-107.0	-73.8	-122.3	-124.1	-125.7
B PC 0.3	-47.2	-59.2	-96.9	-123.1	-272.1	-153.8	-86.2	-62.0	-135.3	-119.4	-132.8	-101.9
B PC 0.4	-161.7	-282.2	-242.9	-222.5	-288.9	-266.0	-299.8	-186.2	-253.2	-261.7	-225.9	-166.5
B GGBS 0.0	-99.4	-83.8	-38.5	-26.4	-168.1	-74.4	-170.2	-54.3	-60.1	-65.5	-77.2	-73.6
B GGBS 0.1	-269.0	-314.3	-234.9	-252.4	-395.4	-306.5	-299.1	-285.7	-249.1	-255.8	-240.0	-241.4
B GGBS 0.2	-209.4	-217.7	-195.8	-172.0	-312.0	-152.4	-178.4	-132.3	-132.8	-124.3	-139.7	-133.0
B GGBS 0.3	-237.2	-168.0	-235.1	-189.8	-371.6	-251.3	-222.4	-216.6	-185.1	-182.5	-181.3	-182.6
B GGBS 0.4	-185.9	-142.6	-161.0	-132.2	-299.8	-173.3	-170.0	-111.4	-108.6	-135.5	-195.1	-177.5
B FA 0.0	-52.1	-59.3	-51.1	-21.5	-212.2	-20.8	-1.3	-1.5	36.8	13.6	-19.5	-31.1
B FA 0.1	-178.6		-182.5	-140.6	-318.3	-179.9	-143.6	-192.2	-89.4	-100.7	-108.1	-108.0
B FA 0.2	-291.6		-183.2	-125.8	-318.9	-210.3	-215.3	-192.0	-165.8	-211.4	-214.3	-232.5
B FA 0.3	-147.3		-148.5	-79.3	-286.0	-126.1	-168.8	-104.4	-134.0	-132.8	-153.5	-126.1
B FA 0.4	-174.4	-194.2	-167.6	-148.1	-341.6	-159.6	-140.1	-144.1	-129.9	-226.0	-186.5	-157.9

Table A- 3 Monthly average Half-cell potential readings for Specimens A 1 and B made of all binder types for the third year

Test	25	26	27	28	29	30	31	32	33	34	35	36
reference	month											
A1 PC	-411.3	-407.7	-403.0	-393.7	-414.3	-128.3	-342.0	-348.0	-367.0	-346.7	-321.7	-362.0
A1GGBS	-361.7	-372.7	-367.3	-366.0	-373.0	-353.7	-379.7	-325.7	-295.0	-343.0	-267.7	-333.7
A1 FA	-361.7	-372.7	-367.3	-366.0	-373.0	-353.7	-379.7	-325.7	-295.0	-343.0	-267.7	-333.7
B PC 0.0	-49.9	-50.2	-51.2	-57.9	-42.2	-44.4	-12.0	-66.8	-58.8	-47.0	-11.6	-17.5
B PC 0.1	-75.4	-70.8	-85.4	-71.5	-65.2	-95.8	-41.6	-68.7	-114.5	-93.8	-68.0	-84.5
B PC 0.2	-130.0	-127.6	-134.6	-128.7	-149.6	-116.6	-53.5	-308.9	-319.0	-252.4	-254.1	-289.1
B PC 0.3	-109.8	-111.1	-133.9	-159.7	-132.6	-131.1	-131.0	-150.3	-145.5	-113.2	-157.4	-133.7
B PC 0.4	-214.7	-227.4	-177.4	-245.8	-279.4	-224.0	-241.9	-251.7	-304.7	-280.2	-294.2	-333.0
B GGBS 0.0	-80.7	-75.8	-76.8	-95.2	-80.3	-85.1	-102.5	-121.8	-150.8	-120.9	-82.8	-58.0
B GGBS 0.1	-231.3	-232.3	-264.1	-259.1	-250.0	-280.4	-282.0	-279.1	-298.1	-250.4	-184.4	-232.6
B GGBS 0.2	-140.2	-115.0	-95.6	-87.5	-111.6	-89.9	-116.9	-130.3	-147.8	-96.9	-59.4	-125.3
B GGBS 0.3	-156.3	-154.9	-170.2	-158.1	-163.3	-170.6	-163.1	-236.4	-249.2	-155.6	-75.9	-75.7
B GGBS 0.4	-156.2	-135.6	-199.8	-219.7	-184.8	-173.6	-99.0	-144.7	-147.7	-146.6	-98.0	-96.3
B FA 0.0	-27.9	-20.2	-15.6	-31.8	-41.5	-35.7	23.2	-8.6	-62.7	-36.4	6.6	-45.2
B FA 0.1	-135.3	-153.9	-159.9	-179.8	-166.6	-152.3	-109.1	-100.1	-310.3	-189.3	-150.8	-195.1
B FA 0.2	-195.1	-145.7	-187.2	-203.3	-175.8	-192.7	-150.0	-173.0	-215.3	-197.5	-181.4	-216.7
B FA 0.3	-205.0	-134.1	-129.8	-129.9	-110.6	-103.8	-98.7	-151.7	-146.8	-84.0	-66.5	-149.5
B FA 0.4	-176.2	-134.1	-108.0	-154.2	-159.0	-162.8	-87.7	-156.6	-85.3	-34.8	-83.6	-134.3

Table A- 4 Monthly average Half-cell potential readings for Specimens A 2 and C made of all binder types for 14 months

Test reference	1 month	2 month	3 month	4 month	5 month	6 month	7 month	8 month	9 month	10 month	11 month	12 month	13 month	14 month
A2 PC	-101.3	-390.7	-279.7	-397.3	-362.0	-535.7	-465.0	-473.7	-481.7	-340.7	-412.7	-380.3	-251.7	-306.0
A2 GGBS	15.3	-317.3	-244.0	-256.3	-308.0	-472.0	-468.0	-488.3	-490.0	-472.7	-367.0	-377.0	-255.3	-339.3
A2 FA	-57.7	-400.7	-201.0	-347.3	-348.0	-437.0	-447.7	-474.0	-469.7	-454.3	-447.7	-435.7	-278.7	-328.3
C PC 0.1	-36.0	-503.3	-167.3	-230.0	-216.0	-367.7	-316.3	-342.3	-311.7	-269.3	-287.0	-232.0	-233.7	-248.7
C PC 0.2	-24.3	-545.3	-225.7	-271.3	-249.0	-395.0	-281.0	-330.7	-273.7	-256.7	-266.0	-184.3	-217.0	-190.7
C PC 0.3	-23.0	-499.7	-231.0	-272.3	-254.3	-363.0	-247.3	-331.7	-296.7	-272.7	-344.7	-351.0	-227.3	-329.7
C PC 0.4	-36.3	-417.7	-236.0	-297.0	-291.3	-380.7	-313.0	-384.7	-389.7	-382.3	-367.7	-278.3	-242.3	-326.3
C GGBS 0.1	-62.0	-404.0	-204.0	-176.3	-175.7	-245.0	-255.3	-205.7	-227.0	-228.7	-258.0	-264.0	-251.0	-262.7
C GGBS 0.2	-131.3	-458.3	-225.7	-225.0	-248.3	-225.0	-225.3	-236.3	-194.7	-236.7	-235.7	-239.7	-238.0	-247.0
C GGBS 0.3	-58.7	-392.3	-238.7	-232.3	-215.3	-281.3	-243.0	-241.3	-224.7	-214.3	-229.7	-221.3	-168.3	-187.7
C GGBS 0.4	-92.7	-519.7	-261.7	-197.3	-203.3	-339.3	-216.3	-261.7	-258.0	-272.3	-318.0	-297.3	-259.3	-327.7
C FA 0.1	-26.7	-394.7	-237.7	-231.0	-230.0	-230.3	-220.0	-231.7	-235.3	-235.3	-217.0	-125.7	-217.3	-210.0
C FA 0.2	-61.3	-370.3	-210.7	-200.0	-230.0	-273.0	-247.0	-284.0	-226.0	-296.0	-252.0	-208.3	-228.7	-224.3
C FA 0.3	-64.7	-394.7	-248.7	-271.0	-259.3	-304.7	-214.7	-249.7	-188.3	-207.0	-203.3	-246.7	-249.3	-172.0
C FA 0.4	26.0	-150.3	-174.0	-275.0	-287.7	-315.7	-195.0	-302.0	-266.0	-305.0	-316.3	-297.3	-263.7	-292.3

Table A- 5 Monthly average LPR readings for Specimens A 1 and B made of all binder types for the first year

Test	1	2	3	4	5	6	7	8	9	10	11	12
reference	month											
A1 PC	0.1	0.1	0.4	0.6	0.5	0.4	1.1	1.0	1.5	2.8	3.0	2.5
A1GGBS	0.1	0.1	0.2	0.6	0.5	0.3	0.7	1.1	0.9	1.0	1.1	0.8
A1 FA	0.1	0.1	0.4	0.5	0.8	0.6	0.7	0.7	1.0	0.9	1.3	1.5
B PC 0.0	0.1	0.1	0.1	0.1	0.1	0.1	0.2	0.2	0.2	0.2	0.1	0.1
B PC 0.1	0.1	0.1	0.1	0.1	0.1	0.1	0.2	0.3	0.5	0.6	0.5	0.5
B PC 0.2	0.1	0.1	0.1	0.1	0.1	0.2	0.3	0.3	0.2	0.3	0.5	0.5
B PC 0.3	0.1	0.1	0.1	0.2	0.2	0.2	0.2	0.4	0.2	0.2	0.5	0.7
B PC 0.4	0.1	0.1	0.1	0.1	0.2	0.2	0.2	0.3	0.4	0.3	0.5	0.6
B GGBS 0.0	0.1	0.1	0.2	0.1	0.1	0.1	0.2	0.2	0.1	0.2	0.2	0.1
B GGBS 0.1	0.1	0.1	0.1	0.2	0.1	0.1	0.2	0.3	0.3	0.3	0.4	0.4
B GGBS 0.2	0.1	0.1	0.1	0.1	0.1	0.1	0.0	0.3	0.3	0.3	0.3	0.3
B GGBS 0.3	0.1	0.1	0.1	0.1	0.2	0.1	0.0	0.3	0.2	0.2	0.3	0.3
B GGBS 0.4	0.1	0.1	0.1	0.2	0.1	0.2	0.0	0.2	0.2	0.2	0.5	0.6
B FA 0.0	0.1	0.1	0.1	0.1	0.1	0.1	0.2	0.2	0.2	0.2	0.1	0.1
B FA 0.1	0.1	0.1	0.1	0.1	0.1	0.2	0.2	0.3	0.3	0.2	0.3	0.5
B FA 0.2	0.1	0.1	0.1	0.1	0.1	0.1	0.2	0.5	0.6	0.7	0.3	0.5
B FA 0.3	0.1	0.1	0.1	0.1	0.1	0.2	0.2	0.3	0.3	0.3	0.4	0.4
B FA 0.4	0.1	0.1	0.1	0.2	0.1	0.1	0.2	0.2	0.2	0.3	0.5	0.6

Table A- 6 Monthly average LPR readings for Specimens A 1 and B made of all binder types for the second year

Test reference	13 month	14 month	15 month	16 month	17 month	18 month	19 month	20 month	21 month	22 month	23 month	24 month
A1 PC	2.1	1.7	2.4	3.1	3.4	4.7	7.0	7.7	6.5	5.9	5.9	5.7
A1GGBS	0.8	1.4	1.5	2.1	2.2	3.2	2.6	3.3	3.9	3.9	4.5	4.7
A1 FA	1.3	1.5	2.0	1.8	3.0	2.4	3.0	3.6	4.0	3.6	4.2	3.6
B PC 0.0	0.1	0.1	0.0	0.0	0.1	0.5	0.7	0.5	0.8	0.7	0.4	0.6
B PC 0.1	0.5	0.6	0.4	0.9	1.1	1.4	1.7	2.0	2.2	2.0	2.3	1.8
B PC 0.2	0.6	0.7	0.8	1.0	1.1	1.3	1.4	1.3	1.0	0.8	1.3	1.5
B PC 0.3	0.7	0.9	0.7	1.0	0.9	1.5	1.3	1.1	1.9	1.4	1.3	1.6
B PC 0.4	0.9	0.6	0.6	0.7	1.0	1.5	1.8	1.5	1.8	1.8	1.8	1.9
B GGBS 0.0	0.2	0.1	0.1	0.0	0.0	0.5	0.5	0.6	0.7	0.7	0.6	0.7
B GGBS 0.1	0.4	0.4	0.5	0.6	0.5	0.6	1.2	0.7	0.6	0.6	0.6	0.6
B GGBS 0.2	0.4	0.3	0.4	0.5	0.6	0.8	0.7	0.6	0.7	0.5	0.6	0.7
B GGBS 0.3	0.3	0.4	0.5	0.6	0.7	0.9	0.8	0.7	0.7	0.7	0.9	0.7
B GGBS 0.4	0.5	0.6	0.8	0.8	0.7	0.6	0.6	0.5	0.7	0.6	0.6	0.8
B FA 0.0	0.4	0.2	0.0	0.0	0.0	0.5	0.5	0.5	0.4	0.4	0.5	0.4
B FA 0.1	0.4	0.6	0.6	0.6	0.9	1.9	1.5	1.7	1.4	1.3	1.3	1.6
B FA 0.2	0.7	0.6	0.7	0.7	0.9	1.7	1.7	1.6	1.6	1.2	1.4	1.7
B FA 0.3	0.5	0.5	0.6	0.6	0.7	1.1	1.1	1.0	1.1	0.8	0.8	1.0
B FA 0.4	0.6	0.8	0.8	0.8	0.8	0.8	0.7	0.6	0.7	0.6	0.8	0.6

Table A-7 Monthly average LPR readings for Specimens A 1 and B made of all binder types for the third year

Test	25	26	27	28	29	30	31	32	33	34	35	36
reference	month											
A1 PC	5.9	5.8	5.6	6.0	5.8	5.8	6.1	6.0	7.2	6.7	6.3	6.3
A1GGBS	4.6	4.5	3.9	4.4	4.6	3.9	4.6	3.5	3.9	3.9	4.0	2.6
A1 FA	3.8	3.1	3.0	2.6	5.0	4.7	4.0	5.1	3.9	4.4	5.2	3.6
B PC 0.0	0.6	0.6	0.4	0.6	0.4	0.3	0.3	0.7	0.7	0.9	0.8	0.8
B PC 0.1	1.9	2.0	2.1	2.1	2.1	2.1	2.3	2.3	2.6	2.3	2.3	2.4
B PC 0.2	1.9	1.9	2.2	2.2	2.3	3.0	3.3	3.4	3.9	3.7	3.8	4.3
B PC 0.3	1.8	2.2	2.1	2.5	2.2	2.3	2.5	0.9	1.1	2.0	1.2	2.7
B PC 0.4	1.6	1.8	2.3	2.4	2.4	2.3	2.4	1.8	2.3	2.6	3.4	3.5
B GGBS 0.0	0.7	0.6	0.7	0.7	0.5	0.6	0.7	0.7	0.8	0.7	0.8	0.7
B GGBS 0.1	0.6	0.5	0.5	0.7	0.7	0.7	0.5	0.6	0.7	0.8	0.8	0.7
B GGBS 0.2	0.8	0.8	0.8	0.7	0.7	0.7	0.8	0.7	0.7	0.6	0.6	0.7
B GGBS 0.3	0.8	0.7	0.7	0.7	0.7	0.6	0.7	0.8	0.9	0.7	0.7	0.7
B GGBS 0.4	0.7	0.7	0.7	0.7	0.8	0.7	0.7	0.6	0.7	0.7	0.7	0.6
B FA 0.0	0.4	0.5	0.4	0.4	0.4	0.5	0.5	0.4	0.5	0.5	0.5	0.5
B FA 0.1	1.5	1.6	1.8	1.8	1.7	1.9	1.7	1.4	2.5	2.0	2.0	2.1
B FA 0.2	1.6	1.5	1.4	1.5	1.7	1.8	1.7	1.5	2.0	1.8	1.9	2.0
B FA 0.3	1.0	0.9	0.9	1.1	0.9	1.0	1.1	1.0	1.1	1.0	1.0	1.0
B FA 0.4	0.7	1.0	0.8	0.8	0.7	0.7	0.7	0.6	0.8	1.0	1.1	1.3

Table A- 8 Monthly average LPR readings for Specimens A2 and C made of all binder types for 14 months

Test reference	1 month	2 month	3 month	4 month	5 month	6 month	7 month	8 month	9 month	10 month	11 month	12 month	13 month	14 month
A2 PC	0.2	0.4	1.0	3.9	4.9	5.5	6.5	6.9	7.7	7.4	9.2	11.4	8.4	9.0
A2 GGBS	0.2	0.3	4.3	1.8	3.0	3.8	3.4	4.4	4.4	4.6	4.2	5.1	4.3	4.6
A2 FA	0.1	0.4	2.0	3.1	3.4	4.1	4.0	4.3	4.9	5.4	5.4	5.2	4.5	4.6
C PC 0.1	0.2	0.4	2.5	1.5	1.7	3.6	4.7	4.4	4.7	3.9	3.7	3.4	2.4	2.7
C PC 0.2	0.2	0.8	2.3	1.9	2.3	4.7	5.4	4.3	4.6	3.4	3.1	2.8	2.0	2.1
C PC 0.3	0.2	0.7	2.5	1.9	2.6	4.3	3.9	4.1	4.0	3.3	5.4	4.8	3.0	3.6
C PC 0.4	0.2	1.0	2.0	3.3	3.5	4.5	5.5	5.3	6.1	6.6	6.2	6.3	5.2	6.8
C GGBS 0.1	0.2	0.7	3.0	1.7	2.1	2.4	2.5	2.3	2.7	2.2	2.6	2.7	2.1	2.1
C GGBS 0.2	0.2	0.8	5.0	1.9	2.0	2.5	2.3	1.9	2.1	1.9	2.0	2.4	2.0	2.1
C GGBS 0.3	0.2	1.0	4.0	1.5	1.7	2.0	2.0	1.7	1.7	1.5	1.5	1.6	1.5	1.5
C GGBS 0.4	0.1	0.6	1.1	1.7	1.5	1.6	2.2	2.0	2.3	2.0	2.5	2.3	2.5	2.0
C FA 0.1	0.2	0.8	2.7	1.7	1.9	2.0	1.9	1.8	2.0	1.7	1.6	2.0	1.5	1.5
C FA 0.2	0.1	0.7	2.9	1.6	2.1	2.3	2.6	2.6	2.6	3.1	2.2	2.3	1.4	1.9
C FA 0.3	0.1	0.9	2.6	2.7	3.1	2.9	3.0	2.5	2.8	2.9	2.2	2.5	1.5	2.2
C FA 0.4	0.2	0.6	1.1	1.4	2.0	2.1	1.5	2.0	2.3	2.1	2.1	2.3	2.4	2.5

Table A- 9 Monthly average ZRA readings for Specimens A2 and C made of all binder types for the first year

Test ref.	1 month	2 month	3 month	4 month	5 month	6 month	7 month	8 month	9 month	10 month	11 month	12 month
A1 PC	0.03	1	3	2	1	1	3	1	0.7	1	0.4	2
A1GGBS	0.38	0.6	0.7	0.8	0.9	0.5	1.7	0.9	0.8	0.9	0.6	0.2
A1 FA	0.06	1	1	0.5	0.9	1	1.6	1	1	1	0.8	1
B PC 0.0	0.02	0.4	0.5	0.25	0.15	0.8	0.7	0.3	0.21	0.35	0.23	0.5
B PC 0.1	0.21	0.55	0.85	0.55	0.6	1.5	0.3	0.45	0.3	0.45	0.07	0.55
B PC 0.2	0.12	0.35	1.5	1.3	1.4	1.6	0.31	0.35	0.24	0.65	3.04	1.1
B PC 0.3	0.03	0.21	0.45	0.5	0.45	0.95	0.65	0.35	0.8	0.75	0.75	0.5
B PC 0.4	0.03	0.65	0.8	0.4	0.15	0.75	0.75	0.55	0.24	0.3	2.9	2.6
B GGBS 0.0	0.03	0.5	0.2	0.3	0.45	0.45	0.3	0.2	0.26	0.3	0.24	0.5
B GGBS 0.1	0.02	0.4	0.7	0.55	0.45	0.3	0.6	0.25	0.5	0.45	0.35	0.3
B GGBS 0.2	0.03	1.3	0.6	0.7	0.45	0.4	0.85	0.65	0.35	0.55	0.3	0.75
B GGBS 0.3	0.02	0.5	0.75	0.6	0.5	0.75	0.6	0.55	0.2	0.35	0.85	0.9
B GGBS 0.4	0.03	0.4	0.45	0.4	0.6	0.55	0.4	0.45	0.45	0.3	0.55	0.7
B FA 0.0	0.02	0.75	0.45	0.65	0.17	0.1	0.55	0.25	0.25	0.25	0.9	0.2
B FA 0.1	0.03	0.85	0.65	0.6	0.65	0.7	0.8	0.65	0.4	0.4	0.55	0.95
B FA 0.2	0.03	2	0.45	0.6	0.85	0.8	1.4	0.6	0.35	0.9	1.3	1
B FA 0.3	0.03	0.4	0.3	0.6	0.4	0.75	0.8	0.8	0.4	0.6	0.7	1.7
B FA 0.4	0.21	0.35	0.3	0.6	0.35	0.7	0.62	0.75	0.7	0.8	0.35	0.7

Table A- 10 Monthly average ZRA readings for Specimens A2 and C made of all binder types for the second year

Test ref.	13 month	14 month	15 month	16 month	17 month	18 month	19 month	20 month	21 month	22 month	23 month	24 month
A1 PC	3	3	3	0.7	3	2	2	2.7	2.4	2.4	2.2	2.3
A1GGBS	1	0.7	0.7	0.7	0.8	0.7	0.6	0.6	0.5	0.8	0.8	0.8
A1 FA	1	0.9	0.9	1	1	0.8	0.9	0.8	0.7	0.6	0.6	0.7
B PC 0.0	0.55	0.6	0.55	0.5	0.15	0.15	0.25	0.4	0.3	0.4	0.4	0.3
B PC 0.1	1.15	0.9	0.7	1	2	0.35	0.35	0.2	0.35	0.45	0.4	0.45
B PC 0.2	3.85	3.5	0.9	2.5	0.85	0.75	0.65	0.6	0.45	0.85	0.75	0.7
B PC 0.3	0.65	1	0.4	0.8	1.25	0.65	0.6	0.95	0.7	0.85	1.5	0.8
B PC 0.4	0.8	3.5	1.85	0.75	0.85	0.8	0.85	0.55	0.55	0.7	0.75	0.55
B GGBS 0.0	0.25	0.35	0.5	0.4	0.5	0.3	0.4	0.5	0.15	0.25	0.3	0.2
B GGBS 0.1	0.25	0.7	0.4	0.3	0.4	0.4	0.3	0.4	0.3	0.55	0.4	0.3
B GGBS 0.2	1.3	1.45	0.7	0.75	0.5	1.3	1.8	0.65	0.55	0.7	0.6	0.55
B GGBS 0.3	0.8	0.95	0.6	0.6	0.55	0.8	0.75	0.45	0.65	0.55	0.45	0.55
B GGBS 0.4	0.7	0.6	0.35	0.4	0.7	0.85	0.5	0.6	0.45	0.8	0.65	0.6
B FA 0.0	0.5	0.07	0.7	0.51	0.4	0.3	0.5	0.1	0.5	0.4	0.35	0.3
B FA 0.1	0.8	0.51	0.75	0.26	0.85	0.7	0.9	0.75	0.6	0.4	0.25	0.4
B FA 0.2	1	1.1	0.45	0.5	0.4	0.7	0.3	0.4	0.6	0.55	0.6	0.4
B FA 0.3	1.2	1.2	0.7	0.7	1.7	0.75	0.7	0.4	0.35	0.65	0.7	0.85
B FA 0.4	0.55	1.3	0.7	0.55	0.7	0.6	0.65	0.25	0.4	0.85	0.6	0.75

Table A- 11 Monthly average ZRA readings for Specimens A2 and C made of all binder types for the third year

Test ref.	25 month	26 month	27 month	28 month	29 month	30 month	31 month	32 month	33 month	34 month	35 month	36 month
A1 PC	2.2	2.4	2.4	2.6	2.5	2.7	2	2.1	2.2	2.3	2.6	3.3
A1GGBS	0.9	0.7	0.7	0.8	0.8	0.7	0.6	0.5	0.6	0.8	0.7	1.2
A1 FA	0.5	0.5	0.7	0.6	0.6	0.6	0.6	0.6	0.6	0.8	0.7	0.6
B PC 0.0	0.35	0.45	0.35	0.35	0.35	0.3	0.1	0.15	0.5	1.1	0.8	1.15
B PC 0.1	0.45	0.5	0.5	0.4	0.35	0.35	0.2	0.3	0.7	0.25	1.25	1
B PC 0.2	0.75	0.55	0.55	0.55	0.45	0.5	0.55	0.4	0.8	0.5	2.05	1.2
B PC 0.3	0.8	0.7	0.7	0.7	0.7	0.7	0.65	0.55	0.4	0.6	1.6	0.75
B PC 0.4	0.65	0.7	0.75	0.85	0.7	0.55	0.6	0.4	0.45	0.45	0.25	1.05
B GGBS 0.0	0.2	0.25	0.3	0.35	0.4	0.3	0.15	0.2	0.35	0.35	0.7	0.4
B GGBS 0.1	0.2	0.25	0.35	0.4	0.4	0.45	0.25	0.35	0.6	0.3	0.35	0.4
B GGBS 0.2	0.45	0.55	0.45	0.55	0.55	0.45	0.25	0.5	0.6	0.45	1.95	0.5
B GGBS 0.3	0.65	0.55	0.4	0.3	0.45	0.45	0.6	0.55	0.65	0.35	0.4	0.4
B GGBS 0.4	0.55	0.6	0.6	0.6	0.65	0.75	0.55	0.6	0.55	0.6	0.55	0.55
B FA 0.0	0.4	0.4	0.3	0.2	0.3	0.4	0.4	0.2	0.5	0.55	0.2	0.25
B FA 0.1	0.5	0.45	0.35	0.35	0.4	0.45	0.45	0.4	0.55	0.4	0.4	0.3
B FA 0.2	0.7	0.5	0.45	0.55	0.7	0.8	0.9	0.35	0.4	0.7	0.5	0.6
B FA 0.3	0.85	0.5	0.5	0.5	0.7	0.7	0.4	0.4	0.9	1.15	1	0.55
B FA 0.4	0.95	0.75	0.9	0.75	0.55	0.6	0.45	0.65	0.45	0.25	0.4	0.25

Table A- 12 Monthly average ZRA readings for Specimens A2 and C made of all binder types for 14 months

Test ref.	1 month	2 month	3 month	4 month	5 month	6 month	7 month	8 month	9 month	10 month	11 month	12 month	13 month	14 month
A2 PC	0.3	0.3	0.1	1	1.5	3.4	2.8	2.8	2.4	1.6	1.8	2	2	2.7
A2 GGBS	0.3	0.2	0.3	0.3	0.5	0.9	1	1	1.1	1	0.6	0.5	0.8	1.3
A2 FA	0.2	0.2	0.1	0.5	0.6	0.7	1.2	1.1	1.4	1.2	1.1	1	1	1
C PC 0.1	0.2	1	0.4	0.5	0.7	2.7	1.9	1.7	1.4	2	0.8	0.5	1.1	1.1
C PC 0.2	0.3	0.5	0.3	2.6	1.1	1.7	4.2	2.8	1	1.5	1.1	0.2	1.2	1.4
C PC 0.3	0.3	1	0.2	0.5	1.2	2.4	1.8	1.4	1.2	1.6	1.2	1.2	0.8	1.2
C PC 0.4	0.1	0.7	0.3	0.2	0.7	0.7	0.6	0.7	1.6	4.3	1.4	0.8	0.8	1.5
C GGBS 0.1	0.1	0.3	0.3	0.3	0.3	0.4	0.3	0.2	0.5	0.3	0.5	0.4	0.3	0.5
C GGBS 0.2	0.3	0.4	0.4	0.3	0.2	0.5	0.2	0.3	0.5	0.7	0.7	0.1	0.5	1.2
C GGBS 0.3	0.2	0.4	0.3	0.3	0.3	0.4	0.4	0.3	0.3	0.5	0.5	0.3	0.2	0.4
C GGBS 0.4	0.1	0.3	0.3	0.2	0.2	0.5	0.3	0.3	0.5	0.2	0.8	0.3	0.2	0.8
C FA 0.1	0.1	0.3	0.4	0.3	0.4	0.5	0.3	0.4	0.2	0.4	0.3	0.3	0.2	0.2
C FA 0.2	0.2	0.8	0.6	0.7	0.7	1	0.8	0.8	0.7	1.2	0.7	0.8	0.4	0.9
C FA 0.3	0.4	1	2	0.9	0.9	1	0.5	0.6	0.7	0.3	0.5	0.4	0.3	0.5
C FA 0.4	0.08	0.7	0.2	1.4	0.5	2	0.3	0.6	0.7	0.8	0.6	0.4	0.3	0.3

Appendix B Raw data in a long format

Table B- 1 The long format of the raw data for testing the effect of crack width on corrosion in Specimen types B made of PC measured via LPR

width	month	corrosion	next	width	month	corrosion	next	width	month	corrosion
0	1	0.06		0	7	0.21		0	13	0.09
0.1	1	0.08		0.1	7	0.16		0.1	13	0.5
0.2	1	0.06		0.2	7	0.26		0.2	13	0.64
0.3	1	0.06		0.3	7	0.2		0.3	13	0.72
0.4	1	0.06		0.4	7	0.17		0.4	13	0.89
0	2	0.07		0	8	0.2		0	14	0.09
0.1	2	0.08		0.1	8	0.29		0.1	14	0.56
0.2	2	0.09		0.2	8	0.31		0.2	14	0.68
0.3	2	0.08		0.3	8	0.36		0.3	14	0.88
0.4	2	0.08		0.4	8	0.32		0.4	14	0.55
0	3	0.07		0	9	0.2		0	15	0.05
0.1	3	0.08		0.1	9	0.45		0.1	15	0.43
0.2	3	0.07		0.2	9	0.19		0.2	15	0.79
0.3	3	0.08		0.3	9	0.22		0.3	15	0.73
0.4	3	0.07		0.4	9	0.44		0.4	15	0.55
0	4	0.12		0	10	0.22		0	16	0.04
0.1	4	0.12		0.1	10	0.6		0.1	16	0.9
0.2	4	0.13		0.2	10	0.33		0.2	16	1
0.3	4	0.15		0.3	10	0.22		0.3	16	0.96
0.4	4	0.11		0.4	10	0.31		0.4	16	0.72
0	5	0.11		0	11	0.29		0	17	0.05
0.1	5	0.13		0.1	11	0.5		0.1	17	1.1
0.2	5	0.13		0.2	11	0.51		0.2	17	1.1
0.3	5	0.15		0.3	11	0.5		0.3	17	0.85
0.4	5	0.15		0.4	11	0.45		0.4	17	1
0	6	0.1		0	12	0.05		0	18	0.5
0.1	6	0.14		0.1	12	0.5		0.1	18	1.37
0.2	6	0.18		0.2	12	0.54		0.2	18	1.31
0.3	6	0.16		0.3	12	0.67		0.3	18	1.5
0.4	6	0.2		0.4	12	0.58		0.4	18	1.54

width	month	corrosion	next	width	month	corrosion	next	width	month	corrosion
0	19	0.67		0	25	0.65		0	31	0.5
0.1	19	1.72		0.1	25	1.91		0.1	31	2.32
0.2	19	1.37		0.2	25	1.89		0.2	31	3.27
0.3	19	1.28		0.3	25	1.82		0.3	31	2.53
0.4	19	1.8		0.4	25	1.58		0.4	31	2.37
0	20	0.5		0	26	0.62		0	32	0.72
0.1	20	1.96		0.1	26	1.99		0.1	32	2.28
0.2	20	1.26		0.2	26	1.94		0.2	32	3.39
0.3	20	1.07		0.3	26	2.2		0.3	32	0.88
0.4	20	1.45		0.4	26	1.85		0.4	32	1.79
0	21	0.7		0	27	0.52		0	33	0.67
0.1	21	2.24		0.1	27	2.06		0.1	33	2.56
0.2	21	0.97		0.2	27	2.23		0.2	33	3.87
0.3	21	1.94		0.3	27	2.07		0.3	33	1.1
0.4	21	1.83		0.4	27	2.29		0.4	33	2.3
0	22	0.64		0	28	0.61		0	34	0.83
0.1	22	2.02		0.1	28	2.05		0.1	34	2.26
0.2	22	0.79		0.2	28	2.24		0.2	34	3.68
0.3	22	1.36		0.3	28	2.45		0.3	34	1.95
0.4	22	1.76		0.4	28	2.38		0.4	34	2.59
0	23	0.57		0	29	0.41		0	35	0.73
0.1	23	2.3		0.1	29	2.13		0.1	35	2.28
0.2	23	1.33		0.2	29	2.28		0.2	35	3.83
0.3	23	1.28		0.3	29	2.22		0.3	35	1.17
0.4	23	1.76		0.4	29	2.41		0.4	35	3.4
0	24	0.65		0	30	0.42		0	36	0.75
0.1	24	1.8		0.1	30	2.06		0.1	36	2.4
0.2	24	1.54		0.2	30	2.95		0.2	36	4.26
0.3	24	1.61		0.3	30	2.33		0.3	36	2.65
0.4	24	1.89		0.4	30	2.25		0.4	36	3.46

Table B- 2 The long format of the raw data for testing the effect of crack width on corrosion in Specimen type B made of PC measured via ZRA

width	month	corrosion	next	width	month	corrosion	next	width	month	corrosion
0	1	0.02		0	7	0.7		0	13	0.55
0.1	1	0.21		0.1	7	0.3		0.1	13	1.15
0.2	1	0.12		0.2	7	0.31		0.2	13	3.85
0.3	1	0.03		0.3	7	0.65		0.3	13	0.65
0.4	1	0.03		0.4	7	0.75		0.4	13	0.8
0	2	0.4		0	8	0.3		0	14	0.6
0.1	2	0.55		0.1	8	0.45		0.1	14	0.9
0.2	2	0.35		0.2	8	0.35		0.2	14	3.5
0.3	2	0.21		0.3	8	0.35		0.3	14	1
0.4	2	0.65		0.4	8	0.9		0.4	14	1.2
0	3	0.5		0	9	0.21		0	15	0.55
0.1	3	0.85		0.1	9	0.3		0.1	15	0.7
0.2	3	1.5		0.2	9	0.24		0.2	15	0.9
0.3	3	0.45		0.3	9	0.8		0.3	15	0.4
0.4	3	0.8		0.4	9	0.24		0.4	15	1.3
0	4	0.25		0	10	0.35		0	16	0.5
0.1	4	0.55		0.1	10	0.45		0.1	16	1
0.2	4	1.3		0.2	10	0.65		0.2	16	2.5
0.3	4	0.5		0.3	10	0.75		0.3	16	0.8
0.4	4	0.4		0.4	10	0.6		0.4	16	0.75
0	5	0.15		0	11	0.23		0	17	0.15
0.1	5	0.6		0.1	11	0.07		0.1	17	2
0.2	5	1.4		0.2	11	3.04		0.2	17	0.85
0.3	5	0.45		0.3	11	0.9		0.3	17	1.25
0.4	5	0.15		0.4	11	1.6		0.4	17	0.85
0	6	0.8		0	12	0.5		0	18	0.15
0.1	6	1.5		0.1	12	0.55		0.1	18	0.35
0.2	6	1.6		0.2	12	1.1		0.2	18	0.75
0.3	6	0.95		0.3	12	0.7		0.3	18	0.65
0.4	6	0.75		0.4	12	1.3		0.4	18	0.8

width	month	corrosion	next	width	month	corrosion	next	width	month	corrosion
0	19	0.25		0	25	0.35		0	31	0.1
0.1	19	0.35		0.1	25	0.45		0.1	31	0.2
0.2	19	0.65		0.2	25	0.75		0.2	31	0.55
0.3	19	0.6		0.3	25	0.8		0.3	31	0.65
0.4	19	0.85		0.4	25	0.65		0.4	31	0.6
0	20	0.4		0	26	0.45		0	32	0.15
0.1	20	0.2		0.1	26	0.5		0.1	32	0.3
0.2	20	0.6		0.2	26	0.55		0.2	32	0.4
0.3	20	0.95		0.3	26	0.7		0.3	32	0.55
0.4	20	0.9		0.4	26	0.9		0.4	32	0.4
0	21	0.3		0	27	0.35		0	33	0.5
0.1	21	0.35		0.1	27	0.5		0.1	33	0.7
0.2	21	0.45		0.2	27	0.55		0.2	33	0.8
0.3	21	0.7		0.3	27	0.7		0.3	33	0.4
0.4	21	0.55		0.4	27	0.75		0.4	33	0.88
0	22	0.4		0	28	0.35		0	34	1.1
0.1	22	0.45		0.1	28	0.4		0.1	34	0.25
0.2	22	0.85		0.2	28	0.55		0.2	34	0.5
0.3	22	0.85		0.3	28	0.7		0.3	34	0.6
0.4	22	1		0.4	28	0.85		0.4	34	0.45
0	23	0.4		0	29	0.35		0	35	0.8
0.1	23	0.4		0.1	29	0.35		0.1	35	1.25
0.2	23	0.75		0.2	29	0.45		0.2	35	1.3
0.3	23	1.5		0.3	29	0.7		0.3	35	1.6
0.4	23	0.75		0.4	29	0.7		0.4	35	0.5
0	24	0.3		0	30	0.3		0	36	1.15
0.1	24	0.45		0.1	30	0.35		0.1	36	1
0.2	24	0.7		0.2	30	0.5		0.2	36	1.2
0.3	24	0.8		0.3	30	0.7		0.3	36	0.75
0.4	24	0.55		0.4	30	0.88		0.4	36	1.05

Table B- 3 The long format of the raw data for testing the effect of crack width on corrosion in Specimen type B made of GGBS measured via LPR

width	month	Corrosion	next	width	month	Corrosion	next	width	month	Corrosion
0	1	0.07		0	7	0.17		0	13	0.17
0.1	1	0.08		0.1	7	0.21		0.1	13	0.36
0.2	1	0.07		0.2	7	0.02		0.2	13	0.36
0.3	1	0.07		0.3	7	0.02		0.3	13	0.31
0.4	1	0.07		0.4	7	0.01		0.4	13	0.46
0	2	0.08		0	8	0.16		0	14	0.12
0.1	2	0.09		0.1	8	0.33		0.1	14	0.37
0.2	2	0.09		0.2	8	0.32		0.2	14	0.29
0.3	2	0.09		0.3	8	0.25		0.3	14	0.35
0.4	2	0.08		0.4	8	0.24		0.4	14	0.55
0	3	0.2		0	9	0.13		0	15	0.06
0.1	3	0.09		0.1	9	0.33		0.1	15	0.54
0.2	3	0.08		0.2	9	0.33		0.2	15	0.4
0.3	3	0.08		0.3	9	0.24		0.3	15	0.48
0.4	3	0.09		0.4	9	0.21		0.4	15	0.83
0	4	0.12		0	10	0.2		0	16	0.04
0.1	4	0.16		0.1	10	0.27		0.1	16	0.6
0.2	4	0.13		0.2	10	0.26		0.2	16	0.53
0.3	4	0.14		0.3	10	0.2		0.3	16	0.57
0.4	4	0.18		0.4	10	0.2		0.4	16	0.75
0	5	0.11		0	11	0.22		0	17	0.02
0.1	5	0.13		0.1	11	0.36		0.1	17	0.54
0.2	5	0.12		0.2	11	0.28		0.2	17	0.58
0.3	5	0.15		0.3	11	0.25		0.3	17	0.67
0.4	5	0.12		0.4	11	0.5		0.4	17	0.66
0	6	0.1		0	12	0.05		0	18	0.5
0.1	6	0.11		0.1	12	0.4		0.1	18	0.59
0.2	6	0.14		0.2	12	0.28		0.2	18	0.8
0.3	6	0.13		0.3	12	0.3		0.3	18	0.9
0.4	6	0.2		0.4	12	0.6		0.4	18	0.64

width	month	Corrosion	next	width	month	Corrosion	next	width	month	Corrosion
0	19	0.49		0	25	0.69		0	31	0.7
0.1	19	1.16		0.1	25	0.59		0.1	31	0.53
0.2	19	0.73		0.2	25	0.75		0.2	31	0.83
0.3	19	0.77		0.3	25	0.76		0.3	31	0.69
0.4	19	0.63		0.4	25	0.75		0.4	31	0.72
0	20	0.61		0	26	0.63		0	32	0.66
0.1	20	0.68		0.1	26	0.54		0.1	32	0.6
0.2	20	0.64		0.2	26	0.76		0.2	32	0.67
0.3	20	0.7		0.3	26	0.67		0.3	32	0.79
0.4	20	0.55		0.4	26	0.67		0.4	32	0.65
0	21	0.67		0	27	0.68		0	33	0.8
0.1	21	0.61		0.1	27	0.52		0.1	33	0.73
0.2	21	0.66		0.2	27	0.84		0.2	33	0.68
0.3	21	0.68		0.3	27	0.66		0.3	33	0.9
0.4	21	0.66		0.4	27	0.73		0.4	33	0.69
0	22	0.69		0	28	0.73		0	34	0.73
0.1	22	0.59		0.1	28	0.69		0.1	34	0.78
0.2	22	0.5		0.2	28	0.73		0.2	34	0.61
0.3	22	0.72		0.3	28	0.66		0.3	34	0.73
0.4	22	0.58		0.4	28	0.73		0.4	34	0.66
0	23	0.63		0	29	0.5		0	35	0.76
0.1	23	0.65		0.1	29	0.71		0.1	35	0.79
0.2	23	0.63		0.2	29	0.69		0.2	35	0.63
0.3	23	0.87		0.3	29	0.73		0.3	35	0.7
0.4	23	0.61		0.4	29	0.81		0.4	35	0.68
0	24	0.65		0	30	0.63		0	36	0.7
0.1	24	0.57		0.1	30	0.73		0.1	36	0.73
0.2	24	0.69		0.2	30	0.68		0.2	36	0.68
0.3	24	0.72		0.3	30	0.61		0.3	36	0.67
0.4	24	0.75		0.4	30	0.74		0.4	36	0.62

Table B- 4 The long format of the raw data for testing the effect of crack width on corrosion in Specimen type B made of GGBS measured via ZRA

width	month	corrosion	next	width	month	corrosion	next	width	month	corrosion
0	1	0.03		0	7	0.3		0	13	0.25
0.1	1	0.02		0.1	7	0.6		0.1	13	0.25
0.2	1	0.03		0.2	7	0.85		0.2	13	1.3
0.3	1	0.02		0.3	7	0.6		0.3	13	0.8
0.4	1	0.02		0.4	7	0.4		0.4	13	0.7
0	2	0.5		0	8	0.2		0	14	0.35
0.1	2	0.4		0.1	8	0.25		0.1	14	0.7
0.2	2	1.3		0.2	8	0.65		0.2	14	1.45
0.3	2	0.5		0.3	8	0.55		0.3	14	0.95
0.4	2	0.4		0.4	8	0.45		0.4	14	0.6
0	3	0.2		0	9	0.26		0	15	0.5
0.1	3	0.7		0.1	9	0.5		0.1	15	0.4
0.2	3	0.6		0.2	9	0.35		0.2	15	0.7
0.3	3	0.75		0.3	9	0.2		0.3	15	0.6
0.4	3	0.7		0.4	9	0.45		0.4	15	0.35
0	4	0.3		0	10	0.3		0	16	0.4
0.1	4	0.55		0.1	10	0.45		0.1	16	0.3
0.2	4	0.7		0.2	10	0.55		0.2	16	0.75
0.3	4	0.6		0.3	10	0.35		0.3	16	0.6
0.4	4	0.5		0.4	10	0.3		0.4	16	0.4
0	5	0.45		0	11	0.24		0	17	0.5
0.1	5	0.45		0.1	11	0.35		0.1	17	0.4
0.2	5	0.45		0.2	11	0.3		0.2	17	0.5
0.3	5	0.5		0.3	11	0.85		0.3	17	0.55
0.4	5	0.6		0.4	11	0.55		0.4	17	0.7
0	6	0.45		0	12	0.5		0	18	0.3
0.1	6	0.3		0.1	12	0.3		0.1	18	0.4
0.2	6	0.4		0.2	12	0.75		0.2	18	1.3
0.3	6	0.75		0.3	12	0.9		0.3	18	0.8
0.4	6	0.55		0.4	12	0.7		0.4	18	0.85

width	month	corrosion	next	width	month	corrosion	next	width	month	corrosion
0	19	0.4		0	25	0.2		0	31	0.15
0.1	19	0.3		0.1	25	0.2		0.1	31	0.25
0.2	19	1.8		0.2	25	0.45		0.2	31	0.25
0.3	19	0.75		0.3	25	0.65		0.3	31	0.6
0.4	19	0.5		0.4	25	0.55		0.4	31	0.55
0	20	0.5		0	26	0.25		0	32	0.2
0.1	20	0.4		0.1	26	0.25		0.1	32	0.35
0.2	20	0.65		0.2	26	0.55		0.2	32	0.5
0.3	20	0.45		0.3	26	0.55		0.3	32	0.55
0.4	20	0.6		0.4	26	0.6		0.4	32	0.6
0	21	0.15		0	27	0.3		0	33	0.35
0.1	21	0.3		0.1	27	0.35		0.1	33	0.6
0.2	21	0.55		0.2	27	0.45		0.2	33	0.6
0.3	21	0.65		0.3	27	0.4		0.3	33	0.65
0.4	21	0.45		0.4	27	0.6		0.4	33	0.55
0	22	0.25		0	28	0.35		0	34	0.35
0.1	22	0.55		0.1	28	0.4		0.1	34	0.3
0.2	22	0.7		0.2	28	0.55		0.2	34	0.45
0.3	22	0.55		0.3	28	0.3		0.3	34	0.35
0.4	22	0.8		0.4	28	0.6		0.4	34	0.6
0	23	0.3		0	29	0.4		0	35	0.7
0.1	23	0.4		0.1	29	0.4		0.1	35	0.35
0.2	23	0.6		0.2	29	0.55		0.2	35	1.95
0.3	23	0.45		0.3	29	0.45		0.3	35	0.4
0.4	23	0.65		0.4	29	0.65		0.4	35	0.55
0	24	0.2		0	30	0.3		0	36	0.4
0.1	24	0.3		0.1	30	0.45		0.1	36	0.4
0.2	24	0.55		0.2	30	0.45		0.2	36	0.5
0.3	24	0.55		0.3	30	0.45		0.3	36	0.4
0.4	24	0.6		0.4	30	0.75		0.4	36	0.55

Table B- 5 The long format of the raw data for testing the effect of crack width on corrosion in Specimen type B made of FA measured via LPR

width	month	corrosion	next	width	month	corrosion	next	width	month	corrosion
0	1	0.07		0	7	0.15		0	13	0.35
0.1	1	0.08		0.1	7	0.17		0.1	13	0.21
0.2	1	0.06		0.2	7	0.19		0.2	13	0.35
0.3	1	0.08		0.3	7	0.16		0.3	13	0.54
0.4	1	0.08		0.4	7	0.15		0.4	13	0.63
0	2	0.08		0	8	0.19		0	14	0.16
0.1	2	0.07		0.1	8	0.29		0.1	14	0.3
0.2	2	0.08		0.2	8	0.23		0.2	14	0.3
0.3	2	0.07		0.3	8	0.32		0.3	14	0.52
0.4	2	0.08		0.4	8	0.21		0.4	14	0.75
0	3	0.11		0	9	0.15		0	15	0.03
0.1	3	0.05		0.1	9	0.33		0.1	15	0.31
0.2	3	0.07		0.2	9	0.29		0.2	15	0.33
0.3	3	0.07		0.3	9	0.32		0.3	15	0.58
0.4	3	0.06		0.4	9	0.2		0.4	15	0.8
0	4	0.13		0	10	0.2		0	16	0.04
0.1	4	0.14		0.1	10	0.21		0.1	16	0.29
0.2	4	0.12		0.2	10	0.35		0.2	16	0.36
0.3	4	0.13		0.3	10	0.3		0.3	16	0.64
0.4	4	0.15		0.4	10	0.26		0.4	16	0.77
0	5	0.11		0	11	0.06		0	17	0.02
0.1	5	0.13		0.1	11	0.33		0.1	17	0.43
0.2	5	0.12		0.2	11	0.16		0.2	17	0.43
0.3	5	0.12		0.3	11	0.43		0.3	17	0.67
0.4	5	0.14		0.4	11	0.48		0.4	17	0.8
0	6	0.1		0	12	0.11		0	18	0.48
0.1	6	0.15		0.1	12	0.25		0.1	18	0.93
0.2	6	0.13		0.2	12	0.25		0.2	18	0.85
0.3	6	0.2		0.3	12	0.42		0.3	18	1.08
0.4	6	0.14		0.4	12	0.57		0.4	18	0.8

width	month	corrosion	next	width	month	corrosion	next	width	month	corrosion
0	19	0.47		0	25	0.38		0	31	0.45
0.1	19	0.77		0.1	25	0.77		0.1	31	0.86
0.2	19	0.84		0.2	25	0.81		0.2	31	0.87
0.3	19	1.12		0.3	25	0.96		0.3	31	1.11
0.4	19	0.7		0.4	25	0.7		0.4	31	0.7
0	20	0.48		0	26	0.45		0	32	0.43
0.1	20	0.87		0.1	26	0.78		0.1	32	0.7
0.2	20	0.81		0.2	26	0.76		0.2	32	0.74
0.3	20	1.03		0.3	26	0.93		0.3	32	1
0.4	20	0.6		0.4	26	1		0.4	32	0.6
0	21	0.43		0	27	0.43		0	33	0.48
0.1	21	0.71		0.1	27	0.92		0.1	33	1.26
0.2	21	0.81		0.2	27	0.71		0.2	33	0.98
0.3	21	1.08		0.3	27	0.86		0.3	33	1.06
0.4	21	0.7		0.4	27	0.8		0.4	33	0.8
0	22	0.43		0	28	0.43		0	34	0.5
0.1	22	0.63		0.1	28	0.91		0.1	34	1.01
0.2	22	0.58		0.2	28	0.74		0.2	34	0.9
0.3	22	0.76		0.3	28	1.07		0.3	34	0.97
0.4	22	0.6		0.4	28	0.8		0.4	34	1
0	23	0.45		0	29	0.44		0	35	0.45
0.1	23	0.67		0.1	29	0.86		0.1	35	1.01
0.2	23	0.72		0.2	29	0.85		0.2	35	0.96
0.3	23	0.81		0.3	29	0.94		0.3	35	1.02
0.4	23	0.8		0.4	29	0.7		0.4	35	1.1
0	24	0.43		0	30	0.49		0	36	0.48
0.1	24	0.78		0.1	30	0.93		0.1	36	1.07
0.2	24	0.84		0.2	30	0.89		0.2	36	0.98
0.3	24	0.96		0.3	30	1.03		0.3	36	0.97
0.4	24	0.6		0.4	30	0.7		0.4	36	1.3

Table B- 6 The long format of the raw data for testing the effect of crack width on corrosion in Specimen type B made of FA measured via ZRA

width	month	corrosion	next	width	month	corrosion	next	width	month	corrosion
0	1	0.02		0	7	0.55		0	13	0.5
0.1	1	0.03		0.1	7	0.8		0.1	13	0.8
0.2	1	0.03		0.2	7	1.4		0.2	13	1
0.3	1	0.03		0.3	7	0.8		0.3	13	1.2
0.4	1	0.21		0.4	7	0.62		0.4	13	0.55
0	2	0.75		0	8	0.25		0	14	0.07
0.1	2	0.85		0.1	8	0.65		0.1	14	0.51
0.2	2	2		0.2	8	0.6		0.2	14	1.1
0.3	2	0.4		0.3	8	0.8		0.3	14	1.2
0.4	2	0.35		0.4	8	0.75		0.4	14	1.3
0	3	0.45		0	9	0.25		0	15	0.7
0.1	3	0.65		0.1	9	0.4		0.1	15	0.75
0.2	3	0.45		0.2	9	0.35		0.2	15	0.45
0.3	3	0.3		0.3	9	0.4		0.3	15	0.7
0.4	3	0.3		0.4	9	0.7		0.4	15	0.7
0	4	0.65		0	10	0.25		0	16	0.51
0.1	4	0.6		0.1	10	0.4		0.1	16	0.26
0.2	4	0.6		0.2	10	0.9		0.2	16	0.5
0.3	4	0.6		0.3	10	0.6		0.3	16	0.7
0.4	4	0.6		0.4	10	0.8		0.4	16	0.55
0	5	0.17		0	11	0.9		0	17	0.4
0.1	5	0.65		0.1	11	0.55		0.1	17	0.85
0.2	5	0.85		0.2	11	1.3		0.2	17	0.4
0.3	5	0.4		0.3	11	0.7		0.3	17	1.7
0.4	5	0.35		0.4	11	0.35		0.4	17	0.7
0	6	0.1		0	12	0.2		0	18	0.3
0.1	6	0.7		0.1	12	0.95		0.1	18	0.7
0.2	6	0.8		0.2	12	1		0.2	18	0.7
0.3	6	0.75		0.3	12	1.7		0.3	18	0.75
0.4	6	0.7		0.4	12	0.7		0.4	18	0.6

width	month	corrosion	next	width	month	corrosion	next	width	month	corrosion
0	19	0.5		0	25	0.4		0	31	0.4
0.1	19	0.9		0.1	25	0.5		0.1	31	0.45
0.2	19	0.3		0.2	25	0.7		0.2	31	0.9
0.3	19	0.7		0.3	25	0.85		0.3	31	0.4
0.4	19	0.65		0.4	25	0.95		0.4	31	0.45
0	20	0.1		0	26	0.4		0	32	0.2
0.1	20	0.75		0.1	26	0.45		0.1	32	0.4
0.2	20	0.4		0.2	26	0.5		0.2	32	0.35
0.3	20	0.4		0.3	26	0.5		0.3	32	0.4
0.4	20	0.25		0.4	26	0.75		0.4	32	0.65
0	21	0.5		0	27	0.3		0	33	0.5
0.1	21	0.6		0.1	27	0.35		0.1	33	0.55
0.2	21	0.6		0.2	27	0.45		0.2	33	0.4
0.3	21	0.35		0.3	27	0.5		0.3	33	0.9
0.4	21	0.4		0.4	27	0.9		0.4	33	0.45
0	22	0.4		0	28	0.2		0	34	0.55
0.1	22	0.4		0.1	28	0.35		0.1	34	0.4
0.2	22	0.55		0.2	28	0.55		0.2	34	0.7
0.3	22	0.65		0.3	28	0.5		0.3	34	1.15
0.4	22	0.85		0.4	28	0.75		0.4	34	0.25
0	23	0.35		0	29	0.3		0	35	0.2
0.1	23	0.25		0.1	29	0.4		0.1	35	0.4
0.2	23	0.6		0.2	29	0.7		0.2	35	0.5
0.3	23	0.7		0.3	29	0.7		0.3	35	1
0.4	23	0.6		0.4	29	0.55		0.4	35	0.4
0	24	0.3		0	30	0.4		0	36	0.25
0.1	24	0.4		0.1	30	0.45		0.1	36	0.3
0.2	24	0.4		0.2	30	0.8		0.2	36	0.6
0.3	24	0.85		0.3	30	0.7		0.3	36	0.55
0.4	24	0.75		0.4	30	0.6		0.4	36	0.25

Table B- 7 The long format of the raw data for testing the effect of crack width on corrosion in Specimen type C made of PC measured via LPR

width	month	corrosion	next	width	month	corrosion
0	1	0.09		0	8	0.40
0.1	1	0.20		0.1	8	4.40
0.2	1	0.20		0.2	8	4.25
0.3	1	0.20		0.3	8	4.13
0.4	1	0.20		0.4	8	3.12
0	2	0.11		0	9	0.54
0.1	2	0.41		0.1	9	4.68
0.2	2	0.80		0.2	9	4.63
0.3	2	0.67		0.3	9	4.00
0.4	2	1.00		0.4	9	3.39
0	3	0.11		0	10	0.62
0.1	3	2.52		0.1	10	3.92
0.2	3	2.31		0.2	10	3.44
0.3	3	2.50		0.3	10	3.25
0.4	3	1.30		0.4	10	3.67
0	4	0.29		0	11	0.41
0.1	4	1.48		0.1	11	3.72
0.2	4	1.94		0.2	11	3.06
0.3	4	1.94		0.3	11	5.38
0.4	4	2.70		0.4	11	3.88
0	5	0.32		0	12	0.40
0.1	5	1.68		0.1	12	3.44
0.2	5	2.25		0.2	12	2.81
0.3	5	2.63		0.3	12	4.81
0.4	5	2.30		0.4	12	3.50
0	6	0.40		0	13	0.50
0.1	6	3.60		0.1	13	2.36
0.2	6	4.69		0.2	13	2.00
0.3	6	4.31		0.3	13	3.00
0.4	6	2.50		0.4	13	3.25
0	7	0.40		0	14	0.67
0.1	7	4.68		0.1	14	2.72
0.2	7	5.44		0.2	14	2.06
0.3	7	3.94		0.3	14	3.63
0.4	7	3.10		0.4	14	3.78

Table B- 8 The long format of the raw data for testing the effect of crack width on corrosion in Specimen type C made of PC measured via ZRA

width	month	corrosion	next	width	month	corrosion
0	1	0.02		0	8	0.5
0.1	1	0.2		0.1	8	1.7
0.2	1	0.3		0.2	8	2.8
0.3	1	0.3		0.3	8	1.4
0.4	1	0.1		0.4	8	0.7
0	2	0.25		0	9	0.4
0.1	2	1		0.1	9	1.4
0.2	2	0.5		0.2	9	1
0.3	2	1		0.3	9	1.2
0.4	2	0.7		0.4	9	1.6
0	3	0.3		0	10	0.4
0.1	3	0.4		0.1	10	2
0.2	3	0.3		0.2	10	1.5
0.3	3	0.2		0.3	10	1.6
0.4	3	0.3		0.4	10	4.3
0	4	0.35		0	11	0.45
0.1	4	0.5		0.1	11	0.8
0.2	4	2.6		0.2	11	1.1
0.3	4	0.5		0.3	11	1.2
0.4	4	0.2		0.4	11	1.4
0	5	0.5		0	12	0.35
0.1	5	0.7		0.1	12	0.5
0.2	5	1.1		0.2	12	0.2
0.3	5	1.2		0.3	12	1.2
0.4	5	0.7		0.4	12	0.8
0	6	0.6		0	13	0.35
0.1	6	2.7		0.1	13	1.1
0.2	6	1.7		0.2	13	1.2
0.3	6	2.4		0.3	13	0.8
0.4	6	0.7		0.4	13	0.8
0	7	0.5		0	14	0.5
0.1	7	1.9		0.1	14	1.1
0.2	7	4.2		0.2	14	1.4
0.3	7	1.8		0.3	14	1.2
0.4	7	0.6		0.4	14	1.5

Table B- 9 The long format of the raw data for testing the effect of crack width on corrosion in Specimen type C made of GGBS measured via LPR

width	month	corrosion	next	width	month	corrosion
0	1	0.07		0	8	0.40
0.1	1	0.2		0.1	8	2.3
0.2	1	0.2		0.2	8	1.9
0.3	1	0.2		0.3	8	1.7
0.4	1	0.1		0.4	8	2
0	2	0.12		0	9	0.50
0.1	2	0.7		0.1	9	2.7
0.2	2	0.8		0.2	9	2.1
0.3	2	1		0.3	9	1.7
0.4	2	0.6		0.4	9	2.3
0	3	0.17		0	10	0.55
0.1	3	3		0.1	10	2.2
0.2	3	5		0.2	10	1.9
0.3	3	4		0.3	10	1.5
0.4	3	1.1		0.4	10	2
0	4	0.13		0	11	0.55
0.1	4	1.7		0.1	11	2.6
0.2	4	1.9		0.2	11	2
0.3	4	1.5		0.3	11	1.5
0.4	4	1.7		0.4	11	2.5
0	5	0.22		0	12	0.68
0.1	5	2.1		0.1	12	2.7
0.2	5	2		0.2	12	2.4
0.3	5	1.7		0.3	12	1.6
0.4	5	1.5		0.4	12	2.3
0	6	0.30		0	13	0.69
0.1	6	2.4		0.1	13	2.1
0.2	6	2.5		0.2	13	2
0.3	6	2		0.3	13	1.5
0.4	6	1.6		0.4	13	2.5
0	7	0.50		0	14	0.71
0.1	7	2.5		0.1	14	2.1
0.2	7	2.3		0.2	14	2.1
0.3	7	2		0.3	14	1.5
0.4	7	2.2		0.4	14	2

Table B- 10 The long format of the raw data for testing the effect of crack width on corrosion in Specimen type C made of GGBS measured via ZRA

width	month	corrosion	next	width	month	corrosion
0	1	0.03		0	8	0.3
0.1	1	0.1		0.1	8	0.2
0.2	1	0.3		0.2	8	0.3
0.3	1	0.2		0.3	8	0.3
0.4	1	0.1		0.4	8	1
0	2	0.2		0	9	0.25
0.1	2	0.3		0.1	9	0.5
0.2	2	0.4		0.2	9	0.5
0.3	2	0.4		0.3	9	0.3
0.4	2	0.3		0.4	9	0.8
0	3	0.3		0	10	0.35
0.1	3	0.3		0.1	10	0.3
0.2	3	0.4		0.2	10	0.7
0.3	3	0.3		0.3	10	0.5
0.4	3	0.3		0.4	10	0.7
0	4	0.45		0	11	0.4
0.1	4	0.3		0.1	11	0.5
0.2	4	0.3		0.2	11	0.7
0.3	4	0.3		0.3	11	0.5
0.4	4	0.2		0.4	11	0.8
0	5	0.3		0	12	0.35
0.1	5	0.3		0.1	12	0.4
0.2	5	0.2		0.2	12	0.1
0.3	5	0.3		0.3	12	0.3
0.4	5	0.2		0.4	12	0.3
0	6	0.5		0	13	0.35
0.1	6	0.4		0.1	13	0.3
0.2	6	0.5		0.2	13	0.5
0.3	6	0.4		0.3	13	0.2
0.4	6	0.5		0.4	13	0.4
0	7	0.35		0	14	0.4
0.1	7	0.3		0.1	14	0.5
0.2	7	0.2		0.2	14	1.2
0.3	7	0.4		0.3	14	0.4
0.4	7	0.6		0.4	14	0.8

Table B- 11 The long format of the raw data for testing the effect of crack width on corrosion in Specimen type C made of FA measured via LPR

width	month	corrosion	next	width	month	corrosion
0	1	0.07		0	8	0.30
0.1	1	0.20		0.1	8	1.80
0.2	1	0.10		0.2	8	2.55
0.3	1	0.10		0.3	8	2.53
0.4	1	0.20		0.4	8	2.00
0	2	0.13		0	9	0.40
0.1	2	0.80		0.1	9	2.00
0.2	2	0.67		0.2	9	2.55
0.3	2	0.88		0.3	9	2.76
0.4	2	0.60		0.4	9	2.00
0	3	0.15		0	10	0.26
0.1	3	2.70		0.1	10	1.70
0.2	3	2.85		0.2	10	3.10
0.3	3	2.65		0.3	10	2.94
0.4	3	1.10		0.4	10	2.10
0	4	0.20		0	11	0.40
0.1	4	1.70		0.1	11	1.60
0.2	4	1.60		0.2	11	2.15
0.3	4	2.71		0.3	11	2.24
0.4	4	1.40		0.4	11	2.10
0	5	0.20		0	12	0.40
0.1	5	1.90		0.1	12	2.00
0.2	5	2.05		0.2	12	2.30
0.3	5	3.12		0.3	12	2.47
0.4	5	2.00		0.4	12	2.10
0	6	0.30		0	13	0.44
0.1	6	2.00		0.1	13	1.50
0.2	6	2.25		0.2	13	1.40
0.3	6	2.88		0.3	13	1.53
0.4	6	2.10		0.4	13	2.00
0	7	0.33		0	14	0.35
0.1	7	1.90		0.1	14	1.50
0.2	7	2.60		0.2	14	1.90
0.3	7	3.00		0.3	14	2.24
0.4	7	1.50		0.4	14	2.50

Table B- 12 The long format of the raw data for testing the effect of crack width on corrosion in Specimen type C made of FA measured via ZRA

width	month	corrosion	next	width	month	corrosion
0	1	0.02		0	8	0.35
0.1	1	0.10		0.1	8	0.40
0.2	1	0.20		0.2	8	0.80
0.3	1	0.40		0.3	8	0.60
0.4	1	0.08		0.4	8	0.60
0	2	0.45		0	9	0.40
0.1	2	0.30		0.1	9	0.20
0.2	2	0.80		0.2	9	0.70
0.3	2	1.00		0.3	9	0.70
0.4	2	0.70		0.4	9	0.70
0	3	0.55		0	10	0.30
0.1	3	0.40		0.1	10	0.40
0.2	3	0.60		0.2	10	1.20
0.3	3	2.00		0.3	10	0.30
0.4	3	0.20		0.4	10	0.80
0	4	0.25		0	11	0.40
0.1	4	0.30		0.1	11	0.30
0.2	4	0.70		0.2	11	0.70
0.3	4	0.90		0.3	11	0.50
0.4	4	1.40		0.4	11	0.60
0	5	0.50		0	12	0.43
0.1	5	0.40		0.1	12	0.30
0.2	5	0.70		0.2	12	0.80
0.3	5	0.90		0.3	12	0.40
0.4	5	0.50		0.4	12	0.40
0	6	0.51		0	13	0.40
0.1	6	0.50		0.1	13	0.20
0.2	6	1.00		0.2	13	0.40
0.3	6	1.00		0.3	13	0.30
0.4	6	2.00		0.4	13	0.30
0	7	0.40		0	14	0.50
0.1	7	0.30		0.1	14	0.20
0.2	7	0.80		0.2	14	0.90
0.3	7	0.50		0.3	14	0.50
0.4	7	0.30		0.4	14	

Table B- 13 The long format of the raw data for testing the effect of CRACK DEPTH on corrosion in Specimen types A1 and B made of PC measured via LPR

Types	month	corrosion	next	Types	month	corrosion
A1	1	0.07		A1	19	7.00
В	1	0.06		В	19	1.80
A1	2	0.09		A1	20	7.67
В	2	0.08		В	20	1.45
A1	3	0.4		A1	21	6.50
В	3	0.07		В	21	1.83
A1	4	0.56		A1	22	5.90
В	4	0.11		В	22	1.76
A1	5	0.47		A1	23	5.87
В	5	0.15		В	23	1.76
A1	6	0.37		A1	24	5.67
В	6	0.20		В	24	1.89
A1	7	1.1		A1	25	5.90
В	7	0.17		В	25	1.58
A1	8	1		A1	26	5.83
В	8	0.32		В	26	1.85
A1	9	1.47		A1	27	5.60
В	9	0.44		В	27	2.29
A1	10	2.8		A1	28	6.00
В	10	0.31		В	28	2.38
A1	11	2.96		A1	29	5.80
В	11	1.60		В	29	2.41
A1	12	2.5		A1	30	5.84
В	12	0.58		В	30	2.25
A1	13	2.1		A1	31	6.10
В	13	0.89		В	31	2.37
A1	14	1.67		A1	32	6.00
В	14	0.55		В	32	1.79
A1	15	2.37		A1	33	7.20
В	15	0.55		В	33	2.30
A1	16	3.10		A1	34	6.70
В	16	0.72		В	34	2.59
A1	17	3.40		A1	35	6.30
В	17	1.00		В	35	3.40
A1	18	4.73		A1	36	6.30
В	18	1.54		В	36	3.46

Table B- 14 The long format of the raw data for testing the effect of CRACK DEPTH on corrosion in Specimen types A1 and B made of PC measured via ZRA

Types	month	corrosion	next	Types	month	corrosion
A1	1	0.03		A1	19	2
В	1	0.03		В	19	0.85
A1	2	1		A1	20	2.7
В	2	0.65		В	20	0.9
A1	3	3		A1	21	2.4
В	3	0.8		В	21	0.9
A1	4	2		A1	22	2.4
В	4	0.4		В	22	1
A1	5	1		A1	23	2.2
В	5	0.15		В	23	0.75
A1	6	1		A1	24	2.3
В	6	0.75		В	24	0.55
A1	7	3		A1	25	2.2
В	7	0.75		В	25	0.65
A1	8	1		A1	26	2.4
В	8	0.9		В	26	0.9
A1	9	0.7		A1	27	2.4
В	9	0.24		В	27	0.75
A1	10	1		A1	28	2.6
В	10	0.3		В	28	0.85
A1	11	0.4		A1	29	2.5
В	11	1.6		В	29	0.7
A1	12	2		A1	30	2.7
В	12	1.3		В	30	1
A1	13	3		A1	31	2
В	13	0.8		В	31	0.6
A1	14	3		A1	32	2.1
В	14	1.2		В	32	0.4
A1	15	3		A1	33	2.2
В	15	1.3		В	33	0.88
A1	16	0.7		A1	34	2.3
В	16	0.75		В	34	0.8
A1	17	3		A1	35	2.6
В	17	0.85		В	35	0.9
A1	18	2		A1	36	3.3
В	18	0.8		В	36	1.05

Table B- 15 The long format of the raw data for testing the effect of CRACK DEPTH on corrosion in Specimen types A1 and B made of GGBS measured via LPR

Types	month	corrosion	next	Types	month	corrosion
A1	1	0.08		A1	19	2.6
В	1	0.07		В	19	0.63
A1	2	0.08		A1	20	3.3
В	2	0.08		В	20	0.55
A1	3	0.23		A1	21	3.86
В	3	0.09		В	21	0.66
A1	4	0.6		A1	22	3.9
В	4	0.18		В	22	0.58
A1	5	0.5		A1	23	4.5
В	5	0.12		В	23	0.61
A1	6	0.3		A1	24	4.68
В	6	0.2		В	24	0.75
A1	7	0.67		A1	25	4.55
В	7	0.01		В	25	0.75
A1	8	1.07		A1	26	4.46
В	8	0.24		В	26	0.67
A1	9	0.87		A1	27	3.9
В	9	0.21		В	27	0.73
A1	10	1		A1	28	4.38
В	10	0.2		В	28	0.73
A1	11	1.07		A1	29	4.55
В	11	0.5		В	29	0.81
A1	12	0.8		A1	30	3.9
В	12	0.61		В	30	0.74
A1	13	0.8		A1	31	4.6
В	13	0.46		В	31	0.71
A1	14	1.35		A1	32	3.51
В	14	0.55		В	32	0.65
A1	15	1.47		A1	33	3.9
В	15	0.83		В	33	0.69
A1	16	2.12		A1	34	3.9
В	16	0.75		В	34	0.68
A1	17	2.21		A1	35	4
В	17	0.66		В	35	0.67
A1	18	3.2		A1	36	2.6
В	18	0.64		В	36	0.62

Table B- 16 The long format of the raw data for testing the effect of CRACK DEPTH on corrosion in Specimen types A1 and B made of GGBS measured via ZRA

Types	month	corrosion	next	Types	month	corrosion
A1	1	0.38		A1	19	0.6
В	1	0.02		В	19	0.5
A1	2	0.6		A1	20	0.8
В	2	0.4		В	20	0.6
A1	3	0.7		A1	21	0.8
В	3	0.7		В	21	0.45
A1	4	0.8		A1	22	0.8
В	4	0.5		В	22	0.8
A1	5	0.9		A1	23	0.8
В	5	0.6		В	23	0.65
A1	6	0.5		A1	24	0.8
В	6	0.55		В	24	0.6
A1	7	1.7		A1	25	0.9
В	7	0.4		В	25	0.55
A1	8	0.9		A1	26	0.7
В	8	0.45		В	26	0.6
A1	9	0.8		A1	27	0.7
В	9	0.45		В	27	0.6
A1	10	0.9		A1	28	0.8
В	10	0.3		В	28	0.6
A1	11	0.6		A1	29	0.8
В	11	0.55		В	29	0.65
A1	12	0.2		A1	30	0.7
В	12	0.7		В	30	0.75
A1	13	1		A1	31	0.9
В	13	0.7		В	31	0.55
A1	14	0.7		A1	32	0.8
В	14	0.6		В	32	0.6
A1	15	0.7		A1	33	0.9
В	15	0.35		В	33	0.55
A1	16	0.7		A1	34	0.8
В	16	0.4		В	34	0.6
A1	17	0.8		A1	35	0.7
В	17	0.7		В	35	0.55
A1	18	0.7		A1	36	1.2
В	18	0.85		В	36	0.55

Table B- 17 The long format of the raw data for testing the effect of CRACK DEPTH on corrosion in Specimen types A1 and B made of FA measured via LPR

Types	month	corrosion	next	Types	month	corrosion
A1	1	0.05		A1	19	3
В	1	0.08		В	19	0.7
A1	2	0.08		A1	20	3.6
В	2	0.08		В	20	0.6
A1	3	0.4		A1	21	3.96
В	3	0.06		В	21	0.7
A1	4	0.5		A1	22	3.6
В	4	0.15		В	22	0.6
A1	5	0.8		A1	23	4.24
В	5	0.14		В	23	0.8
A1	6	0.63		A1	24	3.6
В	6	0.14		В	24	0.6
A1	7	0.73		A1	25	3.84
В	7	0.15		В	25	0.7
A1	8	0.7		A1	26	3.08
В	8	0.21		В	26	1
A1	9	1		A1	27	3
В	9	0.2		В	27	0.8
A1	10	0.87		A1	28	2.6
В	10	0.26		В	28	0.8
A1	11	1.3		A1	29	4.9
В	11	0.48		В	29	0.7
A1	12	1.52		A1	30	4.7
В	12	0.6		В	30	0.7
A1	13	1.34		A1	31	4.03
В	13	0.6		В	31	0.7
A1	14	1.5		A1	32	5.07
В	14	0.75		В	32	0.6
A1	15	2		A1	33	3.9
В	15	0.77		В	33	0.8
A1	16	1.8		A1	34	4.42
В	16	0.77		В	34	1
A1	17	2.96		A1	35	5.15
В	17	0.8		В	35	1.1
A1	18	2.4		A1	36	3.55
В	18	0.8		В	36	1.3

Table B- 18 The long format of the raw data for testing the effect of CRACK DEPTH on corrosion in Specimen types A1 and B made of FA measured via ZRA

Types	month	corrosion	next	Types	month	corrosion
A1	1	0.06		A1	19	0.9
В	1	0.21		В	19	0.65
A1	2	1		A1	20	0.8
В	2	0.35		В	20	0.25
A1	3	1		A1	21	0.7
В	3	0.3		В	21	0.4
A1	4	0.5		A1	22	0.6
В	4	0.6		В	22	0.85
A1	5	0.9		A1	23	0.6
В	5	0.35		В	23	0.6
A1	6	1		A1	24	0.7
В	6	0.7		В	24	0.75
A1	7	1.6		A1	25	0.5
В	7	0.62		В	25	0.95
A1	8	1		A1	26	0.5
В	8	0.75		В	26	0.75
A1	9	1		A1	27	0.7
В	9	0.7		В	27	0.9
A1	10	1		A1	28	0.6
В	10	0.8		В	28	0.75
A1	11	0.8		A1	29	0.6
В	11	0.35		В	29	0.55
A1	12	1		A1	30	0.6
В	12	0.7		В	30	0.6
A1	13	1		A1	31	0.6
В	13	0.55		В	31	0.45
A1	14	0.9		A1	32	0.6
В	14	1.3		В	32	0.65
A1	15	0.9		A1	33	0.6
В	15	0.7		В	33	0.45
A1	16	1		A1	34	0.8
В	16	0.55		В	34	0.25
A1	17	1		A1	35	0.7
В	17	0.7		В	35	0.4
A1	18	0.8		A1	36	0.6
В	18	0.6		В	36	0.25

Table B- 19 The long format of the raw data for testing the effect of CRACK DEPTH on corrosion in Specimen types A2 and C made of PC measured via LPR (left) and ZRA (right)

	LPR			ZRA	
Types	month	corrosion	Types	month	corrosion
A2	1	0.2	A2	1	0.3
С	1	0.2	С	1	0.1
A2	2	0.4	A2	2	0.3
С	2	1	С	2	0.7
A2	3	1	A2	3	0.1
С	3	1.3	С	3	0.3
A2	4	3.85	A2	4	1
С	4	2.7	С	4	0.2
A2	5	4.85	A2	5	1.5
С	5	2.3	С	5	0.7
A2	6	5.5	A2	6	3.4
С	6	2.5	С	6	0.7
A2	7	6.5	A2	7	2.8
С	7	3.1	С	7	0.6
A2	8	6.85	A2	8	2.8
С	8	3.11	С	8	0.7
A2	9	7.65	A2	9	2.4
С	9	3.3	С	9	1.6
A2	10	7.35	A2	10	1.6
С	10	3.6	С	10	2.5
A2	11	9.15	A2	11	1.8
С	11	3.7	С	11	1.4
A2	12	11.53	A2	12	2
С	12	3.7	С	12	0.8
A2	13	8.35	A2	13	2
С	13	3.2	С	13	0.8
A2	14	9	A2	14	2.7
С	14	3.7	С	14	1.5

Table B- 20 The long format of the raw data for testing the effect of CRACK DEPTH on corrosion in Specimen types A2 and C made of GGBS measured via LPR (left) and ZRA (right)

	LPR			ZRA	
Types	month	corrosion	Types	month	corrosion
A2	1	0.2	A2	1	0.3
С	1	0.1	С	1	0.1
A2	2	0.3	A2	2	0.2
С	2	0.6	С	2	0.3
A2	3	4.3	A2	3	0.3
С	3	1.1	С	3	0.3
A2	4	1.8	A2	4	0.3
С	4	1.7	С	4	0.2
A2	5	3	A2	5	0.5
С	5	1.5	С	5	0.2
A2	6	3.8	A2	6	0.9
С	6	1.6	С	6	0.5
A2	7	3.4	A2	7	1
С	7	1.6	С	7	0.6
A2	8	4.3	A2	8	1
С	8	2	С	8	1
A2	9	4.3	A2	9	1.1
С	9	2.3	С	9	0.8
A2	10	4.6	A2	10	1
С	10	2	С	10	0.7
A2	11	4.2	A2	11	0.6
С	11	2.5	С	11	0.8
A2	12	5.1	A2	12	0.5
С	12	2.3	С	12	0.3
A2	13	4.3	A2	13	0.8
С	13	2.5	С	13	0.4
A2	14	4.5	A2	14	1.3
С	14	2	С	14	0.8

Table B- 21 The long format of the raw data for testing the effect of CRACK DEPTH on corrosion in Specimen types A2 and C made of FA measured via LPR (left) and ZRA (right)

Types	month	corrosion	Types	month	corrosion
A2	1	0.1	A2	1	0.2
С	1	0.2	С	1	0.08
A2	2	0.4	A2	2	0.2
С	2	0.6	С	2	0.7
A2	3	2	A2	3	0.1
С	3	1.1	С	3	0.2
A2	4	3.1	A2	4	0.5
С	4	1.4	С	4	1.4
A2	5	3.4	A2	5	0.6
С	5	2	С	5	0.5
A2	6	4	A2	6	0.7
С	6	2.1	С	6	2
A2	7	4	A2	7	1.2
С	7	1.5	С	7	0.3
A2	8	4.3	A2	8	1.1
С	8	1.4	С	8	0.6
A2	9	4.8	A2	9	1.4
С	9	2	С	9	0.7
A2	10	5.4	A2	10	1.2
С	10	2.1	С	10	0.8
A2	11	5.4	A2	11	1.1
С	11	2.1	С	11	0.6
A2	12	5.2	A2	12	1
С	12	2.3	С	12	0.4
A2	13	4.5	A2	13	1
С	13	2.1	С	13	0.3
A2	14	4.6	A2	14	1
С	14	2.3	С	14	0.3

Table B- 22 The long format of the raw data for testing the effect of BINDER TYPE on corrosion in Specimen type A1 made of all the binder types measured via LPR

Mix	month	corrosion	next	Mix	month	corrosion	next	Mix	month	corrosion
PC	1	0.07		PC	13	2.13		PC	25	5.90
GGBS	1	0.08		GGBS	13	0.80		GGBS	25	4.55
FA	1	0.05		FA	13	1.34		FA	25	3.84
PC	2	0.09		PC	14	1.67		PC	26	5.84
GGBS	2	0.08		GGBS	14	1.35		GGBS	26	4.46
FA	2	0.08		FA	14	1.53		FA	26	3.08
PC	3	0.40		PC	15	2.37		PC	27	5.59
GGBS	3	0.23		GGBS	15	1.47		GGBS	27	3.90
FA	3	0.40		FA	15	2.00		FA	27	3.00
PC	4	0.57		PC	16	3.10		PC	28	6.02
GGBS	4	0.63		GGBS	16	2.12		GGBS	28	4.38
FA	4	0.53		FA	16	1.80		FA	28	2.60
PC	5	0.47		PC	17	3.41		PC	29	5.82
GGBS	5	0.50		GGBS	17	2.21		GGBS	29	4.55
FA	5	0.80		FA	17	2.96		FA	29	4.98
PC	6	0.37		PC	18	4.74		PC	30	5.84
GGBS	6	0.33		GGBS	18	3.21		GGBS	30	3.90
FA	6	0.63		FA	18	2.40		FA	30	4.72
PC	7	1.10		PC	19	6.99		PC	31	6.10
GGBS	7	0.67		GGBS	19	2.60		GGBS	31	4.64
FA	7	0.73		FA	19	3.00		FA	31	4.03
PC	8	1.00		PC	20	7.67		PC	32	5.99
GGBS	8	1.08		GGBS	20	3.29		GGBS	32	3.51
FA	8	0.70		FA	20	3.60		FA	32	5.07
РС	9	1.47		PC	21	6.50		PC	33	7.17
GGBS	9	0.87		GGBS	21	3.86		GGBS	33	3.90
FA	9	0.97		FA	21	3.96		FA	33	3.90
PC	10	2.80		PC	22	5.92		PC	34	6.67
GGBS	10	1.00		GGBS	22	3.90		GGBS	34	3.90
FA	10	0.87		FA	22	3.60		FA	34	4.42
PC	11	2.97		PC	23	5.87		PC	35	6.34
GGBS	11	1.07		GGBS	23	4.51		GGBS	35	3.99
FA	11	1.27		FA	23	4.24		FA	35	5.16
PC	12	2.50		PC	24	5.69		PC	36	6.29
GGBS	12	0.83		GGBS	24	4.68		GGBS	36	2.60
FA	12	1.52		FA	24	3.60		FA	36	3.55

Table B- 23 The long format of the raw data for testing the effect of BINDER TYPE on corrosion in Specimen type A1 made of all the binder types measured via ZRA

Mix	month	corrosion	next	Mix	month	corrosion	next	Mix	month	corrosion
PC	1	0.1		PC	13	3.0		PC	25	2.2
GGBS	1	0.4		GGBS	13	1.0		GGBS	25	0.9
FA	1	0.1		FA	13	1.0		FA	25	0.5
PC	2	1.0		PC	14	3.0		PC	26	2.4
GGBS	2	0.6		GGBS	14	0.7		GGBS	26	0.7
FA	2	1.0		FA	14	0.9		FA	26	0.5
PC	3	3.0		PC	15	3.0		PC	27	2.4
GGBS	3	0.7		GGBS	15	0.7		GGBS	27	0.7
FA	3	1.0		FA	15	0.9		FA	27	0.7
PC	4	2.0		PC	16	0.7		PC	28	2.6
GGBS	4	0.8		GGBS	16	0.7		GGBS	28	0.8
FA	4	0.5		FA	16	1.0		FA	28	0.6
PC	5	1.0		PC	17	3.0		PC	29	2.5
GGBS	5	0.9		GGBS	17	0.8		GGBS	29	0.8
FA	5	0.9		FA	17	1.0		FA	29	0.6
PC	6	1.0		PC	18	2.0		PC	30	2.7
GGBS	6	0.5		GGBS	18	0.7		GGBS	30	0.7
FA	6	1.0		FA	18	0.8		FA	30	0.6
PC	7	3.0		PC	19	2.0		PC	31	2.0
GGBS	7	1.7		GGBS	19	0.6		GGBS	31	0.9
FA	7	1.6		FA	19	0.9		FA	31	0.6
PC	8	1.0		PC	20	2.7		PC	32	2.1
GGBS	8	0.9		GGBS	20	0.8		GGBS	32	0.8
FA	8	1.0		FA	20	0.8		FA	32	0.6
PC	9	0.7		PC	21	2.4		PC	33	2.2
GGBS	9	0.8		GGBS	21	0.8		GGBS	33	0.9
FA	9	1.0		FA	21	0.7		FA	33	0.6
PC	10	1.0		PC	22	2.4		PC	34	2.3
GGBS	10	0.9		GGBS	22	0.8		GGBS	34	0.8
FA	10	1.0		FA	22	0.6		FA	34	0.8
PC	11	0.4		PC	23	2.2		PC	35	2.6
GGBS	11	0.6		GGBS	23	0.8		GGBS	35	0.7
FA	11	0.8		FA	23	0.6		FA	35	0.7
РС	12	2.0		PC	24	2.3		PC	36	3.3
GGBS	12	0.2		GGBS	24	0.8		GGBS	36	1.2
FA	12	1.0		FA	24	0.7		FA	36	0.6

Table B- 24 The long format of the raw data for testing the effect of BINDER TYPE on corrosion in Specimen type B made of all the binder types measured via LPR

Mix	month	corrosion	next	Mix	month	corrosion	next	Mix	month	corrosion
PC	1	0.06		PC	13	0.89		PC	25	1.58
GGBS	1	0.07		GGBS	13	0.46		GGBS	25	0.75
FA	1	0.08		FA	13	0.63		FA	25	0.70
PC	2	0.08		PC	14	0.55		PC	26	1.85
GGBS	2	0.08		GGBS	14	0.55		GGBS	26	0.67
FA	2	0.08		FA	14	0.75		FA	26	1.00
PC	3	0.07		PC	15	0.55		PC	27	2.29
GGBS	3	0.09		GGBS	15	0.83		GGBS	27	0.73
FA	3	0.06		FA	15	0.80		FA	27	0.80
PC	4	0.11		PC	16	0.72		PC	28	2.38
GGBS	4	0.18		GGBS	16	0.75		GGBS	28	0.73
FA	4	0.15		FA	16	0.77		FA	28	0.80
PC	5	0.15		PC	17	1.00		PC	29	2.41
GGBS	5	0.12		GGBS	17	0.66		GGBS	29	0.81
FA	5	0.14		FA	17	0.80		FA	29	0.70
PC	6	0.20		PC	18	1.54		PC	30	2.25
GGBS	6	0.20		GGBS	18	0.64		GGBS	30	0.74
FA	6	0.14		FA	18	0.80		FA	30	0.70
PC	7	0.17		PC	19	1.80		PC	31	2.37
GGBS	7	0.01		GGBS	19	0.63		GGBS	31	0.72
FA	7	0.15		FA	19	0.70		FA	31	0.70
PC	8	0.32		PC	20	1.45		PC	32	1.79
GGBS	8	0.24		GGBS	20	0.55		GGBS	32	0.65
FA	8	0.21		FA	20	0.60		FA	32	0.60
PC	9	0.44		PC	21	1.83		PC	33	2.30
GGBS	9	0.21		GGBS	21	0.66		GGBS	33	0.69
FA	9	0.20		FA	21	0.70		FA	33	0.80
PC	10	0.31		PC	22	1.76		PC	34	2.59
GGBS	10	0.20		GGBS	22	0.58		GGBS	34	0.66
FA	10	0.26		FA	22	0.60		FA	34	1.00
PC	11	0.45		PC	23	1.76		PC	35	3.40
GGBS	11	0.50		GGBS	23	0.61		GGBS	35	0.68
FA	11	0.48		FA	23	0.80		FA	35	1.10
РС	12	0.58		PC	24	1.89		PC	36	3.46
GGBS	12	0.60		GGBS	24	0.75		GGBS	36	0.62
FA	12	0.57		FA	24	0.60		FA	36	1.30

Table B- 25 The long format of the raw data for testing the effect of BINDER TYPE on corrosion in Specimen type B made of all the binder types measured via ZRA

Mix	month	corrosion	next	Mix	month	corrosion	next	Mix	month	corrosion
PC	1	0.03		PC	13	0.8		PC	25	0.65
GGBS	1	0.03		GGBS	13	0.7		GGBS	25	0.55
FA	1	0.21		FA	13	0.55		FA	25	0.95
PC	2	0.65		PC	14	1.2		PC	26	0.9
GGBS	2	0.4		GGBS	14	0.6		GGBS	26	0.6
FA	2	0.35		FA	14	1.3		FA	26	0.75
PC	3	0.8		PC	15	1.3		PC	27	0.75
GGBS	3	0.45		GGBS	15	0.35		GGBS	27	0.5
FA	3	0.3		FA	15	0.7		FA	27	0.9
PC	4	0.4		PC	16	0.75		PC	28	0.85
GGBS	4	0.6		GGBS	16	0.4		GGBS	28	0.6
FA	4	0.6		FA	16	0.55		FA	28	0.75
PC	5	0.15		PC	17	0.85		PC	29	0.7
GGBS	5	0.6		GGBS	17	0.75		GGBS	29	0.55
FA	5	0.35		FA	17	0.7		FA	29	0.55
PC	6	0.75		PC	18	0.8		PC	30	0.88
GGBS	6	0.55		GGBS	18	0.85		GGBS	30	0.55
FA	6	0.7		FA	18	0.6		FA	30	0.6
PC	7	0.75		PC	19	0.85		PC	31	0.6
GGBS	7	0.4		GGBS	19	0.5		GGBS	31	0.55
FA	7	0.62		FA	19	0.65		FA	31	0.45
PC	8	0.9		PC	20	0.9		PC	32	0.4
GGBS	8	0.45		GGBS	20	0.6		GGBS	32	0.55
FA	8	0.75		FA	20	0.25		FA	32	0.65
PC	9	0.24		PC	21	0.55		PC	33	0.88
GGBS	9	0.45		GGBS	21	0.45		GGBS	33	0.55
FA	9	0.7		FA	21	0.4		FA	33	0.45
PC	10	0.3		PC	22	1		PC	34	0.8
GGBS	10	0.3		GGBS	22	0.8		GGBS	34	0.5
FA	10	0.8		FA	22	0.85		FA	34	0.25
PC	11	1.6		PC	23	0.75		PC	35	0.5
GGBS	11	0.55		GGBS	23	0.65		GGBS	35	0.55
FA	11	0.35		FA	23	0.6		FA	35	0.4
РС	12	1.3		PC	24	0.55		PC	36	1.05
GGBS	12	0.7		GGBS	24	0.6		GGBS	36	0.55
FA	12	0.7		FA	24	0.75		FA	36	0.25

Table B- 26 The long format of the raw data for testing the effect of BINDER TYPE on corrosion in Specimen type A2 made of all the binder types measured via LPR

Mix	time	corrosion	next	Mix	time	corrosion
PC	1	0.20		PC	8	6.85
GGBS	1	0.20		GGBS	8	4.40
FA	1	0.10		FA	8	4.30
PC	2	0.40		PC	9	7.65
GGBS	2	0.30		GGBS	9	4.30
FA	2	0.40		FA	9	4.80
PC	3	1.00		PC	10	7.35
GGBS	3	4.30		GGBS	10	4.60
FA	3	2.00		FA	10	5.40
PC	4	3.85		PC	11	9.15
GGBS	4	1.80		GGBS	11	4.10
FA	4	3.13		FA	11	5.30
PC	5	4.85		PC	12	11.35
GGBS	5	3.00		GGBS	12	5.10
FA	5	3.40		FA	12	5.30
PC	6	5.50		PC	13	8.35
GGBS	6	3.80		GGBS	13	4.27
FA	6	4.00		FA	13	4.50
PC	7	6.50		PC	14	9.00
GGBS	7	3.40		GGBS	14	4.57
FA	7	4.00		FA	14	4.60

Table B- 27 The long format of the raw data for testing the effect of BINDER TYPE on corrosion in Specimen type A2 made of all the binder types measured via ZRA

Mix	time	corrosion	next	Mix	time	corrosion
PC	1	0.3		PC	8	2.8
GGBS	1	0.3		GGBS	8	1
FA	1	0.2		FA	8	1.1
PC	2	0.3		PC	9	2.4
GGBS	2	0.2		GGBS	9	1.1
FA	2	0.2		FA	9	1.4
PC	3	0.1		PC	10	1.6
GGBS	3	0.3		GGBS	10	1
FA	3	0.1		FA	10	1.2
PC	4	1		PC	11	1.8
GGBS	4	0.3		GGBS	11	0.6
FA	4	0.5		FA	11	1.1
PC	5	1.5		PC	12	2
GGBS	5	0.5		GGBS	12	0.5
FA	5	0.6		FA	12	1
PC	6	3.4		PC	13	2
GGBS	6	0.9		GGBS	13	0.8
FA	6	0.7		FA	13	1
PC	7	2.8		PC	14	2.7
GGBS	7	1		GGBS	14	1.3
FA	7	1.2		FA	14	1

Table B- 28 The long format of the raw data for testing the effect of BINDER TYPE on corrosion in Specimen type C made of all the binder types measured via LPR

next

	1	1
Mix	month	corrosion
PC	1	0.20
GGBS	1	0.10
FA	1	0.20
PC	2	1.00
GGBS	2	1.00
FA	2	1.30
PC	3	2.00
GGBS	3	2.00
FA	3	3.00
PC	4	3.30
GGBS	4	2.40
FA	4	2.40
PC	5	3.50
GGBS	5	2.80
FA	5	2.70
PC	6	3.80
GGBS	6	2.00
FA	6	2.70
PC	7	3.67
GGBS	7	2.00
FA	7	2.80

Mix	month	corrosion
PC	8	3.53
GGBS	8	2.40
FA	8	3.20
PC	9	5.55
GGBS	9	2.70
FA	9	2.70
PC	10	6.00
GGBS	10	3.00
FA	10	3.30
PC	11	5.64
GGBS	11	2.50
FA	11	2.70
PC	12	5.73
GGBS	12	2.80
FA	12	3.90
PC	13	4.73
GGBS	13	2.50
FA	13	2.10
PC	14	6.18
GGBS	14	2.60
FA	14	3.20

Table B- 29 The long format of the raw data for testing the effect of BINDER TYPE on corrosion in Specimen type C made of all the binder types measured via ZRA

Mix	month	corrosion	next	Mix	month	corrosion
PC	1	0.1		PC	8	0.7
GGBS	1	0.1		GGBS	8	1
FA	1	0.08		FA	8	0.6
PC	2	0.7		PC	9	1.6
GGBS	2	0.3		GGBS	9	0.8
FA	2	0.7		FA	9	0.7
PC	3	0.3		PC	10	4.3
GGBS	3	0.3		GGBS	10	0.7
FA	3	0.2		FA	10	0.8
PC	4	0.2		PC	11	1.4
GGBS	4	0.2		GGBS	11	0.8
FA	4	1.4		FA	11	0.6
PC	5	0.7		PC	12	0.8
GGBS	5	0.2		GGBS	12	0.3
FA	5	0.5		FA	12	0.4
PC	6	0.7		PC	13	0.8
GGBS	6	0.5		GGBS	13	0.4
FA	6	2		FA	13	0.3
PC	7	0.6		PC	14	1.5
GGBS	7	0.6		GGBS	14	0.8
FA	7	0.3		FA	14	0.3

Appendix C Codes used in R studio

R Studio is a software which requires certain codes in order to execute the statistical analysis. First, packages such as "readxl" and "ggplot2" should be installed within the software. After this, the effect of crack width on corrosion has been tested. The code is provided below to test the effect of crack width on corrosion:

1. input_data = read_excel('location of the excel document should be indicated here')

The next code is necessary to test whether the right document has been selected.

print(input_data)

The data frame has to be created in the next code.

3.df<as.data.frame(matrix(unlist(input_data),nrow=length(unlist(input_data[1]))))
names(df) <- c('width','month','corrosion')

df\$corrosion <- as.numeric(as.character(df\$corrosion))</pre>

The next code allows for significance test to be performed in respect with crack widths.

4. model.1 <- aov(corrosion ~ width, df) summary(model.1)

However, above code does not show the significance level between all considered crack widths, and it has to be followed by post-hoc test shown below.

5. my_data <- aov(corrosion~as.factor (width), data=df)

TukeyHSD(my_data)

The next step is to build a boxplot where the number of tests should be indicated. It should be stopped at 14 months when types A2 and C specimens are tested as they have readings only for 14 months.

```
6.df$time<factor(df$time,levels=c("1","2","3","4","5","6","7","8","9","10","11","12", '13','14', '15', '16', '17', '18','19','20', '21', '22', '23', '24', '25', '26', '27', '28', '29', '30', '31', '32', '33', '34', '35', '36'))
```

The next set of codes are used for boxplot specifications such as the title, the position of the mean values the font size and colour of the boxplots and so on.

7. df\$width = as.character(df\$width)
ggplot(df, aes(x=width, y=corrosion, fill=width)) +
geom_boxplot() +

```
ggtitle('Effect of crack width on corrosion rate Specimen type A1 made of PC')+
theme(plot.title = element_text(hjust=0.5)) +
xlab('Crack width') +
ylab('Corrosion rate mA/cm2') +
ylim(0, 5) +
stat_summary(fun="mean", geom="point", aes(group=width),
position = position_dodge(0.8), shape=21, size=0.5, color="red", fill="red")+
stat_summary(fun = mean, geom = "text", col =
"black",size=3,position=position_dodge(0.8),
vjust =0.5, aes(label = paste0(round(..y.., digits = 1))))
```

To test the effect of crack depths, a new excel document should be crated with corrosion rates between A1 and B as well as between A2 and C are included. The first code remines the same except for the location of the excel sheet (the last part of the code in brackets). Next, the code for checking the correctness of the selected excel sheet the code number 2 remains the same. After this, data frame should be changed as the variables in this test are different.

```
3.df<as.data.frame(matrix(unlist(input_data),nrow=length(unlist(input_data[1]))))
names(df) <- c('Types', 'time','corrosion')
df$corrosion <- as.numeric(as.character(df$corrosion))
```

The codes number 4, 5, and 6 remain the same. However the last code will change due to different variables being tested which is shown below.

```
7. ggplot(df, aes(x=Types, y=corrosion, fill=Types))+
 geom_boxplot()+
 ggtitle('Effect of crack depth on corrosion rate specimens made of FA')+
 theme(plot.title = element_text(hjust=0.5))+
 xlab('Specimen type')+
 ylab('Corrosion rate mA/cm2')+
 ylim(0, 12) +
 stat_summary(fun="mean", geom="point", aes(group=Types),
position = position_dodge(0.8), shape=21, size=0.5, color="red", fill="red")+
stat_summary(fun
                              'mean'.
                                          geom
                                                            "text".
                                                                      col
"black", size=4, position=position dodge(0.9),
vjust =1.5, aes(group=Types, label = paste0(round(..y.., digits = 1))))
```

For testing the effect of cement type, the first code remains the same except for the location of the excel document. Since the variables tested here are different, the dataframe should be changed as follows:

```
3.df<as.data.frame(matrix(unlist(input_data),nrow=length(unlist(input_data[1]))))
names(df) <- c( 'Mix','month','corrosion')
df$corrosion <- as.numeric(as.character(df$corrosion))

The codes number 4, 5, and 6 remain the same. However the last code will change due to different variables being tested which is shown below.

7. data_new <- df  # Duplicate data
data_new$Mix <- factor(data_new$Mix, # Reorder factor levels
```

```
data_new$Mix <- factor(data_new$Mix,
c("PC", "GGBS", "FA"))
#print(data_new)
#data_new %>% filter(Mix == "PFA")
ggplot(data_new, aes(x=Mix, y=corrosion, fill=Mix))+
geom_boxplot()+
ggtitle('Effect of cement on corrosion rate of Specimen type C')+
theme(plot.title = element_text(hjust=0.5))+
xlab('Cement type')+
ylab('Corrosion rate mA/cm2')+
ylim(0, 7) +
stat_summary(fun="mean", geom="point", aes(group=Mix),
position = position_dodge(0.8), shape=21, size=0.5, color="red", fill="red")+
stat_summary(fun
                             'mean'.
                                                          "text".
                                         geom
                                                    =
                                                                     col
                                                                             =
"black", size=3, position=position dodge(0.9),
```

vjust =1.5, aes(group=Mix, label = paste0(round(..y.., digits = 1))))

Appendix D Analysis of the last 3, 6, and 9 months

This Appendix shows the results obtained for the last 3, 6 and 9 months in isolation in order to check wether the results are consistent. First ANOVA results are presented in a table followed by post-hoc test and then the boxplots illustrating the results visually. Table D-1 and D-2 show the ANOVA and post-hoc test results for the last 9, 6 and 3 months respectively. Whereas Figures D-1, D-2 and D3 represent the boxplots of effect of crack widths on corrosion rates for the last 9, 6 and 3 months respectively.

Table D- 1 ANOVA results for different crack widths in specimens B and C made of PC and measured with both measurement techniques.

Ф	re Je		Measurement techniques						
sur	t ag	Specimen	LF	PR	ZRA				
Measure	Meas	type	F Test statistic	Significance level	F Test statistic	Significance level			
	ths	В	F(1)= 16.56	<i>p</i> < 0.05	F(1) =3.5	p = 0.07			
6	9 months	С	<i>F(4)</i> = 32.94	p < 0.05	<i>F(4)</i> = 3.02	p < 0.05			
	ths	В	F(1)= 8.12	p < 0.05	<i>F(1)</i> = 3.18	p = 0.4			
9	months	С	F(4)=22.36	p < 0.05	<i>F(4)</i> = 2.97	p < 0.05			
	ths	В	F(1)= 4.92	p < 0.05	F(1)=0.26	p = 0.6			
3	3 months	С	F(4)=17.57	p < 0.05	<i>F(4)</i> = 1.44	p = 0.29			

Table D- 2 Post Hoc Test of multiple comparisons on the effect of crack width on corrosion for specimens B and C made of PC measured via LPR and ZRA

	7	Comparison	Measurement techniques				
Space de	combination	Linear	Polarisation	Zero Resistance			
esu tain	Specific en type			sistance	Ammeter		
Re obt		widths	Mean	Sig.	Mean	Sig.	
		0; 0.1; 0.2; 0.3; 0.4	Diff.	Sig.	Diff.	Sig.	
с ө	c 0 D	0.1 vs 0	1.6	<i>p</i> < 0.05	NA	NA	
the B	0.2 vs 0	2.6	<i>p</i> < 0.05	NA	NA		

				ı	1	
		0.3 vs 0	1.3	<i>p</i> < 0.05	NA	NA
		0.4 vs 0	1.9	<i>p</i> < 0.05	NA	NA
		0.2 vs 0.1	1	<i>p</i> < 0.05	NA	NA
		0.3 vs 0.1	-0.3	p = 0.67	NA	NA
		0.4 vs 0.1	0.3	p = 0.72	NA	NA
		0.3 vs 0.2	-1.3	<i>p</i> < 0.05	NA	NA
		0.4 vs 0.2	-0.7	p < 0.05	NA	NA
		0.4 vs 0.3	0.6	p = 0.09	NA	NA
		0.1 vs 0	3.24	<i>p</i> < 0.05	1.01	p = 0.09
		0.2 vs 0	3.12	<i>p</i> < 0.05	1.23	<i>p</i> < 0.05
		0.3 vs 0	3.57	<i>p</i> < 0.05	00.97	p = 0.11
		0.4 vs 0	2.87	p < 0.05	0.93	p = 0.14
		0.2 vs 0.1	-0.13	p = 0.99	0.21	p = 0.98
	С	0.3 vs 0.1	0.32	p = 0.89	-0.04	p = 1
		0.4 vs 0.1	-0.37	p = 0.83	-0.09	p = 1
		0.3 vs 0.2	0.45	p = 0.72	-0.26	p = 0.96
		0.4 vs 0.2	-0.24	p = 0.96	-0.30	p = 0.94
		0.4 vs 0.3	-0.69	p = 0.31	-0.04	p = 0.99
		0.1 vs 0	1.6	<i>p</i> < 0.05	NA	NA
	В	0.2 vs 0	2.9	<i>p</i> < 0.05	NA	NA
		0.3 vs 0	1.1	<i>p</i> < 0.05	NA	NA
		0.4 vs 0	1.9	<i>p</i> < 0.05	NA	NA
		0.2 vs 0.1	1.3	<i>p</i> < 0.05	NA	NA
		0.3 vs 0.1	-0.5	p = 0.31	NA	NA
"		0.4 vs 0.1	0.3	p = 0.8	NA	NA
6 months		0.3 vs 0.2	-1.8	<i>p</i> < 0.05	NA	NA
nor		0.4 vs 0.2	-1	<i>p</i> < 0.05	NA	NA
		0.4 vs 0.3	0.8	<i>p</i> < 0.05	NA	NA
ast		0.1 vs 0	2.95	<i>p</i> < 0.05	0.74	p = 0.33
In the last		0.2 vs 0	2.47	<i>p</i> < 0.05	0.66	p = 0.45
L L		0.3 vs 0	3.48	<i>p</i> < 0.05	0.79	p = 0.27
_		0.4 vs 0	3.05	p < 0.05	1.32	<i>p</i> < 0.05
	С	0.2 vs 0.1	-0.47	p = 0.78	-0.08	p = 0.99
	C	0.3 vs 0.1	0.54	p = 0.69	0.05	p = 0.99
		0.4 vs 0.1	0.1	p = 0.99	0.58	p = 0.56
		0.3 vs 0.2	1.1	p = 0.14	0.13	p = 0.99
		0.4 vs 0.2	0.58	p = 0.64	0.67	p = 0.44
		0.4 vs 0.3	-0.43	p = 0.83	0.53	p = 0.65
		0.1 vs 0	1.6	<i>p</i> < 0.05	NA	NA
8		0.2 vs 0	3.2	<i>p</i> < 0.05	NA	NA
last	В	0.3 vs 0	0.9	<i>p</i> < 0.05	NA	NA
In the last months		0.4 vs 0	2.2	<i>p</i> < 0.05	NA	NA
In t		0.2 vs 0.1	1.5	<i>p</i> < 0.05	NA	NA
-		0.3 vs 0.1	-0.7	p = 0.26	NA	NA

		0.4 vs 0.1	0.6	p = 0.39	NA	NA
		0.3 vs 0.2	-2.2	<i>p</i> < 0.05	NA	NA
		0.4 vs 0.2	-1	<i>p</i> < 0.05	NA	NA
		0.4 vs 0.3	1.2	<i>p</i> < 0.05	NA	NA
		0.1 vs 0	2.32	<i>p</i> < 0.05	NA	NA
		0.2 vs 0	1.76	p < 0.05	NA	NA
	С	0.3 vs 0	3.29	p < 0.05	NA	NA
		0.4 vs 0	2.98	<i>p</i> < 0.05	NA	NA
		0.2 vs 0.1	-0.55	p = 0.99	NA	NA
		0.3 vs 0.1	0.97	p = 0.89	NA	NA
		0.4 vs 0.1	0.67	p = 0.83	NA	NA
		0.3 vs 0.2	1.52	p = 0.72	NA	NA
		0.4 vs 0.2	1.21	p = 0.96	NA	NA
		0.4 vs 0.3	-0.30	p = 0.31	NA	NA

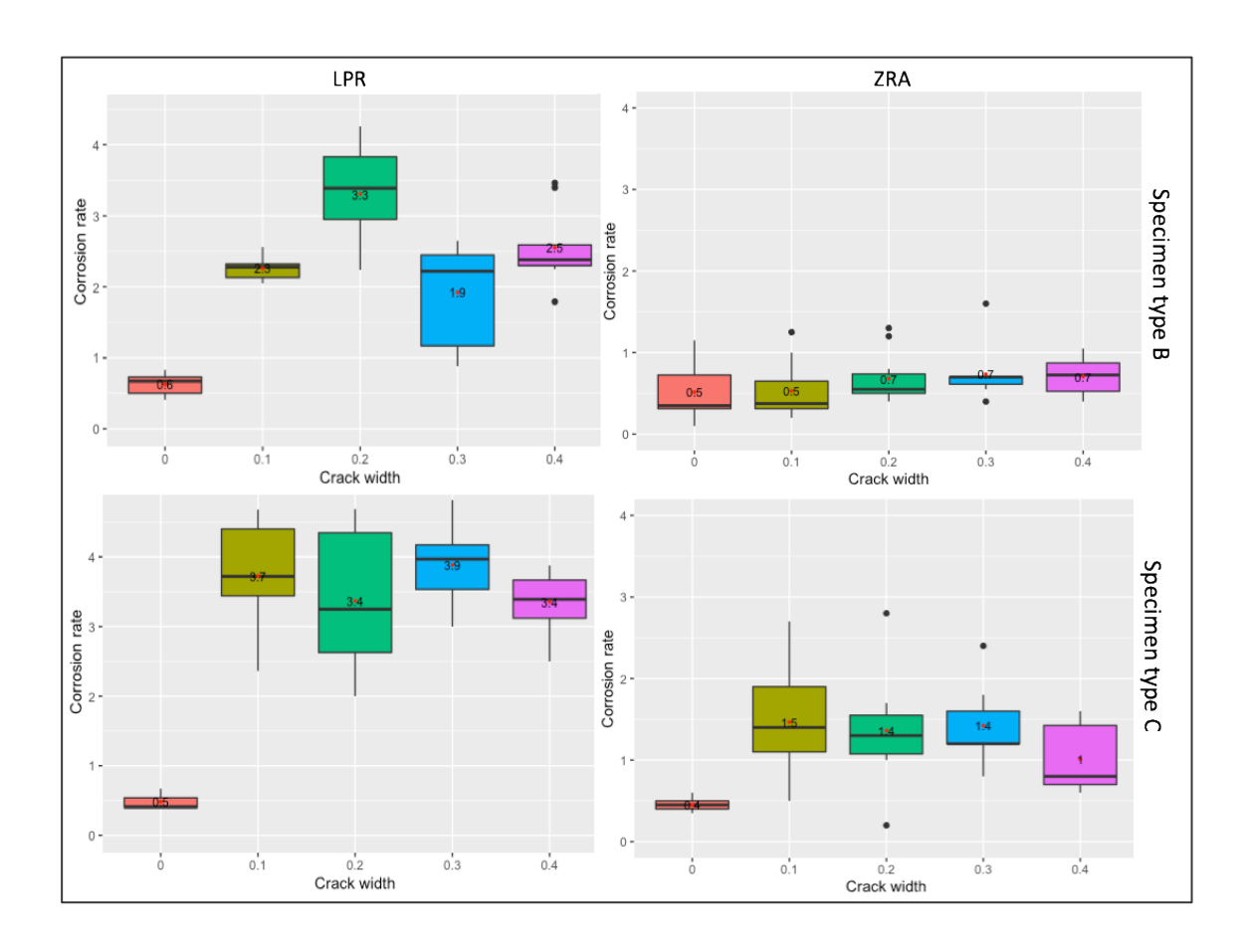


Fig. D- 1 Corrosion rates (μ A/cm²) experienced by specimen types B and C made of PC for the last 9 months measured via LPR and ZRA.

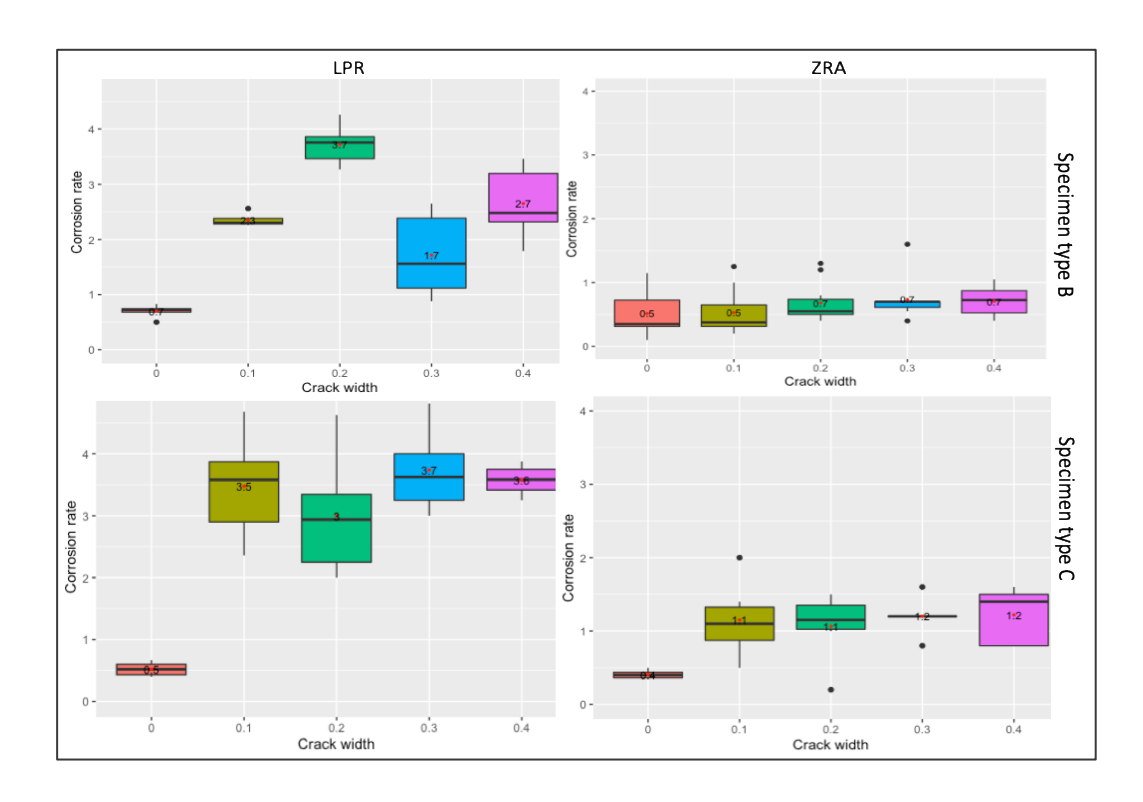


Fig. D- 2 Corrosion rates (μ A/cm²) experienced by specimen types B and C made of PC for the last 6 months measured via LPR and ZRA.

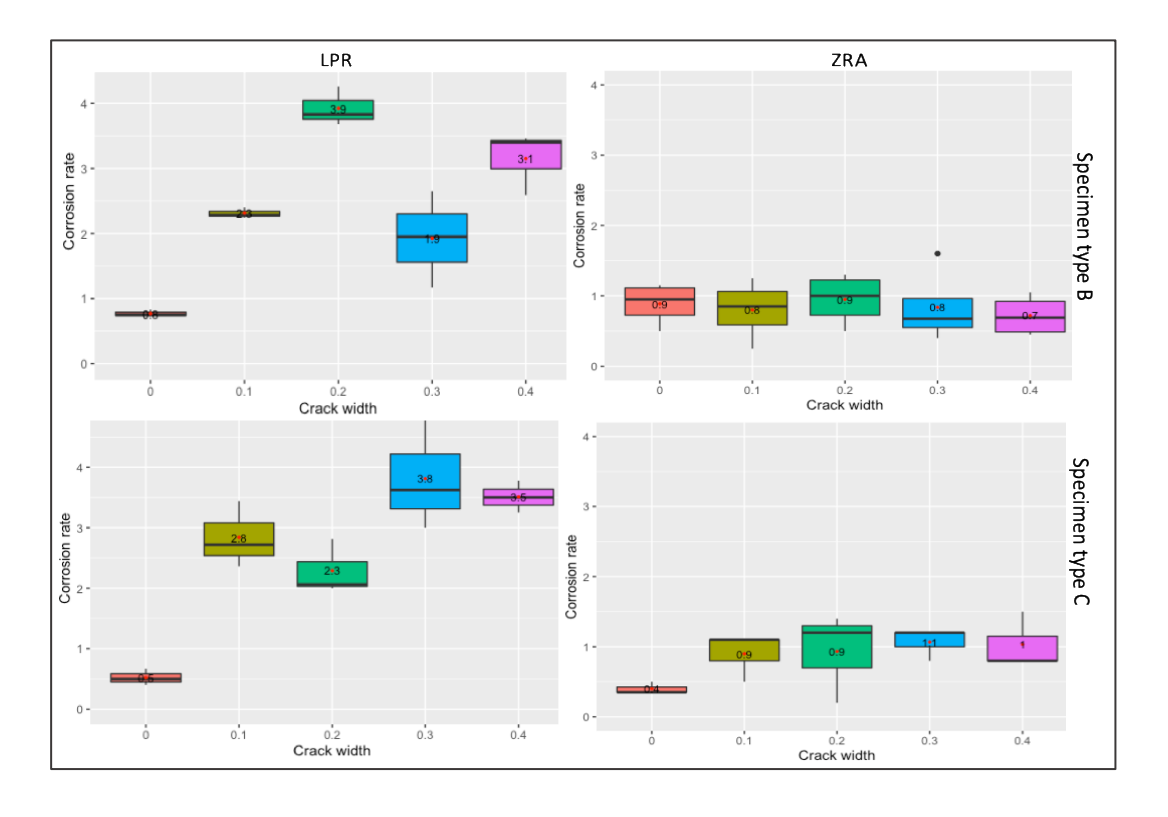


Fig. D- 3 Corrosion rates (μ A/cm²) experienced by specimen types B and C made of PC for the last 6 months measured via LPR and ZRA.

Table D- 3 ANOVA results for different crack widths in specimens B and C made of GGBS and measured with both measurement techniques.

Ф	<u>e</u>		Measurement techniques					
sur	t age	Specimen	LF	PR	ZI	RA		
Mea	Measure ment age	type	F Test statistic	Significance level	F Test statistic	Significance level		
	ths	В	F(1)= 0.62	p = 0.44	F(1) =5.67	p = 0.06		
6	9 months	С	F(1)= 14.89	p < 0.05	F(1)=7.3	p < 0.05		
	ths	В	F(1)= 0.51	p = 0.7	<i>F</i> (1)= 3.01	p = 0.1		
9	months	С	F(1)=10.1	p < 0.05	F(1)= 3.36	p = 0.1		
	ths	В	F(1)= 2.88	p = 0.11	F(1)=0.22	p = 0.66		
3	3 months	С	F(1)=4.96	p < 0.05	F(1)= 0.11	p = 0.74		

Table D- 4 Post Hoc Test of multiple comparisons on the effect of crack width on corrosion for specimens B and C made of GGBS measured via LPR and ZRA

	Specim	Comparison	Measurement techniques				
lts ied		combination	Linear	Polarisation	Zero Resistance		
Results obtained	en type	between crack	Res	sistance	Amn	neter	
8 . g	Cirtype	widths	Mean	Sig.	Mean	Sig.	
		0; 0.1; 0.2; 0.3; 0.4	Diff.	Olg.	Diff.	Olg.	
		0.1 vs 0	NA	NA	NA	NA	
		0.2 vs 0	NA	NA	NA	NA	
		0.3 vs 0	NA	NA	NA	NA	
		0.4 vs 0	NA	NA	NA	NA	
	В	0.2 vs 0.1	NA	NA	NA	NA	
SL	Б	0.3 vs 0.1	NA	NA	NA	NA	
ontl		0.4 vs 0.1	NA	NA	NA	NA	
Ш 6		0.3 vs 0.2	NA	NA	NA	NA	
ast		0.4 vs 0.2	NA	NA	NA	NA	
In the last 9 months		0.4 vs 0.3	NA	NA	NA	NA	
ln t		0.1 vs 0	1.86	<i>p</i> < 0.05	0.02	p = 0.09	
		0.2 vs 0	1.59	p < 0.05	0.16	p = 0.41	
		0.3 vs 0	1.12	p < 0.05	0.01	p = 0.99	
		0.4 vs 0	1.61	p < 0.05	0.29	<i>p</i> < 0.05	
	С	0.2 vs 0.1	-0.27	p = 0.10	0.14	p = 0.51	
		0.3 vs 0.1	0.73	<i>p</i> < 0.05	-0.01	p = 1	
		0.4 vs 0.1	-0.24	p = 0.16	0.28	p = 0.03	

		0.3 vs 0.2	-0.47	<i>p</i> < 0.05	-0.16	p = 0.43
		0.4 vs 0.2	0.02	p = 0.99	0.13	p = 0.58
		0.4 vs 0.3	0.5	p < 0.05	0.29	p < 0.05
		0.1 vs 0	NA	NA	NA	NA
		0.2 vs 0	NA	NA	NA	NA
		0.3 vs 0	NA	NA	NA	NA
		0.4 vs 0	NA	NA	NA	NA
	Ь	0.2 vs 0.1	NA	NA	NA	NA
	В	0.3 vs 0.1	NA	NA	NA	NA
		0.4 vs 0.1	NA	NA	NA	NA
ths		0.3 vs 0.2	NA	NA	NA	NA
nor		0.4 vs 0.2	NA	NA	NA	NA
6 r		0.4 vs 0.3	NA	NA	NA	NA
In the last 6 months		0.1 vs 0	1.79	<i>p</i> < 0.05	NA	NA
Je l		0.2 vs 0	1.47	p < 0.05	NA	NA
n #		0.3 vs 0	0.93	p < 0.05	NA	NA
		0.4 vs 0	1.65	<i>p</i> < 0.05	NA	NA
	С	0.2 vs 0.1	-0.32	p = 0.06	NA	NA
	O	0.3 vs 0.1	-0.85	<i>p</i> < 0.05	NA	NA
		0.4 vs 0.1	-0.13	p = 0.75	NA	NA
		0.3 vs 0.2	-0.53	<i>p</i> < 0.05	NA	NA
		0.4 vs 0.2	0.18	p = 0.48	NA	NA
		0.4 vs 0.3	0.72	<i>p</i> < 0.05	NA	NA
		0.1 vs 0	NA	NA	NA	NA
		0.2 vs 0	NA	NA	NA	NA
		0.3 vs 0	NA	NA	NA	NA
		0.4 vs 0	NA	NA	NA	NA
	В	0.2 vs 0.1	NA	NA	NA	NA
	ט	0.3 vs 0.1	NA	NA	NA	NA
S		0.4 vs 0.1	NA	NA	NA	NA
utp		0.3 vs 0.2	NA	NA	NA	NA
In the last 3 months		0.4 vs 0.2	NA	NA	NA	NA
13		0.4 vs 0.3	NA	NA	NA	NA
lasi		0.1 vs 0	1.61	<i>p</i> < 0.05	NA	NA
þe		0.2 vs 0	1.47	<i>p</i> < 0.05	NA	NA
In t		0.3 vs 0	0.84	<i>p</i> < 0.05	NA	NA
		0.4 vs 0	1.57	<i>p</i> < 0.05	NA	NA
	С	0.2 vs 0.1	-0.13	p = 0.94	NA	NA
	_	0.3 vs 0.1	-0.77	<i>p</i> < 0.05	NA	NA
		0.4 vs 0.1	-0.33	p = 0.99	NA	NA
		0.3 vs 0.2	-0.63	p < 0.05	NA	NA
		0.4 vs 0.2	0.1	p = 0.97	NA	NA
		0.4 vs 0.3	0.73	<i>p</i> < 0.05	NA	NA

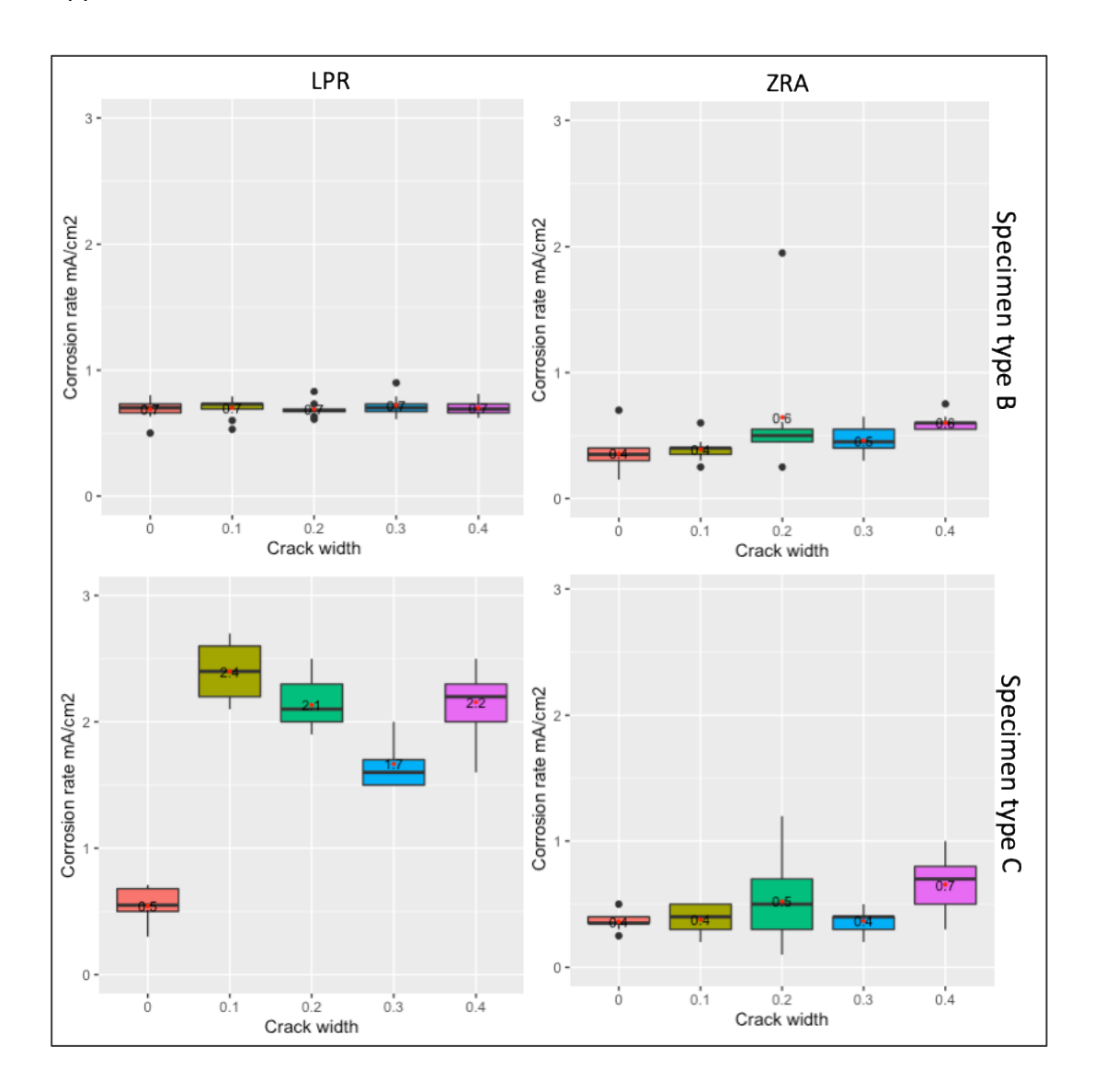


Fig. D- 4 Corrosion rates (μ A/cm²) experienced by specimen types B and C made of GGBS for the last 9 months measured via LPR and ZRA.

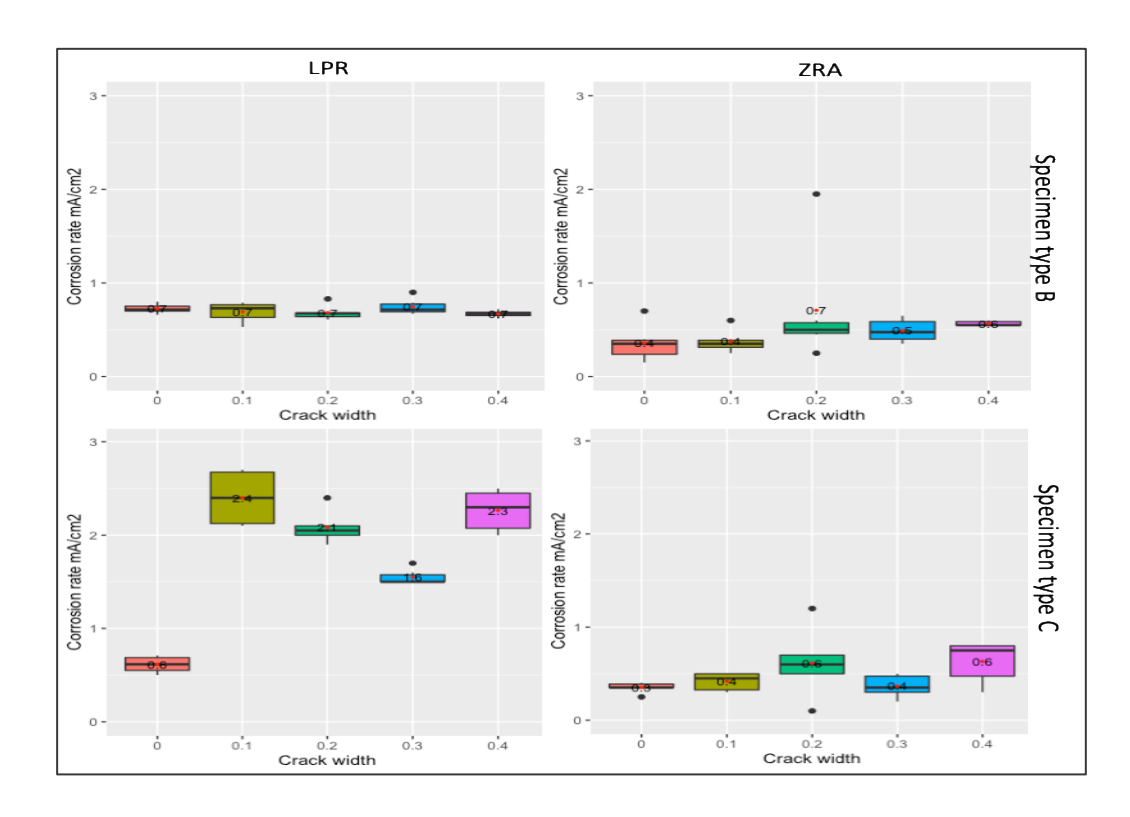


Fig. D- 5 Corrosion rates ($\mu A/cm^2$) experienced by specimen types B and C made of GGBS for the last 6 months measured via LPR and ZRA.

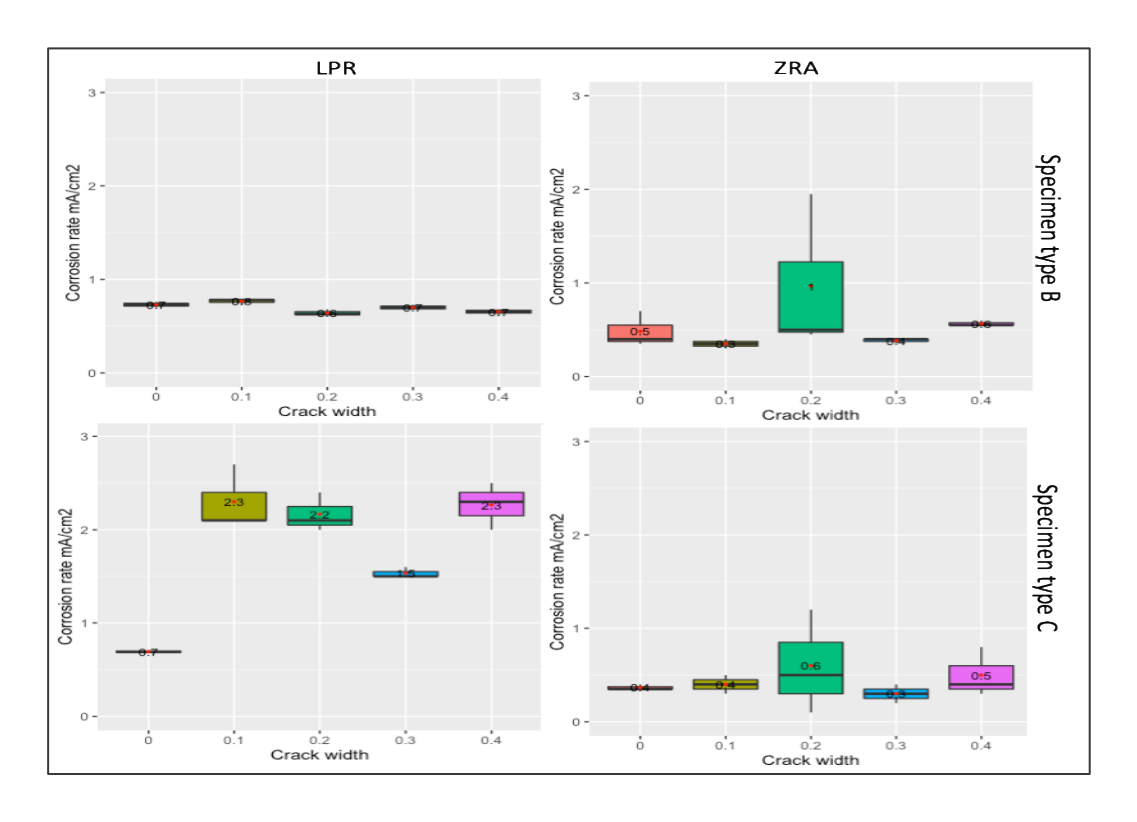


Fig. D- 6 Corrosion rates (μ A/cm²) experienced by specimen types B and C made of GGBS for the last 3 months measured via LPR and ZRA.

Appendix

Table D- 5 ANOVA results for different crack widths in specimens B and C made of FA and measured with both measurement techniques.

Ф	<u>e</u>		Measurement techniques					
sur	t age	Specimen	LF	PR	ZI	RA		
Mea	Measure ment age	type	F Test statistic	Significance level	F Test statistic	Significance level		
t 9	ıths	В	F(1)= 17.37	p < 0.05	F(1) =11.58	p < 0.05		
Las	Last 9 months	С	F(1)= 58.37	<i>p</i> < 0.05	F(1)= 4.5	p < 0.05		
9 .	ths	В	F(1)= 12.24	p < 0.05	F(1)= 3.14	p = 0.1		
Last	months	С	F(1)=29.5	p < 0.05	<i>F(1)</i> = 7.31	p = 0.1		
t 3	ths	В	F(1)= 11.16	<i>p</i> < 0.05	F(1)= 1.04	p = 0.32		
Last	Last 3 months	С	F(1)= 13.18	p < 0.05	F(1)= 5.11	p < 0.05		

Table D- 6 Post Hoc Test of multiple comparisons on the effect of crack width on corrosion for specimens B and C made of FA measured via LPR and ZRA

		Comparison	Measurement techniques				
Results obtained	Specim	combination		Polarisation	Zero Resistance		
Results obtained	en type	between crack	Res	sistance	Amr	neter	
R, do	on typo	widths	Mean	Sig.	Mean	Sig.	
		0; 0.1; 0.2; 0.3; 0.4	Diff.	olg.	Diff.	oig.	
		0.1 vs 0	0.49	<i>p</i> < 0.05	0.1	p = 0.88	
		0.2 vs 0	0.40	<i>p</i> < 0.05	0.27	<i>p</i> < 0.05	
		0.3 vs 0	0.54	<i>p</i> < 0.05	0.35	<i>p</i> < 0.05	
	В	0.4 vs 0	0.39	<i>p</i> < 0.05	0.19	p = 0.13	
		0.2 vs 0.1	-0.1	p = 0.53	0.19	p = 0.15	
ıths		0.3 vs 0.1	0.05	p = 0.91	0.27	<i>p</i> < 0.05	
mor		0.4 vs 0.1	-0.10	p = 0.41	0.12	p = 0.58	
st 9		0.3 vs 0.2	0.14	p = 0.13	0.1	p = 0.83	
e la:		0.4 vs 0.2	-0.01	p = 0.99	-0.1	p = 0.91	
In the last 9 months		0.4 vs 0.3	-0.15	p = 0.08	-0.16	p = 0.33	
		0.1 vs 0	1.42	<i>p</i> < 0.05	-0.12	p = 0.94	
		0.2 vs 0	1.95	p < 0.05	0.40	<i>p</i> < 0.05	
		0.3 vs 0	2.16	p < 0.05	0.12	p = 0.88	
		0.4 vs 0	1.69	p < 0.05	0.26	p = 0.32	
	С	0.2 vs 0.1	0.53	p < 0.05	0.50	<i>p</i> < 0.05	
		0.3 vs 0.1	0.73	<i>p</i> < 0.05	0.22	p = 0.46	

		0.4 vs 0.1	0.27	p = 0.45	0.35	p = 0.08
		0.4 vs 0.1 0.3 vs 0.2	0.27	p = 0.43 $p = 0.72$		
		0.4 vs 0.2	-0.27	p = 0.72 $p = 0.45$	-0.28	p = 0.24
				•	-0.14	p = 0.81
		0.4 vs 0.3	-0.47	p < 0.05	0.13	p = 0.85
		0.1 vs 0	0.51	<i>p</i> < 0.05	NA	NA
		0.2 vs 0	0.43	<i>p</i> < 0.05	NA	NA
		0.3 vs 0	0.55	p < 0.05	NA	NA
		0.4 vs 0	0.42	p < 0.05	NA	NA
	В	0.2 vs 0.1	-0.07	p = 0.87	NA	NA
	J	0.3 vs 0.1	0.05	p = 0.97	NA	NA
(O		0.4 vs 0.1	-0.1	p = 0.76	NA	NA
ths		0.3 vs 0.2	0.12	p = 0.54	NA	NA
nor		0.4 vs 0.2	-0.02	p = 1	NA	NA
6 r		0.4 vs 0.3	-0.14	p = 0.41	NA	NA
In the last 6 months		0.1 vs 0	1.34	p < 0.05	-0.14	p = 0.64
e l		0.2 vs 0	1.86	p < 0.05	0.38	<i>p</i> < 0.05
u #		0.3 vs 0	1.98	p < 0.05	0.04	p = 0.99
_		0.4 vs 0	1.76	p < 0.05	0.11	p = 0.79
	0	0.2 vs 0.1	0.52	p = 0.14	0.52	p < 0.05
	С	0.3 vs 0.1	0.65	p < 0.05	0.18	p = 0.38
		0.4 vs 0.1	0.42	p = 0.31	0.25	p = 0.12
		0.3 vs 0.2	0.13	p = 0.97	-0.33	p < 0.05
		0.4 vs 0.2	-0.1	p = 0.98	-0.27	p = 0.1
		0.4 vs 0.3	-0.23	p = 0.82	0.1	p = 0.96
		0.1 vs 0	0.61	<i>p</i> < 0.05	NA	NA
		0.2 vs 0	0.48	p < 0.05	NA	NA
		0.3 vs 0	0.53	p < 0.05	NA	NA
		0.4 vs 0	0.57	p < 0.05	NA	NA
		0.2 vs 0.1	-0.13	p = 0.46	NA	NA
	В	0.3 vs 0.1	-0.1	p = 0.82	NA	NA
		0.4 vs 0.1	-0.4	p = 0.99	NA	NA
ths		0.3 vs 0.2	0.05	p = 0.96	NA	NA
nor		0.4 vs 0.2	0.1	p = 0.74	NA	NA
3 п		0.4 vs 0.3	0.05	p = 0.97	NA	NA
In the last 3 months		0.1 vs 0	1.27	p < 0.05	-0.21	p = 0.37
<u>8</u>		0.2 vs 0	1.47	p < 0.05	0.26	p = 0.21
‡	С	0.3 vs 0	1.68	p < 0.05	0.04	p = 0.99
		0.4 vs 0	1.80	p < 0.05	-0.11	p = 0.85
		0.2 vs 0.1	0.20	p = 0.95	0.47	<i>p</i> < 0.05
		0.3 vs 0.1	0.41	p = 0.61	0.17	p = 0.57
		0.4 vs 0.1	0.53	p = 0.38	0.1	p = 0.88
		0.3 vs 0.2	0.21	p = 0.94	-0.30	p = 0.11
			, J.— .	, , , , , ,	, 5.55	, ,
		0.4 vs 0.2	0.33	p = 0.76	-0.37	<i>p</i> < 0.05

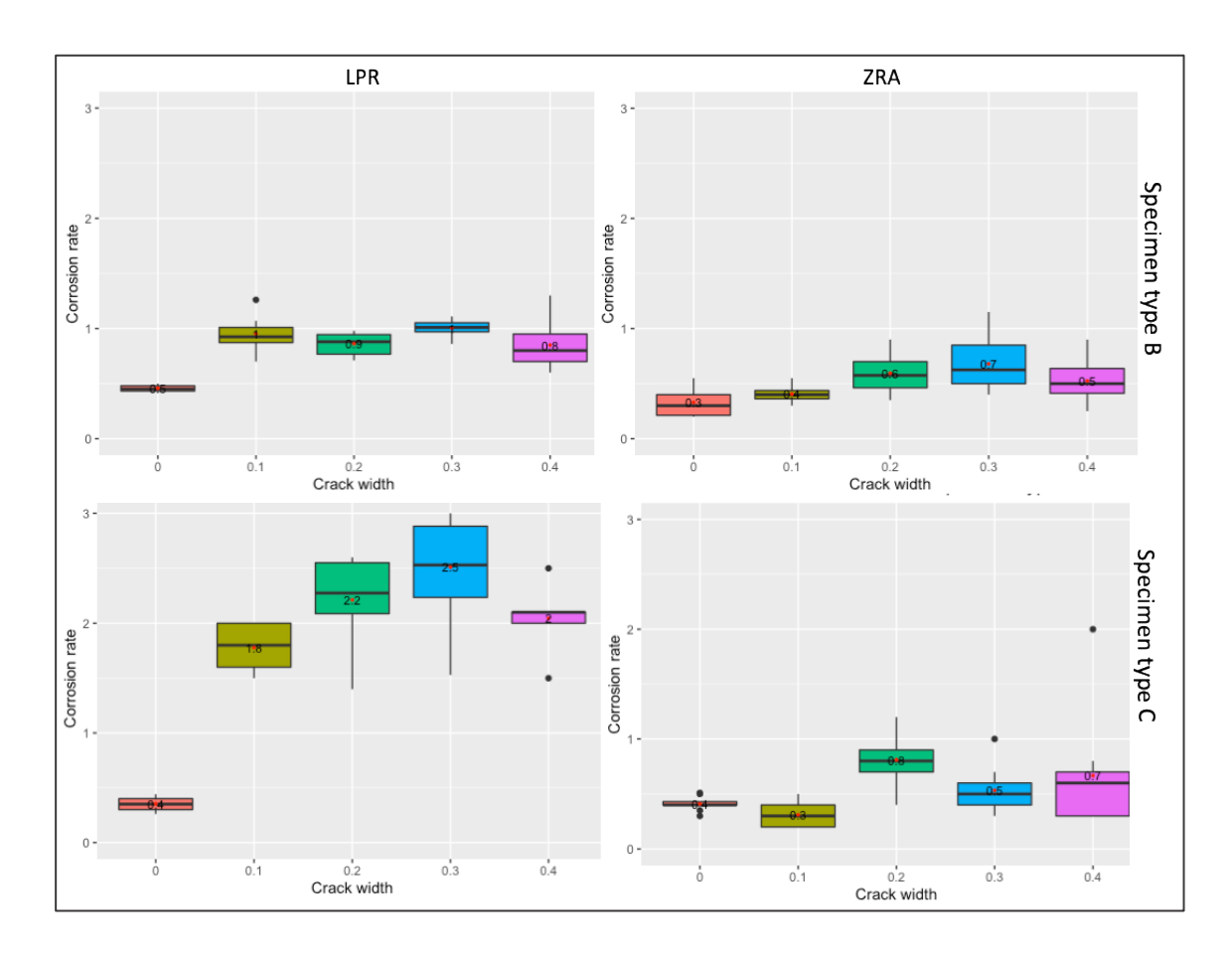


Fig. D- 7 Corrosion rates (μ A/cm²) experienced by specimen types B and C made of FA for the last 9 months measured via LPR and ZRA.

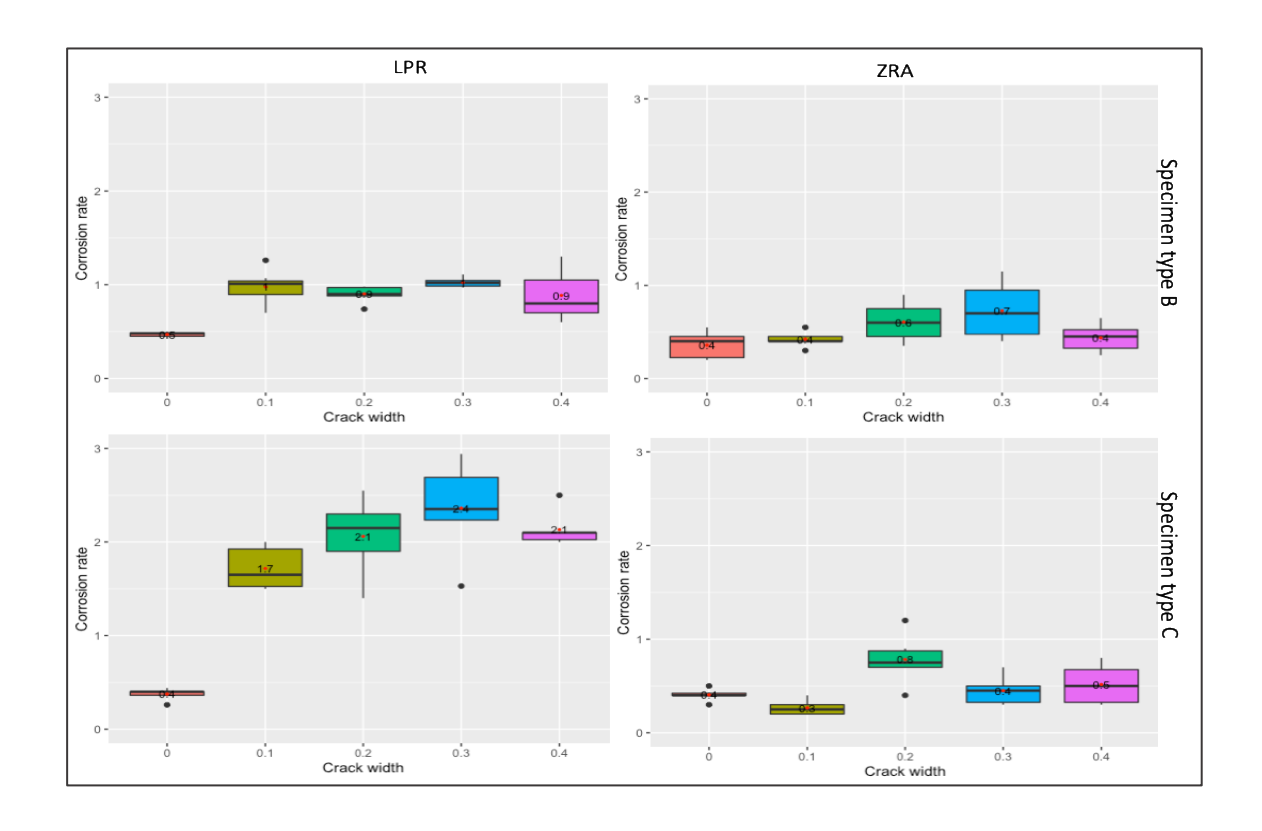


Fig. D- 8 Corrosion rates (μ A/cm²) experienced by specimen types B and C made of FA for the last 6 months measured via LPR and ZRA.

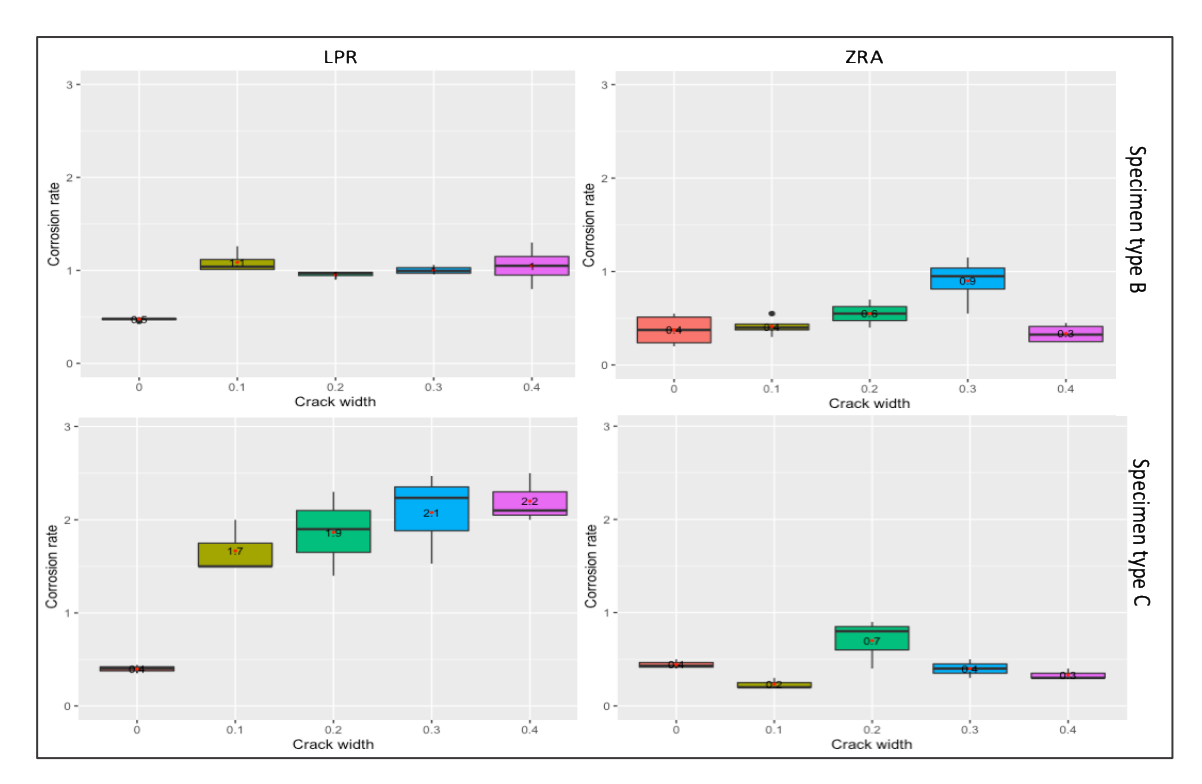


Fig. D- 9 Corrosion rates (μ A/cm²) experienced by specimen types B and C made of FA for the last 3 months measured via LPR and ZRA.

Appendix E Effect of crack depth

In this Appendix, the effect of crack depth has been assessed on the results obtained in the last 26 months since the corrosion rate was negligible during the first 10 months. First, ANOVA test of variance results are shown in tables followed by boxplots. The order of results is following: The effect of crack depth was tested between specimen types A1 and B made of PC, GGBS and FA measured by both techniques.

Table E- 1 ANOVA results for different crack depths (Specimen types A1 and B) in specimens made of all cement types over the last 26 months readings and measured through both measurement techniques.

Specimen types	Specimen types Measurement		Significance level
A1 and B	techniques		
PC	LPR	F(1)= 81.39	p < 0.05
	ZRA	F(1) =97.5	p < 0.05
GGBS	LPR	F(1)= 94.61	p < 0.05
	ZRA	F(1) = 20.41	p < 0.05
FA	LPR	F (1)= 100	p < 0.05
	ZRA	F(1) = 5.1	p < 0.05

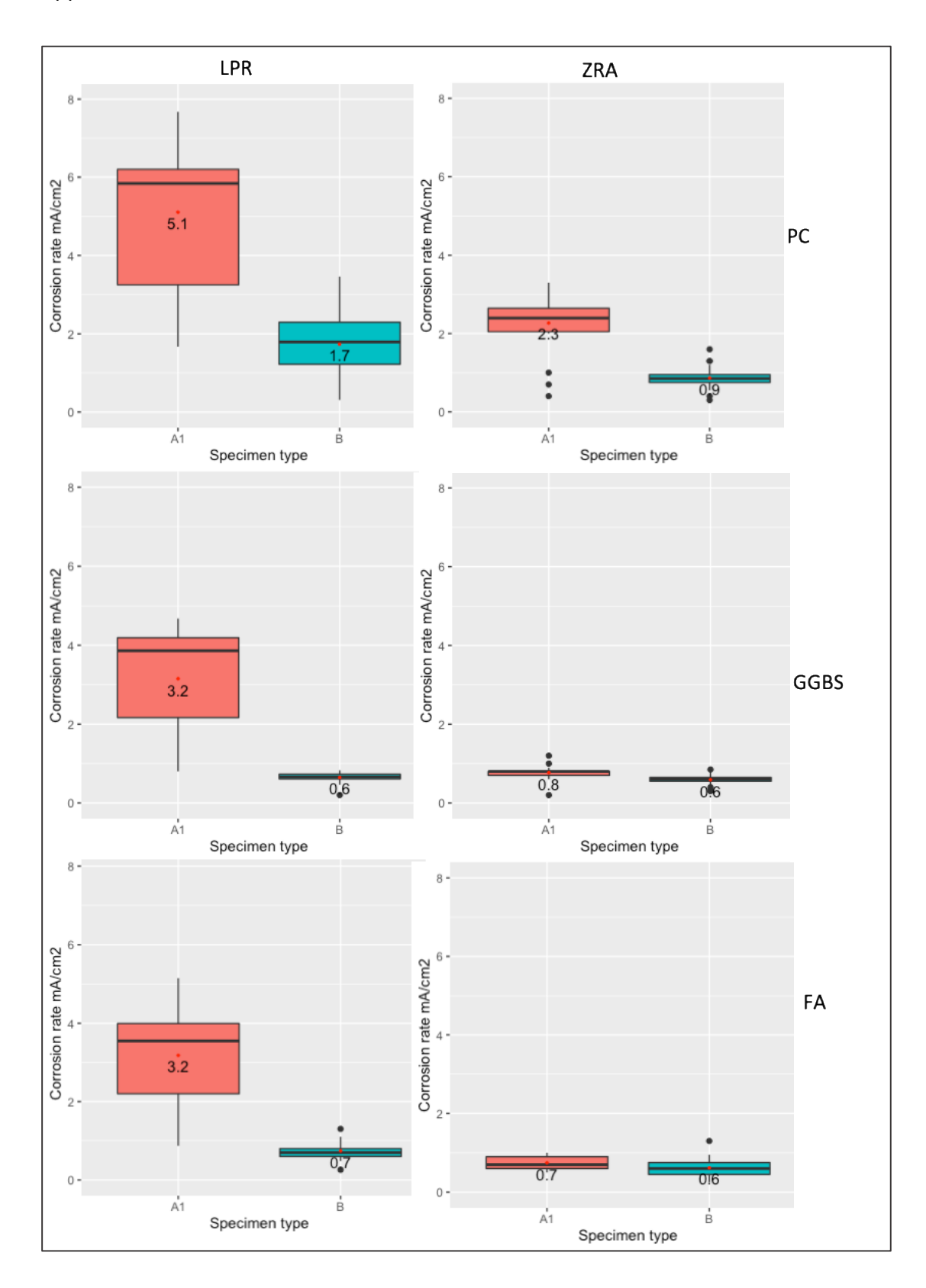


Fig. E- 1 Corrosion rates ($\mu A/cm^2$) experienced by specimen designs A1 and B during last 26 months.

Appendix F Resutls of specimen design A2

This appendix presents the results obtained from specimen design A2 on the effect of cement type on corrosion of the reinforcement.

Table F- 1ANOVA results for Specimen type A2 through both measurement techniques

Measurement technique	F Test statistic	Significance level
LPR	F (2)= 4.33	<i>p</i> < 0.05
ZRA	F (2) =10.45	<i>p</i> < 0.05

Table F- 2 Post Hoc Test of multiple comparisons on the effect of cement type on corrosion among specimen type A2 measured via LPR and ZRA.

Measurement techniques								
Linear I	Zero	Resistar	nce Amm	eter				
Binder type	Compa rison	Mean Diff.	Sig.	Binder type	Compa rison	Mean Diff.	Sig.	
1. PC 100%	1-2	2.42	p < 0.05	1. PC 100%	1-2	1.06	p < 0.05	
2. GGBS 65%	3-2	0.22	p = 0.99	2. GGBS 65%	3-2	0.11	p = 0.91	
3 FA 30%	3-1	-2.19	p < 0.05	3. FA 30%	3-1	-0.96	p < 0.05	

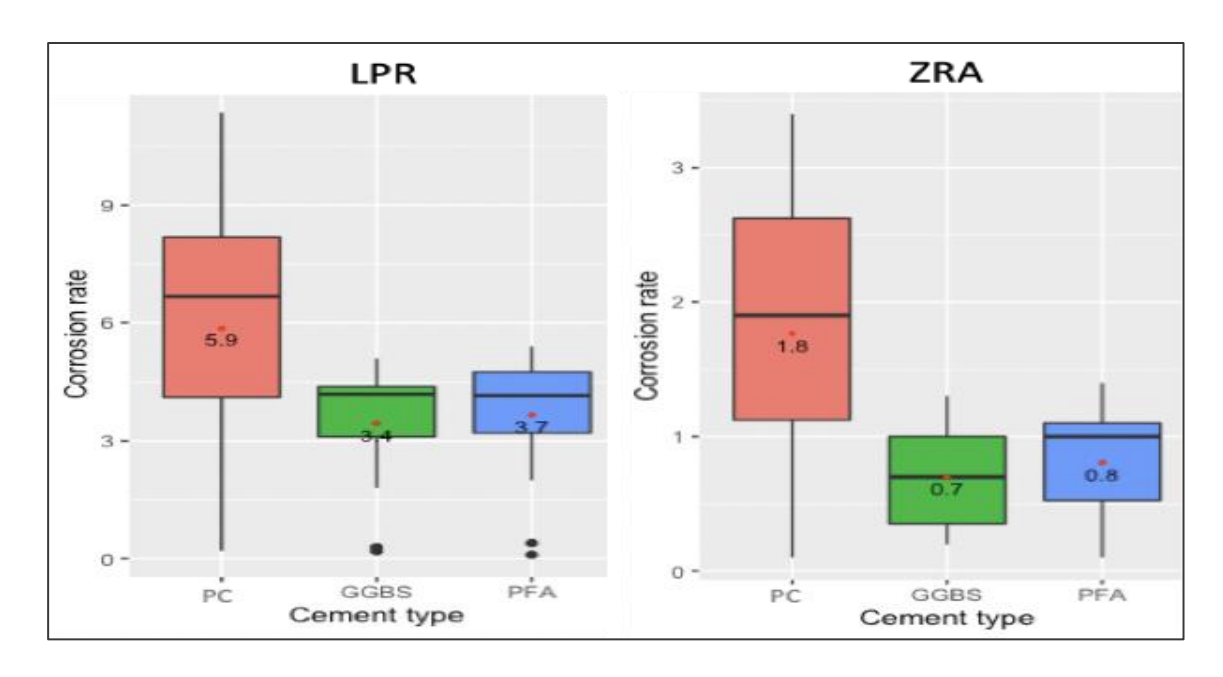


Fig. F- 1 Corrosion rates ($\mu A/cm^2$) in Specimen type A2 obtained via LPR and ZRA.